

**From Lake to Ocean:
Disentangling past and present depositional
processes and environmental conditions
of sub-Antarctic South Georgia
using molecular and isotopic tools**

Sandra Jivcov

**From Lake to Ocean:
Disentangling past and present depositional
processes and environmental conditions
of sub-Antarctic South Georgia
using molecular and isotopic tools**

Inaugural-Dissertation
zur
Erlangung des Doktorgrades
der Mathematisch-Naturwissenschaftlichen Fakultät
der Universität zu Köln

vorgelegt von
Sandra Jivcov
aus Temeschburg, Rumänien

Köln, 2019

Berichterstatter: Prof. Dr. Martin Melles
(Gutachter) Prof. Dr. Janet Rethemeyer

Tag der mündlichen Prüfung: 13. Juni 2018

Abstract

The sub-Antarctic is a key region for the understanding of the coupling of Northern and Southern Hemispheres' reactions to climate change. Until now, only few marine sedimentary records from this region were investigated because they are often lacking in eligible material for radiocarbon dating. Here, this topical problem is addressed by compound-specific radiocarbon analysis (CSRA) of biomarkers, derived from sedimentary records of South Georgia. Intrinsic characteristics of different biomarkers as well as depositional processes were investigated, in order to identify suitable compounds for the development of confident sediment chronologies. Environmental changes in the study area were traced on the basis of comprehensive multi-proxy analyses of marine and lacustrine sedimentary records.

Radiocarbon ages of *n*-fatty acids, *n*-alkanes, *n*-alcohols, total organic carbon (TOC) and macrofossils of a coastal marine sediment core (Co1305) of Little Jason Lagoon and a lacustrine sediment core (Co1308) of Allen Lake A were measured, in order to identify sources of the organic matter and to assess timescales of sediment transport. Similar temporal offsets of c. 1,900 to 2,600 years between production and deposition of co-occurring plant macrofossils and high molecular weight (HMW) *n*-fatty acids and *n*-alkanes point to common origins and transport pathways of these different sample types. Preservation and retention of the organic matter on land seems to be favored by climatic conditions.

Sedimentary bedrock is another source of land-derived organic carbon (OC) in the study area. Petrogenic OC is commonly free of ^{14}C and therefore influences radiocarbon ages of bulk sediments considerably. In order to quantify the contributions of OC from petrogenic, terrigenous (plants and soils) and marine sources to the surface sediments of different aquatic environments (a lake, a marine inlet, two fjords and an off-shore site), three end-member mass balance calculations were successfully applied. A clear spatial trend in the proportions of ancient OC in the sediments indicates that export of petrogenic carbon is mainly controlled by the activity of glaciers in the supply area. Correlation of ice-rafted debris (IRD) with high TOC ages of the coastal marine downcore record Co1305 supports that mechanical erosion of the bedrock by glaciers most efficiently mobilizes ancient OC.

Because of the influence of differently "aged" material from various sources on land, radiocarbon ages of terrigenous components or of TOC cannot be used for a chronological purpose in the coastal marine setting of Little Jason Lagoon. CSRA revealed that ^{14}C ages of mainly marine biomarkers (*n*-C₁₆ fatty acids and *n*-C₂₂ alcohols) likely yield more conf-

ident approximations of the time of sediment formation at this site. Proportions of terrigenous homologues, contributing to sedimentary pools of n -C₁₆ fatty acids and n -C₂₂ alcohols, seem to be related to the individual diagenetical behaviors of the respective biomarkers. ¹⁴C ages of co-occurring n -C₁₆ fatty acids and n -C₂₂ alcohols indicate that post-depositional processes change proportions of marine and terrigenous homologues of n -C₁₆ fatty acids to a higher extend than of n -C₂₂ alcohols. It seems therefore advantageous to combine n -C₁₆ fatty acid ages along with n -C₂₂ alcohol ages to improve the accuracy of the marine sediment chronology, particularly for the lower part of the sedimentary record Co1305.

Sedimentation is assumed to have started c. 10,000 cal BP in the setting of Little Jason Lagoon. The record Co1308 of Allen Lake A is going back to c. 7,500 cal BP. A marked environmental change was encountered in both records to have happened around 4,000 cal BP, when climatic conditions ameliorated after a cold phase. A marked vegetational change at this time in the setting of Allen Lake A seems to have caused several sedimentological and geochemical changes in the lacustrine record. Where sedimentary proxies of the lacustrine record Co1308 reveal a long term trend of successively ameliorating climatic conditions since c. 7,500 cal BP, various environmental changes, including glacier fluctuations and variations in marine and terrigenous productivity, are indicated in the record of Little Jason Lagoon. Combination of comprehensive information of both sedimentary records enabled the identification of system dependent variability of the different aquatic environments as well as environmental transitions of a likely regional extend.

Kurzfassung

Für das Verständnis des Zusammenhangs von nord- und südhemispherischen Reaktionen auf Klimaänderungen ist die sub-Antarktis eine Schlüsselregion. Bisher wurden nur wenige marine Sedimentarchive aus dieser Region untersucht, weil es meist an geeignetem Material, das zur Radiokarbondatierung verwendet werden kann, mangelt. In dieser Arbeit wurde die Methode der komponentenspezifischen Radiokarbondatierung von Biomarkern genutzt, um Altersdatenpunkte für aquatische Ablagerungsräume Südgeorgiens zu generieren. Durch die Untersuchung von Ablagerungsprozessen und intrinsischen Eigenschaften spezifischer Komponenten, konnten geeignete Biomarker für die Erstellung verlässlicher Sedimentchronologien identifiziert werden. Mithilfe einer umfassenden, auf einem marinen und einem lacustrinen Sedimentkern basierenden, Multi-Proxy-Analyse konnten Umweltveränderungen im Untersuchungsgebiet rekonstruiert werden.

Radiokarbonalter von *n*-Fettsäuren, *n*-Alkanen, *n*-Alkoholen, des Gesamtkohlenstoff und von Makrofossilien aus einem küstennahen marinen Sedimentkern (Co1305) und aus einem Seekern (Co1308) wurden gemessen, um die Quellen des organischen Material aufzuschlüsseln, sowie die Dauer des Sedimenttransports zu bestimmen. Ein ähnlicher zeitlicher Versatz von etwa 1.900 bis 2.600 Jahren zwischen Produktion und Ablagerung, gleichzeitig eingetragener Landpflanzenbiomarker und makroskopischer Pflanzenteile deutet auf gemeinsame Quellen des Materials hin. Die Erhaltung und Zwischenspeicherung der Organik an Land scheint durch klimatische Bedingungen gesteuert zu sein. Sedimentgestein bildet eine weitere Quelle, aus der organischer Kohlenstoff in die aquatischen Ablagerungsräume eingetragen werden kann. Dieses Material ist üblicherweise frei von ^{14}C , und wirkt sich somit stark auf die Radiokarbonalter der Gesamtorganik des Sediments aus. Um die Anteile organischen Kohlenstoffs aus unterschiedlichen Quellen in Oberflächensedimenten verschiedener aquatischer Ablagerungsräume, darunter ein See, eine Lagune, zwei Fjorde und eine off-shore Site, zu quantifizieren, wurden Massenbilanzen mit drei Endmembern (fossil, marin, terrestrisch (Pflanzen und Böden)) verwendet. Der räumliche Verteilung fossilen Kohlenstoffs deutet darauf hin, dass der Eintrag ^{14}C -freier Organik maßgeblich von der mechanischen Erosion des Gesteins durch Gletscher bestimmt wird. Durch den Einfluss von vorgealterter Organik aus verschiedenen Quellen an Land, können weder die Alter von Landpflanzenbiomarkern noch die der Gesamtorganik für die Erstellung eines Altersmodell für den Kern Co1305 ge-

nutzt werden. Die Ergebnisse der komponentenspezifischen Radiokarbondatierung weisen darauf hin, dass Biomarker die aus hauptsächlich marinen Quellen stammen ($n\text{-C}_{16}$ Fettsäuren und $n\text{-C}_{22}$ Alkohole) verlässliche Sedimentalter liefern können. Die von Land eingetragenen Anteile an $n\text{-C}_{16}$ Fettsäuren und $n\text{-C}_{22}$ Alkoholen im Sediment, scheinen von dem jeweiligen diagenetischen Verhalten der Biomarker abhängig zu sein. Mit zunehmender Tiefe im Kern verändert sich die anfängliche Zusammensetzung von $n\text{-C}_{16}$ Fettsäuren stärker, als die der $n\text{-C}_{22}$ Alkohole. Daher ist es von großem Vorteil die Altersinformationen beider Biomarker zu kombinieren um ein präzises Altersmodell für den marinen Ablagerungsraum zu entwickeln. Der marine Sedimentkern Co1305 hat ein Gesamtalter von ca. 10.000 Jahren und der Sediment-kern Co1308 aus dem See reicht ungefähr 7.500 Jahre zurück. Eine deutliche Veränderung der Umwelt scheint sich vor etwa 4.000 Jahren zugetragen zu haben, als sich die klimatischen Bedingungen nach einer Phase niedriger Temperaturen verbessert haben. In dem Einzugsgebiet der Sees scheint sich die Vegetation zu dieser Zeit stark verändert zu haben, womit viele sedimentologische und geochemische Veränderungen im Sedimentkern begründet werden können. Generell scheint es, dass in den Sedimenten des Sees ein Langzeittrend aufgezeichnet ist, der von sich kontinuierlich verbessernden klimatischen Bedingungen während des Holozäns zeugt, wobei die Sedimente des Lagunenkerns Hinweise auf eine größere Variabilität unterschiedlicher Umweltbedingungen liefert (z.B. Veränderung der Gletscheraktivität sowie der marinen und terrestrischen Produktivität). Durch die Kombination der umfassenden sedimentologischen und geochemischen Daten aus beiden Kernen ist es schließlich möglich sowohl Klimaänderung von regionalem Ausmaß zu identifizieren als auch spezifische lokale Prozesse, die den unterschiedlichen Charakteristika der jeweiligen Ablagerungsräume zuzuschreiben sind.

Acknowledgement

The realization of this thesis was possible by courtesy of the German Research Foundation (DFG), who funded this project within the priority program of Antarctic research (Schwerpunktprogramm SSP 1158 Antarktischforschung).

First and foremost, I would like to thank Sonja Berg for giving me the opportunity to participate in this project. I am very grateful for her supervision, her unequivocal support and for always having time and advice. Her patience and constructive problem solving abilities seemed to be inexhaustible.

I would like to thank Martin Melles and Janet Rethemeyer for reviewing this thesis and for joining the thesis committee. I owe many thanks to both for enabling my participation in drilling campaigns, in a research cruise on RV Meteor and in national and international conferences.

I would like to thank Stephe Kusch for the profound discussions concerning the interpretation and presentation of my data and for always having good advice and great ideas. I will never forget the great time we spent on Meteor.

I would like to thank Matthias Thienemann for being the best room mate ever. We had a lot of fun during cigarette breaks, ice cream breaks, coffee breaks, soft drink breaks, walks with Zora, and also in the office.

Another person who really enriched my time in Cologne was Janna Just. I am very grateful to Janna for many productive discussions we had on my data but in particular I want to thank her very much for always encouraging me when I had the impression that challenges were too huge to manage.

I would like to thank Thorsten Domann for his help in the lab and his contribution to this project by his BSc thesis.

I am grateful to Bianca Stapper, Stephan John, Wolf Dumann and Anja Wotte for their advice in the lab. Special thanks to Ulrike Patt and Lana John for the preparation of samples for radiocarbon analysis and to Doro Klinghardt and Nicole Mantke for measuring TOC and CNS and XRF.

I would like to thank all my other colleagues from the institute for the nice work atmosphere.

Contents

1	Introduction	1
1.1	Paleoclimatic Evolution of the Sub-Antarctic	2
1.1.1	Last Glacial Termination	2
1.1.2	Holocene Climatic Variability	4
1.2	Global Carbon Cycle	5
1.3	Objectives	8
2	Methodological Approaches	9
2.1	Radiocarbon Analysis	9
2.2	Compound-Specific Radiocarbon Analysis	12
2.3	Biomarker Analysis	13
3	Study Area	17
3.1	South Georgia	17
3.2	Cumberland Bay Area	18
4	Sources and Fates of Lipid Biomarkers	21
4.1	Introduction	21
4.2	Material and Methods	22
4.2.1	Sediment and Plant Samples	22
4.2.2	Grain Size Analysis	22
4.2.3	Elemental Analysis	22
4.2.4	Radiocarbon Analysis of Bulk Sediments and Macrofossils	23
4.2.5	Lipid Analysis	23
4.2.6	Gas Chromatography	25
4.2.7	Preparative Capillary Gas Chromatography	26
4.3	Results	31
4.3.1	Lithology	31
4.3.2	Radiocarbon Inventories of Biomarkers and of TOC	32
4.3.3	TOC, IRD and Biomarker Records of Co1305	36
4.3.4	Contemporary Plant Samples	37
4.4	Discussion	39

4.4.1	Diversity of Biomarker Sources on Land and in the Ocean	39
4.4.2	Processes Explaining Biomarker Distributions and ^{14}C Variability in the record Co1305	42
4.5	Interpretation	49
4.5.1	Evaluation of Depositional Processes in the Course of the Sedimenta- tion History of Little Jason Lagoon	49
4.5.2	Considerations for Sediment Chronologies	51
4.5.3	Considerations for Paleoenvironmental Reconstructions	53
4.6	Conclusion	54
5	Disentangling Lateral Age Distribution of Surface Sediments in different Aquatic Environments of South Georgia by Quantification of OC Sources	55
5.1	Introduction	55
5.2	Samples and Methods	57
5.2.1	Sediment Samples	57
5.2.2	High Performance Liquid Chromatography	57
5.2.3	Radiocarbon Analysis	58
5.2.4	Elemental Analysis	58
5.2.5	Determination of Distances between Sedimentary Sites and Major Supply Areas on Land	58
5.2.6	#Ringstetra Index	58
5.2.7	Three Endmember $\Delta^{14}\text{C}$ Mass Balances	59
5.3	Results	59
5.3.1	Lateral Distribution of TOC Concentrations and Radiocarbon Ages .	59
5.3.2	Lateral Distribution of Sedimentary Biomarkers	61
5.3.3	Proportions of Terrigenous, Aquatic and Ancient OC in Surface Sed- iments of Different Aquatic Environments	63
5.4	Discussion	67
5.4.1	Terrigenous OC	67
5.4.2	Aquatic OC	69
5.4.3	Ancient OC	70
5.4.4	OC Distributions in Fjords and Off-Shore	71
5.4.5	OC Distributions in the Costal Marine Inlet (LJL)	74
5.4.6	OC Distributions in the Lacustrine Environment (ALA)	75
5.5	Conclusion	76
6	Environmental History of South Georgia	79
6.1	Introduction	79
6.2	Material and Methods	80
6.2.1	Samples	80
6.2.2	Radiocarbon Analysis	80

6.2.3	Biomarker Analysis	81
6.2.4	Elemental Data	81
6.2.5	Carbon Preference Index	81
6.2.6	BIT Index	82
6.2.7	Tex ₈₆ ^L	82
6.2.8	MBT'/CBT	82
6.2.9	MSAT	83
6.3	Results and Discussion	83
6.3.1	Sediment Chronology - Co1308	84
6.3.2	Sediment Chronology - Co1305	86
6.3.3	Mean Residence Time of Organic Matter in Terrestrial Reservoirs	89
6.3.4	Biomarkers and Proxies - Co1308	90
6.3.5	Biomarkers and Proxies - Co1305	93
6.3.6	GDGT-derived Temperature Reconstructions - Co1305	96
6.3.7	GDGT-derived Temperature Reconstructions - Co1308	100
6.3.8	Evaluation of Temperature Reconstructions	101
6.4	Interpretation	103
6.4.1	Start of Sedimentation in LJL: > 15,200 - < 11,200 cal BP	103
6.4.2	Lacustrine Stage of LJL: < 11,200 - c. 7,300 cal BP	104
6.4.3	Mid-Holocene Hypsithermal: c. 7,500 (7,300) - 5,800 cal BP	105
6.4.4	"Neoglacial": c. 5,800 - c. 4,500 cal BP	107
6.4.5	Late Holocene Hypsithermal: c. 4,500 - c. 2,700 cal BP	108
6.4.6	Climate Deterioration : c. 2,700 - c. 800 cal BP	110
6.4.7	High Climatic Variability: c. 800 cal BP - Today	110
6.5	Conclusions	111
7	Summarizing Remarks and Perspectives	113

List of Figures

1.1	Carbon Cycle	7
2.1	Molecular Structures of GDGTs	15
3.1	Maps of the Study Area	18
3.2	View over Little Jason Lagoon and Allen Lake A	19
4.1	Biomarker Analysis: Extraction and Separation of Procedure	23
4.2	CSRA: Scheme of the Laboratory Procedure	29
4.3	Lithology of the Core Co1305	31
4.4	A: $\Delta^{14}\text{C}$ Values of Biomarkers and TOC of core Co1305. B: $\Delta^{14}\text{C}$ Offsets between Biomarkers and TOC in ‰	35
4.5	IRD, TOC and Biomarker Concentrations of the Record Co1305	37
4.6	Biomarker Inventories of Contemporary Plant Samples	38
4.7	Kelp, Tussock Grass and Moss in the Study Area	41
4.8	Preservation Conditions in the Sediments of Co1305	46
4.9	Correlation of $n\text{-C}_{16}$ and $n\text{-C}_{26}$ Fatty Acid Abundances in the Record Co1305	46
4.10	$\Delta^{14}\text{C}$ offsets between $n\text{-C}_{29}$ alkanes, $n\text{-C}_{22}$ Alcohols, $n\text{-C}_{26}$ Alcohols, $n\text{-C}_{26}$ Fatty Acids, TOC and $n\text{-C}_{16}$ fatty acids in ‰	48
4.11	Overview of $\Delta^{14}\text{C}$ Values of $n\text{-C}_{16}$ Fatty Acids, $n\text{-C}_{22}$ Alcohols and TOC, Preservation Conditions and IRD-derived Influences on Marine Reservoir Ef- fects in the Record Co1305	52
5.1	Location Maps of the Study Sites	60
5.2	Distribution of Surface Sediments Parameters	62
5.3	Ternary Mixing Diagrams: Aquatic, Terrigenous and Ancient OC in Surface Sediments	66
5.4	Concentrations of brGDGTs against HMW n -fatty acids for all Investigated Sites	67
5.5	Proportions of Aquatic, Terrigenous and Ancient OC in Surface Sediments of Fjord and Off-Shore Sites	71
5.6	Proportions of Aquatic, Terrigenous and Ancient OC in Surface Sediments of Little Jason Lagoon and Allen Lake A	75

6.1	Age Model of the Record Co1308	85
6.2	Age Model of the Record Co1305	86
6.3	Lithological Profile of the Core Co1308, Biomarker and Proxy Records against Sediment Age	90
6.4	Biomarker and Proxy Records of Co1305 against Sediment Age	94
6.5	GDGT-derived Temperature Reconstructions	98
6.6	Regional Overview of Climatic Reconstructions compared to Data of this Study	108
6.7	Biomarker and Proxy Records of Co1305 and Co1308 against Time	109

List of Tables

4.1	Biomarkers used for CSRA, Contaminations and C Yields	32
4.2	Radiocarbon Data of TOC and Biomarker, with Respective Corrections . . .	34
5.1	Locations and Properties of the Study Sites	60
5.2	Biomarker Concentrations and TOC Ages Of Surface Sediements	61
5.3	Input Parameters for Mass Balance Calculations and Resulting Proportions	64
6.1	Radiocarbon Data of the Record Co1308	84
6.2	Radiocarbon Data of the Record Co1305	87
6.3	Results of Temperature Reconstructions, BIT Indices and #Ringtetra Indices of the Record Co1305	99
6.4	Results of Temperature Reconstructions and #Ringtetra Indices of the Record Co1308	100
6.5	Basal Peat and Lake Sediment Radiocarbon Dates from South Georgia . . .	105

Chapter 1

Introduction

Past climatic and environmental changes are recorded in archives like aquatic sediments, tree rings, speleothems and ice cores. Physical and chemical properties of these archives provide evidences of the paleoenvironmental evolution in different resolutions and on different time scales. Marine and lacustrine sedimentary archives are particularly important for the reconstruction of paleoenvironmental conditions, since they can provide long and continuous records which often contain a multitude of high resolution information and since they are accessible in most parts of the world (Mollenhauer and Eglinton, 2007). However, sites of paleoenvironmental investigations are globally not evenly distributed. Whereas most evidences of climatic and environmental conditions of the Last Glacial Maximum (LGM) and of the Holocene were derived from marine and terrestrial archives from the Northern Hemisphere and from low latitude regions of the Southern Hemisphere, reconstructions from the high latitudes of the Southern Hemisphere are scarce (Xiao et al., 2016). Latter largely rely on Antarctic ice core records (Landais et al., 2015).

A substantial lack in high-resolution records is given for the the sub-Antarctic and particularly the Atlantic sector of the Southern Ocean. The scarcity of terrestrial records can be simply attributed to the very small land masses that exist in form of six island groups in the Southern Ocean. However, the marine sector of the sub-Antarctic is as well a major blank area of paleoenvironmental records. Missing chronological markers, few or badly preserved macroscopic remains that can be used for radiocarbon analysis, the insufficiently constrained marine reservoir age variability and the mixture of organic carbon from different sources complicates the development of accurate marine sediment chronologies in this region (Licht et al., 1998; Andrews et al., 1999; Domack et al., 2001; Ohkouchi, 2003; Rosenheim et al., 2008, 2013; Subt et al., 2016).

The need for more high-resolution records from the sub-Antarctic is, however, not only related to the aim of simply extending the global net of paleoenvironmental study sites. It seems that characteristic oceanic and atmospheric circulation patterns of this region play a particularly important role for the global climate dynamics. The Southern Ocean, as major component in the carbon cycle, is an important driving force of the global climatic evolution (Xiao et al., 2016). The Polar Frontal Zone (PFZ) surrounding the Antarctic landmass in

the Southern Ocean, currently at 48° - 61° S, divides the convergence region to the north from the divergence region to the south (Taylor et al., 1978). The PFZ seems to be a major climatic boundary between Antarctica and the temperate regions of the Southern Hemisphere and it possibly divides the response patterns to climatic forcings between Antarctica and the rest of the world (Bard et al., 1997; Broecker, 1998). Paleoenvironmental records from the sub-Antarctic are therefore of great interest to investigate climatic connections and to provide information on the role of the PFZ in the Earth's climate system.

South Georgia, one of the islands of the Atlantic sector of sub-Antarctic, is located south of the recent position of the PFZ ($54^{\circ}17'S$, $36^{\circ}30'W$). Depositional sites on land and at the coast of the island can provide high-resolution records of paleoenvironmental changes of this area. Compound-specific radiocarbon analysis (CSRA) of biomarkers has great potential to overcome the regionally common difficulties of radiocarbon dating (Ohkouchi, 2003). In order to determine eligible compounds that yield good estimates of the time of sediment formation, biomarker sources, redistribution processes and timescales of these processes need to be investigated. On the basis of accurate marine and lacustrine sediment chronologies, paleoenvironmental reconstructions can contribute to a refined understanding of regional environmental processes and the role of the sub-Antarctic for the global climatic evolution.

1.1 Paleoclimatic Evolution of the Sub-Antarctic

1.1.1 Last Glacial Termination

The Last Glacial Termination started around 20,000 years BP with the collapse of the very large Northern Hemisphere (NH) ice sheets that were build up during the Pleistocene. Fresh-water inflow into the Atlantic Ocean is assumed to have played a significant role for the following climatic changes (Marson et al., 2014).

In Antarctica, full glacial conditions persisted until c. 18,000 years BP. A first warming pulse is attributed to a weakened Atlantic Meridional Overturning Circulation (AMOC), which reduced the heat transfer from the south to the north. Increasing sea-surface temperatures (SST) in the Southern Ocean resulted and the latitudinal SST gradients facilitated the southward shift of the Southern Westerlies. Strengthening of these winds produced ocean upwelling and further warming in the Southern Ocean and Antarctica (Denton et al., 2010).

The propagation of oceanic and atmospheric changes (bipolar seesaw) led to alternating stadial and interstadial conditions, that were anti-phased between the NH and Antarctica. Melt water contributions from Antarctica and feedback effects due to an increasing atmospheric CO_2 level are assumed to have led to further decoupling of the hemispheres with the beginning of the initial warming (Bianchi and Gersonde, 2004). The asynchronous response to climatic forcings for the NH and Antarctica after the LGM is evidenced by ice core records (Blunier et al., 1998). For the tropical to temperate regions of the Southern

Hemisphere, paleoenvironmental records point to a climatic evolution in concert with the Northern Hemisphere (Bard et al., 1997).

The location of the sub-Antarctic island of South Georgia, south of the recent position of the PFZ, led to several studies that attempted to identify the timing and the coupling of climatic transitions in this area. The maximum extent of the ice cover during the LGM and the timing of subsequent deglaciation in phase or out of phase with Antarctic and NH glaciations are major concerns in these studies (Clapperton et al., 1989; Bentley et al., 2007; Rosqvist and Schuber, 2003; Hodgson et al., 2014).

For the reconstruction of the glaciation history of South Georgia, terrestrial (Sugden and Clapperton, 1977; Clapperton et al., 1989; Bentley et al., 2007) as well as submarine geomorphological evidences (Graham et al., 2008; Hodgson et al., 2014) have been studied. Radiocarbon and cosmogenic isotope dating of moraines was performed (Bentley et al., 2007) and basal ages of peat accumulation (Smith, 1981; Barrow, 1983; Gordon, 1987; Clapperton et al., 1989; Van der Putten et al., 2004; Van Der Putten and Verbruggen, 2005) and of lacustrine sedimentation (Rosqvist et al., 1999; Rosqvist and Schuber, 2003; Van Der Putten and Verbruggen, 2005) were determined.

Two conflicting LGM models have been inferred based on these studies: 1. a glaciation restricted to the inner fjords of the island or 2. an extensive shelf-wide glaciation.

Rosqvist et al. (1999) suggested that deglaciation started before 18.6 ka BP, based on the onset of lacustrine sedimentation in Block lake on Tønsberg Peninsula. Ice-free conditions at that time support the hypothesis of a restricted glaciation during the LGM, also favored by Bentley et al. (2007), based on geomorphological evidences. These studies suggest that South Georgia was responding similar to Antarctica and that the boundary between Antarctic and Northern Hemisphere ‘signals’ was located at or north of the Antarctic PFZ.

Thirty years before, the investigation of the submarine morphology led Sugden and Clapperton (1977) to the assessment that South Georgia was covered by ice up to the continental shelf break. Increasing evidence for the extensive glaciation is provided by recent studies, which are based on bathymetric investigations (Graham et al., 2008; Hodgson et al., 2014) in combination with marine sedimentary records (Graham et al., 2017) and modeling of relative sea levels (Barlow et al., 2016).

In contrast to the radiocarbon age evidence of the Block Lake record (18.6 ka BP), peat and lake sediment accumulation prior to 11.6 ka BP is absent in most records from South Georgia (Smith, 1981; Barrow, 1983; Gordon, 1987; Clapperton et al., 1989; Van der Putten et al., 2004; Van Der Putten and Verbruggen, 2005). The prominent gap between 18.6 ka BP and the start of the Holocene can possibly be attributed to glacier re-advances during the Antarctic cold reversal (ACR), which interrupted the warming trend after the LGM. Glacier re-advances are documented in fjords of the north-eastern shore of the island between c. 15,170 and 13,340 cal years BP (Graham et al., 2017). The authors of this study concluded that the LGM glaciation was extensive up to 19 ka BP but the sensitivity of the glaciers to climate variability during the last termination was more significant than previ-

ously implied. To explain the ice-free conditions prior to 18.6 ka BP on Tønsberg Peninsula, they proposed initial glacier retreat from an extensive extension during the LGM by 18 ka BP, at least to the fjord mouths. Rapid shelf deglaciation is supposed to be characterized by thinning of the ice-surface profile, in order to maintain fjord glaciers while leaving the present-day peninsulas deglaciated. In a regional context, they conclude that initial glacier retreat around South Georgia was slightly earlier than at more northern latitudes and was not forced atmospherically but by warming of the ocean or rising sea-levels. Meltwater pulses sourced from Antarctica are one plausible trigger for initiating landward ice-cap retreat. In contrast to the initial warming, the subsequent ACR appears to be remarkably in phase with evidences from Patagonian mountain glaciers, supporting the notion that the cooling was broadly synchronous across the southern mid-latitudes and the Southern Hemisphere glacial systems (Graham et al., 2017).

1.1.2 Holocene Climatic Variability

The Holocene, which started c. 11,000 yrs BP in the Southern Hemisphere with the establishment of the interglacial climate, is generally assumed to represent a relatively stable interglacial period (Nielsen et al., 2004). However, distinct periods of significant rapid climate change during the Holocene were identified (Mayewski et al., 2004).

At the beginning of the Holocene (11,000 - 9,500 yrs BP), the Southern Hemisphere high latitudes were characterized by warm conditions (Bentley et al., 2009). Most of the peat and lacustrine records from South Georgia start their formation at that time (Smith, 1981; Barrow, 1983; Gordon, 1987; Clapperton et al., 1989; Van der Putten et al., 2004; Van Der Putten and Verbruggen, 2005), documenting an important environmental transition at the beginning of the Holocene. Deglaciation of the coastal zones (< 50 m) of the island of South Georgia was mostly accomplished between c. 9,600 and 8,660 yrs BP (Smith, 1981; Clapperton et al., 1989; Van Der Putten and Verbruggen, 2005). Vegetation seems to have rapidly colonized these ice-free zones and peat growth, that started at the same time, contained nearly all plant species already soon after the deglaciation (Barrow, 1978; Smith, 1981; Björck et al., 1991; Rosqvist et al., 1999; Van Der Putten and Verbruggen, 2005).

A cooling trend, accompanied by the re-advance of sea-ice between 9,000 and 7,000 yrs BP, is documented in several records from the Atlantic sector of the Southern Ocean. The regional extend of this climatic event is assumed to be related to the reinforcement and northward expansion of the Weddell Gyre circulation (Bianchi and Gersonde, 2004). It seems that after this climate deterioration generally cool climatic conditions persisted in the sub-Antarctic until 4500 cal BP, including a warm phase between c. 7,000 to 6,000 yrs BP (Mayewski et al., 2004; Bentley et al., 2009; Strother et al., 2015). The transition from the mid to the late Holocene in the sub-Antarctic region is characterized by a warming trend that started around 4500 yrs cal BP (Bentley et al., 2009). After a period of probably alternating climatic conditions between 3,500 and 2,500 yrs BP (Mayewski et al., 2004), a

generally cooler phase started around 2,500 yrs BP and persisted until the present rapid, regionally variable, warming of the last decades (Bentley et al., 2009; Strother et al., 2015). Some major climatic transitions during the Holocene are apparently of a regional extent and can be traced in several paleoclimatic records from sub-Antarctic (and Antarctic) region. However, the supposed timings of these climatic transitions as well as the duration of distinct climatic phases differs between the investigated settings. The differences in the paleoclimatic records may be explained by locally variable environmental conditions. However, they can also reflect the limitation of a low resolution age control in many high-latitude paleoclimate records (Strother et al., 2015).

The quality of the radiocarbon chronology of each individual sedimentary record depends on the resolution of the data and the knowledge of the ^{14}C ages of carbon sources, incorporated in the dated material. Samples of a known origin, like planktic foraminifera, are generally assumed to give best approximations of the sediment formation ages (Pearson and Eglinton, 2000; Mollenhauer and Eglinton, 2007). However, for sedimentary records from the Southern Atlantic Ocean good chronological control is often complicated, since sediments are frequently lacking in macroscopic remains that can be attributed to a definite source (Andrews et al., 1999). Moreover chronological markers like ash layers from well-dated eruptions are mostly absent (Hall et al., 2010). When bulk sediments are analyzed, the samples can contain organic carbon (OC) with highly variable ^{14}C inventories. Surface sediments in the sub-Antarctic often exhibit old ^{14}C ages because of the admixture of ancient OC (Licht et al., 1996; Andrews et al., 1999; Ohkouchi, 2003).

Knowledge about carbon sources and processes associated to the carbon cycle is therefore very important for the interpretation of radiocarbon data and for the establishment of confident chronologies for sub-Antarctic marine sedimentary records.

1.2 Global Carbon Cycle

Carbon is a major component of living organisms as well as of their habitats. It is present in a multitude of carbon reservoirs on earth, like in the earths' crust, in oceans, in terrestrial and aquatic biospheres as well as in the atmosphere. Carbon can be present in form of inorganic compounds like CO_2 or CH_4 as well as in form of organic compounds like sugars and lipids (Bolin, 1970). Transformation of inorganic carbon into organic carbon (and vice versa) is often associated with exchange processes between different carbon reservoirs. Transformation and exchange processes together constitute the carbon cycle (fig. 1.1). Timescales of carbon transition between distinct reservoirs can be highly variable, ranging from instantaneous reactions to millions of years. To understand the factors that affect ^{14}C concentrations in specific environments, the relative sizes of and interactions between the reservoirs need to be considered (Bowman, 1990).

Carbon occurs in three isotopes: two stable isotopes (^{12}C and ^{13}C) and one radioactive isotope (^{14}C). The natural abundance of these isotopes in the atmosphere has a proportion of 98.9 to 1.1 to 1×10^{-10} (e.g. Wood, 2015). The cosmogenic nuclide ^{14}C is formed in the lower stratosphere by collision between a neutron deriving from cosmic radiation and ^{14}N , under the emission of a proton. The mean residence time for a molecule of CO_2 in the atmosphere before it is removed to another reservoir is about 3 years (Schlesinger et al., 1995).

Photosynthetic fixation of inorganic CO_2 and its subsequent reduction to organic compounds (autotrophic production of biomass) is a short-time process. Conversion of organic carbon into inorganic carbon and its release from the biosphere to the atmosphere by respiration of living organisms and the remineralization of dead organic material happens as well over short timescales.

The flux of carbon into the ocean is driven by sinking of dead phytoplankton, exporting carbon in its biomass to the deep ocean. Additionally, CO_2 enters the ocean because of the increasing concentration in the atmosphere (Schlesinger et al., 1995). The marine carbon reservoir is much larger than the atmospheric one. High residence times of ^{14}C in the ocean are a consequence of the limited exchange between these different sized reservoirs. The ocean surface water is therefore depleted in ^{14}C with respect to the atmosphere, since the decay of ^{14}C occurring in this marine reservoir can be quite severe. Concentrations of ^{14}C generally decrease with water depth but they also vary geographically. Dispersion depends on circulation patterns of the water masses e.g. upwelling and downwelling, vertical mixing of water masses or stratification and on exposure times of a water masses to the atmosphere. Exchange of CO_2 between ocean and atmosphere can be inhibited by ice-cover or can vary because of climatic changes or variable wind conditions (Gordon and Harkness, 1992; Smitenberg et al., 2004; Uchikawa et al., 2008).

The terrestrial carbon reservoir (organic carbon of the recent terrestrial biomass and soils) is 3–5 times greater than the carbon reservoir of the atmosphere (Tao et al., 2015). Over long timescales the terrestrial biosphere and the atmosphere exhibit equilibrium conditions because most carbon that is fixed in terrestrial biomass returns quickly to the atmosphere by respiration. Over shorter timescales the atmosphere is sensitive to imbalances with the other larger carbon reservoirs (Galy et al., 2015).

A long-term control of the global carbon cycle is the weathering of kerogen in shales (Hedges, 1992). Oxidation of petrogenic carbon during erosion, transport and postdepositional processes releases CO_2 to the atmosphere, a process that would not have happened directly because rock reservoirs and atmosphere are disconnected (Cui et al., 2017).

All reservoirs can be seen as sources or sinks for carbon. Exchange fluxes, synthesis of new substrates, diagenesis and decomposition are influencing carbon in its source region, on its pathway and in its sink regions (Blair and Aller, 2012). The export of carbon from terrestrial reservoirs to the ocean can involve several cycles of mobilization and retention, so that timescales between production of the organic matter and the final burial in the sediments can be very variable. Environmental factors as well as intrinsic reactivities of carbon com-

pounds control these carbon cycles and therefore the composition, concentration and ^{14}C activity of sedimentary organic matter. Climatic factors can influence the turnover time, with faster turnover of organic matter in tropical climates than in high latitude regions (Douglas et al., 2014). Properties of the watershed, topography and drainage systems (e.g. the efficiency of riverine export or the ice flux of glaciers) are as well important factors for the export of carbon from terrestrial reservoirs to the ocean.

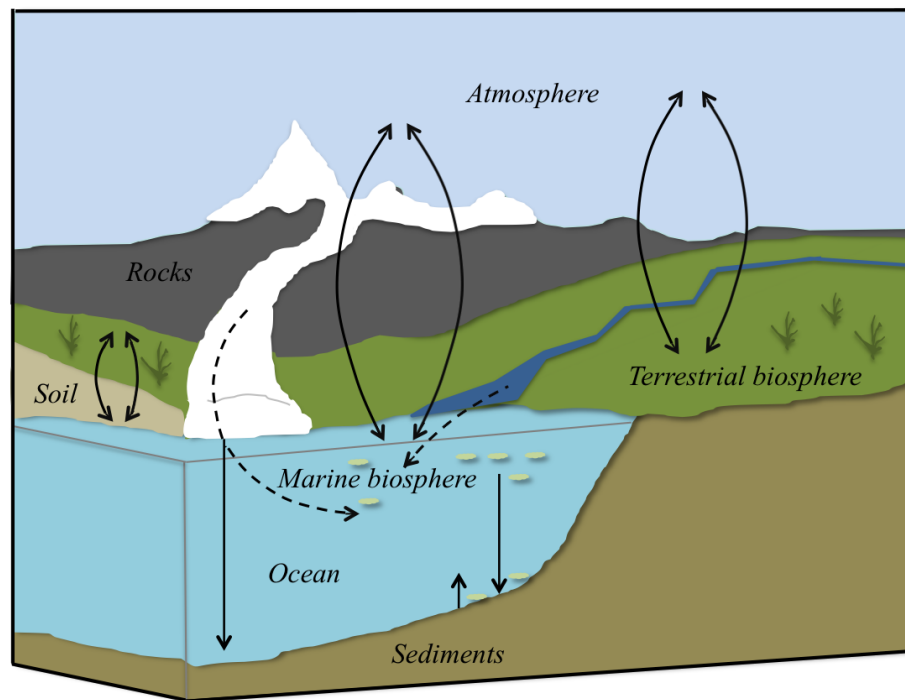


Figure 1.1: Schematic illustration of the carbon cycle. Solid arrows mark the exchange pathways of carbon between different reservoirs. Dashed arrows mark the transport pathways of carbon from land to the ocean.

1.3 Objectives

Sediments are mostly characterized by a heterogenous composition of organic matter from autochthonous and allochthonous sources. Sedimentological and diagenetic processes control the composition and the ^{14}C inventories of the sedimentary organic matter. Understanding these processes is of crucial importance for the interpretation of past environmental changes that are recorded in sedimentary archives. The establishment of reliable sediment chronologies is the most important prerequisite for paleoenvironmental investigations, but in sub-Antarctic environment often difficult to accomplish.

This thesis aims to improve the knowledge of depositional processes in lacustrine and coastal marine environments of South Georgia and to derive confident sediment chronologies for these archives.

Main objectives of this thesis are:

1. to disentangle sources of organic carbon in different aquatic environments of South Georgia,
2. to quantify contributions from these sources to surface sediments,
3. to investigate the effects of source composition and biogeochemical as well as depositional processes on radiocarbon inventories of individual biomarkers,
4. to develop confident sediment chronologies based on compound-specific radiocarbon data of biomarkers,
5. to obtain information about paleoenvironmental and -climatological changes in the study area during the Holocene.

Chapter 2

Methodological Approaches

2.1 Radiocarbon Analysis

^{14}C is a radioactive isotope and therefore characterized by its decay. Exchange of carbon between living organisms and the atmosphere ends when at the time when the organism dies. From this time on, ^{14}C which is contained in the biomass of the respective organism, starts to decay with a half life time of 5,730 years. Radiocarbon (^{14}C) can be used for the determination of the age of carbon-containing materials. The remaining ^{14}C concentration of a sample can be measured and compared to the ^{14}C concentration at the time when decay started. Radiocarbon dating is an important method for the investigation of sedimentary records that formed in the last 50,000 years (Ingalls and Pearson, 2005).

Walter Libby established a method for the detection of radioactive decay of ^{14}C (Libby et al., 1949). The decay was directly measured by counting of emitted β -particles. In 1977, this highly time intensive procedure was replaced by the direct measurement of ^{14}C contents of a sample using accelerator mass spectrometry (AMS) (Muller, 1977). The AMS technology not only allowed to reduce the measuring time significantly but also the sample size by three orders of magnitude to $< 1\text{mg}$ (Ingalls and Pearson, 2005).

Radioactive decay is not predictable for single ^{14}C atoms. It happens randomly regardless of the time an atom has existed. Considering a quantity of ^{14}C atoms the decay follows an exponential decay rate.

$$dN/dt = -\lambda N, \tag{2.1}$$

where N is the number of atoms and λ is the decay constant.

The average time that an atom remains stable is called mean life time, τ and is 8033 years (Stuiver and Polach, 1977).

The exponential decay can also be characterized by the half-life $t_{1/2}$, the time when half of the initial atoms are decayed that is 5730 years:

$$t_{1/2} = \ln(2)/\lambda = \tau \ln(2). \quad (2.2)$$

Reporting Radiocarbon Data Radiocarbon data are reported as fraction modern carbon (fMC), representing the $^{14}\text{C}/^{12}\text{C}$ ratio of the sample relative to the $^{14}\text{C}/^{12}\text{C}$ ratio of a reference standard:

$$fMC = \frac{{}^{14}\text{C}/{}^{12}\text{C}_{\text{sample}}}{{}^{14}\text{C}/{}^{12}\text{C}_{\text{standard}}}. \quad (2.3)$$

The $^{14}\text{C}/^{12}\text{C}$ ratios of both sample and the "modern" international standard need to be corrected for carbon isotopic fractionation.

The $^{14}\text{C}/^{12}\text{C}$ ratio of the modern standard is defined as 95% of the radiocarbon concentration of NBS Oxalic Acid I in AD 1950 normalized to $\delta^{13}\text{C}$ VPDB of -19 ‰ (with respect to Pee Dee Belemnite). 1950 is the year to which all radiocarbon ages are referred, termed present (Stuiver and Polach, 1977).

$${}^{14}\text{C}/{}^{12}\text{C}_{\text{standard},\delta^{13}\text{C}} = 0.95 * {}^{14}\text{C}/{}^{12}\text{C}_{\text{standard}} * \frac{(1 - 19/1000)^2}{(\delta^{13}\text{C}/1000)}. \quad (2.4)$$

The $^{14}\text{C}/^{12}\text{C}$ ratio of a sample is affected by isotopic fractionation in nature, which happens at different rates for different organisms or in different regions. In order to ensure that samples from different environments can be compared, the reported $^{14}\text{C}/^{12}\text{C}$ ratio of a sample is normalized to a $\delta^{13}\text{C}$ value of -25‰ VPDB (Stuiver and Polach, 1977).

$${}^{14}\text{C}/{}^{12}\text{C}_{\text{sample},\delta^{13}\text{C}} = 0.95 * {}^{14}\text{C}/{}^{12}\text{C}_{\text{sample}} * \frac{(1 - 25/1000)^2}{(\delta^{13}\text{C}/1000)}. \quad (2.5)$$

The reported fMC is further corrected for processing blanks as well as for statistical uncertainty of the AMS measurement.

Radiocarbon data can also be reported in $\Delta^{14}\text{C}$ notation. The $\Delta^{14}\text{C}$ value corrects the fMC value for the decay that happened between collection and measurement of a sample so that repeated measurements of the same sample performed in different years obtain the same results.

$$\Delta^{14}C = (fMC/e^{\lambda(y-1950)} - 1) * 1000\text{‰}, \quad (2.6)$$

where y is the year of collection and λ is $1/8267 \text{ yr}^{-1}$ (8267 yrs being the mean life time of ^{14}C according to its half life time of 5,730 years).

fMC values can be converted to conventional radiocarbon ages, when assuming that atmospheric ^{14}C concentration is constant over time:

$$^{14}\text{C Age} = -8033 * \ln(fMC). \quad (2.7)$$

Conventional radiocarbon ages can be reported in years BP, referred to 1950, which equals 0 years BP. Conventional radiocarbon ages cannot be determined for younger samples. Samples originating after 1950 are termed $>$ modern (Stuiver and Polach, 1977).

Calibration of Radiocarbon Data Direct conversion of conventional radiocarbon ages into calendar years is not possible, because atmospheric ^{14}C concentrations are not constant over time. Reasons for the atmospheric ^{14}C variability are changes in the cosmic radiation, which influences the production of ^{14}C in the atmosphere, as well as variable exchange rates between the atmosphere and other carbon reservoirs (Suess, 1986; Bard et al., 1998). In addition to the natural variability, human activities like burning of fossil fuel or nuclear weapon testing led to significant changes in the atmospheric ^{14}C concentrations. Since industrialization, burning of fossil carbon sources (which are free of ^{14}C) caused a high release of $^{12}\text{CO}_2$ to the atmosphere, diluting the atmospheric ^{14}C concentration (suess-effect) (Suess, 1955). In contrast, nuclear weapon testing caused atmospheric ^{14}C concentrations to almost double in the 1960s. Uptake of atmospheric CO_2 by biospheres and hydrospheres reduced the concentration of atmospheric ^{14}C to almost pre-bomb values in recent times (Turnbull et al., 2017). Due to these natural and anthropogenic impacts on the variability of the atmospheric ^{14}C concentration, conventional radiocarbon ages have to be compared with independently derived ages to yield calendar ages (Bard et al., 1990; Reimer et al., 2004; Hogg et al., 2016). Age information derived from e.g. dendrochronologically dated tree rings, uranium-thorium dated corals or varve-counted lake sediments is included in international calibration data sets such as IntCal13, Marine13 or SHcal13 (Reimer et al., 2013). This data can be accessed using calibration programs, to determine the probability distribution of the samples true age, in confidence intervals of 68% (1sigma) or 95% (2sigma), reported as calibrated ages.

For the calibration of conventional radiocarbon ages of marine samples, marine reservoir effects have to be considered. Other than terrigenous primary production, using CO_2 from the atmosphere, marine organisms consume dissolved inorganic carbon (DIC) from ambient water of the ocean and therefore incorporate the ^{14}C signature of the oceans' DIC in their tissue (Stuiver and Polach, 1977). The difference between ^{14}C concentrations of the atmo-

sphere and the DIC of the surface ocean waters, translates into a globally averaged marine reservoir age of c. 400 years (Hughen et al., 2004). This global marine reservoir effect (R) is included in the Marine13 calibration curve (Reimer et al., 2013), which is based on a model of Stuiver and Pearson (1993). The local deviation from R is defined as the regional marine reservoir effect, ΔR (Stuiver et al., 1986).

In sub-Antarctic marine environments up-welling of ^{14}C -depleted deep and intermediate water masses, old ^{14}C from melting glacier ice and seasonally persisting sea ice cover that is preventing exchange with the atmosphere result in marine reservoir ages of 700 to 1300 yrs. This difference has to be accounted when conventional radiocarbon ages of marine samples are converted to calibrated calendar ages (Bard, 1988; Southon et al., 1990; Gordon and Harkness, 1992; Stuiver and Pearson, 1993; Eglinton et al., 1997; Berkman and Forman, 1996; Hall et al., 2010; Ohkouchi and Eglinton, 2008).

Dating of known-age marine samples like shells or marine mammal bones (e.g. Gordon and Harkness, 1992) from the same locality is one possibility to derive information on the local deviation from R. However, to establish chronologies for marine records, it is important to consider that temporal variability of ΔR can have an impact on the accuracy of age determinations (e.g. Sarnthein et al., 2015; Wündsche et al., 2016). Past surface water reservoir ages can be derived from ^{14}C records of planktic foraminifera by comparison with past atmospheric ^{14}C values. But without knowing the explicit time of deposition, absolute changes in reservoir ages cannot be determined. Another rare but valuable opportunity to study marine reservoir ages is the application of reservoir age independent dating techniques like uranium-thorium dating of deep water corals e.g. in the Drake Passage (Burke and Robinson, 2012) or the Ross sea (Hall et al., 2010) or ^{226}Ra dating of barite in the deep open Southern Atlantic Ocean (53°S, 4°W) (Van Beek et al., 2002). However, despite all the elaborated methods it remains very hard to determine absolute reservoir age variability of the Southern Ocean. Therefore, in many studies constant ΔR value are applied for the reservoir correction of the whole records (Wündsche et al., 2016).

2.2 Compound-Specific Radiocarbon Analysis

Most samples used for radiocarbon dating are total organic carbon (TOC) samples, which contain a mixture of organic materials from unknown sources and with unknown relative contributions. Radiocarbon ages of such TOC samples are complicated to interpret, so that their application for chronological purposes is often precluded. The problems associated to the mixing of carbon sources can be circumvented by compound-specific radiocarbon analysis (CSRA) of biomarkers of known origin (Eglinton et al., 1997; Pearson et al., 2001; Smittenberg et al., 2004; Mollenhauer and Rethemeyer, 2009).

In settings where sediment chronologies are hard to establish, like Antarctic and sub-Antarctic marine environments, CSRA is a particularly valuable tool (Ohkouchi, 2003; Ohk-

ouchi and Eglinton, 2008; Yamane et al., 2014).

Additional to chronological applications, CSRA can also be used to yield information on the origin and refractivity of organic matter in sediments. It can provide an enhanced understanding of biogeochemical and sedimentological processes that are affecting sedimentary biomarker records. The fate of organic carbon, in terms of transport pathways, residence times in intermediate reservoirs and burial in aquatic sediments can be traced (Eglinton et al., 1996, 1997; Pearson and Eglinton, 2000; Pearson et al., 2001; Uchida et al., 2001; Rethemeyer et al., 2004; Mollenhauer et al., 2005; Ziolkowski and Druffel, 2009).

Radiocarbon dating on a molecular level is enabled by high-precision AMS systems combined with preparative capillary gas chromatography (PCGC). PCGC allows the isolation of target compounds from complex heterogenous samples in sufficient quantities and high purity (Eglinton et al., 1996, 1997).

The small sample size requirement for CSRA is the greatest advantage of this method (Uchikawa et al., 2008). However, the potential of CSRA is constrained by the purity to which target material can be isolated by PCGC and by the capability of AMS systems to measure very small samples (Ingalls and Pearson, 2005). CSRA is theoretically possible for samples as small as 10 μg . CSRA involves a multiple step purification procedure for the collection of a single compound of high purity (Ziolkowski and Druffel, 2009). Each step of the sample treatment procedure can add small amounts of carbon from unknown sources and with unknown isotopic composition to the sample. With decreasing sample size, the uncertainty due to blank contamination increases (Rethemeyer et al., 2004). Correction for contamination with modern and fossil carbon can be assessed by isotopic mass balance corrections, using fossil and modern standards, respectively, that were processed with the same techniques as the samples. The procedural blank of ultra-small samples can place a practical limit to the accuracy of CSRA (Mollenhauer and Rethemeyer, 2009).

2.3 Biomarker Analysis

Biomarkers are molecular (chemical) fossils that can be found in recent environmental samples and in geological archives (Eglinton and Calvin, 1967). They have chemical structures which can be assigned to certain precursor organisms (Simoneit, 2004). Biomarkers developed into an important tool for paleoenvironmental studies. Particularly in sedimentary archives in which macro remains or pollen have a low resolution or are badly preserved, biomarkers can provide information on the origin of the organic matter, the depositional setting and the carbon cycle (Diefendorf and Freimuth, 2016). To derive information of present to past time changes, these compounds need to be sufficiently refractory so that they are preserved in the investigated sedimentary archives (Eglinton et al., 1997).

Biomarkers investigated in this study comprise *n*-alkanes, *n*-alcohols and *n*-fatty acids as well as glycerol dialkyl glycerol tetraethers (GDGTs).

***n*-Alkyl Compounds:** Long-chain odd-numbered *n*-alkanes ($>C_{27}$) and long-chain even-numbered *n*-fatty acids ($>C_{26}$) and *n*-alcohols ($>C_{26}$) are major components of epicuticular waxes from vascular plant leaves (Eglinton and Hamilton, 1967). *n*-Alkanes are highly resistant to diagenetic alteration (Cranwell, 1981) and can therefore be used to trace the pathway of terrigenous organic matter and to reconstruct paleoenvironmental changes (Ishiwatari et al., 1994; Pearson and Eglinton, 2000; Uchikawa et al., 2008). *n*-Fatty acids are more sensitive to degradation, so that they can be influenced by early diagenetic processes (Bol et al., 1996). In marine environments, *n*-fatty acids with chain-lengths of C_{14} to C_{18} are primarily produced by phytoplankton in the surface water but they are ubiquitous in all organisms (Volkman et al., 1980).

Glycerol Dialkyl Glycerol Tetraether (GDGT): Glycerol dialkyl glycerol tetraethers (GDGTs) are membrane lipids that are synthesized by archaea and bacteria which occur ubiquitously in environments like oceans, lakes, soils and peats worldwide. Despite the great variety of sources, the origin of several GDGTs has been identified unambiguously, so that these GDGTs can be used as lipid biomarkers in paleoenvironmental studies (Schouten et al., 2013). Basically, they can be subdivided into two distinct classes: isoprenoid GDGTs (isoGDGT) and branched GDGTs (brGDGTs) (Naeher et al., 2014).

Isoprenoid GDGTs are membrane lipids that are produced by archaea (Schouten et al., 2000). In marine environments isoGDGTs always contain crenarchaeol, a specific isoprenoid membrane lipid that is derived from archaea of the phylum *Thaumarchaeota*, formerly known as *Crenarchaeota* (Schouten et al., 2013). A unique characteristic of crenarchaeol is a cyclohexane moiety that could not be encountered in any other isoGDGT (Damsté et al., 2002). Despite of low abundances in peat and soils (Weijers et al., 2006), crenarchaeol has been found to occur predominantly in marine environments (Hopmans et al., 2004) and can therefore be used to characterize marine paleo-productivity.

Branched GDGTs were first discovered in peat bogs (Schouten et al., 2000). The origin of these membrane lipids is yet not completely understood, but to the current knowledge a group of anaerobic soil bacteria (Acidobacteria) produce this kind of membrane lipids (Weijers et al., 2007). In contrast to archaeal GDGTs, bacterial GDGTs are characterized by carbon skeletons that are not isoprenoid but comprise branched carbon chains (Peterse et al., 2009). These branched GDGTs have 4 to 6 methyl groups and 0 to 2 cyclopentyl moieties that are attached to their *n*-alkyl chains (Weijers et al., 2007).

Fig. 2.1 gives an overview of the molecular structures of the GDGTs that are investigated in this study.

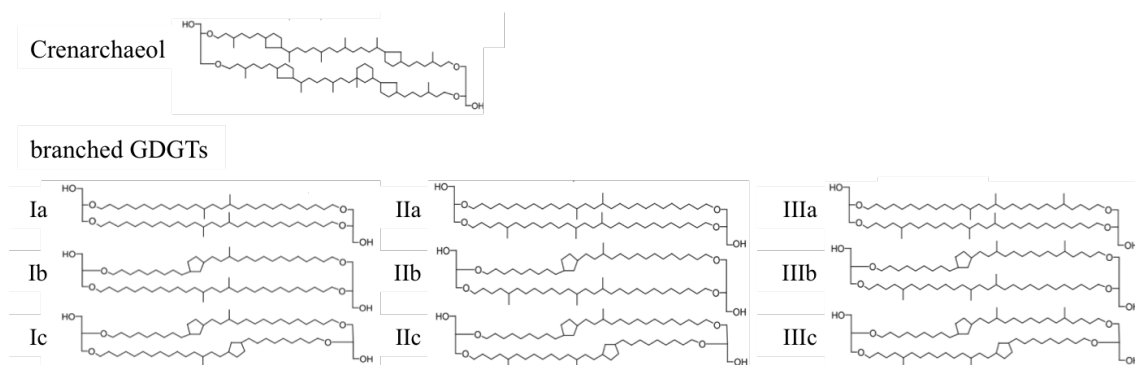


Figure 2.1: Molecular Structures of GDGTs investigated in this study

Chapter 3

Study Area

3.1 South Georgia

South Georgia (54°S, 36°W) is located on the North Scotia Ridge, which forms the eastward extending tectonic arc between Antarctica and America. The island probably maintained its position on the Scotia plate relative to the South American plate since the late Miocene and is probably still uplifting, because of the convergence of the South American and Scotia plates (Graham et al., 2008). The island has a narrow and long extension (35 km wide and 190 km long) and a high altitudinal gradient. The steep mountainous terrain rises up to 2934 m. A 30 -100 km wide continental shelf extends offshore from the coast (Fretwell et al., 2009). Glacial advances during the Pleistocene have carved deep fjords, particularly into the northern coast of the island. Today, glaciers are covering about 58 % of South Georgia (Clapperton et al., 1989), commencing at the high, axial, NNW-SSE crossing mountain ridge of Allardyce Range and mostly terminating as tidewater glaciers at the sea (Gordon et al., 2008). Suites of moraines document former glaciations, particularly along the north-east coast (Bentley et al., 2007). Radial, deep cross-shelf troughs are a prominent feature on the seafloor around South Georgia. They have a strong sense of drainage to the north of the island. Glacier mass balance exhibits a strong north-south gradient over the island (Graham et al., 2008). The highly sensitive maritime glaciological regime of South Georgia experiences strong glacier fluctuation, with significant retreat recorded in 90% of its glaciers over the past \sim 60 years (Graham et al., 2017).

The island of South Georgia is located close to the global climate boundaries in the Southern Ocean, south of the PFZ and north of the average Antarctic sea-ice limit (Gordon et al., 2008). Climatic conditions are determined by the influence of the PFZ and the Westerlies, which lead to a cold and wet regime (Van der Putten et al., 2009). The mean annual air temperature is 2.5°C and the ocean is mostly ice-free. Mean precipitation amounts of about 1600 mm per year are recorded at King Edward Point (Clapperton et al., 1989). However, orographic controls lead to a local temperature variability. The Allardyce Ranges are sheltering the north-east coast from prevailing south-westerly winds, leading to Föhn conditions with temperatures rising up to 20°C on the leeward north-east coast (Gordon et al., 2008).

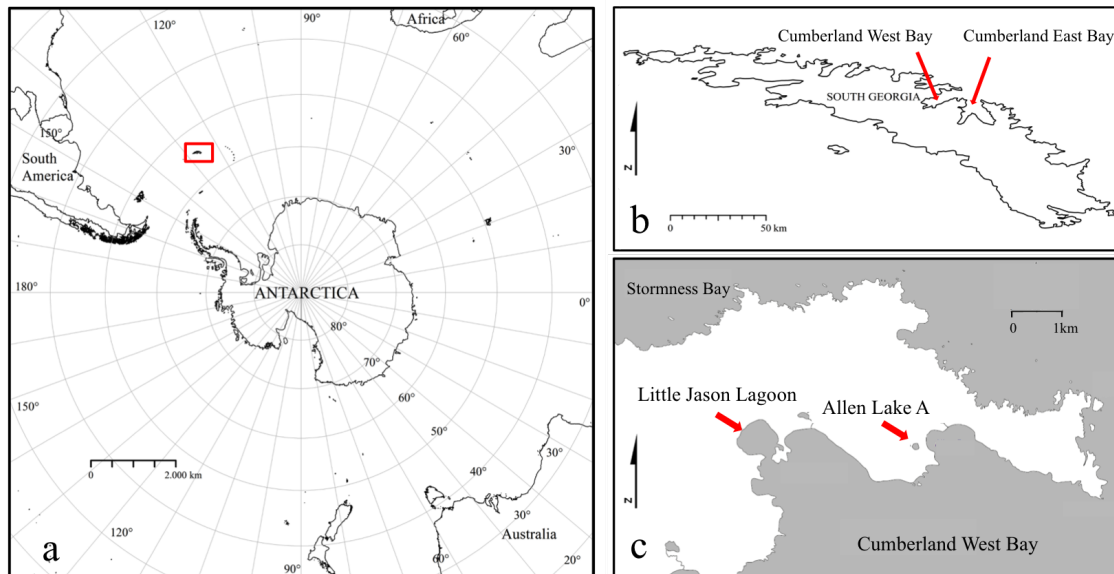


Figure 3.1: Maps of the study area. a: Location of the island of South Georgia in the Southern Ocean, b: Map of South Georgia with Cumberland West and East Bays, c: Lewin Peninsula to the north of Cumberland West Bay with study sites Little Jason Lagoon and Allen Lake A.

In the coastal lowlands, Tussock grass is the climax vegetation and the most widespread and productive community (Leader-Williams et al., 1987). In the north-eastern part of the island it extends from sea-level to about 110 m on north-facing slopes, and to about 70 m on south-facing slopes. Towards higher altitudes, this community is replaced by bryophyte assemblages and lichen. Extensive peat formation is favored by high annual precipitation and cold temperatures (Van der Putten et al., 2009).

The complex water-mass circulation pattern around South Georgia is influenced by the latitudinal variation of the PFZ and the intensity of the Southern Westerly Wind belt (Graham et al., 2017). Sea-surface temperatures exhibit strong north-south gradients on either side of the island and Antarctic sea-ice limits fluctuate between the southern and northern extents of the island (Bentley et al., 2007). Oceanographic conditions around South Georgia lead to large phytoplankton blooms, which are particularly intense on the northern shelf area with peak concentrations in austral summer (Borrione and Schlitzer, 2013).

3.2 Cumberland Bay Area

The investigated sites of this study are located at the north-eastern shore of South Georgia on the Lewin peninsula, to the north of Cumberland Bay (fig: 3.1). The geological setting of this area is characterized by shales and greywackes of the Cumberland series that crop out in the western part of South Georgia (Gregory, 1915) and absence of calcite (Skidmore,

1972). The Cumberland Bay is the largest of the bays on the island and is divided into the Cumberland West Bay and the Cumberland East Bay (Geprägs et al., 2016), both approximately 18 km long. The bays are U-shaped fjord basins which are encompassed by sparsely vegetated, steep slopes. At the heads of the fjords, tidewater glaciers are calving into the sea (Gordon et al., 2008).

Cumberland East Bay has a shallow inner basin (up to 190 m deep) that is divided from the deep outer basin (up to 270 m deep) by a moraine. The outer basin in turn is bounded by an outer moraine (Hodgson et al., 2014). The Nordenskjöld Glacier, one of the largest glaciers of South Georgia, is calving into the main fjord of Cumberland East Bay (Gordon et al., 2008). Two tributary fjords, the Moraine Fjord and King Edward Cove, enter the main fjord. The Hamberg Glacier and Harker Glacier terminate in the Moraine Fjord, whereas King Edward Cove is not glacierized (Hodgson et al., 2014). The Nordenskjöld glaciers show signs of retreat but the fluctuation is small, the Harker Glacier is the only advancing glacier of the north-east coast and the Hamberg Glacier shows fast retreat in recent times (Gordon et al., 2008). Both basins are sediment-filled, as being typical for high-latitude fjords, in which sediment accumulation rates are exceptionally high (Graham et al., 2017).

Cumberland West Bay is up to 265 m deep. Several submerged promontories are indicating truncated moraines but no inner basin is present like in Cumberland East Bay (Hodgson et al., 2014). The Neumayer Glacier is discharging into Cumberland West Bay. The glacier has retreated significantly in recent times (Gordon et al., 2008). The main fjord of Cumberland West Bay has also two tributary fjords, Harpon Bay and Mercer Bay, which are both partially enclosed by moraines (Gordon et al., 2008). The Lyell Glacier discharging in Harpon Bay has changed little in recent times, whereas the Geikie Glacier discharging



Figure 3.2: a: View over Little Jason Lagoon, b: view over Allen Lake A.

in Mercer Bay as well as the the Neumayer Glacier retreated significantly (Gordon et al., 2008).

On the south-eastern shore of Lewin Peninsula, the western boundary of Cumberland West Bay, a marine inlet, named Little Jason Lagoon, is shaping the coastline (fig: 3.2a). The inlet is connected with the ocean by a shallow sill (~ 1 m). Maximum depth of Little Jason Lagoon is 24 m. The shore of the inlet is vegetated and steep, rocky mountain slopes encounter the inlet on the backside.

Allen Lake A (fig: 3.2b) is a small and shallow (1.1 m deep) lake on Lewin Peninsula. It is located 24 m a.s.l. and has a richly vegetated catchment (Melles et al., 2013).

Chapter 4

Sources and Fates of Lipid Biomarkers

4.1 Introduction

Lipid biomarkers are derived from a multitude of aquatic and terrigenous source organisms and are supplied via different pathways to sedimentary sites. Several factors, including intrinsic reactivities of individual compounds as well as environmental conditions, determine the composition of biomarkers in the sediments. However, initial concentrations, proportions and radiocarbon inventories of sedimentary biomarkers can change over time, due to post-depositional processes (Mollenhauer and Eglinton, 2007).

In order to facilitate conclusive interpretations of biomarker records, it is therefore necessary to identify biomarker sources as well as biogeochemical and sedimentological processes. Compound-specific radiocarbon analysis (CSRA) is a powerful tool to this end, since effects of selective preservation, variable transport mechanisms, intermediate storage and mixing of biomarkers are expressed in the radiocarbon signatures of the respective compounds (Mollenhauer and Rethemeyer, 2009).

Distributions and radiocarbon inventories of high molecular weight (HMW) *n*-alkanes, of *n*-C₂₂ and *n*-C₂₆ alcohols and of *n*-C₁₆ and *n*-C₂₆ fatty acids of the sedimentary record Co1305 of Little Jason Lagoon are investigated in this chapter, in order to derive information on biomarker origins as well as on pre- and post-depositional processes in the setting of Little Jason Lagoon. Since CSRA can also be used as alternative dating option, the evaluation of specific characteristics of co-occurring biomarkers additionally holds the opportunity to identify compounds that have great potential to yield reliable age estimates of sediment formation in the investigated coastal marine setting.

4.2 Material and Methods

4.2.1 Sediment and Plant Samples

During the cruise ANT-XXIX/4 of RV Polarstern in March-April 2013, sediment cores were recovered within the marine inlet of Little Jason Lagoon (LJL). Drilling was performed from a floating platform, using gravity corer (GC) for the uppermost sediments and percussion piston corer (PC) for the sediments down to the base of the embayment (Bohrmann, 2013). At site Co1305, 18 coresections with maximum length of 3 m per section, were recovered. Coring was performed with minimum 1 m overlap, to facilitate correlation of the sediment sections. To prevent fast decomposition of the organic material in the sediments, the cores were stored at 4°C prior to processing. Correlation of sediment sections was performed by Sonja Berg, University of Cologne, based on core descriptions, water content and XRF data and resulted in a composite record of 11.04 m length. Subsampling was performed on half cores of the sedimentary sequences, comprised in the composite record. For biomarker analyses, subsamples of 5 cm were taken in a resolution of approximately 50 cm down to a composite depth of 9.7 m. Between 9.7 m and the base of the composite core, subsamples of 3 cm were taken, approximately every 25 cm. The subsamples for biomarker analyses were recovered just from the inner part of the cores to avoid contamination resulting from the interaction of the sediments with the liner and to exclude vertical relocation of the material due to the coring process. After subsampling for biomarker analysis, the remaining sediments were continuously subsampled into 2 cm slices.

Plant samples, including tussock grass, unspecified mosses and kelp, were collected in the catchment of LJL during the expedition. Like the sediment cores, plant samples were stored at 4°C, prior to processing. In the lab, they were cut into pieces with solvent-cleaned scissors and soil adhered to the plant samples was mechanically removed.

All samples (sediments and plants) were freeze-dried and sediment samples were subsequently homogenized using a mortar and pestle.

4.2.2 Grain Size Analysis

Grain sizes analysis was conducted by Sonja Berg, University of Cologne. Sediment samples (6-25 g) were wet sieved on a 1mm steel mesh sieve. Grains > 1 mm were counted and normalized to the dry weight (DW) of the sediment (Berg et al., 2019)

4.2.3 Elemental Analysis

Total carbon (TC) and total inorganic carbon (TIC) contents were measured on ground aliquots of 80 sediment subsamples, using a DIMATOC 2000 carbon analyzer (Dimatec Corp., Germany). Total organic carbon (TOC) was calculated from the difference of the measured TC and TIC contents.

4.2.4 Radiocarbon Analysis of Bulk Sediments and Macrofossils

For radiocarbon analysis, aliquots of sediment samples were checked under a microscope and potential contaminants were removed. Subsequently, inorganic carbon was removed from the samples by extraction with 1% HCl. Reaction time with HCl lasted for 1 hour at 60°C and then over night at room temperature. Afterwards, samples were washed with demineralized water to pH > 5. Samples were dried at 60°C and were then converted to graphite with H₂ over iron as catalyst (Rethemeyer et al., 2013). Combustion and graphitization was carried out with an Automated Graphitisation Equipment (AGE), interfaced to an elemental analyzer (VarioMicroCube, Elementar, Germany) (Wacker et al., 2010). AMS measurements were carried out at the CologneAMS facility (Dewald et al., 2013). ¹⁴C concentrations were reported as fraction modern carbon (fMC), $\Delta^{14}\text{C}$ (‰) and conventional ¹⁴C ages according to (Stuiver and Polach, 1977).

4.2.5 Lipid Analysis

The extraction procedure is illustrated schematically in fig. 4.1.

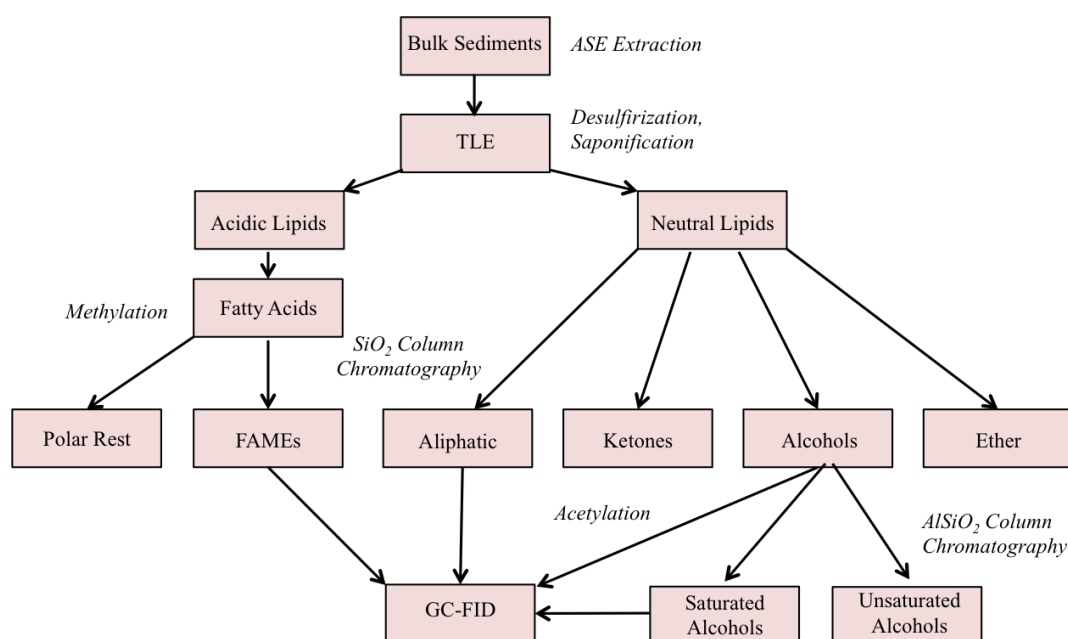


Figure 4.1: Scheme of the extraction and separation steps for lipid biomarkers analysis, in direction of the arrows: Extraction of total lipids (TLE) with ASE extraction, desulfurization and saponification of the samples, separation of neutral and acidic lipids, methylation of acidic lipids, separation of neutral lipid fraction and fatty acid fraction into polarity fractions by silica gel column chromatography, acetylation of alcohol fraction, GC-FID measurements of FAME, aliphatic and alcohol fractions, separation of alcohol fraction into saturated and unsaturated alcohols by silica gel and silver nitrate column chromatography.

Extraction of Total Lipids: Solvent extractable lipids were released from freeze-dried and homogenized sediment samples (10.7-27.3 g) and plant samples (1-5.4 g) by accelerated

solvent extraction (Dionex ASE 300, Thermo) with dichloromethane:methanol (9:1,v:v) at 120 °C and 75 bar for one cycle and with a heating time of 6 min and a static time of 20 min.

The total lipid extract (TLE) of sediment samples can contain elemental sulfur, which is a product of diagenesis. When measuring a sample, the sulfur peak can mask other compounds and can also damage the measuring device. To remove the obstructive sulfur from the sample, the TLE of each sediment sample was desulfurized using activated copper. The TLE solution was then concentrated by rotary evaporation under near vacuum and was subsequently transferred into 8 ml vials. The remaining solvent was removed under N₂, so that only the dry TLE remained in the vial.

Separation of Neutral and Acid Fractions: Fatty acids in the TLE are often bound in complex molecules, which cannot be measured easily. To break the ester bonds of these molecules and therefore to enhance the recovery of fatty acids, the TLE of sediment and plant samples was saponified with 0.5 M KOH in methanol:water (9:1,v:v) at 80°C for 2 h. The air in the vial was replaced by N₂ before the vial was closed. After reaction, the saponified TLE was dried under N₂. The saponification additionally facilitates the separation of fatty acids from neutral lipids, since fatty acids are then present as soaps and as such they are more soluble in water than in organic solvents.

For the separation of neutral lipids and fatty acids, demineralized H₂O and dichloromethane (c. 1:1, v:v) was added to the dry, saponified TLE. To completely dissolve the dry TLE in the added solvents and to yield a uniform suspension, samples were mixed with a Vortex mixer for approximately 30 sec. The suspension was then separated into a dichloromethane phase (containing the neutral lipids) and a H₂O phase (containing the fatty acids) by centrifugation of the samples for c. 5 min with 1200 runs/min. The dichloromethane phase of each sample was subsequently transferred into a new vial, respectively. After transfer, new dichloromethane was added to the sample and the separating procedure was repeated (5-25 times) until the dichloromethane phase of each sample remained clear after centrifugation. After the last transfer of the dichloromethane phase, hydrochloric acid (37%) was added to the residual saponified extracts to reduce the pH of the solution to <1. In the acidic solution, fatty acids become soluble in organic solvents again. The acid fraction was then isolated with dichloromethane by the same procedure as the neutral lipids, with turns of mixing, centrifugation and transfer of the dichloromethane phase into new vials. These steps were repeated 6-30 times for each of the respective samples, until the dichloromethane phase remained clear. The extracted acid fractions were then dried under N₂.

The fatty acids in the acid fraction cannot directly be analyzed by gaschromatographic (GC) procedures, since they are quite polar and therefore interact strongly with the stationary phase (the silica column in the GC device). Derivatization (methylation) of the fatty acids to fatty acid methyl ester (FAMES) reduce their polarity, and by that they become GC-amenable. For this purpose, MeOH(¹⁴C dated):HCl (95:5, v:v) was added to the dry acid fractions and air was replaced by N₂ in the vial. Reaction took place over night at

80°C. In order to quantify the introduced radiocarbon of the added methyl group, ^{14}C dated methanol was used for derivatization of the fatty acids. After reaction, the methylated acid fractions were dried under N_2 . To extract the FAMES, hexane and demineralized H_2O (c. 1:1; v:v) were added to the methylated acid fractions and turns of mixing, centrifugation and transfer of the hexane phase into new vials were performed, as previously described. 6-20 repetitions of these steps for each respective sample yielded a clear hexane phase at the end of the procedure.

Separation of Polarity Fractions: Neutral lipids contain a mixture of various lipids. Therefore, the extracted neutral lipid fractions were divided into four polarity fractions by silica gel column chromatography (4 cm x 0,5 cm, deactivated, 60 Å) and by elution with organic solvents of successively increasing polarity. Column chromatography relies on the effect that polar compounds interact more strongly with the silica gel than non-polar compounds, so that they move more slowly through the column than the non-polar compounds. Elution of the neutral fraction, successively with hexane, dichlormethane:hexane (1:1; v:v), chloroform and then with methanol, yielded an aliphatic fraction, a ketone fraction, an alcohol fraction and a polar fraction. Elution was performed with 8 ml of the respective solvents and eluted fractions were recovered in fresh 8 ml vials. For the recovery of the alcohol fraction only, 2 x 8 ml of chloroform were used, since mobilization of alcohols in chloroform is relatively slow. After recovery, the 2 x 8 ml were concentrated by evaporation under N_2 and combined in one vial. Alcohols are not directly GC-amenable, so that they were derivatized with acetic anhydride (^{14}C dated):pyridine (1:1; v:v) for 2 hours at 80°C. Just like the added methyl group in the FAMES, adding an acetyl group to the alcohols, alters the carbon composition and therefore the radiocarbon concentration of the respective compounds. In order to correct for this effect, acetic anhydride was ^{14}C dated, prior to utilization. The acetylation of the alcohol fraction leads to alcohol derivatives of low polarity and high stability.

The fatty acid fractions contain, besides the desired FAMES, some residuals and potentially some water that was not completely evaporated after methylation. Separation of the FAME fraction from the residuals was achieved by silica gel column chromatography (4 cm x 0,5 cm, deactivated, 60 Å) and with Na_2SO_4 on top of the silica gel, to remove the water from the sample. Elution of the fatty acid fraction was performed with hexane to recover the FAMES and then with methanol to recover the polar residuals.

4.2.6 Gas Chromatography

From aliphatic, alcohol and the FAME fractions of all sediment and plant samples, aliquots of 1%-10% (depending on the TOC content of the respective sample) were analyzed by gas chromatography. The utilized measuring device comprises a gas-chromatograph (GC-HP 7890B, Agilent Technologies, Palo Alto, CA) with flame ionization detection (FID) and is equipped with a silica column (50 m x 0,2 mm i.d. and 0,33 μm film thickness, Agilent

J&W). Compounds in the respective aliquots of the analyzed aliphatic, alcohol and FAME fractions were identified and quantified relative to authentic external standards.

4.2.7 Preparative Capillary Gas Chromatography

Separation of Saturated and Unsaturated Compounds: Beside the desired saturated alcohols, the alcohol fraction also contains high amounts of unsaturated compounds. For preparative capillary gas chromatography (PCGC), co-elution of different compounds hamper the confident identification and isolation of individual alcohols. Therefore, prior to PCGC, the alcohol fractions were separated into saturated and unsaturated sub-fractions, so that isolation of the desired compounds can be achieved without contamination of co-elutants. Silica gel impregnated with silver nitrate was used for column chromatography (4 cm x 0,5 cm, deactivated, 60 Å), in order to separate the saturated from the unsaturated alcohols. Silver nitrate prolongs the time that unsaturated compounds need to pass the silica gel column, since they bind to the compounds that contain double bonds (unsaturated compounds). The saturated alcohol fraction was eluted with 8 ml of ethyl acetate and successively, the unsaturated fraction was eluted with 8 ml of methanol. Performance of the separation procedure was checked by GC measurements and compounds of the saturated alcohol fraction were quantified in reference to external standards.

Selection of Biomarkers: Based on the quantified concentrations of the compounds and on their potential to derive from either marine or terrestrial sources, the following compounds have been selected for PCGC: *n-C*₂₅, *n-C*₂₇, *n-C*₂₉, *n-C*₃₁, *n-C*₃₃ and *n-C*₃₅ alkanes from the aliphatic fraction, *n-C*₁₄, *n-C*₁₆, *n-C*₂₂, *n-C*₂₆, *n-C*₂₈ alcohols and phytol from the saturated alcohol fraction and *n-C*₁₄, *n-C*₁₆, *n-C*₁₈, *n-C*₂₆, *n-C*₂₈ and *n-C*₃₀ fatty acids from the FAME fraction. Six evenly distributed depths of the composite were chosen that exhibited concentrations of the selected compounds of high enough concentrations to potentially yield sufficient carbon for AMS measurements. Two additional depths were chosen for the generally higher concentrated *n*-fatty acids, complementing the resolution to a set of 8 depths for this lipid class.

Isolation of Lipid Biomarkers and Quantification of C Yields: Great care during sample procedure is a prerequisite to achieve samples of high purity (Eglinton et al., 1997). In order to avoid contaminations, all equipment like vials, glass pipettes and traps as well as aluminum foil have been combusted at 450°C for 4 hours, prior to utilization. Solvents that were added to the samples or that were used for rinsing, were first checked for contamination by GC-FID measurements.

For isolation of the selected biomarker compounds, a PCGC system, composed of a GG-FID 7890A GC (Agilent Technologies, Palo Alto, CA), with a cold injection system (CIS, Gerstel GmbH, Germany) and interfaced to a preparative collection device (PFC, Gerstel GmbH, Germany), was used. The PFC device is equipped with six glass traps, in which the single compounds were collected, and one waste trap, in which the rest of the respective sample

was collected.

Injection volume per run was 5 μl . The CIS temperature program was set from 40 °C, at a rate of 12 °C/min, to 350 °C and isothermal for 5 min and then to 340°C at a rate of 12 °C/min and isothermal for 4 min. Individual compounds were separated on a 50 m fused-silica capillary column with 0.53 mm inner diameter and film thickness 0.5 μm (RTX-1, RESTEK; film thickness 0.5 μm) and with helium as carrier gas with a constant flow rate of 50 ml/min. For processing of *n*-alkane and *n*-alcohol samples, the GC oven temperature was programmed from 40 °C isothermal for 1 min to 200°C, at a rate of 15 °C/min, and then to 320 °C at a rate of 6 °C/min and isothermal for 20 min. For the processing of *n*-fatty acid samples, the GC oven temperature was programmed from 40 °C isothermal for 1 min to 150°C, at a rate of 20 °C/min, and then to 320 °C at a rate of 10 °C/min and isothermal for 12.5 min.

1% of the sample, eluting from the column, was diverted to the FID and 99% was transferred to the PFC. The temperature of the FID was constant at 300°C and air and hydrogen flows were constant at 300 and 35 ml/min, respectively, with helium as makeup gas at 25 ml/min. The PFC switch temperature and the transfer line were heated to 320°C, like the oven, so that the compounds do not precipitate before they reach the traps.

Before isolation of the compounds, reasonable sample concentrations as well as the time windows of their elution were determined by test runs. To avoid isotopic fractionations, the time windows were chosen as large as possible to isolate the entire peak, but as narrow as possible to obtain high purity. Carbon isotopes show an inverse isotope effect during gas chromatographic separation, so that heavy carbon isotopes elute slightly earlier than the lighter isotopes (Zencak et al., 2007). Therefore, the time window was determined with great care to ensure the start of the peak was covered. For each processed sample, a new CIS inlet liner was used to avoid carry over from the previous sample.

For processing, the samples were divided and transferred with dichloromethane into 5 vials. The concentration levels were chosen so as to achieve good separation of the eluants (not too high concentrations), and to isolate most of the sample with the least possible number of runs (not too low concentrations). Each sample was repeatedly injected 5-10 times per vial. The number of injections was decided based on the solvent volume, with a view to preventing variations in peak widths and in retention times caused by increasing sample concentration due to evaporation. When the respective number of injections from each of the 5 vials was performed, the remaining sample volumes were combined and divided into 3 vial, and again a respective number of injections was performed. The number of vials was further reduced to two and then to one. The idea behind this procedure was to maximize the yield of compounds which is particularly relevant when sample size is low. The retention time was frequently checked, and the trapping windows were adjusted if necessary. Each of the selected compounds was isolated individually in the traps of PFC device. After isolating the single compounds, the glass traps were rinsed with 1 ml of dichloromethane into 2 ml glass vials. To determine purity and yields, an aliquot of 1 μl was taken from the dissolved sample with a cleaned syringe and injected manually on-column to a GC-

FID 7890B (Agilent Technologies, Palo Alto, CA). C yields of all isolated compounds as well as of contaminations in the respective samples were quantified in reference to external standards. Samples with high contaminations or low C yields were rejected from further analysis. Compounds from potentially marine as well as from terrigenous sources with sufficient yields of C ($>10 \mu\text{g}$), with contaminations $< 3.5\%$ and in the best case available in all of the selected depths, were further prepared for AMS measurement. However, one should bear in mind that purity determination just covers contaminations that are amenable to gas chromatography, so that other contamination, e.g. particulate organic carbon, cannot be detected (Zencak et al., 2007).

Isolated $n\text{-C}_{16}$ and $n\text{-C}_{26}$ fatty acids as well as $n\text{-C}_{22}$ and $n\text{-C}_{26}$ alcohols had high enough C yields and were further processed individually. Concentrations of individual n -alkanes were generally too low for CSRA in all depths, so that two HMW n -alkanes from each sample depth were combined for radiocarbon measurement. Before combining them, the samples had to be cleaned, since the proportions of the contaminations were quite high in every sample due to the low concentration of the respective compounds. Contaminations were successfully eliminated from most n -alkane compounds by elution of the samples with hexane over a column of silica gel (2 cm x 0,5 cm, deactivated, 60 Å). The purest two, successive n -alkanes were pooled, resulting in combinations of $n\text{-C}_{27}+n\text{-C}_{29}$, $n\text{-C}_{29}+n\text{-C}_{31}$ or $n\text{-C}_{31}+n\text{-C}_{33}$ alkanes. In the following all these combinations of two respective n -alkanes are referred as $n\text{-C}_{27-33}$ alkanes.

The described isolation procedure as well as the following transfer, evacuation, combustion and purification procedures are illustrated schematically in fig. 4.2.

Transfer, Evacuation, Combustion, Purification and Measurement: All equipment used for sample preparation was previously combusted for 4 hours. Glass pipettes, long glass flasks and pincettes were combusted at 450°C . Quartz tubes, CuO and silver (Ag) wire were combusted twice at 900°C .

Sample vials were covered with combusted aluminum foil to avoid contamination and solvent was removed from the samples by evaporation over night. Dry samples were then dissolved again in small volumes of dichloromethane and transferred with glass pipettes into quartz tubes of 6 mm diameter. The quartz tubes were placed into long glass flasks and attached to a rotary evaporator. Dichloromethane was evaporated under near vacuum until it was completely removed from the samples. C. 150 mg of CuO was added as oxidant to the dry samples in the 6 mm quartz tubes, and c. 60 mg of Ag wire was added to trap sulfur and halogens and to reduce the development of NO_x during combustion (Wild et al., 1998). The 6 mm quartz tubes were placed into larger quartz tubes, which were then attached to a vacuum line. The tubes were evacuated to a pressure of 10^{-5} mbar while immersed in dry ice/EtOH (-78°C) to prevent the loss of highly volatile compounds. When pressure was reached, the dry ice/EtOH trap was replaced by a liquid N₂ trap and the quartz tubes were sealed using a propane burner. The samples were combusted in the sealed quartz glass tubes over night at 900°C . Combustion converts carbon into CO₂ but also yields water and

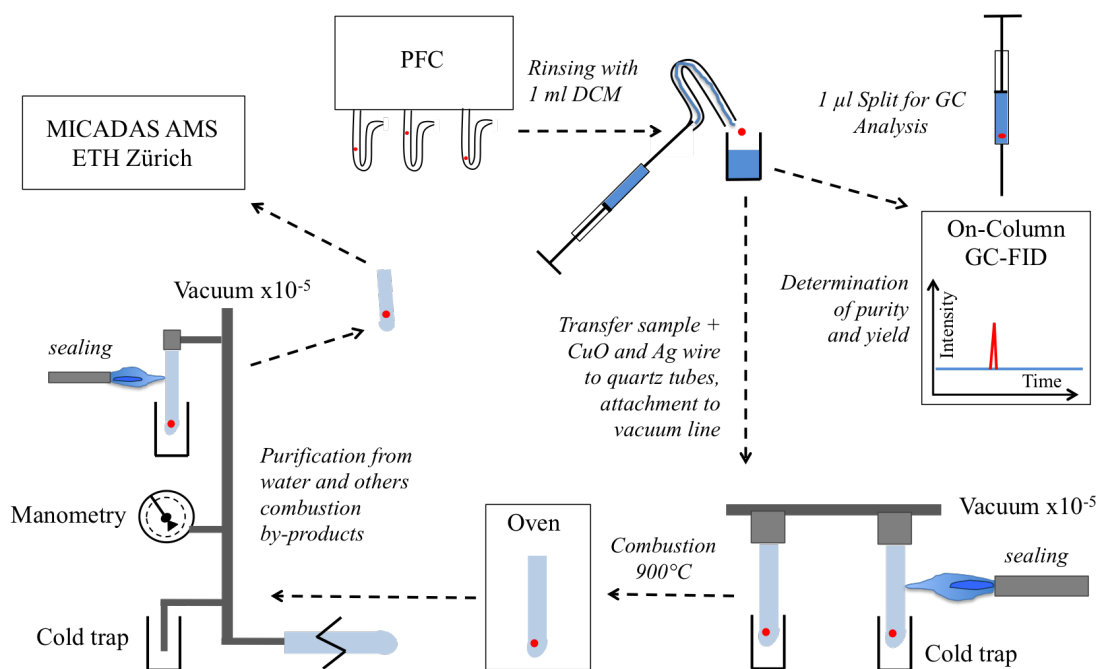


Figure 4.2: Scheme of the laboratory procedure for CSRA in direction of the arrows: Isolation of single compounds in traps of the PFC device, rinsing of traps, determination of purity and yield and transfer of the samples to quartz tubes together with CuO and Ag wire, evacuation of and sealing of the samples, combustion of the samples, removal of water and combustion by-products, quantification of the CO₂ and sealing of the samples, submission to ETH Zürich for AMS measurement.

other combustion by-products.

Water and condensable by-products were removed from the gas samples in a second vacuum line through a series of cold traps. The purified CO₂ was quantified by manometry, which refers to the measurement of the gas pressure in a defined space of the vacuum line. Samples that yielded more than 60 µg C were split in the vacuum line into two sub-samples by freezing a part of the gas in a cold trap, sealing the other part of the gas into small borosilicate tubes of 4 mm diameter, and then releasing the remaining gas and sealing it into a second tube. The purified CO₂ samples were sent to the AMS facility in Zürich, where they were measured with a MICADAS AMS with gas ion source.

Corrections for Blank and Derivatization: It is possible that during PCGC isolation procedure and subsequent handling, extraneous carbon contaminates the samples (Eglinton et al., 1997). Therefore, results of the CSRA have to be corrected for this extraneous carbon: modern contamination in the fossil standard (octadecan) and fossil contamination in the modern standard (squalane) were determined using ¹⁴C concentrations of the treated and the untreated standard materials for isotopic mass balance calculations:

$$fMC_{OctaPrep} = x * fMC_{OctaUn} + (1 - x) * fMC_{ContMod} \quad (4.1)$$

$$fMC_{SquaPrep} = x * fMC_{SquaUn} + (1 - x) * fMC_{ContFoss} , \quad (4.2)$$

where $fMC_{OctaPrep}$ and $fMC_{SquaPrep}$ are the measured fMC values of the processed standards, fMC_{OctaUn} and fMC_{SquaUn} are the fMC values of the unprocessed standards and $fMC_{ContMod}$ and $fMC_{ContFoss}$ are the fMC values of the modern and the fossil contamination, respectively. For $fMC_{ContMod}$ the recent value of the atmosphere (1.02) and for $fMC_{ContFoss}$ the value 0 (no ^{14}C activity) was applied in the calculations.

In order to derive fMC values, corrected for contaminations (fMC_{Corr}), modern and fossil contaminations were combined to $fMC_{ContMod+Foss}$. The respective contaminations were normalized to sample size, since depending on the amount of analyzed carbon, the magnitude of the carbon background correction varies between samples (Douglas et al., 2014):

$$fMC_{Corr} = x * fMC_{Free} + (1 - x) * fMC_{ContMod+Foss} . \quad (4.3)$$

Results have to be further corrected for the carbon that was added due to derivatization, since this additional carbon alters the ^{14}C content of the sample.

Correction for derivatization can be achieved as follows:

$$fMC_{Measured} = C_n * fMC_{Free} + C_{(n+1)}/C_n * fMC_{Methanol} , \quad (4.4)$$

or

$$fMC_{Measured} = C_n * fMC_{Free} + C_{(n+1)}/C_n * fMC_{EthylAcetat} , \quad (4.5)$$

with C_n delimiting the carbon number of the respective compound.

The propagated uncertainties were calculated as follows:

$$\sqrt{(E_{Sample})^2 + (E_{Methanol})^2 + (E_{SquaUn})^2 + (E_{SquaPrep})^2 + (E_{OctaUn})^2 + (E_{OctaPrep})^2} , \quad (4.6)$$

with E = error in fMC. Equation 4.6 is an example for n -fatty acids. $E_{Methanol}$ was replaced with $E_{EthylAcetat}$ for n -alcohols and was excluded for n -alkanes.

Conversion of fMC to $\Delta^{14}C$ values and ^{14}C ages follow equations 2.6 and 2.7 respectively, according to the established conventions (Stuiver and Polach, 1977).

4.3 Results

4.3.1 Lithology

The 11.04 m long sediment core Co1305 comprises the complete postglacial sedimentation record of the marine inlet, indicated by radiocarbon data of plant remains from the lower part of the core that exhibit a ^{14}C age of c. 15,200 years (details in chapter 6). The base of the record is formed by diamictic sediments that are pointing to a former glaciation of the site. The diamicton is overlain by well stratified sediments that are then passing over into massive muds of silt and clay (Berg et al., 2019). Four Units can be subdivided in the record based on $\delta^{13}\text{C}$ analyses of bulk TOC and on diatom assemblages (Berg et al., 2019): Unit I (11.04–10.42 m) comprises the diamictic base of the record. Unit II (10.42–9.96 m) is composed of stratified lake sediments. The lacustrine stage of the record ends with a transition from lacustrine to marine between 9.96–9.78 m, which is termed Unit III. A fully marine sequence follows in Unit IV, from 9.78 m to the surface of the core (fig. 4.3).

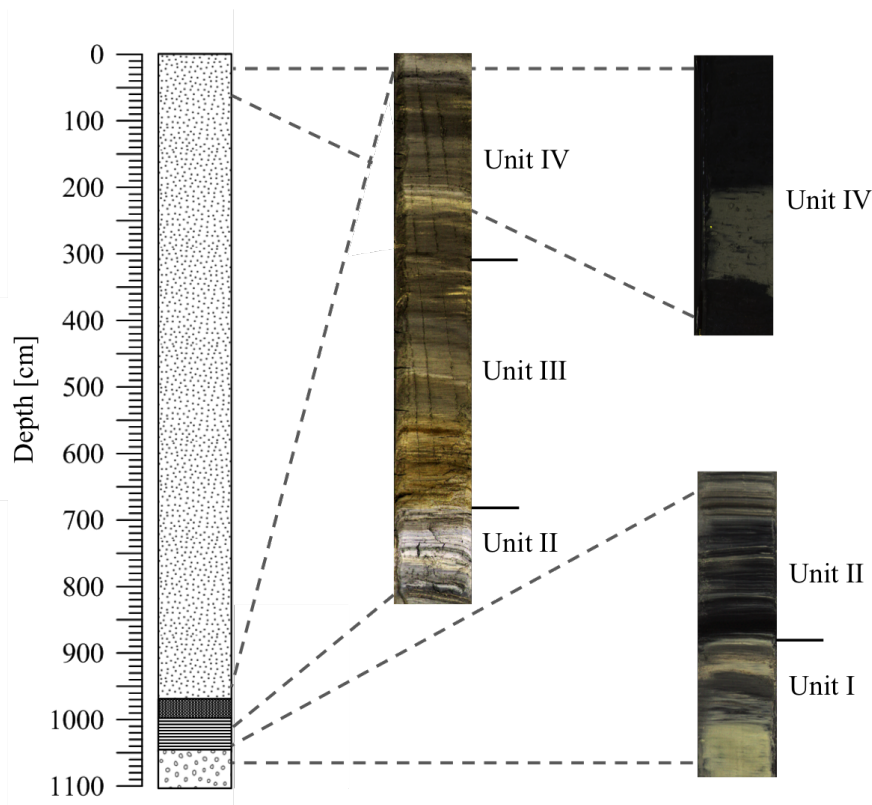


Figure 4.3: Lithological profile of sediment core Co1305 with subdivisions of Units I-IV. Diamictic sediments of Unit I (11.04–10.42 m) are marked with circles, lacustrine sediments of Unit II (10.42–9.96 m) are marked by horizontal lines, transition from lacustrine to marine sediments of Unit III (9.96 –9.78 m) is marked by horizontal lines with dark background, marine sediments of Unit IV (9.78 m–surface) are marked with small dots. Scans of exemplary core sections are displayed on the right-hand side of the figure.

4.3.2 Radiocarbon Inventories of Biomarkers and of TOC

In tab. 4.1, the analyzed compounds, their respective sample depths, the number of runs that were performed to isolate the compounds, their contaminations and their C yields are listed. No correlation is given between the number of prep-runs and the contaminations ($r^2=0.01$) or between C yields and contaminations ($r^2=0.03$). Samples with C yields too high for AMS gas measurement ($> 60 \mu\text{g}$) were split during the gas cleaning procedure in the vacuum line.

Table 4.1: Biomarkers chosen for CSRA of the core Co1305: "Sample" is referring to the biomarker class and "compound" to the chain-length of the analyzed biomarkers. "Prep-runs" are showing the number of injections that were performed for each compound during preparative capillary gas chromatography (PCGC). "Contaminations (%)" were quantified on an on-column GC-FID together with C concentration (C [μg] GC-FID). Concentration "C [μg] vacuum line" are referring to the C amounts that were calculated based on manometry measurements during purification of the combusted sample. Underlined values indicate C yields that are too high for AMS (MICADAS) measurement ($>60 \mu\text{g}$). For the samples with too high amounts of C, just the submitted split of the samples is listed under "C [μg] Vacuum Line".

Depth [cm]	Sample Type	Compound	Prep-Runs	Contamination [%]	C [μg] GC-FID	C [μg] Vacuum Line
4-9	fatty acids	<i>n</i> -C ₂₆	47	0	15.1	21
4-9	alkanes	<i>n</i> -C ₂₉₊₃₁	43	0.5	11.2	22
4-9	alcohols	<i>n</i> -C ₂₂	73	1.6	22.1	28
4-9	alcohols	<i>n</i> -C ₂₆	73	2.2	63.5	57
103-108	fatty acids	<i>n</i> -C ₁₆	82	0.7	<u>92.1</u>	36
103-108	fatty acids	<i>n</i> -C ₂₆	82	0	11.3	23
308-313	fatty acids	<i>n</i> -C ₁₆	51	0.5	<u>96</u>	39
308-313	fatty acids	<i>n</i> -C ₂₆	51	3.2	40	42
308-313	alkanes	<i>n</i> -C ₂₉₊₃₁	40	0.6	11.4	16
308-313	alcohols	<i>n</i> -C ₂₂	105	1.7	49.4	31
468-473	fatty acids	<i>n</i> -C ₁₆	53	0.6	74.5	57
468-473	fatty acids	<i>n</i> -C ₂₆	53	0.2	35.2	39
468-473	alkanes	<i>n</i> -C ₂₇₊₂₉	68	1.8	11.3	15
468-473	alcohols	<i>n</i> -C ₂₆	63	0.9	<u>155.3</u>	36
612-617	fatty acids	<i>n</i> -C ₁₆	57	0.6	<u>138.9</u>	48
612-617	fatty acids	<i>n</i> -C ₂₆	57	0.3	85.1	60
612-617	alkanes	<i>n</i> -C ₂₇₊₂₉	52	0	10.8	14
612-617	alcohols	<i>n</i> -C ₂₂	76	1.2	68.8	55
612-617	alcohols	<i>n</i> -C ₂₆	76	1.4	<u>91.5</u>	55
720-725	fatty acids	<i>n</i> -C ₁₆	55	0.5	<u>121.5</u>	48
720-725	fatty acids	<i>n</i> -C ₂₆	55	0.5	<u>89.4</u>	44
720-725	alkanes	<i>n</i> -C ₃₁₊₃₃	40	5	8.5	12
720-725	alcohols	<i>n</i> -C ₂₂	25	3.4	20.1	33
820-823	fatty acids	<i>n</i> -C ₁₆	63	1.8	44.1	40
820-823	fatty acids	<i>n</i> -C ₂₆	63	0.6	34.9	34
988-991	fatty acids	<i>n</i> -C ₁₆	46	1.9	<u>231.8</u>	50
988-991	fatty acids	<i>n</i> -C ₂₆	46	0.7	<u>164.2</u>	54
988-991	alkanes	<i>n</i> -C ₂₉₊₃₁	46	2.6	7.1	17
988-991	alcohols	<i>n</i> -C ₂₂	86	0.8	34.9	39
988-991	alcohols	<i>n</i> -C ₂₆	86	1.0	36.9	43

The C yield of these samples is underlined in row 6. C amounts of the respective analyzed subsamples are listed rightmost of tab. 4.1.

$\Delta^{14}\text{C}$ Values of Bulk TOC and Biomarker Compounds: Results of radiocarbon measurements (fMC) of bulk TOC samples and of isolated lipid biomarkers were converted to $\Delta^{14}\text{C}$ (‰) and to ^{14}C ages. In tab. 4.2, fMC results of the AMS measurements are listed in row 4. The fMC values that were corrected for exogenous carbon and for derivatization (if required) are displayed in row 5. The corrected fMC values, converted into $\Delta^{14}\text{C}$ (‰) and ^{14}C ages, are listed in rows 6 and 7, respectively. For comparison of radiocarbon inventories, the Δ -notation is used.

The $n\text{-C}_{26}$ alcohol sample at 612–617 cm core depth is excluded from further analysis, because it exhibits an unrealistically high $\Delta^{14}\text{C}$ value (underlined in row 6). Since no particularly severe contamination could be detected in this sample before evacuation, a contamination with modern ^{14}C during subsequent sample procedure is likely. It is possible that atmospheric CO_2 diffused into the sample tube through a micro crack in the glass.

$\Delta^{14}\text{C}$ values of all remaining samples range between -81.7 ± 12.9 ‰ for the $n\text{-C}_{26}$ alcohols at 4–9 cm core depth to -702.8 ± 2.4 ‰ for TOC in 988–991 cm. $\Delta^{14}\text{C}$ values inside each sample class are decreasing with core depth, with an exception between 720 and 825 cm, where a reversal is occurring for $n\text{-C}_{16}$ fatty acids (fig. 4.4 A). Overall, TOC is the sample class with the lowest $\Delta^{14}\text{C}$ values or exhibits, in an error of 2σ , the same value as the most depleted biomarker compound at the respective depth. Just at 103–108 cm depth, $n\text{-C}_{26}$ fatty acids are more depleted than TOC. The most enriched compounds in all sample depths, except in the uppermost, are $n\text{-C}_{16}$ fatty acids and/or $n\text{-C}_{22}$ alcohols. In the upper part of the core (308–313 cm), $n\text{-C}_{16}$ fatty acids are more enriched than $n\text{-C}_{22}$ alcohols. At 612–617 cm core depth, $n\text{-C}_{16}$ fatty acids and $n\text{-C}_{22}$ alcohols exhibit the same $\Delta^{14}\text{C}$ values in an error of 2σ , whereas in the lower part of the sediment core (720–725 and 988–993 cm), $n\text{-C}_{16}$ fatty acids are more depleted than $n\text{-C}_{22}$ alcohols (fig. 4.4 A). $n\text{-C}_{27-33}$ alkanes and $n\text{-C}_{26}$ fatty acids exhibit the same $\Delta^{14}\text{C}$ values, in an error of 2σ , at all but one sample depths. At 720–725 cm, the $\Delta^{14}\text{C}$ value of $n\text{-C}_{27-33}$ alkanes is lower than that of $n\text{-C}_{26}$ fatty acids. $\Delta^{14}\text{C}$ values of $n\text{-C}_{26}$ alcohols were determined for three depths only. At the uppermost depth (4–9 cm), $n\text{-C}_{26}$ alcohols are most enriched in ^{14}C , compared to all other samples. At 468–473 cm, the $\Delta^{14}\text{C}$ value of $n\text{-C}_{26}$ alcohols lies between the more enriched $n\text{-C}_{16}$ fatty acids and $n\text{-C}_{22}$ alcohols and the more depleted $n\text{-C}_{26}$ fatty acids, $n\text{-C}_{27-33}$ alkanes and TOC. At the lowermost depth (988–993 cm), $n\text{-C}_{26}$ alcohols exhibit, in an error of 2σ , the same $\Delta^{14}\text{C}$ value as $n\text{-C}_{16}$, $n\text{-C}_{26}$ fatty acids and $n\text{-C}_{27-33}$ alkanes.

Offsets of $\Delta^{14}\text{C}$ (‰) between Biomarker Compounds and TOC: Fig. 4.4 B is showing the offsets between $\Delta^{14}\text{C}$ values of biomarker compounds and $\Delta^{14}\text{C}$ values of TOC at the respective depths. Offsets between $n\text{-C}_{16}$ fatty acids and TOC, or between $n\text{-C}_{22}$ alcohols and TOC, are largest at all depths, except of the uppermost (4–9 cm). The highest

offset is displayed at 720–725 cm between n -C₁₆ fatty acids and TOC, with -256 ± 10 ‰. For all other depths, offsets between n -C₁₆ fatty acids or n -C₂₂ alcohols and TOC range between -35 ± 15 and -142 ± 13 ‰. n -C₂₆ fatty acids, n -C₂₆ alcohols and n -C_{27–33} alkanes

Table 4.2: Radiocarbon data of TOC and of biomarker compounds of the core Co1305: fMC values are results of AMS measurements (TOC was measured at the AMS facility in Cologne, biomarker compounds were measured at the AMS facility in Zurich). The corrected fMC values include corrections for preparation blank and for derivatization (just for n -fatty acids and n -alcohols). The underlined value was rejected for further analysis. The error is reported as propagated uncertainty. Conversions of fMC to $\Delta^{14}\text{C}$ values and ^{14}C ages are following equations 2.6 and 2.7.

depth [cm]	sample type	compound	measured fMC	corrected fMC	corrected $\Delta^{14}\text{C}$ [‰]	corrected ^{14}C age
0–2	TOC		0.862 ± 0.004		-144.5 ± 4.0	1192 ± 35
4–9	fatty acids	n -C ₂₆	0.847 ± 0.008	0.881 ± 0.012	-126.1 ± 11.6	1022 ± 106
4–9	alkanes	n -C ₂₉₊₃₁	0.879 ± 0.008	0.882 ± 0.012	-124.6 ± 11.6	1008 ± 106
4–9	alcohols	n -C ₂₂	0.838 ± 0.010	0.897 ± 0.014	-109.7 ± 14.3	872 ± 129
4–9	alcohols	n -C ₂₆	0.869 ± 0.008	0.925 ± 0.013	-81.7 ± 12.9	624 ± 113
103–108	fatty acids	n -C ₁₆	0.823 ± 0.007	0.876 ± 0.011	-130.3 ± 10.9	1060 ± 100
103–108	fatty acids	n -C ₂₆	0.723 ± 0.006	0.752 ± 0.010	-254.2 ± 10.4	2295 ± 112
105–107	TOC		0.779 ± 0.004		-226.9 ± 4.0	2003 ± 43
308–313	fatty acids	n -C ₁₆	0.730 ± 0.006	0.778 ± 0.010	-228.4 ± 10.3	2022 ± 107
308–313	fatty acids	n -C ₂₆	0.664 ± 0.006	0.692 ± 0.010	-313.7 ± 10.9	2963 ± 118
308–313	alkanes	n -C ₂₉₊₃₁	0.699 ± 0.009	0.700 ± 0.012	-305.7 ± 11.9	2870 ± 138
308–313	alcohols	n -C ₂₂	0.693 ± 0.009	0.747 ± 0.014	-258.2 ± 10.3	2338 ± 146
310–312	TOC		0.660 ± 0.004		-345 ± 3.6	3337 ± 44
468–473	fatty acids	n -C ₁₆	0.709 ± 0.006	0.756 ± 0.010	-250.1 ± 13.5	2251 ± 110
468–473	fatty acids	n -C ₂₆	0.606 ± 0.006	0.630 ± 0.011	-374.6 ± 10.4	3709 ± 134
468–473	alkanes	n -C ₂₇₊₂₉	0.647 ± 0.009	0.646 ± 0.012	-358.5 ± 12	3505 ± 150
468–473	alcohols	n -C ₂₆	0.652 ± 0.008	0.690 ± 0.013	-315.1 ± 12.6	2979 ± 147
472–474	TOC		0.633 ± 0.003		-372 ± 2.9	3678 ± 37
612–617	fatty acids	n -C ₁₆	0.555 ± 0.005	0.590 ± 0.010	-414.2 ± 9.7	4235 ± 133
612–617	fatty acids	n -C ₂₆	0.518 ± 0.005	0.539 ± 0.010	-465.5 ± 9.6	4970 ± 145
612–617	alkanes	n -C ₂₇₊₂₉	0.561 ± 0.009	0.559 ± 0.012	-444.8 ± 12.1	4666 ± 175
612–617	alcohols	n -C ₂₂	0.572 ± 0.008	0.608 ± 0.013	-396.2 ± 12.7	3992 ± 170
612–617	alcohols	n -C ₂₆	0.797 ± 0.009	0.855 ± 0.013	<u>-151.2 ± 13.2</u>	1255 ± 125
614–616	TOC		0.466 ± 0.003		-537.8 ± 3.0	6138 ± 52
720–725	fatty acids	n -C ₁₆	0.551 ± 0.005	0.544 ± 0.010	-460.5 ± 9.5	4896 ± 145
720–725	fatty acids	n -C ₂₆	0.467 ± 0.005	0.485 ± 0.010	-518.7 ± 9.6	5814 ± 160
720–725	alkanes	n -C ₃₁₊₃₃	0.452 ± 0.009	0.449 ± 0.012	-554.2 ± 12.1	6429 ± 219
720–725	alcohols	n -C ₂₂	0.553 ± 0.008	0.583 ± 0.013	-421.6 ± 12.8	4337 ± 178
722–724	TOC		0.457 ± 0.004		-546.4 ± 3.7	6289 ± 65
820–823	fatty acids	n -C ₁₆	0.538 ± 0.005	0.572 ± 0.010	-432 ± 9.9	4483 ± 139
820–823	fatty acids	n -C ₂₆	0.427 ± 0.005	0.443 ± 0.010	-560.2 ± 9.6	6537 ± 174
848–850	TOC		0.314 ± 0.002		-688.4 ± 1.5	9305 ± 51
988–993	fatty acids	n -C ₁₆	0.357 ± 0.004	0.378 ± 0.009	-625.2 ± 9.3	7822 ± 199
988–991	fatty acids	n -C ₂₆	0.333 ± 0.004	0.344 ± 0.009	-658.7 ± 9.3	8573 ± 219
988–991	alkanes	n -C ₂₉₊₃₁	0.371 ± 0.006	0.366 ± 0.010	-637 ± 10.3	8078 ± 227
988–991	alcohols	n -C ₂₂	0.395 ± 0.006	0.414 ± 0.012	-588.9 ± 11.8	7079 ± 230
988–991	alcohols	n -C ₂₆	0.362 ± 0.006	0.376 ± 0.012	-627.2 ± 11.6	7864 ± 250
990–992	TOC		0.299 ± 0.002		-702.8 ± 2.4	9686 ± 63

mostly exhibit lower offsets of $+27 \pm 11$ to -93 ± 10 ‰ from TOC. Again, 720–725 cm is an exception, showing an offset of -128 ± 10 ‰ between n -C₂₆ fatty acids and TOC.

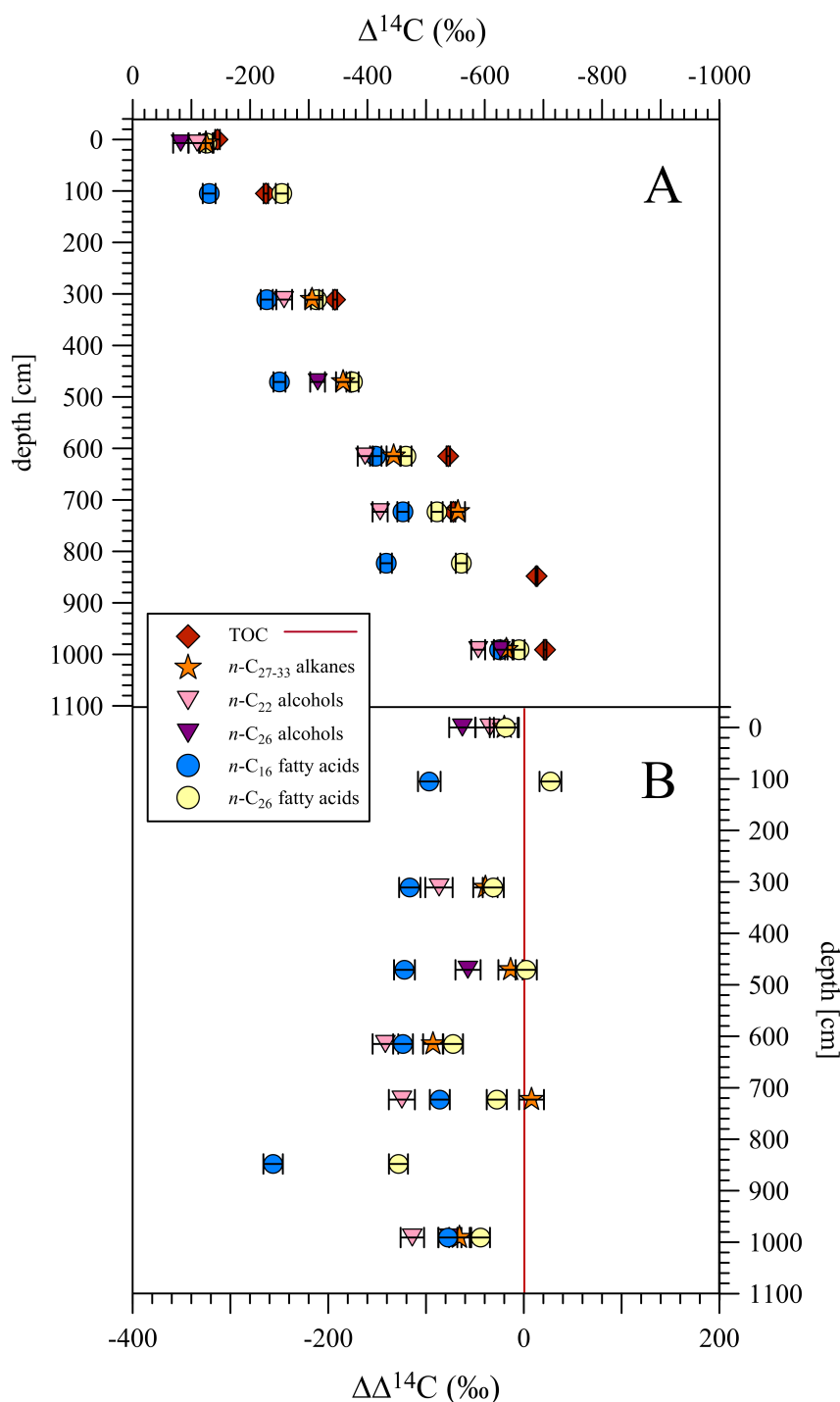


Figure 4.4: **A:** $\Delta^{14}\text{C}$ (‰) of TOC (red diamonds), n -C₂₇₋₃₃ alkanes (orange stars), n -C₂₂ alcohols (rose triangles), n -C₂₆ alcohols (purple triangles), n -C₁₆ fatty acids (blue circles) and n -C₂₆ fatty acids (yellow circles) against core depth. $\Delta^{14}\text{C}$ values are corrected for blank and for derivatization. Error bars display the propagated uncertainty resulting from AMS measurement and corrections. **B:** $\Delta^{14}\text{C}$ (‰) offsets of n -C₂₇₋₃₃ alkanes, n -C₂₂ alcohols, n -C₂₆ alcohols, n -C₁₆ fatty acids, n -C₂₆ fatty acids in reference to TOC (red line). Error bars display the sum of the propagated uncertainties of the respective compound and TOC.

4.3.3 TOC, IRD and Biomarker Records of Co1305

The investigated downcore records of the sediment core Co1305 comprise total organic carbon (TOC), ice-rafted debris (IRD) and the biomarkers that were chosen for CSRA (*n*-C_{27–33} alkanes, *n*-C₂₂ and *n*-C₂₆ alcohols, *n*-C₁₆ and *n*-C₂₆ fatty acids).

Total Organic Carbon (TOC): TOC includes all kinds of organic matter that are preserved in the sediments. TOC concentrations vary between 0.4 and 3 % throughout the entire sedimentary record (fig. 4.5). The diamictic unit I exhibits the lowest TOC concentration of only 0.4 %. In units II and III concentrations are highly variable with values between 1 and 2.5 %. In the lower part of unit IV (up to c. 8 m core depth), TOC concentrations are generally low with values of around 1%. Concentrations then increase rapidly between 8 and 7.5 m core depth from c. 1 to c. 2.2 % and remain relatively stable up to the near surface of the sedimentary record. In the upper 30 cm of the record, TOC concentration increases to a maximum of 3% at the surface of the sediment core.

Ice Rafted Debris (IRD): The sediment fraction > 1 mm is interpreted as IRD that is not transported by run-off or by wind but as frozen particles at the bottom of floating ice blocks and that are subsequently released by the melting ice over the coring site (Grobe, 1987).

The IRD record shows a distinct variability over the four units. In units I - III, varying concentrations of 0.2–0.75 grains/g DW are recorded. In the lower part of Unit IV, IRD counts increase to particularly high, but also variable values between c. 9.2–7.8 m core depth, with maximum concentrations of 1.7 grains/g DW. Counts are low up to c. 6.5 m core depth and then again display high concentrations of a maximum of 1.2 grains/g DW, between c. 6.5 and 6 m. Up to c. 1.5 m, low values of 0–0.5 grains/g DW prevail. Between 1.5 m and the surface, IRD counts are mostly higher than in the phase before but also quite variable with values of 0–0.7 grains/g DW.

Biomarker Concentrations: The highest concentrations as well as the greatest variability are displayed within the *n*-C₁₆ fatty acid record, with concentrations of 11–1016 µg/g OC (fig.4.5). In contrast, the lowest variability is revealed in the *n*-C₂₂ alcohol record, with concentration of 86–651 µg/g OC. *n*-C₂₆ Fatty acids and *n*-C₂₆ alcohols, show a quite similar range of concentrations throughout the record, with values of 39–815 µg/g OC and 22–849 µg/g OC, respectively. The sum of *n*-C₂₇, *n*-C₂₉, *n*-C₃₁ and *n*-C₃₃ alkanes (*n*-C_{27–33} alkanes) is between 12 and 262 µg/g OC.

All biomarker records exhibit low concentrations in units I and II, with an exception of the *n*-C₂₂ alcohols, which display the highest concentration in the lowermost sample (651 µg/g OC). A sharp increase of biomarker concentrations characterizes the transition from unit II to unit III. In unit III, all biomarkers exhibit high concentrations. In the lowest part of unit IV, biomarker concentrations are still relatively high but start to drop until they reach a minimum at c. 8.5 m core depth. After this minimum, all biomarker concentrations increase

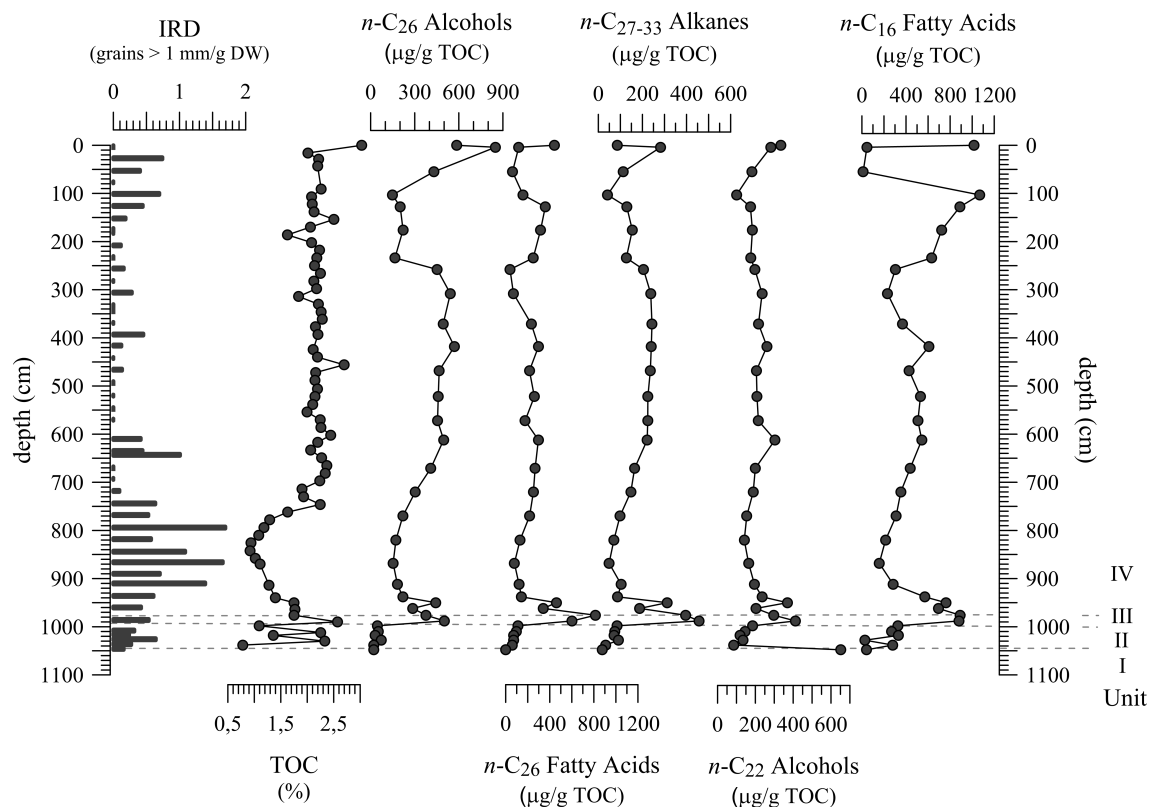


Figure 4.5: IRD, TOC and biomarker concentrations against core depth: The sediment fraction $> 1\text{mm}$ (IRD) is normalized to DW. Discrete values (counts) of IRD are displayed as bars. Concentrations of TOC (red dots) are displayed in %. Biomarker concentrations are normalized to TOC. Boundaries between lithological units I-IV of the sediment core are marked by dashed lines.

successively up to a core depth of c. 7 m and then display relatively stable concentrations up to c. 3.5 m core depth. The so far quite uniform trends of the biomarker records, become more variable in the upper part of the sediment core. Lowest concentrations of $n\text{-C}_{27-33}$ alkanes, $n\text{-C}_{22}$ and $n\text{-C}_{26}$ alcohols are present between c. 2 and 1 m core depth. $n\text{-C}_{16}$ and $n\text{-C}_{26}$ fatty acids exhibit lowest values at c. 2.5 and c. 0.5 m core depth. Exceptionally high concentrations are displayed by $n\text{-C}_{16}$ fatty acids at c. 1 m core depth.

4.3.4 Contemporary Plant Samples

Samples of kelp, tussock grass and moss from the catchment of Little Jason Lagoon were analyzed to derive information on the compositional biomarker fingerprints of these characteristic plant types. Concentrations of odd numbered n -alkanes as well as of even numbered n -alcohols and n -fatty acids of the three contemporary samples are displayed in fig. 4.6. The n -alkane and the n -fatty acid inventories of the kelp are dominated by LMW compounds ($n\text{-C}_{17}$ and $n\text{-C}_{16}$, respectively) and are lacking in HMW compounds. The n -alcohol spectrum of this marine plant species shows high proportions of $n\text{-C}_{16}$, $n\text{-C}_{18}$ and $n\text{-C}_{28}$. The concentrations of n -alkanes, n -fatty acids and n -alcohols differ markedly in the kelp sample. n -Fatty acid concentrations are two orders of magnitude higher than n -alcohol concentra-

tions and four orders of magnitude higher than *n*-alkane concentrations.

The tussock grass exhibits highest proportions of HMW compounds in the spectra of *n*-alkanes and of *n*-alcohols, with peak concentrations of *n*-C₂₉ and *n*-C₃₁ alkanes and *n*-C₂₆ alcohols, respectively. In the *n*-fatty acid spectrum, *n*-C₁₆ and *n*-C₂₀ reveal highest concentrations.

The moss sample and the tussock grass both exhibit highest concentrations of HMW compounds in their *n*-alkane and *n*-alcohol inventories, with peak values for *n*-C₂₉ to *n*-C₃₃ alkanes and for *n*-C₂₂ to *n*-C₂₆ alcohols, respectively. Highest concentrations in the *n*-fatty acid spectrum are displayed by *n*-C₁₆.

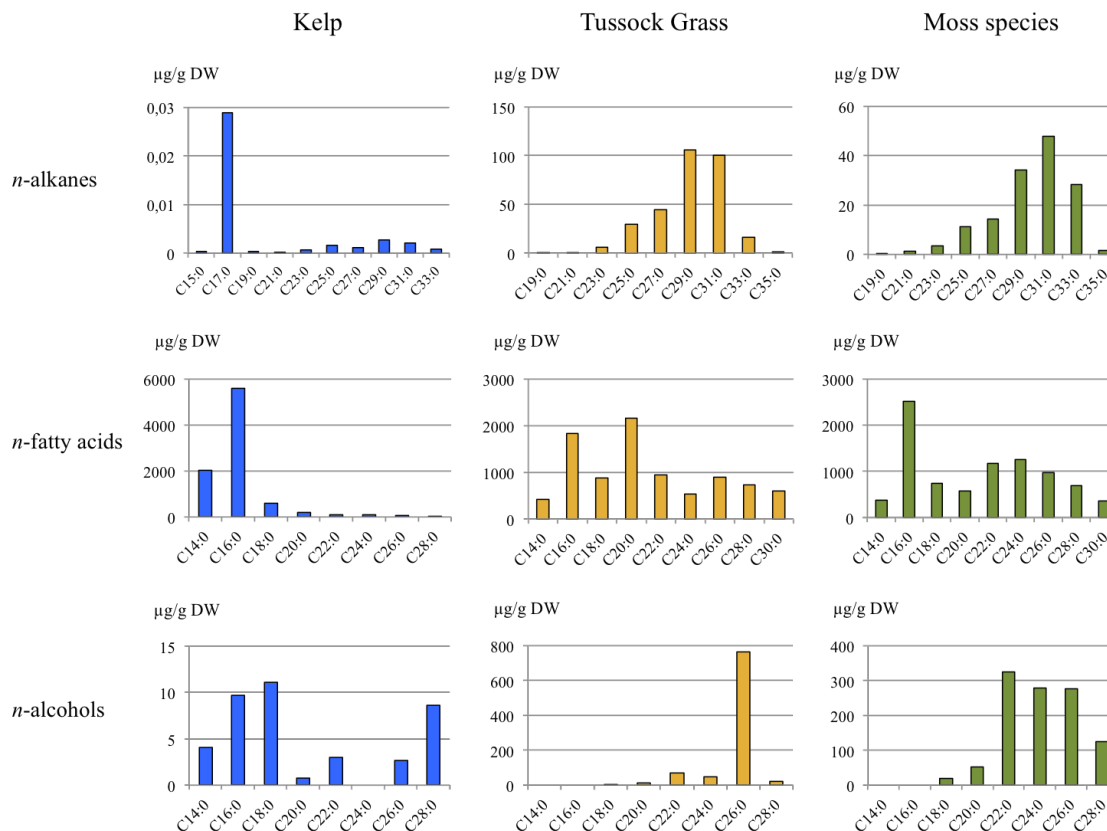


Figure 4.6: Biomarker inventories of contemporary samples, collected in the catchment of Little Jason Lagoon. From left to right: Concentrations of odd-numbered *n*-alkanes (*n*-C₁₅–*n*-C₃₃), even-numbered *n*-fatty acids (*n*-C₁₄–*n*-C₂₈) and even-numbered *n*-alcohols (*n*-C₁₄–*n*-C₂₈) in a kelp sample are displayed as blue bar chart. Concentrations of odd-numbered *n*-alkanes (*n*-C₁₉–*n*-C₃₅), even-numbered *n*-fatty acids (*n*-C₁₄–*n*-C₃₀) and even-numbered *n*-alcohols (*n*-C₁₄–*n*-C₂₈) in a sample of tussock grass are displayed as yellow bar charts. Concentrations of odd-numbered *n*-alkanes (*n*-C₁₉–*n*-C₃₅), even-numbered *n*-fatty acids (*n*-C₁₄–*n*-C₃₀) and even-numbered *n*-alcohols (*n*-C₁₄–*n*-C₂₈) in an unspecified moss sample are displayed as green bar charts. All biomarker concentrations are normalized to DW and are reported in µg/g DW.

4.4 Discussion

4.4.1 Diversity of Biomarker Sources on Land and in the Ocean

Terrigenous Biomarker Sources: Plant types that characterize the vegetation on the island of South Georgia include tussock grass species, spread in the coastal lowlands, as well as moss species, colonizing higher altitudes and steep slopes (Van der Putten et al., 2009). Samples of both of these characteristic plant types reveal considerable proportions of HMW *n*-fatty acids and of HMW *n*-alkanes in their biomarker inventories (fig. 4.6). Contrasting the lipid compositions of the grass and the moss, a sample of marine kelp is virtually lacking in HMW *n*-fatty acids and HMW *n*-alkanes. The absence of these biomarkers is also characteristic for other marine organisms. Only few planktonic sources of HMW *n*-alkanes (Lichtfouse et al., 1994) as well as of HMW *n*-fatty acids (Volkman et al., 1998) were previously reported, but considered mostly negligible in marine sediments. Therefore, it can be assumed that sedimentary HMW *n*-fatty acids and HMW *n*-alkanes in the sediments of the record Co1305 likely derived from land plants, so that these compounds can be interpreted as characteristic biomarkers of the terrestrial vegetation (e.g. Eglinton and Hamilton, 1967; Volkman et al., 1998).

Mostly identical $\Delta^{14}\text{C}$ values of co-occurring *n*-C₂₆ fatty acids and *n*-C_{27–33} alkanes (fig. 4.4) support a common, probably exclusive terrigenous origin of these biomarkers in the investigated coastal marine setting of LJL. Moreover, *n*-C₂₆ fatty acids and *n*-C_{27–33} alkanes not only reveal similar radiocarbon inventories but also a systematically higher depletion in ¹⁴C than *n*-C₁₆ fatty acids or *n*-C₂₂ alcohols of the respective sample depths. This indicates that large proportions of "pre-aged" material might contribute to the sedimentary pools of *n*-C₂₆ fatty acids and *n*-C_{27–33} alkanes.

Marine Biomarker Sources: The ocean around South Georgia is generally highly productive and has rich ecosystems (Borrione and Schlitzer, 2013), characterized by phytoplankton, zooplankton and vertebrate predators (Atkinson et al., 2001). However, strong seasonal gradients in environmental conditions (e.g. sea-ice, light availability, temperature and salinity), common for high-latitude coastal ecosystems, can cause a high variability in the marine productivity as well as a succession in the community structure (Juul-Pedersen et al., 2015). Large phytoplankton blooms that often occur around South Georgia are the main drivers of primary production in this area (Borrione and Schlitzer, 2013), while ice-algae may have seasonal importance (Juul-Pedersen et al., 2015). Small dinoflagellates and diatoms (*Thalassionema* sp.) were found to dominate in the composition of phytoplankton near the northern coast of South Georgia during austral summer (Ward et al., 2005). Besides of phytoplankton, zooplankton produces as well a high amount of biomass around South Georgia, which is 4-5 times larger than the average of the Southern Ocean (Atkinson et al., 2001). Antarctic krill seems to be a dominant species of the zooplankton (Young et al., 2014), although South Georgia, being mostly free of pack-ice, is no typical habitat for krill, a species of the seasonal ice-zone (Atkinson et al., 2001). Different copepod species were

observed to substantially contribute as well to the diversity of zooplankton at the northern coast of the island (Ward et al., 2008).

LMW biomarkers like n -C₁₆ fatty acids are generally considered to mainly originate from phytoplankton in most sedimentary archives (e.g. Volkman et al., 1998). Actually, dominant proportions of n -C₁₆ fatty acids were detected in a multitude of marine phytoplankton species (Ackman, 1989), but apparently, n -C₁₆ fatty acids also dominate in the lipid composition of Antarctic krill around South Georgia (Fricke et al., 1984; Cripps et al., 1999; Phleger et al., 2002; Ju and Harvey, 2004), as well as in several copepod species (Albers et al., 1996; Kattner et al., 2003). Therefore, it can be assumed that n -C₁₆ fatty acids might characterize the majority of the marine biomass in the investigated setting, including phytoplankton as well as zooplankton.

High abundances of n -C₁₆ fatty acids in all analyzed plant samples (fig. 4.6) illustrate that this unspecific biomarker is generally produced by all organisms (e.g. Meyers, 1997), including marine as well as terrigenous species. However, fast remineralization of these labile compounds commonly precludes that large fractions of land-derived n -C₁₆ fatty acids can survive lateral transport (Eglinton and Hamilton, 1967). Therefore, sedimentary n -C₁₆ fatty acids can generally be considered to more strongly reflect inputs from the overlying water column (Mollenhauer and Eglinton, 2007).

A predominantly marine origin of n -C₁₆ fatty acids in the sedimentary record of LJJ is likely supported by $\Delta^{14}\text{C}$ values of these compounds that are generally higher than those of co-occurring terrigenous biomarkers (fig. 4.4). The substantial ^{14}C depletion of terrigenous biomarkers in the record can probably be attributed to the retention of land-derived organic matter prior to deposition. n -C₁₆ fatty acids, being relatively more enriched in ^{14}C , therefore seem to unlikely include large proportions of terrigenous biomass but rather to reflect a more recent production and rapid turnover of these compounds. Assuming that marine organic matter probably experienced faster sedimentation than terrigenous material, n -C₁₆ fatty acids can likely be expected to have mainly derived from autochthonous production in the marine inlet.

Considering that autochthonous biomass can possibly be affected by particularly high marine reservoir ages of 700 to 1,300 years in sub-Antarctic regions (Berkman and Forman, 1996), it seems that "pre-aging" of terrigenous organic matter even exceeds the (possibly high) reservoir age of marine organic matter at the study site.

Interestingly, not only n -C₁₆ fatty acids but also n -C₂₂ alcohols are relatively enriched in ^{14}C , compared to the co-occurring terrigenous biomarkers (fig. 4.4). This indicates that n -C₂₂ alcohols in the sediments of LJJ probably derived from mainly marine source organisms as well. This find is surprising, because n -C₂₂ alcohols are often generally attributed to terrigenous sources in the literature (e.g. Meyers, 1997; Volkman et al., 1998).

Marine sources of n -C₂₂ alcohols were investigated only in a few studies, since these compounds are more unusual biomarkers of marine organisms. Anyhow, they were found to be related to macrophyte brownalgae like sea-grass (*Zostera muelleri*) (Johns et al., 1980) or to seagrass-associated algal epiphytes (Jaffé et al., 2001) as well as to cyanobacteria (Filley

et al., 2001).

In lacustrine settings, n -C₂₂ alcohols were found to be mainly derived from submerged or floating macrophytes (Ficken et al., 1998b, 2002). A strong predominance of n -C₂₂ alcohols was also reported for freshwater microalgae (*Eustigmatophytes sp.*) (Volkman et al., 1998). The high concentration of n -C₂₂ alcohols in the lowermost biomarker sample of the Co1305 record (fig. 4.5) might indicate, that such freshwater microalgae were pioneer species in the sedimentary stage of the record that predates the beginning of lacustrine sedimentation.

Reports of marine eustigmatophytes are sparse (Rampen et al., 2014) and even if the abundances of unsaturated alcohols in these species were investigated (Volkman et al., 1992; Méjanelle et al., 2003), there is apparently no data available that reveals the saturated alcohol composition of marine eustigmatophytes. Therefore, the potential role of these species as sources of n -C₂₂ alcohols in the setting of LJJ cannot be evaluated.

It seems that despite of the common, probably mainly marine origin of n -C₁₆ fatty acids and n -C₂₂ alcohols, which is indicated by the relatively enriched $\Delta^{14}\text{C}$ values of these compounds, source organisms of these biomarkers differ. Where n -C₁₆ fatty acids likely derived from most autochthonous species, n -C₂₂ alcohols might have their origin in marine macrophytes. Based on the relatively small abundances of n -C₂₂ alcohols in the analyzed kelp sample (fig. 4.6), this species would not necessarily be considered as main source of these biomarkers. Nevertheless, macrophyte brown algae seem to be a plausible sources of n -C₂₂ alcohols, since kelp is a dominant species of the intertidal waters of the Southern Ocean, producing immense quantities of biomass around South Georgia (Fraser et al., 2009), (fig. 4.7). Several macrofossils of kelp that were recovered from the sediments of LJJ (details in chapter 6), moreover document the presences of kelp in the marine inlet of LJJ.



Figure 4.7: Left: Kelp near to the coast, Middle: Tussock grass stands, Right: Moss bank. Photos by M. Leng and O. Bennike

Mixing of Organic Matter in the Sediments: Organic matter, containing the same compounds, is mostly supplied from multiple sources and via different transport pathways to the sedimentary site (Kusch et al., 2016). Whereas HMW n -fatty acids and n -alkanes seem to originate from sources on land, and n -C₁₆ fatty acids and n -C₂₂ alcohols mainly from marine biomass, the origins of n -C₂₆ alcohols in the sediments of LJJ are more unclear. Like other HMW biomarkers, n -C₂₆ alcohols are often generally attributed to terrigenous

sources (e.g. Volkman et al., 1998; Pancost and Boot, 2004). Distributions of *n*-alcohols in contemporary plants reveal a clear predominance and a high concentration of *n*-C₂₆ alcohols in the grass sample as well as a considerable proportion in the moss sample (fig. 4.6). The proportion of *n*-C₂₆ in the alcohol spectrum of the kelp is similar to that of *n*-C₂₂.

Assuming that kelp is a common marine source of both *n*-C₂₂ and *n*-C₂₆ alcohols, differences in the radiocarbon inventories of these biomarkers may reflect contributions of biomass derived from tussock grass, since this species reveals a clear predominance of *n*-C₂₆ but only a small proportion of *n*-C₂₂ alcohols. Variable mixing proportions of marine and terrigenous sources of *n*-C₂₆ alcohols are likely indicated by $\Delta^{14}\text{C}$ values that are similar to those of *n*-C₁₆ fatty acids and *n*-C₂₂ at 4-9 cm and at 988-991 cm core depth, but differing from those of *n*-C₁₆ fatty acids at 468-473 cm depth (fig. 4.4).

Variable mixing of organic matter from different sources in the sediments of LJJ is also indicated by the radiocarbon inventories of TOC. At 103-108 cm, where a large proportion of marine organic matter is indicated by high concentrations of *n*-C₁₆ fatty acids in the sediments (fig. 4.5), TOC exhibits a $\Delta^{14}\text{C}$ value that likely mainly reflects mixing of marine and terrigenous organic matter (fig. 4.4). At most other depths, TOC reveals a stronger depletion in ¹⁴C than all analyzed biomarkers. This might point to additional, more refractory or "pre-aged" sources of organic matter in the sediments, possibly derived from older soils or petrogenic material. Correlation of low $\Delta^{14}\text{C}$ values of TOC with high IRD concentrations (fig. 4.5 and fig. 4.4) may indicate that glacial activity has a considerable impact on the supply of ¹⁴C-depleted organic material to the site of LJJ .

4.4.2 Processes Explaining Biomarker Distributions and ¹⁴C Variability in the record Co1305

Retention of Organic Matter in Intermediate Reservoirs: Since terrestrial plants metabolize CO₂ from the atmosphere, any deviation of the terrigenous compounds from the atmospheric ¹⁴C signature can be attributed to their retention in intermediate reservoirs, like soils and peat (Kusch et al., 2010b). The degree of ¹⁴C depletion that terrigenous biomarkers exhibit at the time of deposition, therefore, depends on the time lag between production and burial of these compounds (Eglinton et al., 1997).

Several factors can control the terrestrial residence time of individual biomarkers. These factors comprise intrinsic properties of the respective compounds, like molecular structure and size, polarity, reactivity and mineral association, as well as environmental factors like climatic conditions, including temperature, precipitation and wind intensity, catchment size and morphology, as well as drainage regimes and soil characteristics (Hedges et al., 1997; Trumbore, 1997, 2009; Raymond and Bauer, 2001; Drenzek et al., 2007; Mollenhauer and Eglinton, 2007; Douglas et al., 2014).

The potential of individual biomarkers to escape remineralization during retention and on the pathway to a sedimentary site is mainly determined by the reactivity of the compounds

and their physical protection (Eglinton and Hamilton, 1967; Hedges et al., 1997; Mollenhauer and Eglinton, 2007; Drenzek et al., 2007; Kusch et al., 2010b). An important factor determining the intrinsic reactivity of individual biomarkers is their molecular structure. With decreasing chain lengths, reactivities of the compounds generally increase (e.g. Drenzek et al., 2007). Fast remineralization of reactive biomarkers, such as LMW *n*-fatty acids, restricts their potential of "aging" and results in generally young biomarker pools (Kusch et al., 2016). In contrast, relatively low reactivities of HMW biomarkers enhance their potential of preservation during storage and transport on land. At the time of deposition, these biomarkers are therefore more likely "pre-aged", since most durable compounds possibly have already survived a long period of intermediate storage before they reached the sedimentary site (Eglinton et al., 1997; Drenzek et al., 2007; Kusch et al., 2010a, 2016). Association of organic matter with a mineral matrix is generally assumed to further increase the probability of its preservation (Eglinton and Hamilton, 1967; Sun and Wakeham, 1994; Canuel and Martens, 1996; Hedges et al., 1997; Mollenhauer and Eglinton, 2007).

Climatic conditions are the most fundamental environmental factors for the storage of organic matter, since plant production and heterotrophic decomposition are both mainly forced by temperature and precipitation. A strong dependence between soil organic carbon turnover and climate conditions is given, with fast turnover in warm and dry climates and slow turnover in cool and wet environments (Trumbore, 1993; Mollenhauer and Eglinton, 2007; Tao et al., 2015). The climate of South Georgia, characterized by cool and moist conditions, therefore probably favors generally low rates of remineralization and by that the accumulation and retention of organic matter in terrestrial reservoirs. Delayed supply of land-derived organic matter into LJJ is likely reflected by sedimentary *n*-C₂₆ fatty acids and *n*-C_{27–33} alkanes that are generally depleted in ¹⁴C (fig. 4.4).

However, the general conformity of $\Delta^{14}\text{C}$ values of co-occurring *n*-C₂₆ fatty acids and *n*-C_{27–33} alkanes in the sedimentary record Co1305 (fig. 4.4) appears counter-intuitive, since intrinsic reactivities of these individual terrigenous biomarkers differ. HMW *n*-alkanes have particularly low reactivities, allowing even petrogenic contributions to the sedimentary biomarker pools (Ishiwatari et al., 1994), whereas HMW *n*-fatty acids, being relatively more reactive, can be expected to be free of any contribution from petrogenic sources (Mollenhauer and Eglinton, 2007). In accordance to the differing "aging potential" of these biomarkers, HMW *n*-alkanes were found to be more strongly depleted in ¹⁴C than co-occurring HMW *n*-fatty acids in some marine environments (Pearson et al., 2001; Kusch et al., 2010b).

Similar $\Delta^{14}\text{C}$ values of co-occurring *n*-C₂₆ fatty acids and *n*-C_{27–33} alkanes indicate minor contributions of petrogenic *n*-C_{27–33} alkanes to the sediments of LJJ. Instead, considerable fractions of both sedimentary biomarker pools possibly derived from common sources on land and experienced similar processes during their pathway to the depositional site. In order to explain the likely common fate of *n*-C₂₆ fatty acids and *n*-C_{27–33} alkanes, it might be assumed that large proportions of these biomarkers were contemporarily introduced to the site as components of particulate organic matter (POM), namely of plant debris. Contributions of finer material, such as dissolved organic matter (DOM), are probably secondary since

DOM mostly integrates differentially aged biomarkers from more complex sources (Raymond and Bauer, 2001; Blair et al., 2003). An additional argument against the transport of biomarkers as components of DOM is that recurring sorption and desorption processes in subsurface soils would have likely further increased the heterogeneity of the biomarker pools over time (Blair and Aller, 2012). Plant debris as a major source of n -C₂₆ fatty acids and n -C_{27–33} alkanes in the sediments of LJL was possibly mainly derived from soil surfaces rather than from erosion of different soil horizons. Biomarker ages are considered to generally increase with soil depth (Douglas et al., 2014), so that, even if assuming similar pre-aging of n -C₂₆ fatty acids and n -C_{27–33} alkanes in individual plant particles, mixing of plant debris from heterogenous soils would have unlikely resulted in similar $\Delta^{14}\text{C}$ values of the co-occurring compounds, since concentrations of these biomarkers likely differ considerably.

It has been observed that plant debris constitutes a significant fraction of the total soil organic matter in Arctic environments and is therefore an important source of allochthonous OC in marine sediments of these regions (Tesi et al., 2016). Preservation of organic matter in form of plant debris may also be favored in the sub-Antarctic region of South Georgia, since climatic conditions and vegetation types are similar to those of the Arctic. The vegetation in high-latitude environments is composed of plant types like mosses, lichen and evergreen plants, which contain low concentrations of soluble carbohydrates (Hobbie et al., 2000), preventing fast degradation of the biomass. Heterotrophic decomposition is additionally inhibited by cold temperatures in these regions. Intermediate storage of organic matter in soils and peats, which are possibly characterized by water logging or anaerobic conditions, may additionally favor the preservation of plant debris on land.

Long residence times of plant debris on land are indicated by ^{14}C depleted n -C₂₆ fatty acids and n -C_{27–33} alkanes in the sediments. The mountainous catchment of LJL and the high precipitation on South Georgia may generally promote fluvial erosion and transport. However, plant debris hydrologically behaves like sand. Therefore, the capacity of fluvial processes to mobilize it is may limited (Goñi et al., 1998; Bianchi et al., 2002; Wakeham and Canuel, 2016). Moreover, plant tissue probably needs long time to decompose to an extent so that the critical mass (size and the density of the particles) is reached to be mobilized by water.

Besides of the similarities of $\Delta^{14}\text{C}$ values of co-occurring terrigenous biomarkers in the respective samples of the record Co1305, the decrease of radiocarbon concentrations of n -C₂₆ fatty acids and n -C_{27–33} alkanes with depth is also remarkably uniform. Constantly decreasing $\Delta^{14}\text{C}$ values may imply relatively invariable source compositions and transport mechanisms over time and might additionally point to only small influences of variable environmental conditions on the residence time of these biomarkers on land. Erosion and mixing of old and heterogenous soils, as suggested for high energy drainage regimes, resulting from steep reliefs (Raymond and Bauer, 2001), is not indicated in the investigated environment. Assuming a vital role of the mass of the plant debris for its transport, a constant decomposition rate over time may explain the relatively constant terrestrial residence

time throughout the record. The deviation of $\Delta^{14}\text{C}$ values in the uppermost sample from this general trend (fig. 4.4) can most likely be attributed to the effect of bomb ^{14}C rather than to shorter retention of organic matter in recent times.

Post-Depositional Processes: Despite of their likely common sources and fates on land, distributions of $n\text{-C}_{26}$ fatty acids and $n\text{-C}_{27-33}$ alkanes in the sediments of LJL differ, particularly in the upper part of the record (fig. 4.5). Diverging abundances of these biomarkers possibly result from changes in the composition of the terrestrial vegetation over time. But more likely, they indicate that terrigenous biomarker records not only reflect productivity on land but also variable impacts of post-depositional diagenetic alteration in the sediments (Meyers, 1997).

It is well known that diagenetical behaviors of biomarkers differ. Degradation of individual compounds is particularly active in surface sediments. Their concentrations decrease at compound-specific rates and asymptotically approach a more or less stable background value. However, quantitative relations between burial efficiency and redox conditions for different biomarkers remain unclear (Meyers, 1997; Wakeham et al., 1997; Zonneveld et al., 2010).

Since HMW n -fatty acids are inherently more prone to degradation than HMW n -alkanes, ratios of HMW n -fatty acids and HMW n -alkanes can be used as an indicator of sedimentary redox conditions (Cacho et al., 2000; Vonk et al., 2010). The underlying assumption for such ratios is that both biomarkers derive from a common terrestrial source where the ratio is fixed at some constant value. The ratio of $n\text{-C}_{26}$ fatty acids and $n\text{-C}_{29}$ alkanes ($n\text{-C}_{29}$ is the most abundant HMW n -alkane in the tussock grass as well as the moss sample) was calculated in order to trace preservation conditions in the sediments of LJL (fig. 4.8). Since $n\text{-C}_{26}$ fatty acids have greater sensitivity to degradation than $n\text{-C}_{29}$ alkanes, biomarker ratios decrease when degradation is enhanced in the sediments e.g. by more oxic conditions, and vice versa.

Co-variation of $n\text{-C}_{26}$ fatty acid and $n\text{-C}_{29}$ alkane abundances up to c. 3.5 m core depth (fig. 4.5) result in quite constant ratios, which may indicate relatively invariable redox conditions in the lower part of the record (fig. 4.8). Preservation of both biomarkers is possibly mainly determined by the correlation between the rate of sediment accumulation and burial efficiency of organic matter (Müller and Suess, 1979). Climate-driven changes in depositional conditions under which the material is buried can alter the degree of preservation of sedimentary components (Mollenhauer and Eglinton, 2007). Above 3.5 m core depth, more variable biomarker ratios may result because of such changes. Particularly severe degradation is indicated between c. 250 and 350 cm and between 4 and 70 cm core depth (fig. 4.8). Distributions of $n\text{-C}_{16}$ and $n\text{-C}_{26}$ fatty acids are more similar throughout the entire record (fig. 4.9), although chain lengths as well as main sources of these biomarkers differ. LMW n -fatty acids are more reactive than their HMW homologues (Drenzek et al., 2007), resulting in a decomposition rate of $n\text{-C}_{16}$ fatty acids which is 10 times higher during sinking than that of $n\text{-C}_{30}$ fatty acids (Meyers and Ishiwatari, 1993). Therefore it can be assumed

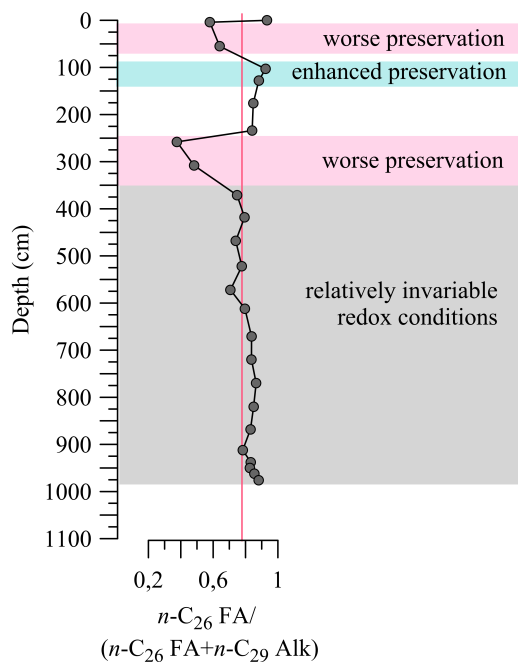


Figure 4.8: Ratio of n -C₂₆ fatty acid and n -C₂₉ alkane abundances for the marine Unit IV of the core Co1305 against depth. Red line marks the mean value of the ratio.

that LMW n -fatty acids also lose higher absolute amounts of their compounds during post-depositional degradation. However, despite of possibly differing rates of remineralization, good correlation ($r^2=0.75$, excluding the samples at 103 cm depth) of n -C₁₆ and n -C₂₆ fatty acid abundances indicates that under variable redox condition in the sediments, inherent diagenetical behaviors of biomarkers from the same lipid class are more similar than of biomarkers with similar chain-lengths (e.g n -C₂₆ fatty acids vs. n -C₂₉ alkanes).

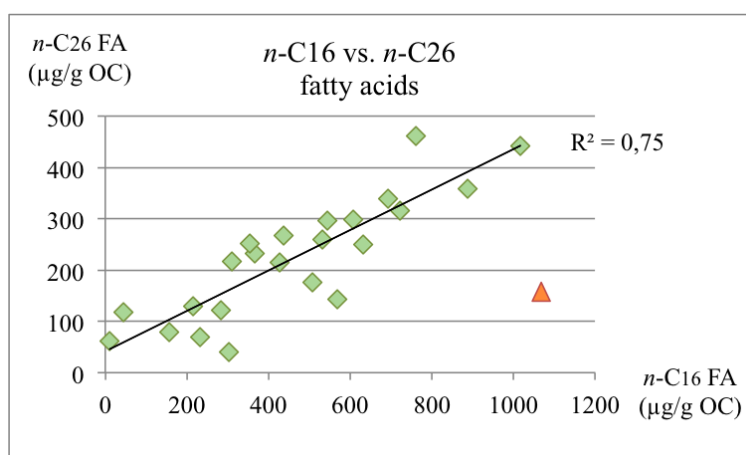


Figure 4.9: Correlation of n -C₁₆ and n -C₂₆ fatty acid abundances in the record Co1305. Correlation coefficient of the data points (green diamonds): $r^2=0.75$. Data point at 103 cm core depth (orange triangle) is deviating from the linear regression.

Preferential Preservation of Allochthonous over Autochthonous Biomarkers

n -C₁₆ Fatty acids and n -C₂₂ alcohols in the sedimentary record of LJJ were considered to mainly originate from autochthonous productivity. However, relatively short distances between source areas of these biomarkers on land and the coastal marine depositional site probably favor distinct allochthonous contributions to the respective sedimentary biomarker pools.

Proportions of land-derived n -C₁₆ fatty acids and of n -C₂₂ alcohols in the sediments are likely related to the intrinsic reactivities of these biomarkers. Whereas fast remineralization of highly reactive n -C₁₆ fatty acids possibly results in relatively small terrigenous contributions, lower reactivities of n -C₂₂ alcohols might allow larger proportions of land-derived compounds in the sediments.

However, post-depositional processes may alter initial marine and terrigenous proportions of n -C₁₆ fatty acids and n -C₂₂ alcohols over time, at likely different rates. It was observed that the general loss of LMW n -fatty acids in sediments is associated with a depletion in ¹³C, indicating increasing terrigenous proportions with depth. Preferential preservation of terrigenous compounds over their marine counterparts likely results because of the persisting physical protection of labile allochthonous biomarkers, which only escaped remineralization on land, because of their association to mineral matrices (Cranwell, 1981; Sun and Wakeham, 1994; Canuel and Martens, 1996; Goñi et al., 1998; Hedges et al., 1999; Ingalls et al., 2004; Mollenhauer and Eglinton, 2007; Zonneveld et al., 2010; Blair and Aller, 2012).

Differing post-depositional alteration of initial proportions of n -C₁₆ fatty acids and n -C₂₂ alcohols is likely indicated by the relation between their $\Delta^{14}\text{C}$ values. At 308-313 cm core depth, n -C₂₂ alcohols are more depleted in ¹⁴C than co-occurring n -C₁₆ fatty acids (fig. 4.10). With depth, a shift in $\Delta^{14}\text{C}$ values towards relatively stronger ¹⁴C depletion of n -C₁₆ fatty acids likely indicates that preferential preservation of terrigenous biomarkers changes initial compositions of n -C₁₆ fatty acids to a higher extent than that of n -C₂₂ alcohols. Besides of the apparently generally differing loss rates of autochthonous fractions of these biomarkers, variable preservation conditions in the sediments may also affect their respective degree of alteration. Moreover, it has to be considered that initial mixing proportions of marine and land-derived biomarkers can vary over time because of changes in marine productivity and terrigenous supply.

Temporal Variability of Marine Reservoir Ages in Little Jason Lagoon: The surface ocean is the interface between the deeper ocean and the atmosphere. The spatial and temporal variability of the surface ocean reservoir age is mainly determined by the effects of upwelling of deep waters (low ¹⁴C activity) and biologically driven draw-down of atmospheric CO₂ (high ¹⁴C activity) into the surface ocean (Eglinton et al., 1997).

Exchange with the open ocean has probably an important impact on the marine reservoir age in the setting of LJJ. However, in this coastal marine environment additional effects may influence the reservoir age variability of the DIC pool. Changes in phytoplankton productivity, community structure, and vertical distribution related to wind-driven upwelling

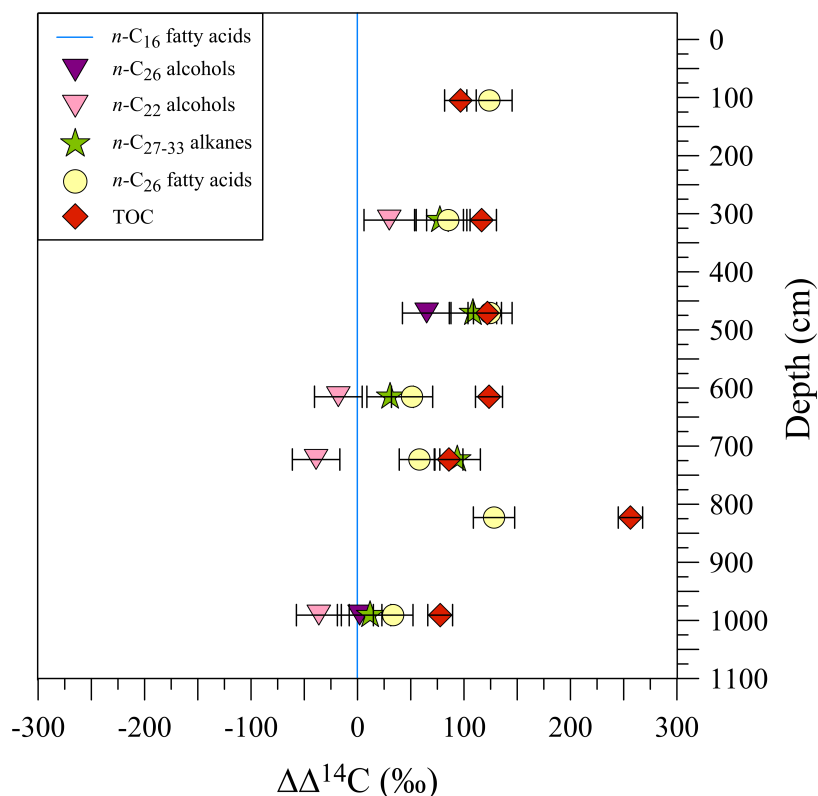


Figure 4.10: $\Delta^{14}\text{C}$ (‰) offsets of $n\text{-C}_{27-33}$ alkanes, $n\text{-C}_{22}$ alcohols, $n\text{-C}_{26}$ alcohols, $n\text{-C}_{26}$ fatty acids, TOC in reference to $n\text{-C}_{16}$ fatty acids (blue line). Error bars display the sum of the propagated uncertainties of the respective samples and $n\text{-C}_{16}$ fatty acids.

and mixing of the water column (Eglinton et al., 1997) might cause a stronger seasonal variation in LJJ than in the open ocean. Moreover, supply of carbon-containing material from land might affect the variability of surface ocean reservoir ages in this setting. Freshwater inflow into the coastal marine inlet, derived from rain or melting snow may introduce a less depleted ^{14}C signature to the site. A temporal variability can therefore result from seasonality effects e.g. snow melt events.

Several studies have shown that glaciers can introduce large amounts of carbon to the marine environment (Hood et al., 2009; Singer et al., 2012; Bhatia et al., 2013; Spencer et al., 2014). Sources of this carbon are included in the melting ice or can be derived from the sediments and the bedrock underneath the glaciers. Melting ice exports dissolved organic and inorganic carbon (DOC and DIC) to the ocean. Erosion of the glacier bed also introduces DOC and DIC, but mostly particulate organic carbon (POC). Investigations of glacier exported POC and DOC showed that ^{14}C depleted organic carbon is generally associated to POC, whereas DOC contains relatively enriched organic carbon (Raymond and Bauer, 2001; Goni et al., 2005; Bhatia et al., 2013; Marwick et al., 2015).

Correlation of ^{14}C depleted TOC with high IRD concentrations (fig. 4.4 and 4.5) may reflect large fractions of ^{14}C -depleted POC that were mobilized by glacier erosion. Assuming that POC cannot be remineralized efficiently during sinking, marine organisms are probably not

affected by its ^{14}C -depleted signature to a high extent. However, if DIC and DOC which was contained in the ice is contemporary introduced to the site, marine organic matter may exhibit particularly higher $\Delta^{14}\text{C}$ values than TOC in the respective sediment depths. The relatively enriched ^{14}C signature of $n\text{-C}_{16}$ fatty acids at 823 cm core depth, in contrast to the relatively depleted ^{14}C signature of TOC, may indicate that glaciers introduced both depleted POC and enriched DOC.

4.5 Interpretation

4.5.1 Evaluation of Depositional Processes in the Course of the Sedimentation History of Little Jason Lagoon

In the analyzed depths of the record Co1305, variable processes have apparently affected the composition and the radiocarbon inventories of biomarkers in the sediments.

4-9 cm: A generally stronger ^{14}C depletion of sedimentary $n\text{-C}_{26}$ fatty acids and $n\text{-C}_{27-33}$ alkanes in contrast to co-occurring $n\text{-C}_{16}$ fatty acids and $n\text{-C}_{22}$ alcohols is revealed in most analyzed samples, clearly indicating long residence times of the terrigenous biomarkers on land. However, $n\text{-C}_{26}$ fatty acids, $n\text{-C}_{27-33}$ alkanes and $n\text{-C}_{22}$ alcohols reveal more similar $\Delta^{14}\text{C}$ values (fig. 4.4). This unlikely points to a faster transport of the organic matter in recent times but rather to bomb ^{14}C , contained in the terrigenous biomass. The relatively more enriched $\Delta^{14}\text{C}$ value of the $n\text{-C}_{26}$ alcohols, in contrast to that of $n\text{-C}_{22}$ alcohols, supports the suggestion of an influence of bomb ^{14}C in the uppermost sample depth. Assuming that both $n\text{-C}_{22}$ alcohols and $n\text{-C}_{26}$ alcohols contain the same contributions from marine sources (presumably from marine macrophytes), the differing radiocarbon inventories of these biomarkers may be explained by high contributions of $n\text{-C}_{26}$ alcohols from tussock grass, a species that revealed only minor proportions of $n\text{-C}_{22}$ alcohols.

103-108 cm: The sediments at 103-108 cm core depth are apparently characterized by high proportions of marine biomass, indicated by highest concentrations of $n\text{-C}_{16}$ fatty acids and generally low abundances of HMW terrigenous biomarkers (4.5). The suggestion of enhanced marine productivity is supported by the deviation of the $n\text{-C}_{16}$ fatty acid concentration from the general co-variation with $n\text{-C}_{26}$ fatty acids towards higher values (fig. 4.9) and by relatively ^{14}C enriched TOC (fig. 4.4). Good preservation conditions in the sediments, indicated by the ratio of $n\text{-C}_{26}$ fatty acids and $n\text{-C}_{29}$ alkanes (fig. 4.8), might have resulted from the high rate of sediment accumulation at that time.

A possible environmental scenario that may have led to this configuration involves unfavorable climatic conditions and sea-ice: Low abundances of terrigenous biomarkers in the sediments may have been caused by low terrestrial productivity due to harsh climatic conditions as well as by hampered input of terrigenous organic matter to the depositional site because of sea-ice. Intense marine productivity and good preservation of the marine biomass

possibly resulted from relatively short events of large phytoplankton blooms in the summer months that may have alternated with a persistent ice-cover on the inlet during the rest of the year. The ice could have diminished the ventilation of the water in the inlet, resulting in lower oxygen levels in the water column and/or at the sediment surface. Enhanced preservation of the marine organic matter in the sediments may result from these conditions. However, high primary production and high sedimentation rates are likely to have a greater influence on the preservations of n -C₁₆ fatty acids in the sediments.

It can be expected that large marine productivity has led to high initial proportions of marine n -C₁₆ fatty acids in the sediments and good preservation conditions may have prevented a significant post-depositional alteration of the initial source composition. Therefore, the $\Delta^{14}\text{C}$ value of n -C₁₆ fatty acids at this depth might reflect the radiocarbon inventory of the marine biomass most accurately in the record.

308-313 cm: The ratio of n -C₂₆ fatty acids and n -C₂₉ alkanes at 308-313 cm core depths clearly points to particularly bad preservation conditions in the sediments (fig. 4.8). It can thus be expected that selective loss of autochthonous n -C₁₆ fatty acids is particularly severe and the relative contribution of allochthonous n -C₁₆ fatty acids therefore quite high at this depth. That is probably even the case unless n -C₁₆ fatty acids are more enriched in ¹⁴C than co-occurring n -C₂₂ alcohols (fig. 4.10), which were assumed to contain initially higher terrigenous proportions.

468-474 cm: n -C₁₆ fatty acids at 468-474 cm core depth seem to be relatively enriched in ¹⁴C, comparing their $\Delta^{14}\text{C}$ values to the samples above and below (fig. 4.4). Relatively small amounts of highly "pre-aged" material in the sediments are indicated by a $\Delta^{14}\text{C}$ value of TOC similar to that of n -C₂₆ fatty acids and n -C₂₇₋₃₃ alkanes at this depth. Low IRD concentrations support a minor input of organic carbon with low ¹⁴C activities from glacier erosion (4.5).

612-617 cm: The low $\Delta^{14}\text{C}$ value of TOC at 612-617 cm core depth coincides with a short period of high IRD concentrations in the record (fig. 4.4 and 4.5). However, since n -C₁₆ fatty acids and n -C₂₂ alcohols are also quite depleted in ¹⁴C, IRD might have not derived from melting glaciers in the catchment of LJL but rather from sea-ice. Other than glaciers, that can export huge quantities of fresh water (potentially relatively enriched in ¹⁴C) due to persistent melting of their ice, the potential of sea-ice is relatively restricted in this regard. Contrary, sea-ice possibly hampers the CO₂ exchange between water and atmosphere and therefore leads to an increasing reservoir age of the surface water mass. Consumption of relatively depleted DIC by marine organisms may then potentially have resulted in relatively low $\Delta^{14}\text{C}$ values of n -C₁₆ fatty acids and n -C₂₂ alcohols at this depth

720-724 cm: An exception to the good agreement between n -C₂₇₋₃₃ n -alkanes and n -C₂₆ fatty acids is displayed at 720-724 cm core depth, with lower $\Delta^{14}\text{C}$ for n -C₂₇₋₃₃ n -alkanes

than for n -C₂₆ fatty acids (fig. 4.4). The combination of n -alkanes of longer chain lengths (n -C₃₁ and n -C₃₃) compared to other sample depths (tab. 4.1) most likely causes this deviation, since intrinsic reactivities of compounds decrease with increasing chain length. However, relatively more depleted n -C₃₃ alkanes may also indicate a differing source composition of this biomarker. Distributions of n -alkanes in the analyzed contemporary plant species reveal that n -C₃₃ alkanes are more characteristic for moss than for grass (fig.4.6). If decomposition and/or transport proceeds more slowly for moss than for the grass, the higher proportion of moss derived n -C₃₃ n -alkanes in the sample may be reflected in the depleted $\Delta^{14}\text{C}$ signature of the n -C_{27–33} n -alkanes at this depth.

n -C₁₆ fatty acids are considerably more depleted in ^{14}C than n -C₂₂ alcohols at 720-724 cm core depth (fig. 4.10). Preservation conditions in the sediments are apparently not particularly bad (fig. 4.8), indicating that the depletion of n -C₁₆ fatty acids might mainly have resulted from the persistently higher loss rate of autochthonous compounds over time, compared to n -C₂₂ alcohols.

820-850 cm: A particularly low $\Delta^{14}\text{C}$ value of TOC indicates high contributions of ^{14}C -depleted material to the sediments between 820 and 850 cm core depth (fig. 4.4). Massive glacier activity, likely indicated by high IRD concentrations (4.5), potentially caused large supply of ^{14}C depleted POC from erosional products to the site. However, the relatively high $\Delta^{14}\text{C}$ value of n -C₁₆ fatty acids at this depth likely indicates that high amounts of melting ice have caused a large input of relatively enriched DIC (from gas inside the ice) and DOC (formed by microbes inside the ice)(Bhatia et al., 2013), which may have lowered local marine reservoir age at this time.

The large difference between the depleted $\Delta^{14}\text{C}$ value of TOC and the relatively enriched $\Delta^{14}\text{C}$ value of n -C₁₆ fatty acids may reflect the contrasting effects of the simultaneous introduction of depleted POC and the enriched DOC and/or DIC to the site.

988-992 cm: Allochthonous proportions are probably above average for both n -C₁₆ fatty acids and n -C₂₂ alcohols at 988–991 cm core depth, since inflow of ocean water during marine transgression has likely introduced distinct amounts of terrigenous biomarkers to the sediments. $\Delta^{14}\text{C}$ values of n -C₁₆ fatty acids and n -C₂₂ alcohols, similar to those of the terrigenous biomarkers, are caused by the enhanced terrigenous supply or possibly reflect a strong alteration of the initial biomarker composition over time. However, the effect of higher proportions of "pre-aged" terrigenous organic matter on the $\Delta^{14}\text{C}$ values of n -C₁₆ fatty acids and n -C₂₂ alcohols is possibly partly compensated by lower reservoir ages at that time, resulting from the mixing of fresh water and ocean water during transgression.

4.5.2 Considerations for Sediment Chronologies

In order to develop sediment chronologies for Antarctic marine records, n -C₁₆ fatty acids were already successfully applied as alternative material to TOC (e.g Ohkouchi, 2003).

However, in coastal marine settings like that of LJJ, allochthonous contributions of n -C₁₆ fatty acids need to be considered, likely introducing a more depleted radiocarbon signature to the sedimentary biomarker pool. Selective preservation of these land-derived fractions in the sediments can further cause an increasing deviation of n -C₁₆ fatty acid ages from the sediment formation age with depth. The relation between $\Delta^{14}\text{C}$ values of n -C₁₆ fatty acids and n -C₂₂ alcohols in the record of LJJ revealed that post-depositional alteration of the composition of n -C₂₂ alcohols likely happens at lower rates than for n -C₁₆ fatty acids. Therefore, it seems advantageous to combine n -C₁₆ fatty acid and n -C₂₂ alcohol ages, in order to enhance the accuracy in the sediment chronology of the record of LJJ. However, variable marine reservoir ages and differing preservation conditions in the course of the sedimentary record also affect the potential of these biomarkers to yield reliable estimates of the time of sediment formation. Particular core depths, which can be assumed to be influenced by such processes are marked in fig. 4.11. Ages of n -C₁₆ fatty acids and of n -C₂₂ alcohols from these depth possibly need to be excluded from chronological applications.

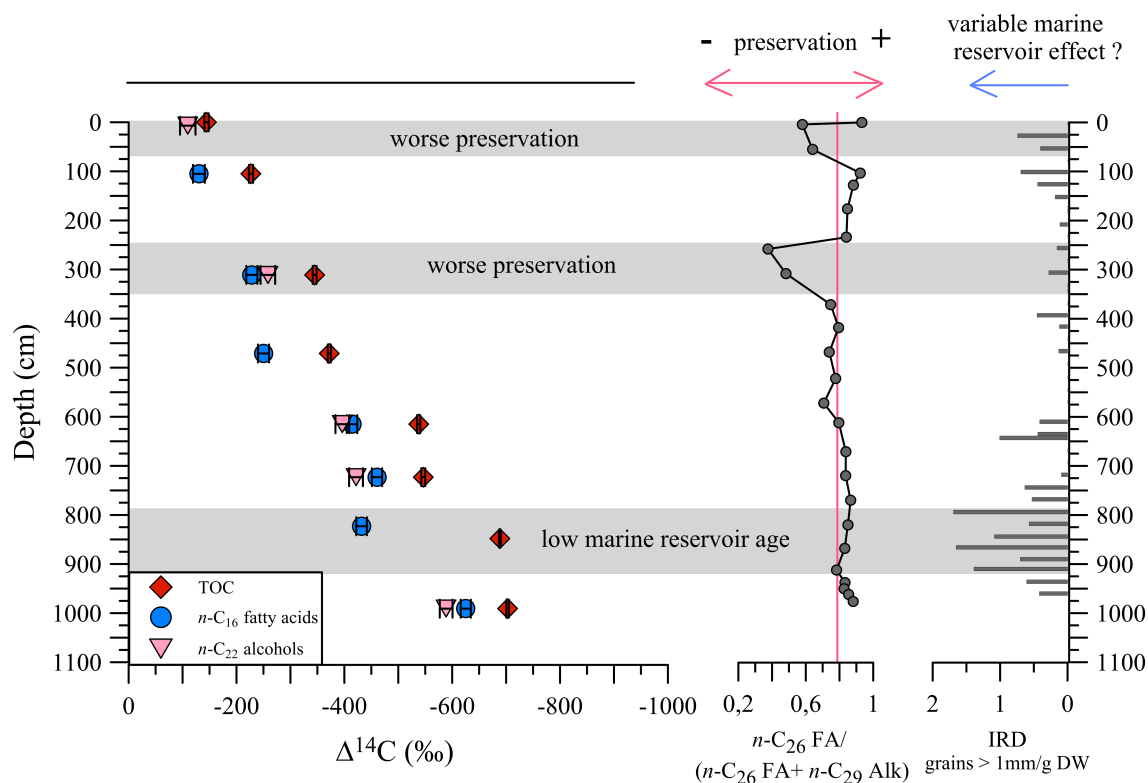


Figure 4.11: On the left-hand side: $\Delta^{14}\text{C}$ (‰) of n -C₂₂ alcohols, n -C₁₆ fatty acids and TOC, in the middle: Ratio of n -C₂₆ fatty acids and n -C₂₉ alkanes, on the right-hand side: IRD concentrations. Grey bars indicate considerable effects of preservation conditions (derived from the ratio of n -C₂₆ fatty acids and n -C₂₉ alkanes) and of possibly variable marine reservoir ages (derived from IRD concentrations) on $\Delta^{14}\text{C}$ of n -C₂₂ alcohols and n -C₁₆ fatty acids

4.5.3 Considerations for Paleoenvironmental Reconstructions

Ubiquitously produced *n*-fatty acids are usually the most abundant lipids in aquatic sediments (Volkman et al., 1998). Therefore, even in settings that are characterized by very low sedimentary TOC concentrations, they can often be detected. However, the interpretation of *n*-fatty acid records in terms of changes in paleo-productivity might be complicated by post-depositional diagenetic alterations of initial biomarker concentrations and proportions. It can be expected that concentrations of all *n*-fatty acids are generally decreasing with depth, as a result of their persistent decomposition over time. However, rates of decomposition strongly differ for individual compounds, so that proportions of different biomarkers are likely changing as well. Preferential degradation of more labile LMW *n*-fatty acids of mostly marine origin in the sediments can therefore lead to overestimating the importance of terrigenous contributions in the record (Meyers, 2003). In addition to the diagenetic alteration of *n*-fatty acid distributions that relies on differing intrinsic reactivities of individual compounds, depositional conditions at the sedimentary site can also modulate the degree of their preservation (Sinninghe Damsté et al., 2002).

Changing redox conditions in the course of the sedimentation history in LJJ are indicated by variable ratios of *n*-C₂₆ fatty acids and *n*-C₂₉ alkanes, particularly in the upper part of the record (fig. 4.8). It seems that LMW *n*-fatty acids as well as HMW *n*-fatty acids are subject to variable diagenetic impacts in distinct phases of the record, so that confident reconstructions of changes in terrigenous or marine productivity cannot be derived from *n*-fatty acid in the setting of LJJ.

HMW *n*-alcohols, like other HMW compounds, are often generally attributed to more or less exclusive terrigenous sources (e.g Volkman et al., 1998). CSRA revealed that *n*-C₂₆ *n*-alcohols in the sediments of LJJ unlikely derived exclusively from terrigenous sources. Therefore, records of *n*-C₂₆ *n*-alcohols cannot be interpreted in terms of terrigenous productivity in the investigated setting but they rather reflect mixing of terrigenous and marine sources.

n-Alkanes are highly resistant to post-depositional diagenetic alteration (e.g Cranwell, 1981) and are therefore often used as proxy to reconstruct paleoenvironmental changes i.e. terrigenous productivity (e.g Ishiwatari et al., 1994). Variable petrogenic contributions of *n*-alkanes can potentially bias vegetation-related signals. Investigation of radiocarbon inventories of *n*-C_{27–33} alkanes and *n*-C₂₆ fatty acids revealed that only minor contributions of petrogenic *n*-alkanes can be expected in the setting of LJJ. It is therefore likely that the *n*-C_{27–33} alkane record traces environmental changes on land most accurately at the study site.

Although *n*-C_{27–33} alkane records seem to be valuable for detecting environmental changes, long time lags between synthesis of plant waxes and their deposition can complicate the interpretation of the records at a high temporal resolution. In accordance to Douglas et al. (2014), it seems therefore imperative to use CSRA sites specifically for testing and resolving such complications.

4.6 Conclusion

CSRA is a powerful tool to trace sources of biomarkers and biogeochemical processes in the setting of LJJ. The generally stronger ^{14}C depletion of $n\text{-C}_{26}$ fatty acids and $n\text{-C}_{27-33}$ alkanes in contrast to co-occurring $n\text{-C}_{22}$ alcohols and $n\text{-C}_{16}$ fatty acids has revealed that transport of $n\text{-C}_{26}$ fatty acids and $n\text{-C}_{27-33}$ alkanes to the sedimentary site is delayed. Faster sedimentation of $n\text{-C}_{22}$ alcohols and $n\text{-C}_{16}$ fatty acids indicates that these biomarkers were mainly produced in the water column, whereas $n\text{-C}_{26}$ fatty acids and $n\text{-C}_{27-33}$ alkanes were derived from terrigenous sources and were stored in intermediate reservoirs prior to deposition. The good matches between radiocarbon inventories of co-occurring $n\text{-C}_{26}$ fatty acids and $n\text{-C}_{27-33}$ alkanes are interpreted as indicator for a common transport mechanism, possibly to the introduction of these biomarkers as constituents of plant debris to the site. Differing distributions of HMW n -fatty acids and HMW n -alkanes revealed variable preservation conditions in the sedimentary record. It seems that HMW n -fatty acid records can be strongly altered due to post-depositional diagenetic processes, so that interpretations of these records in terms of changes in productivity are possibly misleading. HMW n -alkanes seem to trace changes of terrestrial productivity most accurately in this setting, since they are recalcitrant to degradation and since very minor contributions of petrogenic n -alkanes do not alter their concentrations in the sediments to a high extent.

The differences between $\Delta^{14}\text{C}$ values of co-occurring $n\text{-C}_{16}$ fatty acids and $n\text{-C}_{22}$ alcohols indicates variable proportions of marine and terrigenous homologues in the respective sedimentary biomarker pools. It seems that inherent diagenetical behaviors of these biomarkers cause initially higher terrigenous contributions of $n\text{-C}_{22}$ alcohols in the sediments compared to relatively lower land-derived proportions of $n\text{-C}_{16}$ fatty acids. The preferential loss of marine homologues in the sediments however seems to result in increasing terrigenous proportions of $n\text{-C}_{16}$ fatty acids with depth. Relatively more ^{14}C -enriched $n\text{-C}_{22}$ alcohols in deeper sediments therefore potentially better reflect the radiocarbon signature of marine biomass than $n\text{-C}_{16}$ fatty acids.

In order to establish a sediment chronology for the record Co1305, it seems advantageous to combine age information derived from $n\text{-C}_{16}$ fatty acids and from $n\text{-C}_{22}$ alcohols. Possibly varying marine reservoir effects were encountered based on the radiocarbon inventories of $n\text{-C}_{16}$ fatty acids, $n\text{-C}_{22}$ alcohols and TOC in the respective depths together with information of IRD concentrations in the record.

An important finding of this study is that sources of HMW n -alcohols (C_{22} to C_{28}) cannot simply be derived from the chain lengths of these biomarkers, as is commonly assumed when HMW biomarkers are ascribed to terrigenous origins. Therefore, it is crucial before interpreting biomarker data in a paleoenvironmental context to first investigate biomarker sources for each site specifically so that possibly inappropriate allocations of biomarkers to generalized sources can be prevented.

Chapter 5

Disentangling Lateral Age Distribution of Surface Sediments in different Aquatic Environments of South Georgia by Quantification of OC Sources

5.1 Introduction

Several studies revealed that surface sediments of the Southern Ocean often provide radiocarbon ages that exceed marine reservoir ages by hundreds to thousands of years (Gordon and Harkness, 1992; Andrews et al., 1999; Domack et al., 1989; Licht et al., 1998; Ohkouchi, 2003; Ohkouchi and Eglinton, 2008). This reflects the in some cases considerable and spatially highly variable proportion of organic carbon with high or infinite ^{14}C ages, that is sourced from erosion and re-deposition of older land-derived sediments. Site-specific influences on the amount of ^{14}C -free ancient OC can depend for example on sediment accumulation rates and style of deposition. But it has been shown that one major variable, determining bulk sediment ages, is the source of OC (Andrews et al., 1999).

Input of ancient OC is common at sedimentary sites where glaciers erode the bedrock of the catchment (Smith et al., 2015). The shales and greywackes of the Cumberland series (Gregory, 1915) are potential sources of ancient OC in the Cumberland Bay area of South Georgia. Contributions of ^{14}C -depleted OC to the sediments of Little Jason Lagoon are already indicated by TOC ages that exceed the "pre-aged" terrigenous biomarker ages in several depths of the record Co1305 (chapter 4). Highest deviations between TOC and biomarker ages have been found to coincide with phases of high IRD input, pointing to enhanced glacial activity in the watershed of the marine inlet or to the presence of sea-ice. Today, glaciers are retreated from the catchment of Little Jason Lagoon as well as from the

catchment of Allen Lake A (White et al., 2018), so that surface sediments can be expected to lack in OC that is supplied by land-based glaciers. In contrast, the Cumberland Bay fjord system is characterized by several tidewater glaciers, which have the potential to introduce high amounts of allochthonous ^{14}C -depleted organic matter to the sedimentary sites. However, besides of potentially variable ancient OC contributions to the sediments of the different aquatic environments, proportions of autochthonous organic matter (aquatic OC) and of allochthonous plant and soil derived organic matter (terrigenous OC) may also vary, since contrasting water and catchment properties characterize the different settings.

In order to derive information on the impact of these OC sources in surface sediments of the different aquatic environments of the Cumberland Bay area, radiocarbon mass balance calculations can be applied, with aquatic, terrigenous and ancient OC as endmembers. Biomarker ratios of HMW ($n\text{-C}_{26}$, $n\text{-C}_{28}$, $n\text{-C}_{30}$) and LMW ($n\text{-C}_{14}$, $n\text{-C}_{16}$, $n\text{-C}_{18}$) fatty acids as well as of brGDGTs and crenarchaeol can be used to estimate proportional relations between aquatic and terrigenous organic matter in the sediments.

$\Delta^{14}\text{C}$ values for the aquatic, terrigenous and ancient endmembers can be approximated as follows: The ancient endmember can be assumed to consist only of organic matter that is radiocarbon dead, so that $\Delta^{14}\text{C}_{\text{ancient}}$ can be defined as -1000‰ . Results of the radiocarbon analyses of $n\text{-C}_{26}$ fatty acids from the near surface and of a carbonate shell from the surface of the core Co1305 from LJJ (chapter 4 and chapter 6), give best approximations of $\Delta^{14}\text{C}_{\text{terrigenous}}$ and $\Delta^{14}\text{C}_{\text{aquatic}}$ for this environment, with values of -110 and -93‰ , respectively. However, smaller fractions of bomb ^{14}C can possibly be expected in the uppermost 2 cm of the core than in 4-9 cm depth, where the analyzed $n\text{-C}_{26}$ fatty acids come from. To account for this possibility, the range of $\Delta^{14}\text{C}_{\text{terrigenous}}$ can be defined from -110 to -264‰ for the setting of LJJ. -264‰ corresponds to a mean residence time of organic matter in terrestrial reservoirs of 2,400 years. This maximum time of intermediate storage is derived from radiocarbon ages of $n\text{-C}_{26}$ fatty acids in the following analyzed depth (103-108 cm) of the LJJ record, where no influence of bomb ^{14}C is given (details in chapter 6).

For the fjord and off-shore sites, values of $\Delta^{14}\text{C}_{\text{terrigenous}}$ and $\Delta^{14}\text{C}_{\text{aquatic}}$ may be different from those of LJJ. Variable accumulation rates may result in surface sediments that possibly integrate longer or shorter time intervals of sediment formation, and therefore larger or smaller fractions of bomb ^{14}C . The distance of most fjord and off-shore sites to major supply areas on land is greater than for the sites of the marine inlet. The longer transport pathways might promote higher proportions of more refractory ^{14}C -depleted terrigenous organic matter in the surface sediments at these sites. Additionally, it has to be considered that aeolian transport may account for a larger part of land-derived material in the fjord and off-shore environments. The introduced radiocarbon signatures of wind-transported terrigenous organic matter can be relatively enriched in ^{14}C if the material derived from abrasion of plant surfaces, or relatively depleted in ^{14}C if it derived from exposed soils in the catchment. To include all the various possibilities, a range of 0 to -358‰ (0 - 3,500 years) for $\Delta^{14}\text{C}_{\text{terrigenous}}$ can be employed for the fjord and off-shore sites.

$\Delta^{14}\text{C}_{\text{aquatic}}$, particularly at the sites of Cumberland East Bay, may be similar to the values

expected for LJL, since exchange of water is given between these two aquatic environments. However, it has to be considered that marine terminating glaciers likely also introduce ^{14}C -depleted as well as ^{14}C -enriched DIC and DOC to the ocean (chapter 4), that can be incorporated by marine organisms. Moreover, for the fjord but particularly for the off-shore site, mixing with the open ocean surface water is possibly better than in LJL. To account for these possible effects at the fjord and off-shore sites, a range of -56 to -156‰ can be determined for $\Delta^{14}\text{C}_{\text{aquatic}}$. The value of -156‰ corresponds to the highest observed marine reservoir age of 1,300 years for the Southern Ocean (Berkman and Forman, 1996). -56 ‰ represents the global mean marine reservoir age of 400 years. This small value should cover the possibility that inflow of melting ice, that is in good exchange with the atmosphere, locally lowers the marine reservoir age substantially.

For the ALA site, the young TOC age of only 275 ^{14}C years sets the limits for possible $\Delta^{14}\text{C}_{\text{terrigenous}}$ and $\Delta^{14}\text{C}_{\text{aquatic}}$ values. Since input of "pre-aged" terrigenous material is most certainly given and since high concentrations of HMW *n*-fatty acids and of brGDGTs point to a large amount of terrigenous organic matter in the sediments, a lacustrine reservoir effect can very likely be excluded to contribute to the age of the TOC. Therefore, $\Delta^{14}\text{C}_{\text{aquatic}}$ can be defined as 0‰. With $\Delta^{14}\text{C}_{\text{aquatic}} = 0‰$, a maximum proportion of aquatic organic matter derived from *n*-fatty acids ratios, and a proportion of ancient OC > 0%, the maximum value for $\Delta^{14}\text{C}_{\text{terrigenous}}$ is -70‰ for the lacustrine site.

5.2 Samples and Methods

5.2.1 Sediment Samples

Sediment samples from 12 sediment cores, that were retrieved within the fjords of Cumberland West and East Bays, at an off-shore site, in Little Jason Lagoon (LJL) and in Allen Lake A (ALA), were analyzed (fig. 5.1, tab. 5.1). Coring at the fjord and the off-shore sites was conducted with gravity and multi corer. Sediment cores from LJL and from ALA were taken with gravity corer and a percussion piston corer from a floating platform (Bohrmann, 2013). The uppermost two cm of the sediment cores of the sites PS81/258 and PS81/259, located in Cumberland West Bay, PS81/260 and PS81/262 of Cumberland East Bay, Co1302, Co1303, Co1304 and Co1305 of Little Jason Lagoon and Co1308 in Allen Lake A, were subsampled for further analyses. From the sediment cores of the sites PS81/284 of Cumberland West Bay and of site PS81/283 of Cumberland East Bay, subsamples were taken from 5-6 and 1-2 cm core depth, respectively. The amounts of all analyzed sediment samples range between 1.4 g to 53.4 g.

5.2.2 High Performance Liquid Chromatography

Lipid biomarker extraction, separation into polarity fractions and quantification of *n*-fatty acids was described in chapter 4. Prior to the measurement of GDGTs, a GDGT standard

(C₄₆) (Huguet et al., 2006) was admixed to the ether fraction of the biomarker samples. The ether fraction was then filtered over PTFE filters (0,45 μ m x 4mm) using 1 ml of hexane:isopropanol (95:5,v:v). GDGTs were analyzed using an Agilent 1290 UHPLC connected to an Agilent 6460 QQQ equipped with an APCI ion source following the method of (Schouten et al., 2007). GDGTs were analyzed in SIM mode and quantified according to (Huguet et al., 2006).

5.2.3 Radiocarbon Analysis

Pre-treatment and ¹⁴C measurement of bulk sediment samples as well as conversion of fMC data to $\Delta^{14}\text{C}$ values and ¹⁴C ages was performed similarly as described in chapter 4.

5.2.4 Elemental Analysis

Elemental analyses of total nitrogen (TN) and total sulphur (TS) were conducted on ground aliquots of sediment samples with a Vario Micro Cube combustion elemental analyzer (Elementar Corp.). On parallel samples, total carbon (TC) and total inorganic carbon (TIC) contents were measured with a DIMATOC 2000 (Dimatec Corp.). Total organic carbon (TOC) was quantified from the difference between TC and TIC.

5.2.5 Determination of Distances between Sedimentary Sites and Major Supply Areas on Land

The distance between the respective sites and the main input pathway for land-derived organic matter was determined using the Google Earth measuring tool (Google Earth, 2013). The major sources of terrigenous supply in Cumberland East and West Bays are assumed to be the marine terminating glaciers. The distance between the glacier front of the Norden-skjöld glacier and respective sites of Cumberland East Bay, as well as between the glacier front of the Neumayer glacier and the respective sites in Cumberland West Bay, were therefore determined. For the off-shore site (PS81/280), the distance to the closest shore of the island was considered. Unfortunately, the major input pathways into LJL and the circulation patterns within the marine inlet are not clear. It was assumed that a small stream, entering the marine inlet on the western side, provides largest supply of allochthonous organic matter to the sites Co1302, Co1303 and Co1305. Therefore, the distances between the stream and these sites were considered. For the site Co1304, surface run-off derived from the proximal eastern shore of the inlet was assumed to deliver largest parts of land derived organic matter to the site. For the ALA site, the distance to the shore of the hillside of the catchment was determined.

5.2.6 #Ringstetra Index

For the estimation of the influence of *in situ* production of brGDGTs in the water column or in the sediments, the weighted average number of cyclopentane moieties was calculated

for the tetramethylated brGDGTs, according to Sinninghe Damsté (2016), as follows:

$$\#Ringstetra = ([Ib] + 2 * [Ic]) / ([Ia] + [Ib] + [Ic]) . \quad (5.1)$$

Roman numerals refer to brGDGT structures (fig. 2.1).

When $\#Ringstetra > 0.7$, other sources than soil must also contribute to the brGDGTs in the sediments (Sinninghe Damsté, 2016).

5.2.7 Three Endmember $\Delta^{14}\text{C}$ Mass Balances

In order to quantify the contributions of terrigenous, aquatic and ancient endmembers to the various sedimentary environments, a simple ternary mixing model was employed:

$$\Delta^{14}C_{TOC} = x * \Delta^{14}C_{terrigenous} + y * \Delta^{14}C_{aquatic} + (1 - x - y)\Delta^{14}C_{ancient} \quad (5.2)$$

The model is based on $\Delta^{14}\text{C}$ values of TOC and defined minimum and maximum $\Delta^{14}\text{C}$ values of each of the endmembers. The mixing model is further constrained by the ratio of aquatic and terrigenous OC derived from *n*-fatty acids and GDGTs, respectively (Eq. 5.3 and 5.4):

$$\frac{x}{(x + y)} = \frac{\text{HMW } n\text{-fatty acids}}{(\text{HMW } n\text{-fatty acids} + \text{LMW } n\text{-fatty acids})} , \quad (5.3)$$

or

$$\frac{x}{(x + y)} = \frac{(\text{brGDGTs})}{(\text{brGDGTs} + \text{Crenarchaeol})} . \quad (5.4)$$

Computations were performed for each sample with $x/(x + y)$ of *n*-fatty acids and $x/(x + y)$ of GDGTs, respectively. The $\Delta^{14}\text{C}$ values of the aquatic and terrigenous endmembers were varied, and combination of maximum and minimum of each were employed.

5.3 Results

5.3.1 Lateral Distribution of TOC Concentrations and Radiocarbon Ages

TOC concentrations are generally low (0.41 to 0.81%) in the surface sediments of the fjord and off-shore sites (fig. 5.2 B). In the setting of LJJ, surface sediments contain 2.82 - 3.03% of TOC. Particularly high TOC concentration of 12.42% are displayed at the lacustrine site of ALA.

TOC ages also strongly differ between the different aquatic environments. For the fjord and

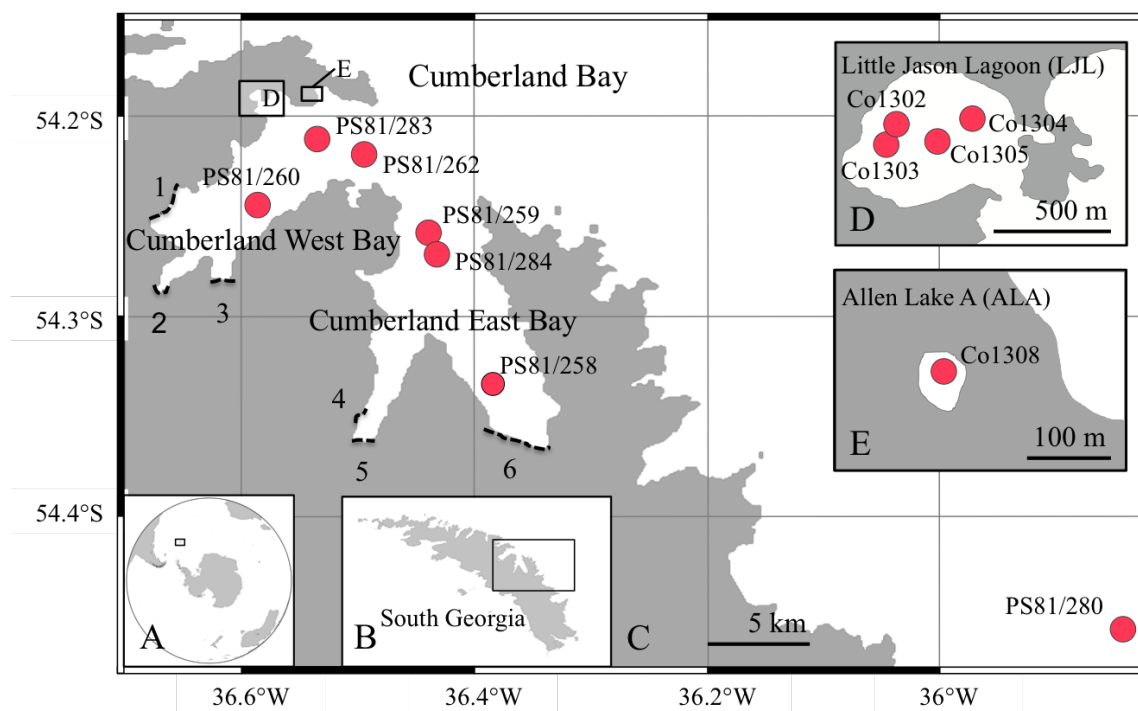


Figure 5.1: Location maps of the study sites: Red dots indicate the coring locations. (A) position of South Georgia in the sub-Antarctic. (B) Study area on the island of South Georgia. (C) Sites of Cumberland West and East Bays and off-shore site. Dashed lines mark the calving fronts of glaciers entering the fjords, 1: Neumayer, 2: Geikie, 3: Lyell, 4: Hamberg, 5: Harker, 6: Nordenskjöld. (D) Sites of the marine inlet, Little Jason Lagoon. (E) Site of Allen Lake A.

Table 5.1: Overview of the coring locations of the investigated environments with their respective coordinates, coring devices that were used to retrieve the sediment cores at these sites: piston percussion corer (PC), gravity corer (GC), multi corer (MUC) and characteristics of the coring locations, including water depth [m] and distance to the main supply area of land derived organic matter [m].

Environment	Coring Location	Latitude South	Longitude East	Coring Device	Water Depth [m]	Distance [m]
Allen Lake	Co1308	54.192000°	36.544750°	PC	1.1	80
	Co1302	54.191667°	36.594300°	GC	15.7	100
Little Jason Lagoon	Co1303	54.192467°	36.594967°	GC	15.8	100
	Co1304	54.192583°	36.588683°	GC	15.7	160
	Co1305	54.192800°	36.591150°	GC	15.8	290
Cumberland West Bay	PS81/258	54.337000°	36.388833°	MUC	178	3,600
	PS81/259	54.261333°	36.437667°	MUC	262	13,800
	PS81/284	54.265167°	36.437167°	GC	259	13,700
Cumberland East Bay	PS81/260	54.246667°	36.582167°	MUC	216	12,300
	PS81/262	54.224833°	36.511833°	MUC	234	18,000
	PS81/283	54.215333°	36.538000°	GC	193	16,200
Off-Shore Site	PS81/280	54.457333°	35.842500°	MUC	237	20,300

Table 5.2: Coring locations of the investigated environments, surface sediment ages and biomarker concentrations in surface sediments

Environment	Site	TOC age ¹⁴ C years	HMW FA [$\mu\text{g/g OC}$]	LMW FA [$\mu\text{g/g OC}$]	brGDGT [$\mu\text{g/g OC}$]	Cren [$\mu\text{g/g OC}$]
Allen Lake	Co1308	273 \pm 37	2471	2806	65.2	0.05
	Co1302	1128 \pm 35	1441	11019	10.4	0.32
Little Jason Lagoon	Co1303	1148 \pm 36	1267	5544	8.5	0.6
	Co1304	1183 \pm 35	657	4719	5.7	0.4
	Co1305	1192 \pm 35	863	3644	1.5	0.3
Cumberland West Bay	PS81/258	8212 \pm 52	419	2071	27.4	546.4
	PS81/259	5154 \pm 46	281	2460	7.3	181.5
	PS81/284	3525 \pm 36	32	423	0.7	12.6
Cumberland East Bay	PS81/260	9911 \pm 65	221	3219	11.8	163.2
	PS81/262	4387 \pm 43	273	2213	8.7	244.5
	PS81/283	12411 \pm 52	30	300	0.6	12.6
Off-Shore Site	PS81/280	2019 \pm 39	84	721	6.3	186.4

the off-shore sites, surface sediment ages range between 2,020 ¹⁴C years at the off-shore site and 12,400 ¹⁴C years at site PS81/283 (fig. 5.2 A). Surface sediments of LJL display a uniform distribution of ages between 1,130 and 1,180 ¹⁴C years. The lacustrine site reveals the youngest sediment age (275 ¹⁴C years) of the investigated aquatic environments.

5.3.2 Lateral Distribution of Sedimentary Biomarkers

Aquatic Biomarkers - LMW *n*-fatty acids and Crenarchaeol: LMW *n*-fatty acids and crenarchaeol are present in all investigated environments (fjord, off-shore, inlet and lacustrine environments). Concentrations of LMW *n*-fatty acids are relatively high at all sites but especially in the surface sediments of LJL, with concentrations of 3,644 to 11,019 $\mu\text{g/g OC}$ (fig. 5.2 C). At the fjord and off-shore sites, concentrations of LMW *n*-fatty acids vary between 300 and 3,219 $\mu\text{g/g OC}$. Sediments of the ALA site display a concentration of LMW *n*-fatty acids of 2,805 $\mu\text{g/g OC}$.

Crenarchaeol has highest absolute abundances at the fjord and off-shore sites (12.6 to 546 $\mu\text{g/g OC}$), excluding site PS81/283, where concentrations of just 0.58 $\mu\text{g/g OC}$ were detected (fig. 5.2 D). Concentrations of crenarchaeol range between 0.26 and 0.56 $\mu\text{g/g OC}$ at the LJL sites. In surface sediments of ALA, crenarchaeol is much less abundant (0.05 $\mu\text{g/g OC}$) than at all other sites.

The highest fractional abundances of both aquatic biomarkers are revealed at the fjord and off-shore sites (fig. 5.2 G,H).

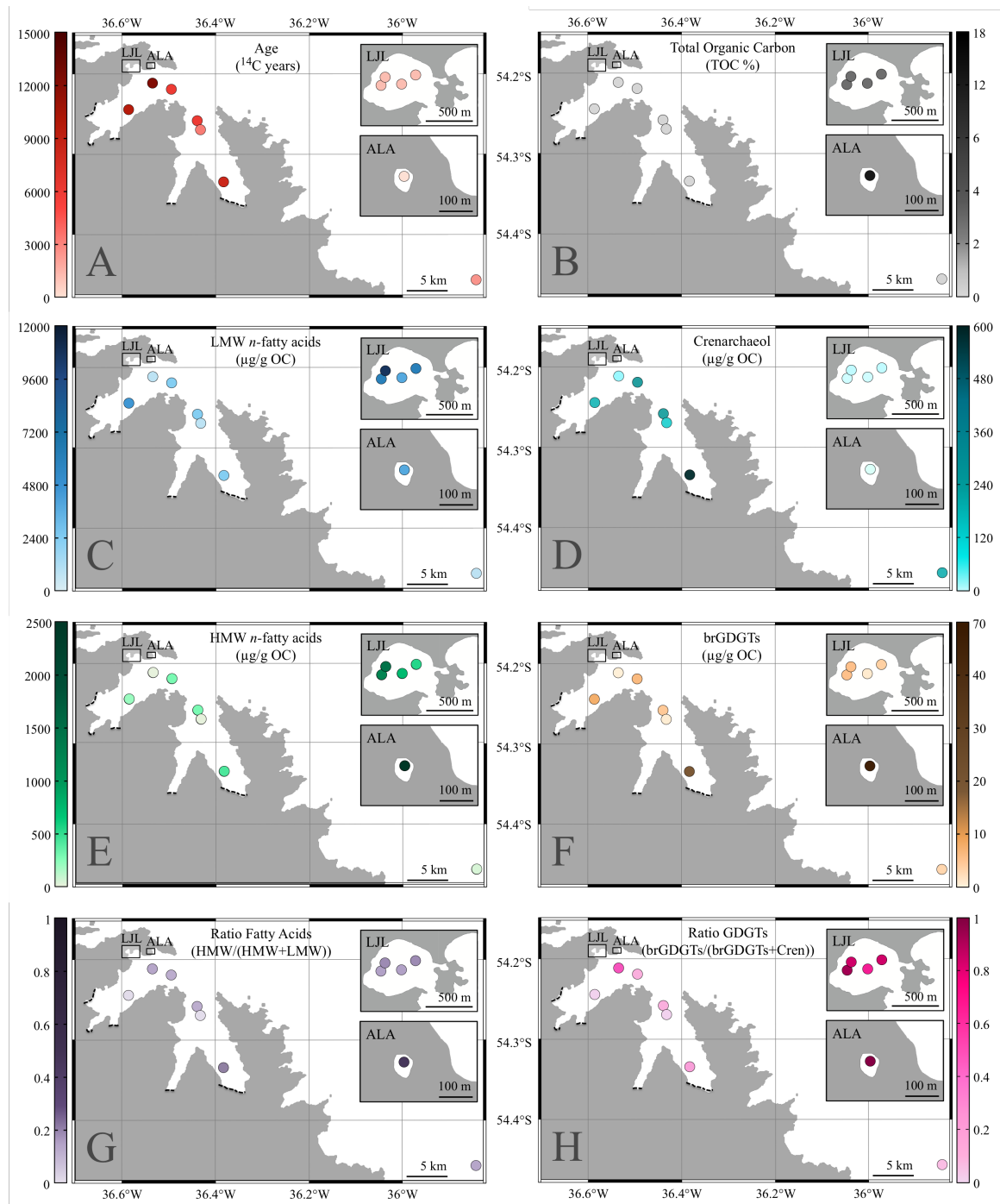


Figure 5.2: Distribution of (A) surface sediment ages in ^{14}C years BP, (B) content of organic carbon in %, (C) concentration of LMW *n*-fatty acids in $\mu\text{g/g OC}$, (D) concentration of crenarchaeol in $\mu\text{g/g OC}$, (E) concentration of HMW *n*-fatty acids in $\mu\text{g/g OC}$, (F) concentration of brGDGTs in $\mu\text{g/g OC}$, (G) ratios of *n*-fatty acids: Proportion of HMW *n*-fatty acids normalized to the sum of HMW and LMW *n*-fatty acids, (H) ratios of GDGTs: Proportion of brGDGTs normalized to the sum of brGDGTs and crenarchaeol.

Terrigenous Biomarkers - HMW *n*-fatty acids and brGDGTs: HMW *n*-fatty acids and brGDGTs were detected in all sediment samples. Particularly high concentrations of HMW *n*-fatty acids (2,471 $\mu\text{g/g OC}$) and of brGDGTs (65.2 $\mu\text{g/g OC}$) occur in the surface sediments of the ALA site (fig. 5.2E, F). A relatively high brGDGTs concentration of 27.4 $\mu\text{g/g OC}$ is also displayed at the fjord site PS81/258. All other marine sites (fjord, off-shore and inlet sites) reveal similarly low abundances of brGDGTs, between 0.7 and 11.7 $\mu\text{g/g OC}$.

In contrast, concentrations of HMW *n*-fatty acids are generally higher at the LJL sites (863-1,441 $\mu\text{g/g OC}$) than at the fjord and off-shore sites (30.4 - 418 $\mu\text{g/g OC}$).

5.3.3 Proportions of Terrigenous, Aquatic and Ancient OC in Surface Sediments of Different Aquatic Environments

Results of the three endmember isotopic mass-balance calculations are displayed in tab. 5.3, including all combinations of minimum and maximum $\Delta^{14}\text{C}$ values for the terrigenous and the aquatic endmembers as well as ratios of these endmembers derived from *n*-fatty acid and GDGT ratios. In order to prevent that proportions of ancient OC < 0% result for the sites of LJL and ALA when GDGT ratios are applied in the calculations, maximum $\Delta^{14}\text{C}$ values of the terrigenous endmember needed to be modified. Maximum $\Delta^{14}\text{C}_{\text{terrigenous}}$ values of -139 were determined for the LJL sites and of -40 for the ALA site.

Ternary mixing plots (fig. 5.3) illustrate that the small difference between minimum and maximum values of $\Delta^{14}\text{C}_{\text{terrigenous}}$, results in a low variability within the obtained OC proportions of the LJL and the ALA sites. More variable OC proportions result from the variation of biomarker ratios in these setting.

For the sites of LJL, employment of *n*-fatty acid ratios in the calculations results in ancient OC proportions of 1.7 to 5.4%, terrigenous OC proportions of 11 to 18.7% and aquatic OC proportions of 76.5 to 85.9%. Based on GDGT ratios, ancient OC proportions of 0.04 to 4.2%, terrigenous OC proportions of 81.2 to 93.9% and aquatic OC proportions of 2.9 to 14.6% are obtained for the LJL sites.

For the ALA site, combinations including *n*-fatty acid ratios yield ancient OC proportions of 0.01 to 4%, terrigenous OC proportions of 54.8 to 57% and aquatic OC proportions of 41.2 to 43%. For GDGT ratios, calculations obtain proportions of 0 to 4% of ancient OC, 96-100% of terrigenous OC and 0% of aquatic OC.

For fjord and the off-shore settings, neither biomarker ratios nor endmember $\Delta^{14}\text{C}$ values vary the obtained OC proportions at the respective sites substantially. However, between the sites, highly variable contributions of OC sources are indicated. The different combinations of endmember $\Delta^{14}\text{C}$ values and biomarker ratios mostly result in smallest proportions of terrigenous OC, with values between 1.8 and 14.9%, for all distributions. The obtained

Table 5.3: Input parameters and results of ^{14}C mass balance calculations: Input parameters employed for calculations are written in italics. Results of the calculations are written in regular font. When two $\Delta^{14}\text{C}$ values are listed in one row, the first was applied for calculation including n -fatty acids ratios and the second for calculations including GDGT ratios. Resulting proportions for all combinations of $\Delta^{14}\text{C}$ values together with n -fatty acid ratios are displayed in columns 6-8 and together with GDGT ratios in columns 9-11.

Station	<i>Input Parameters</i>				Results based on <i>n</i> -Fatty Acid Ratios			Results based on GDGT Ratios		
	$\Delta^{14}\text{C}$ (‰)		<i>Ratios</i>		Terr.	Anc.	Aqua.	Terr.	Anc.	Aqua.
	<i>Terr.</i>	<i>Aqua.</i>	<i>FA</i>	<i>GDGT</i>	(%)	(%)	(%)	(%)	(%)	(%)
PS81/258	<i>0</i>	<i>-56</i>	<i>0.17</i>	<i>0.05</i>	6.2	62.5	31.3	1.9	62.3	35.8
	<i>0</i>	<i>-156</i>	<i>0.17</i>	<i>0.05</i>	6.8	58.9	34.3	2.1	58.1	39.8
	<i>-264</i>	<i>-56</i>	<i>0.17</i>	<i>0.05</i>	6.6	60.1	33.4	1.9	61.6	36.5
	<i>-264</i>	<i>-156</i>	<i>0.17</i>	<i>0.05</i>	7.2	56.0	36.8	2.1	57.2	40.7
PS81/259	<i>0</i>	<i>-56</i>	<i>0.10</i>	<i>0.04</i>	5.5	45.0	49.5	2.2	44.8	53.0
	<i>0</i>	<i>-156</i>	<i>0.10</i>	<i>0.04</i>	6.1	39.3	54.7	2.5	38.6	58.9
	<i>-264</i>	<i>-56</i>	<i>0.10</i>	<i>0.04</i>	5.7	42.9	51.4	2.2	44.0	53.8
	<i>-264</i>	<i>-156</i>	<i>0.10</i>	<i>0.04</i>	6.3	36.6	57.0	2.5	37.6	59.9
PS81/260	<i>0</i>	<i>-56</i>	<i>0.06</i>	<i>0.07</i>	1.9	69.5	28.6	2.1	69.5	28.4
	<i>0</i>	<i>-156</i>	<i>0.06</i>	<i>0.07</i>	2.1	66.1	31.8	2.4	66.2	31.4
	<i>-264</i>	<i>-56</i>	<i>0.06</i>	<i>0.07</i>	1.9	68.8	29.3	2.2	68.7	29.1
	<i>-264</i>	<i>-156</i>	<i>0.06</i>	<i>0.07</i>	2.2	65.2	32.6	2.4	65.2	32.4
PS81/262	<i>0</i>	<i>-56</i>	<i>0.11</i>	<i>0.03</i>	6.4	39.6	54.0	1.8	39.3	58.9
	<i>0</i>	<i>-156</i>	<i>0.11</i>	<i>0.03</i>	7.1	33.3	59.6	2.0	32.4	65.6
	<i>-264</i>	<i>-56</i>	<i>0.11</i>	<i>0.03</i>	6.7	37.1	55.2	1.8	38.6	59.6
	<i>-264</i>	<i>-156</i>	<i>0.11</i>	<i>0.03</i>	7.4	30.2	62.4	2.1	31.5	66.4
PS81/280	<i>0</i>	<i>-56</i>	<i>0.10</i>	<i>0.03</i>	8.2	18.7	73.0	2.4	18.4	79.2
	<i>0</i>	<i>-156</i>	<i>0.10</i>	<i>0.03</i>	9.1	10.2	80.7	2.7	9.0	88.2
	<i>-264</i>	<i>-56</i>	<i>0.10</i>	<i>0.03</i>	8.6	15.5	76.0	2.5	17.4	89.1
	<i>-264</i>	<i>-156</i>	<i>0.10</i>	<i>0.03</i>	9.5	6.3	84.2	2.8	7.9	89.4
PS81/283	<i>0</i>	<i>-56</i>	<i>0.09</i>	<i>0.52</i>	1.8	77.8	20.5	11.3	78.3	10.4
	<i>0</i>	<i>-156</i>	<i>0.09</i>	<i>0.52</i>	2.0	75.4	22.7	11.9	77.2	10.9
	<i>-264</i>	<i>-56</i>	<i>0.09</i>	<i>0.52</i>	1.8	77.1	21.1	14.0	73.3	12.9
	<i>-264</i>	<i>-156</i>	<i>0.09</i>	<i>0.52</i>	2.1	74.5	23.4	14.9	71.4	13.7
PS81/284	<i>0</i>	<i>-56</i>	<i>0.07</i>	<i>0.05</i>	5.1	32.5	62.3	3.4	32.4	64.2
	<i>0</i>	<i>-156</i>	<i>0.07</i>	<i>0.05</i>	5.7	25.2	69.1	3.8	24.9	71.4
	<i>-264</i>	<i>-56</i>	<i>0.07</i>	<i>0.05</i>	5.3	30.5	64.2	3.4	31.1	65.5
	<i>-264</i>	<i>-156</i>	<i>0.07</i>	<i>0.05</i>	5.9	22.8	71.4	3.8	23.3	72.9
Co1302	<i>-110</i>	<i>-93</i>	<i>0.12</i>	<i>0.97</i>	11	4.75	84.2	93.9	3.2	2.9
	<i>-264; -139</i>	<i>-93</i>	<i>0.12</i>	<i>0.97</i>	11.3	2.84	85.9	97	0.04	3
Co1303	<i>-110</i>	<i>-93</i>	<i>0.19</i>	<i>0.94</i>	17.7	4.85	84.2	90.7	3.5	5.8
	<i>-264; -139</i>	<i>-93</i>	<i>0.19</i>	<i>0.94</i>	18.3	1.74	80.0	93.6	0.4	6
Co1304	<i>-110</i>	<i>-93</i>	<i>0.12</i>	<i>0.93</i>	11.6	5.41	83.0	89.4	4	6.7
	<i>-264; -139</i>	<i>-93</i>	<i>0.12</i>	<i>0.93</i>	11.8	3.4	84.8	92.1	1	6.9
Co1305	<i>-110</i>	<i>-93</i>	<i>0.19</i>	<i>0.85</i>	18.1	5.39	76.5	81.2	4.2	14.6
	<i>-264; -139</i>	<i>-93</i>	<i>0.19</i>	<i>0.85</i>	18.7	2.2	79.1	83.5	1.5	15
Co1308	<i>0</i>	<i>0</i>	<i>0.47</i>	<i>1</i>	54.8	4.0	41.2	96	4	0
	<i>-70; -40</i>	<i>0</i>	<i>0.47</i>	<i>1</i>	57	0.01	43	100	0	0

proportions of ancient and of aquatic OC range between 6.3 and 78.3% and between 10.4 and 89.4%, respectively.

Ancient Endmember Variability: Variation of biomarker ratios changes the obtained proportions of ancient OC only to a small extent in all investigated environments. For combinations with constant $\Delta^{14}\text{C}_{\text{terrigenous}}$ and $\Delta^{14}\text{C}_{\text{aquatic}}$ but varied biomarker ratios, derived from GDGTs or from *n*-fatty acids, differences in the calculated ancient OC proportions of 0 to 3.9% result for the fjord and off-shore sites, of 1.2 to 3.3% for the sites of LJL and of 0-2% for the ALA site.

For the sites of LJL and of ALA, also the variation of $\Delta^{14}\text{C}_{\text{terrigenous}}$ and $\Delta^{14}\text{C}_{\text{aquatic}}$ has just a small impact on obtained proportions of ancient OC. Application of minimum and maximum endmember $\Delta^{14}\text{C}$ values results in a variability of 1.9 - 4.2% and of 4% for the sites of LJL and of ALA, respectively.

For the fjord and off-shore sites, variation of endmember $\Delta^{14}\text{C}$ values changes resulting ancient OC proportions by 3.2 -12.4%. However, despite of the somewhat higher variability at these sites, it seems that proportions of ancient OC in the sediments of all environments can be narrowed quite precisely by mass balance calculations.

Terrigenous Endmember Variability: In contrast to ancient OC, the variability in the obtained proportions of terrigenous OC is more strongly affected by differing ratios of fatty acids and GDGTs than by variation of endmember $\Delta^{14}\text{C}$ values. For the fjord and off-shore sites, variation of biomarker ratios in the equations (with constant $\Delta^{14}\text{C}_{\text{terrigenous}}$ and $\Delta^{14}\text{C}_{\text{aquatic}}$) causes a variability of 0.2 to 12.8% in the obtained proportions of terrigenous OC. For the sites of LJL and of ALA, particularly high proportional differences result when *n*-fatty acid or GDGT ratios are employed (63.1 to 85.7% and 23.1 to 41.2%, respectively). When instead biomarker ratios are kept but $\Delta^{14}\text{C}_{\text{terrigenous}}$ and $\Delta^{14}\text{C}_{\text{aquatic}}$ are varied in the calculations, obtained proportions of the terrigenous OC differ by 0.2-3.5% at the fjord and off-shore sites, by 0.2-3.6% at the LJL sites and by 2.3-4% at the ALA site.

Aquatic Endmember Variability: At the sites of LJL and of ALA, obtained aquatic OC proportions are highly dependent on biomarker ratios. Application of *n*-fatty acid or GDGT ratios (with constant $\Delta^{14}\text{C}_{\text{terrigenous}}$ and $\Delta^{14}\text{C}_{\text{aquatic}}$) results in differences of 61.9-82.9% for the proportions of aquatic OC in the setting of LJL, and of 21.1-41.2% in the setting of ALA. Variation of $\Delta^{14}\text{C}_{\text{terrigenous}}$ and $\Delta^{14}\text{C}_{\text{aquatic}}$ only causes differences of 0.1-2.6% for the sites of LJL and of 0-1.7% for the ALA site.

Variability of aquatic OC proportions at the fjord and off-shore sites is affected to a similar extent by variation of $\Delta^{14}\text{C}_{\text{terrigenous}}$ and $\Delta^{14}\text{C}_{\text{aquatic}}$ or of biomarker ratios. Combinations with constant $\Delta^{14}\text{C}_{\text{terrigenous}}$ and $\Delta^{14}\text{C}_{\text{aquatic}}$ but varied biomarker ratios, result in differences of 0.2 -11.7% for aquatic OC proportions at these sites. Keeping biomarker ratios and varying endmember $\Delta^{14}\text{C}$ values causes differences of 3.8 -11.2% in the obtained proportions of aquatic OC.

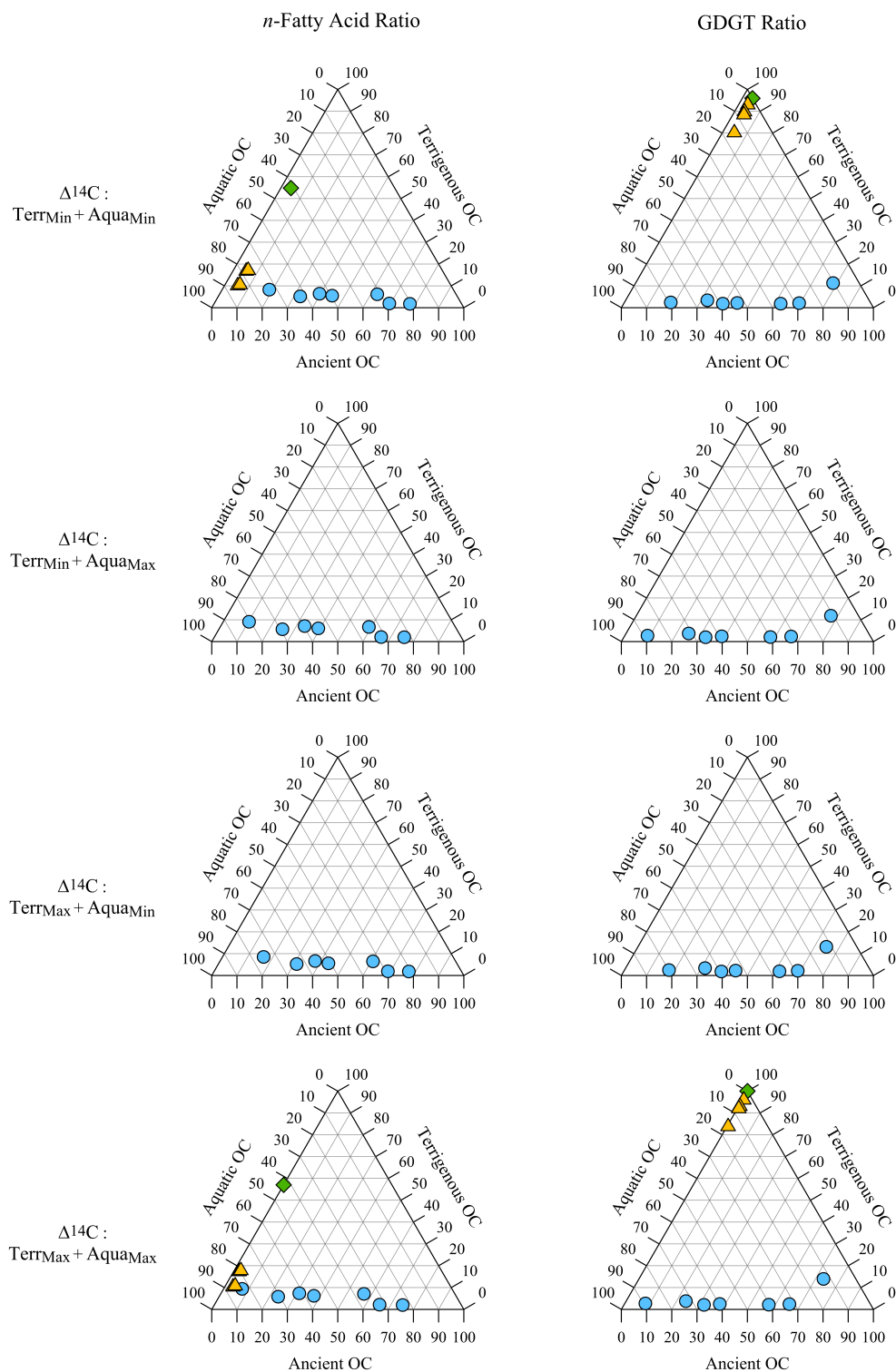


Figure 5.3: Ternary mixing diagrams for aquatic, terrigenous and ancient OC in surface sediments of fjord and off-shore sites (blue circles), marine inlet sites (yellow triangles) and lacustrine site (green diamonds). On the left side: Distributions based on *n*-fatty acid ratios. On the right side: Distributions based on GDGT ratios. From top to bottom: Combinations of applied minimum and maximum $\Delta^{14}\text{C}$ values for terrigenous and aquatic endmembers, respectively: minimum - minimum, minimum - maximum, maximum - minimum and maximum - maximum.

5.4 Discussion

5.4.1 Terrigenous OC

Allochthonous input to the aquatic environments can be derived from multiple sources on land. Actually, terrigenous OC can comprise both recent organic matter sources like plants and soils as well as petrogenic (ancient) sources (Blair and Aller, 2012). However, in this study, "terrigenous" refers just to OC sources which can be traced by terrigenous biomarkers (i.e. brGDGTs and HMW *n*-fatty acids), including plants, soils and peat. Ancient OC can be delimited from these sources, since it is not represented by the terrigenous biomarkers in the sediments.

According to current knowledge, brGDGTs are most likely produced by Acidobacteria in terrestrial environments (Weijers et al., 2007). Their abundances in aquatic sediments document the input of soil and peat derived OC to the sites. In contrast, sedimentary HMW *n*-fatty acids can be derived from organic matter of the standing vegetation, from plant debris that can be incorporated in soils and peat or that is already completely decomposed. Therefore, sedimentary HMW *n*-fatty acids potentially integrate OC from a wide range of plant-derived organic material.

Fig. 5.4 displays the abundances of sedimentary brGDGTs in relation to those of HMW *n*-fatty acids for the investigated sites of the three respective environments (lacustrine, marine inlet, fjord+off-shore).

For the surface sediments of the fjord and off-shore sites, a quite consistent relationship between abundances of brGDGTs and HMW *n*-fatty acids, expressed in a correlation coefficient of $r^2=0.77$ ($n=7$), points to a laterally uniform composition of the terrigenous organic

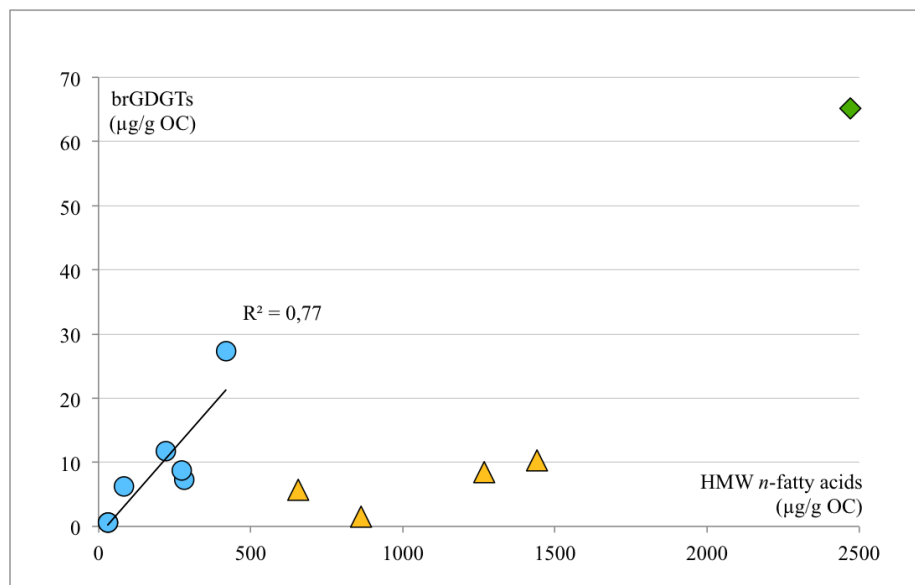


Figure 5.4: Concentrations of brGDGTs against HMW *n*-fatty acids for fjord sites (blue circles), LJL sites (yellow triangles) and ALA site (green diamond)

matter. This could indicate that considerable fractions of both biomarkers derive from common sources and were jointly introduced to the respective sites, most likely as soil-derived organic matter. The role of aeolian transport cannot be clearly delimited but the good agreement between brGDGT and HMW *n*-fatty acid abundances at the fjord and off-shore sites indicates that additional contributions of HMW *n*-fatty acids are either minor or have laterally uniform impacts. Differences in the proportions of sedimentary brGDGTs and HMW *n*-fatty acids are highest between the different aquatic environments. Concentrations of HMW *n*-fatty acids are generally higher at the LJL sites than at the fjord and off-shore sites, whereas concentrations of brGDGTs are similar in both environments (excluding site PS81/258). Conformity of brGDGT abundances across different marine environments may indicate uniform dispersal of soil organic matter in the ocean and a high refractivity of brGDGTs. Higher concentrations of HMW *n*-fatty acids in LJL likely point to an additional fraction of terrigenous organic matter that is preferentially deposited in the inlet. Distinct amounts of unconsolidated plant debris may account for this additional source of terrigenous organic matter in LJL. The hydrological behavior plant debris (details in chapter 4) possibly favored its accumulation at the coast-proximal sites of LJL and hampered the transport off shore. Hydrodynamic sorting of size or density fractions might therefore result in coastal sediments with high proportions of coarse, low-density material, including plant debris (Tesi et al., 2016). High export efficiencies of plant-derived HMW *n*-fatty acids to the more remote and deeper fjord and off-shore sites is possibly additionally prevented by persistent dissolution of the "unprotected" plant tissue in the ocean. In contrast, preservation of soil derived biomarkers is possibly enhanced because of their aggregation with protecting mineral matrices (e.g. Cranwell, 1981).

Despite of the general attribution of brGDGTs to soil bacteria, these biomarkers can also be derived from *in situ* production in the water column or in the sediments (e.g. Peterse et al., 2009; Zell et al., 2015). Based on the observation that *in situ*-produced brGDGTs are characterized by a much higher abundance of cyclic brGDGTs, the #Ringtetra index was proposed for distinguishing between soil-derived and aquatic-derived brGDGTs (Sinninghe Damsté, 2016). With increasing abundances of cyclic brGDGTs, #Ringtetra values increase. Values > 0.7 indicate that other sources than soil must also contribute (Sinninghe Damsté, 2016). In the investigated aquatic environments of South Georgia, *in situ* production is negatively correlated to the total amount of brGDGTs. Small #Ringtetra values of 0.09-0.16 and of 0.07 point to minor abundances of *in situ*-produced brGDGTs in the surface sediments of LJL and of ALA, respectively. At the fjord sites, the threshold value of 0.7 is only exceeded at sites PS81/280 (0.82) and PS81/284 (0.71). However, relatively high indices of 0.40-0.65 possibly point to distinct amounts of *in situ*-brGDGTs, also at the other fjord sites.

As already mentioned, exceptionally high brGDGT concentrations of $27.4 \mu\text{g/g OC}$ (fig. 5.2 F) at site PS81/258, markedly differ from those of all other marine sites. Abundances of HMW *n*-fatty acids are as well particularly high ($418 \mu\text{g/g OC}$) at this site. Apparently,

enhanced input of terrigenous organic matter, possibly together with good preservation conditions in the sediments, characterizes sedimentation at this site. Recent plants and soils are unlikely the source for this massive input, since steep slopes, encompassing Cumberland East Bay, restrict vegetation and soils to the lower altitudes of the catchment, and by that, limit their potential to provide large amounts of recent organic matter to the marine environment. The specifically high input of terrigenous organic matter is most likely explained by glacial supply from the Nordenskjöld Glacier, which erodes the peat bed that is exposed in front of the ice edge and enters Cumberland West Bay proximal to site PS81/258. Radiocarbon dating revealed that the peat sequence in front of the Nordenskjöld Glacier was formed between 2230 ± 70 and 3330 ± 70 yrs BP (Gordon, 1987). Therefore, contributions of aged terrigenous OC from this peat source are likely covered by the range of assumed $\Delta^{14}\text{C}$ values for the terrigenous endmember.

The lacustrine sediments of the ALA site reveal considerably higher concentrations of both, brGDGTs and HMW *n*-fatty acids, than all other sites (fig. 5.2 E, F). The significant role of terrigenous input in ALA is likely a function of a comparatively large catchment area relative to a small lake size. A high TOC concentration of 12.42 % indicates that organic matter constitutes a large fraction of the sediments. The low water depth of c. 1 m possibly facilitates fast sedimentation in this setting and enhances the burial efficiency of organic matter. Additionally, the role of peat as source of terrigenous OC may have to be considered as well, since preservation of organic matter is likely enhanced in peat and since anaerobic conditions potentially favor the production of brGDGTs (Weijers et al., 2004).

5.4.2 Aquatic OC

The aquatic biomarkers, crenarchaeol and LMW *n*-fatty acids, represent different planktonic communities. Crenarchaeol is produced by non-thermophilic Thaumarchaeota (Schouten et al., 2013), whereas LMW *n*-fatty acids are derived from various planktonic species (Volkman et al., 1980), comprising phytoplankton and zooplankton.

Concentrations of crenarchaeol seem to be related to the respective aquatic environments, with highest concentrations at the fjord and the off-shore sites, lower concentrations at the LJL sites and particularly low concentrations at the ALA site. The water depth at the fjord and off-shore sites is substantially deeper than in LJL and ALA (tab. 5.1). A correlation of crenarchaeol concentration with water depth is likely an expression of archaeal habitats since crenarchaeol is favorably produced at the thermocline (Schouten et al., 2013). As the thermocline is 60-120 m deep around South Georgia (Ward et al., 1995), the shallow-water sites of LJL and ALA (tab. 5.1) unlikely provide a favorable habitat for crenarchaeol-producing archaea.

Like for the terrigenous biomarkers, the surface sediments of site PS81/258 also display an exceptionally high concentration of crenarchaeol (fig. 5.2 D). This likely results from a fuelling effect due to the enhanced nutrient supply that is caused by the high input of terrigenous organic matter to the site. However, distinct amounts of allochthonously supplied

crenarchaeol may also contribute, since crenarchaeol was found to occur in soils and peat, however, in way lower amounts than in the ocean (Weijers et al., 2004).

LMW *n*-fatty acid concentrations are particularly high at the sites of LJL (fig. 5.2 C), indicating good production and/or preservation conditions in the inlet. The shallower water depth of LJL, in comparison to the fjord and off-shore sites, possibly enables a faster sedimentation of LMW *n*-fatty acids and therefore may enhance the burial efficiency of these biomarkers in this environment. However, it has to be considered that higher proportions of land derived LMW *n*-fatty acids may contribute to the LJL and ALA sites, due to the proximity of the sites to the terrigenous source area of these biomarkers.

No significant correlation between abundances of LMW *n*-fatty acids and crenarchaeol is given for any of the investigated environments. This lack of coherence between aquatic biomarkers possibly resulted from locally variable planktonic community compositions and/or differing reactivities of LMW *n*-fatty acids and crenarchaeol. To date, the only study that investigated reactivities of co-occurring sedimentary *n*-fatty acids and crenarchaeol was recently published by Kusch et al. (2016). In this work, CSRA data revealed similar reactivities of *n*-fatty acids and crenarchaeol in marine sediments from the Back Sea under variable redox regimes. Although, different reactivities cannot certainly be ruled out based on a single study, variable and complex oceanographic controls, including bathymetry, hydrographic situations, nutrient supply and grazing pressure (Juul-Pedersen et al., 2015) probably mainly determine the magnitude of primary production as well as the abundance and composition of phytoplanktonic species at the different sites and by that the biomarker composition in the sediments.

5.4.3 Ancient OC

The shales and greywackes of the Cumberland series (Gregory, 1915) are a source of ancient OC in the study area. While GDGTs and *n*-fatty acids are good proxies for determining aquatic and terrigenous OC, the bulk sediment ages give a tentative approximation of the impact of ancient OC to the sites, since $\Delta^{14}\text{C}$ of ancient OC is much different from aquatic and terrigenous OC.

Decreasing bulk sediment ages with increasing distance of the sites to the Nordenskjold Glacier in Cumberland East Bay and to the Neumayer Glacier in Cumberland West Bay, respectively (excluding site PS81/283-1) (fig. 5.2), indicate that erosional products of the Cumberland series are discharged by the marine terminating glaciers and are dispersed into the fjords by currents. Physical erosion of sedimentary rocks often accounts for large parts of the input of ancient OC into fjord systems (Cui et al., 2017). In mountainous tributaries large petrogenic POC contribution of up to 80% were found (Häggi et al., 2016).

In LJL and ALA, more local processes like streams and aeolian transport may bring petrogenic material into the system. However, the very similar bulk sediment ages at the four sites of LJL may point to good mixing in the inlet and therefore might indicate that ancient OC is mainly introduced as dissolved fraction within the ocean water from outside of the

inlet rather than as particulate organic matter from the catchment. The young surface sediment age at the ALA site supports the interpretation of a low fluvial and aeolian transport efficiency for ancient OC.

5.4.4 OC Distributions in Fjords and Off-Shore

Although the ratios differ significantly for *n*-fatty acids and GDGTs at the respective fjord and off-shore sites (fig. 5.3), the mixing proportions between the aquatic, terrigenous and ancient endmembers varies in a relatively small range. Moreover, the variation of the aquatic and terrigenous endmember $\Delta^{14}\text{C}$ values also has only a minor effect on the mixing proportions. This relatively small variability can be explained by the high impact of ancient OC. The significantly different $\Delta^{14}\text{C}$ signature of the ancient endmember, weighs much more than shifting relative proportions between aquatic and terrigenous endmembers or varying maximum and minimum $\Delta^{14}\text{C}$ of these endmembers, which have more similar $\Delta^{14}\text{C}$ values than ancient OC. The relatively high contributions of ancient OC to the surface sediments, therefore, mainly determine the variability in the calculated proportions of the three OC sources at the fjord and the off-shore sites. Despite of the relatively small variability, distinct amounts of brGDGTs derived from *in situ* production hamper the quantification of OC sources based on GDGT ratios. Therefore, mean OC proportions resulting only from the calculations with *n*-fatty acids ratios and minimum and maximum $\Delta^{14}\text{C}$ values of aquatic and terrigenous endmembers, displayed in fig. 5.5 for each site, are further discussed.

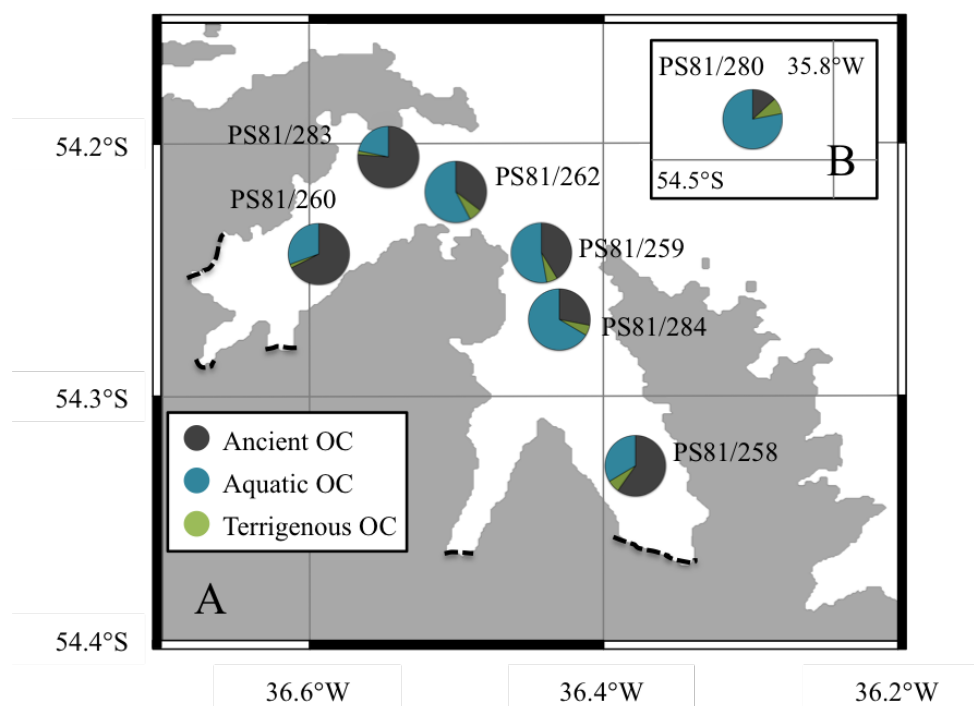


Figure 5.5: Proportions of aquatic (blue), terrigenous (green) and ancient (grey) OC at the respective fjord (map A) and off-shore sites (map B). Proportions are mean values derived from calculations with *n*-fatty acid ratios and minimum and maximum endmember $\Delta^{14}\text{C}$ values

Lateral Trends: Fjords are glacially eroded valleys with steep vertical gradients that were formed during glacial periods. They are often characterized by high terrestrial sediment supply, anoxic or sub-oxic conditions and high sedimentation rates (Huguet et al., 2007; Smith et al., 2015).

Marine terminating glaciers likely deliver largest parts of allochthonous OC as well as distinct amounts of freshwater to the fjords of Cumberland East Bay and Cumberland West Bay. Despite of distinct contributions from smaller glaciers of the tributary fjords, most significant supply is likely derived from the voluminous Neumayer and the Nordenskjöld glaciers.

Distribution patterns of OC sources exhibit clear spatial trends within the fjords and off-shore. Just site PS81/283 does not follow these general trends, possibly because of site-specific characteristics, that will be discussed later.

The marine terminating glaciers in Cumberland East and West Bays apparently supply large amounts of sedimentary material to the fjords. Due to erosion of the local bedrock, ancient OC introduced within the sedimentary load, yields high proportions in the sediments at the glacier proximal sites PS81/258 and PS81/260 (59.8% and 67.5%, respectively)(fig. 5.5). However, lowest TOC concentrations at the sites nearest to the glacier fronts (0.49 % at site PS81/258 and 0.35 % at site PS81/260) (fig. 5.2) point to sediments derived from glacial erosion that are also rich in mineral fractions. Dilution of ancient OC and increasing TOC concentrations indicate that the impact of glacially supplied material on sediment composition decreases with increasing distance to the glaciers. The consistence of these opposing trends is expressed by a high negative correlation ($r^2=-0.98$) between TOC concentrations and ancient OC proportions. It further indicates that largest fractions of ancient OC are introduced from point sources (glaciers) and are then uniformly dispersed within the linear fjords. Terrigenous OC has just minor and relatively similar contributions (2-8.8%) to the sediments. The lack of a clear spatial trend in the proportions of terrigenous OC may indicate, that glaciers do not supply terrigenous OC to the sites, exclusively. During precipitation or snowmelt events, terrigenous organic matter is probably also discharged by surface run-off and irregular small streams directly from the coasts into the fjords. Since terrigenous OC has just minor proportions, sediment composition is mainly characterized by ancient and aquatic OC. Gradients of these OC sources are inversely related, so that proportions of aquatic OC increase towards off-shore conditions.

Site-Specific Variability: Absolute amounts of the different biomarkers vary considerably between the fjord sites. It can therefore be assumed that specific characteristics of the respective settings, e.g. oceanographic conditions or topography, may have variable influences on the productivity of distinct planktonic communities or the deposition and preservation of *n*-fatty acids and GDGTs from land.

Sites PS81/258 and PS81/260, located closest to the glacier fronts of the Nordenskjöld and the Neumayer glacier, respectively, reveal several differences of their biomarker abundances

and sediment ages. The distance between site PS81/260 and the Neumayer glacier with 12.3 km is greater than the distance of 3.6 km between site PS81/258 and the Nordenskjöld glacier (tab. 5.1). However, surface sediments of site PS81/260 are somewhat older (9911 ± 65 ^{14}C years), than those of the site PS81/258 (8212 ± 52 ^{14}C years) (tab. 5.2). This might be explained by differing activities of the glaciers. Whereas low activity characterizes the Nordenskjöld Glacier, the majority of the 20 km long Neumayer Glacier recently falls within the ablation zone, so that the glacier undergoes accelerated retreat (Gordon et al., 2008). Enhanced erosion during glacial retreat (Cui et al., 2016) may be illustrated by the high sediment age at site PS81/260.

Sediments of site PS81/258 are characterized by large amounts of terrigenous biomarkers, likely derived from erosion of the peat bank that is exposed in front of the Nordenskjöld Glacier (Gordon, 1987). Crenarchaeol producing archaea are apparently favored by the nutrient supply, reflected by particularly high crenarchaeol concentrations at this sedimentary site. It seems that other planktonic species do not profit from allochthonous nutrients in a same extend, since LMW *n*-fatty acid concentrations are not as increased at this site (tab. 5.2 and fig. 5.2 C, D). This can possibly be explained by a high turbidity of the ocean water at the site PS81/258, possibly caused by large supply of terrigenous soil (peat) material by the glacier. The habitat of most planktonic species is maybe restricted to a small euphotic zone at the water surface, whereas archaea in deeper waters are possibly more unaffected and can profit from the additional nutrient input at this site.

In contrast, at the site PS81/260, the amount of terrigenous biomarkers is much lower than at the site PS81/258, but the concentration of LMW *n*-fatty acids is quite high (tab. 5.2 and fig. 5.2 C). The apparently large productivity at this site may be associated with the fast retreat of the Neumayer Glacier. Freshwater discharge may cause a stable stratification of the water column in the fjord, which can have important influences on the productivity in this systems, since meltwater introduces nutrients that get mixed within the surface layer, including silica and iron, which are often limiting nutrients for phytoplanktonic production (Atkinson et al., 2001; Borrione and Schlitzer, 2013; Juul-Pedersen et al., 2015).

Atkinson et al. (2001) observed an increase in C/N ratios with increasing water depth at different sites in the Cumberland Bays. Sediments of most of the investigated fjord and off-shore sites of this study reveal C/N ratios of 5-8, typical for marine phytoplankton (e.g Meyers, 1997). Particularly high C/N ratios of 40.7 and 41.8 were detected at the sites PS81/258 and PS81/260, respectively. When nitrogen availability is limited, high marine productivity can generate organic matter that is lipid-rich and nitrogen-poor (Meyers, 1994). Partially decoupled C and N cycles with fast remineralization of N in the surface layer and export of C to the sediments may account for these exceptionally high values (Atkinson et al., 2001), which are similar to the C/N values, reported for inner fjord environments in the Arctic (Winkelmann and Knies, 2005). However, at site PS81/259, which is located relatively far from the Neumayer glacier in Cumberland East Bay, a C/N value of 53.6 can unlikely be explained by exceptionally high marine productivity, since biomarker concen-

trations display quite moderate values. This site is located in the deepest water (262 m) on the oceanward side of the moraine which separates the inner from the outer basin. Possibly, this site is sheltered by the moraine ridge, so that bottom currents cannot disturb the sediments to a high extent and rich benthic communities can possibly evolve at this site. Consequently, preferential diagenetic remineralization and uptake of nitrogen by benthic organisms (Winkelmann and Knies, 2005) and not remineralization in the surface water possibly caused the high C/N value at site PS81/259.

As mentioned, the sediment composition at site PS81/283 does not follow the lateral trend of OC source or age distributions. An exceptionally high TOC age that corresponds to 73.2-78.3% of ancient OC characterize the sediments at this site. The topographically exposed position of PS81/283, located on top of an ancient moraine near the entrance of Cumberland East Bay (Bohrmann, 2013), probably hampers recent sediment accumulation. Winnowing of recent sediments due to ocean currents is indicated by generally low biomarker concentrations (fig. 5.2) in the surface sediments. Exposure of the relict moraine sediment surface is likely. Interestingly, the TOC age of the moraines' surface sediments corresponds to the timing of the ACR. If the material that formed the moraine derived from abrasion of surface sediments in Cumberland East Bay by the advancing Neumayer Glacier during the ACR, the TOC age possibly mainly reflects the age of this material and does not result from the mixing of ancient, marine and terrigenous OC. However, compound-specific radiocarbon data of n -C₁₆ fatty acids from this site (compiled by S. Berg) indicates that at least these compounds derive from recent sedimentation.

5.4.5 OC Distributions in the Costal Marine Inlet (LJL)

The young surface sediment ages set the limits for possible contributions of ancient OC at the LJL sites, so that neither variation of biomarker ratios nor endmember $\Delta^{14}\text{C}$ values change the calculated proportions of ancient OC to a high extent (tab. 5.3). Variation of $\Delta^{14}\text{C}_{\text{terrigenous}}$ and $\Delta^{14}\text{C}_{\text{aquatic}}$ has also only a small effect on the obtained mixing proportions, since the applied minimum and maximum endmember $\Delta^{14}\text{C}$ values are well constrained by the results of the CSRA. However, the very different biomarker ratios have a significant impact on the resulting proportions of aquatic and terrigenous OC. An underestimation of aquatic OC by the GDGT ratio seems likely, because crenarchaeol is not favorably produced in the shallow water of the inlet. Since crenarchaeol unlikely reflects aquatic productivity appropriately in LJL, n -fatty acid ratios are more reliable for the quantification of OC sources in this setting. Means of the resulting proportions derived from calculations with n -fatty acids ratios and variable $\Delta^{14}\text{C}$ values are shown in fig. 5.6. Very similar proportions of the OC sources at all sites possibly point to good mixing within the inlet. Steep gradients, which characterize the watersheds of the settings, generally favor high discharge velocities but also a heterogenous input via discrete streams. Highest concentrations

of HMW fatty acids as well as of brGDGTs (fig. 5.2) at sites Co1302 and Co1303, on the western site of LJJ likely result from their proximity to a permanent stream which enters the inlet close to these sites.

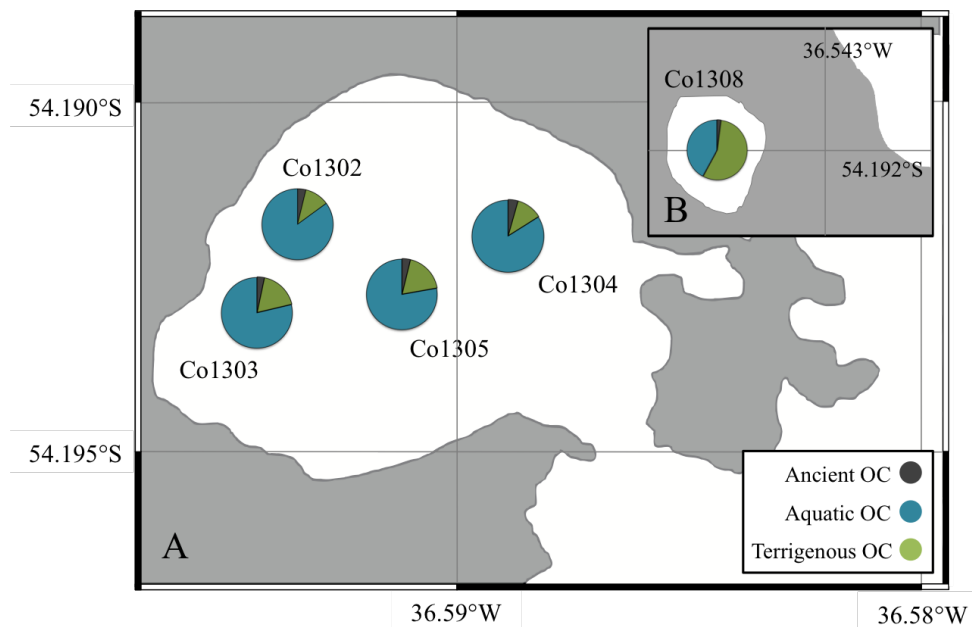


Figure 5.6: Proportions of aquatic (blue), terrigenous (green) and ancient (grey) OC at the respective sites of LJJ (map A) and ALA (map B). Proportions are mean values derived from calculations with n -fatty acid ratios and minimum and maximum endmember $\Delta^{14}\text{C}$ values

5.4.6 OC Distributions in the Lacustrine Environment (ALA)

In the lacustrine environment, high variability of the obtained OC proportions is mainly controlled by the differing biomarker ratios. The application of minimum and maximum endmember $\Delta^{14}\text{C}$ values in the mass balance calculations, affects the results just slightly (tab. 5.3). The composition of the lake sediments is characterized by very small amounts of ancient OC, already indicated by the young sediment age. Substantial input of land-derived biomass to the sediments is reflected by particularly high concentrations of both HMW fatty acids and brGDGTs. It has been suggested that considerable fractions of brGDGTs in lacustrine sedimentary archives can derive from *in situ* production in the water column or in the sediments of the lake (Tierney and Russell, 2009; Loomis et al., 2011; De Jonge et al., 2015; Weber et al., 2015). However, a very low #Ringrtetra value of just 0.1 points to insignificant *in situ* production at the ALA site. Despite of the consistently high concentrations of both terrigenous biomarkers, the proportions of aquatic and terrigenous OC differ strongly, when fatty acid or GDGT ratios are applied in the calculations. The very low concentration of crenarchaeol indicates, that the shallow-lake environment is no favor crenarchaeol production. Possibly, crenarchaeol even do not derived from aquatic production in this setting, but from the high input of soil organic matter. Other than in

marine sediments, where proportions of soil-derived crenarchaeol are mostly insignificant when compared to the high marine production, in the lacustrine environment of ALA, low aquatic productivity and large input of soil organic matter likely increases the proportion of soil-derived crenarchaeol in the sediments significantly. The reliability of the GDGT ratio likely suffers from both the input of soil derived crenarchaeol as well as the very low production in the lake. Therefore, proportions of OC sources derived from *n*-fatty acid ratios more likely reflect the actual composition of the sediments of Allen Lake A. Means of OC proportions derived from *n*-fatty acid ratios and minimum and maximum $\Delta^{14}\text{C}$ values are displayed in fig. 5.6.

In contrast to all marine sites, where concentrations of LMW *n*-fatty acids are about 4-15 times higher than those of HMW *n*-fatty acids, at the ALA site, concentrations of HMW *n*-fatty acids higher than those of LMW *n*-fatty acids. This is probably the result of a lower aquatic productivity combined with high terrigenous input in the lacustrine environment. Large seal populations, which were observed in the vicinity of the lake (Bohrmann, 2013), may introduce considerable amounts of feces into the lake. Eutrophication of the small water mass may result in anoxic conditions in the lake. Good preservation of organic matter due to low oxygen levels might partly explain the particularly high organic content in the sediments of ALA.

5.5 Conclusion

Quantification of OC sources revealed high proportions of ancient OC in the surface sediments of the fjord sites, likely introduced by the marine-terminating glaciers entering Cumberland East and West Bays. At sites of the marine inlet and especially of the lake relatively small contributions of ancient OC were estimated. It seems that chemical weathering and fluvial discharge contributes only minor fractions of ancient OC to the sites, whereas mechanical erosion of the bedrock is likely very efficient in terms of mobilizing ancient OC.

The application of GDGT ratios for estimating the relation between aquatic and terrigenous OC has turned out to be not useful in any of the investigated settings. In the settings of the lake and the marine inlet, GDGT ratios are biased because crenarchaeol is not preferably produced in the shallow waters of these environments. At the fjord and off-shore sites, where absolute amounts of brGDGTs are relatively small, *in situ* production of brGDGTs has a considerable impact. Ratios of *n*-fatty acids seem to have a high potential to reflect aquatic and terrigenous organic matter in all investigated environments reliably. However, it need to be considered that distinct amounts of LMW *n*-fatty acids may derive from land, particularly in settings near to the coast or in the small lake. Well-constrained endmember $\Delta^{14}\text{C}$ values likely further enhance the quality of the mixing model.

In many studies dual mass-balance calculations using $\Delta^{14}\text{C}$ and $\delta^{13}\text{C}$ were applied to determine proportions of three endmembers in sediments (Drenzek et al., 2007; Tao et al., 2015; Galy et al., 2008; Galy and Eglinton, 2011; Kuli et al., 2014; Cui et al., 2016). The

attribution of $\delta^{13}\text{C}$ values to the different endmembers is often a challenge in this approach. In particular, distinguishing and quantifying "pre-aged" terrigenous OC of vascular plant origin and ancient OC from rock erosion can be difficult, because each may be depleted in both $\Delta^{14}\text{C}$ and $\delta^{13}\text{C}$. A confident differentiation between terrigenous OC and ancient OC is, however, extremely important, because different rates of OC cycles in the respective reservoirs have an impact on global biogeochemical cycles. Therefore, quantification of OC sources by $\Delta^{14}\text{C}$ mass balances and using biomarker ratios, e.g. *n*-fatty acids ratios, for characterizing proportions of aquatic and terrigenous OC is possibly a promising approach to overcome these difficulties.

Chapter 6

Environmental History of South Georgia

6.1 Introduction

High-resolution records, which document past climatic and environmental changes, are scarce in the sub-Antarctic. South Georgia, as one of the few landmasses in the Southern Ocean, is an important geographical location for the investigation of paleoenvironmental processes in this region (Gordon et al., 2008). Glacial activity was extensively studied on South Georgia in order to identify major climatic transitions in the past as well as recent climatic trends (Clapperton et al., 1989; Bentley et al., 2007; Gordon et al., 2008; Hodgson et al., 2014; White et al., 2018). However, the investigated geomorphological evidences in these studies document only single, often chronologically poorly constrained, excerpts of the environmental history. Continuous records of lake sediments (Rosqvist and Schuber, 2003) or peat sequences (Van der Putten et al., 2009) provide further insights into the evolution of the terrestrial environment of South Georgia. Correlation of these paleoenvironmental reconstructions is, however, not always fully consistent.

In order to contribute to a refined picture of the environmental history of South Georgia, two continuous sedimentary records are investigated in this chapter, based on a multi-proxy approach. The sediment cores were derived from different aquatic environments, a marine inlet (Little Jason Lagoon) and a lake (Allen Lake A), both located at the north-eastern coast of the island.

The lacustrine sequence Co1308 from Allen Lake A has great potential to reveal a high-resolution record of the evolution of terrestrial biosphere, since sedimentation in this lake is mainly determined by local processes in its small watershed. The coastal-marine sequence Co1305 of Little Jason Lagoon can unveil a multitude of information on past marine and terrestrial biospheres as well as on glacial activity. It may provide an important link between terrestrial and oceanic environments of this region. Deriving reliable age estimates of sediment formation is a topical problem in sub-Antarctic marine environments. Compound-

specific radiocarbon analysis of individual biomarkers was applied to address this challenge, facilitating the development of a confident sediment chronology for the coastal marine record of Little Jason Lagoon. The investigation of lacustrine together with marine sedimentary records from South Georgia, based on the comprehensive analysis of bulk sedimentary and molecular data, enables the identification of significant environmental transitions that are recorded in both settings. Moreover, system dependent variability of processes or differing sensitivities of the environments can be traced. Combination of complementary information from both aquatic environments therefore holds the opportunity to distinguish between regional implications of climatic changes and local processes, and moreover to better constrain the timing of environmental transitions.

6.2 Material and Methods

6.2.1 Samples

Sediment cores from Little Jason Lagoon (Co1305) and from Allen Lake A (Co1308) were investigated to derive high resolution sedimentation histories of these aquatic environments. Coring procedure and subsampling of the composite core Co1305 was described in chapter 4. At site Co1308, coring was performed with a Russian Peat Corer and with c. 50 cm overlap. Five half-cores with maximum length of 1 m per core, were recovered. Prior to processing, all half-cores were stored at 4°C. Correlation of the sediment sections was performed based on XRF data and resulted in a composite record of 2.33 m length. For biomarker analysis, discrete subsamples of 4 cm from the inner part of the cores were taken every 16 cm. The remaining sediments were continuously subsampled into 2 cm slices. All subsamples were freeze-dried and homogenized.

6.2.2 Radiocarbon Analysis

Pre-treatment and subsequent (compound-specific) radiocarbon analysis of biomarker and TOC samples of both records was described in chapters 4 and 5.

In addition to these samples, macrofossils of terrestrial plants (from Co1305 and Co1308) and of marine carbonate shells (from Co1305) were submitted to radiocarbon analysis. Decarbonization with 1% HCl was performed for these samples for 10 h at room temperature, prior to combustion and conversion to elemental carbon (details chapter 4). Radiocarbon measurement was undertaken at the Cologne AMS facility.

Calibration of Radiocarbon Data Radiocarbon ages of all samples were calibrated in order to derive calendar years, using the software CALIB 7.1 (Stuiver, M., Reimer, P.J., and Reimer, R.W., 2018, CALIB 7.1 [WWW program] at <http://calib.org>).

The atmospheric calibration curve SHcal, which was developed for samples of terrigenous

origin from the Southern Hemisphere (McCormac et al., 2004), was used to calibrate radiocarbon ages of HMW biomarkers and of plant macrofossils. It was further applied for the calibration of a ^{14}C age of the lacustrine TOC sample, assuming that sediments of the record Co1308 dominantly consist of terrigenous organic matter and that contained aquatic OC is free from hardwater effects.

Samples of marine origin (marine macrofossils) or of mainly marine origin ($n\text{-C}_{16}$ fatty acids, $n\text{-C}_{22}$ alcohols and TOC) of the record Co1305 were calibrated by means of the calibration curve Marine13 (Reimer et al., 2013). The recent marine reservoir age in the coastal marine setting was determined based on the ^{14}C age (720 years) of a carbonate shell, recovered from the surface sediments of LJJ. The global mean of the marine reservoir effect (400 years), included as default option in the calibration software, was adjusted for the local deviation (ΔR) of +320 years (Stuiver et al., 1986).

The temporal variability of marine reservoir ages cannot be determined based on the present data, so that $\Delta\text{R}=320$ years was applied for the calibration of all marine-derived ages. Variable contributions of terrigenous carbon sources to the $n\text{-C}_{16}$ fatty acid, $n\text{-C}_{22}$ alcohol and TOC samples were neglected for the calibration.

6.2.3 Biomarker Analysis

Extraction of biomarkers from sediment samples of the record Co1305, their separation into polarity fractions and measuring of biomarkers was described in chapter 4 in detail. These procedures were similarly performed for the analysis of biomarker samples of the record Co1308. Briefly, total lipids were extracted from freeze-dried and homogenized biomarker samples (1.5 - 27.3 g) by accelerated solvent extraction. Total lipid extracts were desulfurized and saponified prior to separation into neutral and acid fractions. Extraction of neutral lipids with dichloromethane was repeated 6-13 times for each sample. For the isolation of fatty acids from the remaining solution, 8-33 cycles of dichloromethane extraction were needed. After methylation of the fatty acid fractions, extraction of FAMES with hexane was performed 5-17 times for each of the samples.

6.2.4 Elemental Data

Elemental analyses of total sulphur (S), nitrogen (N), and carbon (C) as well as of total carbon (TC), total organic carbon (TOC) and total inorganic carbon (TIC) was performed on aliquots of the 2 cm sediment subsamples of the record Co1308. The procedures were described in chapter 4 and 5.

C/N ratios were calculated for each sample of Co1308 and Co1305, using the concentrations of TOC and of total N.

6.2.5 Carbon Preference Index

The carbon preference index (CPI) describes those of n -alkanes with an odd number of carbon atoms to the proportion with an even number of carbon atoms. CPI was calculated

for all samples of both records (Co1308 and Co1305) according to Bray and Evans (1961) as follows:

$$CPI_{25-33} = 0.5 * \frac{(C_{25} + C_{27} + C_{29} + C_{31} + C_{33})}{(C_{24} + C_{26} + C_{28} + C_{30} + C_{32})} + \frac{(C_{25} + C_{27} + C_{29} + C_{31} + C_{33})}{(C_{26} + C_{28} + C_{30} + C_{32} + C_{34})}, \quad (6.1)$$

6.2.6 BIT Index

The Branched and Isoprenoid Tetraether (BIT) index is based on the relative abundance of brGDGTs versus crenarchaeol and is calculated according to Hopmans et al. (2004) as follows:

$$BIT = [Ia + IIa + IIIa]/[Ia + IIa + IIIa + crenarchaeol]. \quad (6.2)$$

The BIT index characterizes the relative amounts of soil-derived organic matter in marine and lacustrine sediments. Roman numerals refer to brGDGT structures (fig. 2.1).

6.2.7 Tex_{86}^L

Sea surface temperature (SST) was calculated based on the Tex_{86}^L regional calibration for polar and sub-polar oceans, according to Kim et al. (2010):

$$Tex_{86}^L = LOG(GDGT2/(GDGT1 + GDGT2 + GDGT3)), \quad (6.3)$$

GDGT1, GDGT2, GDGT3 are isoGDGTs, containing 1, 2, and 3 cyclopentane moieties, respectively. The residual standard error for SST estimates, derived from the Tex_{86}^L calibration, is $\pm 4^\circ\text{C}$ (Kim et al., 2010).

6.2.8 MBT'/CBT

Mean annual air temperature (MAAT) and soil pH were calculated according to the revised soil calibration of Peterse et al. (2012), using the Methylation of Branched Tetraethers (MBT') and the Cyclization of Branched Tetraethers (CBT) indices and the following transfer functions:

$$MBT' = [Ia + Ib + Ic]/[Ia + Ib + Ic + IIa + IIb + IIc + IIIa], \quad (6.4)$$

$$CBT = \log([Ib + IIb]/[Ia + IIa]) , \quad (6.5)$$

$$MAAT = 0.81 - 5.567 * CBT + 31 * MBT' , \quad (6.6)$$

$$pH = 7,9 - 1,97 * MBT' . \quad (6.7)$$

Roman numerals refer to brGDGT structures (fig. 2.1). The error for MAAT estimates and soil pH, derived from the soil calibration of Peterse et al. (2012), is $\pm 4.8^\circ\text{C}$ and ± 0.7 , respectively.

6.2.9 MSAT

Mean summer air temperature was calculated according to the regional calibration of Foster et al. (2016):

$$MSAT = 18.7 + (80.3 * Ib) - (25.3 * IIa) - (19.4 * IIIa) + (369.9 * IIIb) \quad (6.8)$$

Roman numerals refer to brGDGT structures (fig. 2.1). The root mean squared error (RMSE) for MSAT estimates derived from the regional calibration is $\pm 2.3^\circ\text{C}$ (Foster et al., 2016).

6.3 Results and Discussion

The establishment of robust sediment chronologies is fundamental for the reconstruction and interpretation of paleoenvironmental changes from sedimentary proxies. Calibrated ^{14}C ages of sedimentary organic material are mostly the basis for the development of sediment chronologies (Mollenhauer and Rethemeyer, 2009). To achieve good chronological control, the investigated organic material has to meet some criteria.

Macrofossils which can be attributed to specific sources are often the preferred sample type for radiocarbon analysis. It is generally assumed that ^{14}C ages of terrestrial macrofossils represent the time of sediment formation in lacustrine sedimentary environments most accurately, since terrestrial plants record the atmospheric radiocarbon signature and since they are assumed to be rapidly transported into the lakes (e.g. Gierga et al., 2016).

In marine sediments, terrestrial macrofossils are often scarce or have experienced interme-

diate storage of unknown duration prior to deposition.

Marine macrofossils are mostly more abundant in these environments and can be used for radiocarbon analysis instead. However, reservoir effects need to be considered when the targeted material has a marine origin.

In sub-Antarctic regions, marine carbonates are often not sufficiently well preserved (e.g. Licht et al., 1998). ^{14}C analysis of TOC is mostly no alternative when macroscopic organic remains are lacking in the sediments, since mixing of allochthonous and autochthonous OC sources complicates the interpretation of ^{14}C ages. When significant contributions of aged or ancient OC are contained in the sediments, ^{14}C analysis can result in a severe overestimation of the time of sediment formation.

An alternative to the radiocarbon analysis of macroscopic remains or TOC is the measurement of ^{14}C concentrations of individual sedimentary biomarkers.

Using terrigenous biomarkers for chronological purposes is problematic for marine sediments because of long residence times of these biomarkers in terrestrial reservoirs (Pearson et al., 2001; Smittenberg et al., 2004; Uchida et al., 2005; Uchikawa et al., 2008). ^{14}C ages of biomarkers that are mainly derived from marine organisms can be expected to reflect the time of sediment deposition in marine environments most accurately (Eglinton et al., 1997; Mollenhauer and Rethemeyer, 2009). Sediment chronologies based on radiocarbon ages of $n\text{-C}_{16}$ fatty acids were already successfully developed for records from the Southern Ocean (Ohkouchi, 2003; Ohkouchi and Eglinton, 2008; Yamane et al., 2014).

6.3.1 Sediment Chronology - Co1308

Sample types that were considered for the establishment of a sediment chronology for the ALA record comprise plant macrofossils as well as $n\text{-C}_{29+31}$ alkanes (tab. 6.1). The organic-rich sediments of the record Co1308, containing large amounts of macroscopic plant remains, enabled the recovery of plant macrofossils from four evenly distributed depths between 16 and 233 cm of the composite core Co1308. From the sediments of 4-8 cm core depth, HMW

Table 6.1: fMC values of biomarker compounds are corrected for blank and derivatization. Calibration ^{14}C ages was performed with Calib 7.1. Calibration curve SHcal was used for terrestrial samples and calibration curve marine13 was used for marine samples and TOC. For marine samples $\Delta\text{R} = 320$ was used. Results cal BP display the median age probability (2 sigma uncertainty). + and - display the age range.

depth [cm]	sample type	compound	F^{14}C	^{14}C age	Cal age		
			fMC	[years BP]	[years BP]	+	-
0–2	TOC		0.967 ± 0.004	273 ± 37	289	40	21
4–8	alkanes	$n\text{-C}_{27}$	0.804 ± 0.007	1751 ± 74	1624	127	196
4–8	alkanes	$n\text{-C}_{29+31}$	0.771 ± 0.006	2090 ± 64	2020	139	153
16–18	terrestrial plant		0.729 ± 0.004	2536 ± 40	2581	159	156
72–79	terrestrial plant		0.588 ± 0.003	4266 ± 44	4742	26	133
144–146	terrestrial plant		0.468 ± 0.003	6106 ± 48	6921	109	143
231–233	terrestrial plant		0.349 ± 0.002	8455 ± 49	9443	83	76

n-alkanes (*n*-C₂₇ and *n*-C₂₉₊₃₁) were submitted to CSRA by Sonja Berg. Calibrated ages of all chosen samples together, display a remarkably consistent (nearly linear) trend, increasing from 2020 yrs cal BP at 4–8 cm with sediment depth to 9443 yrs cal BP at 231–233 cm (fig. 6.1). Extrapolation of this age-depth trend to the surface of the record results in a sediment surface age of c. 1,900 years. The much younger TOC age (289 yrs cal BP) of the surface bulk sediments is not consistent with this age estimate. The difference between the age of the TOC sample and the extrapolated age estimate can have several reasons: 1. A hiatus between the surface and 4 cm core depth, 2. Virtually no sediment accumulation in the last ~ 1,900 years, 3. A large proportion of aquatic organic carbon with an ambient ¹⁴C signature in the TOC sample, or 4. a significant contribution of bomb ¹⁴C to the TOC sample. The first three explanations were all rejected because sediment properties neither indicate a hiatus nor very minor accumulation rates. A high proportion of aquatic organic carbon in the surface sediments, which is indicated by a C/N ratio of 7, is also not supported by biomarker ratios and calculated OC proportions (chapter 5). It seems most likely that surface sediments are rich of terrigenous organic matter which contains bomb ¹⁴C. The whole bomb peak is even possibly integrated in the surface sediments of ALA. Because of the very consistent age-depth trend of macrofossils and *n*-C₂₉₊₃₁ alkanes, an invariable MRT of the terrigenous material of 1,900 years was inferred for the agetmodel. The function, that connects the radiocarbon ages of the considered samples and which was extrapolated to the surface, was simply moved from an origin at 1,900 years to an origin

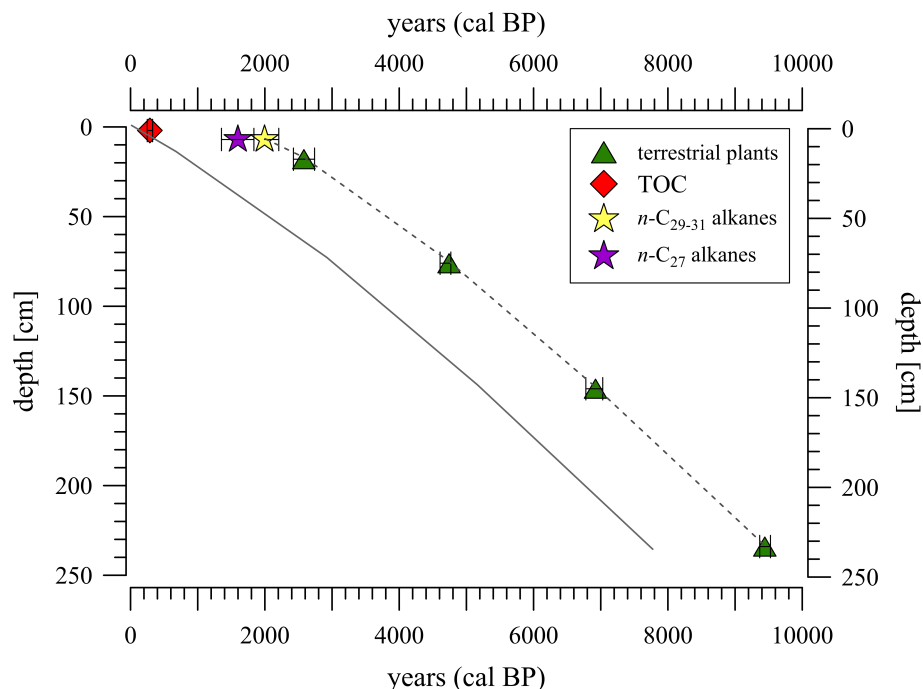


Figure 6.1: Calibrated ages (years BP) of terrestrial macrofossils, TOC, *n*-C_{29–31} alkanes and *n*-C₂₇ alkanes from core Co1308. Dashed line: uncorrected agetmodel resulting from polynomial fitting of calibrated ages of macrofossils and *n*-C_{29–31} alkanes. Solid line: Inferred agetmodel for the record Co1308, corrected for a mean residence time of 1,900 years)

at 0 years, in order to derive a sediment chronology which is corrected for the MRT of terrigenous organic matter on land (fig. 6.1).

6.3.2 Sediment Chronology - Co1305

Different sample types that were obtained from the sedimentary record Co1305 were submitted to radiocarbon analysis. These samples comprise marine and terrigenous macrofossils, various biomarkers as well as TOC of bulk sediments (tab. 6.2). The investigation of radiocarbon inventories of individual biomarkers revealed that HMW *n*-alkanes and *n*-fatty acids, which are derived from terrestrial vegetation, are considerably "pre-aged" at the time deposition (details in chapter 4). Plant macrofossils of a few core depths have similar ^{14}C ages as co-occurring terrigenous biomarkers. Sedimentary *n*-C₁₆ fatty acids and *n*-C₂₂ alcohols are indicated to likely mainly originate from marine sources in the setting of LJJ (details in chapter 4). Calibrated ^{14}C ages of these biomarkers can therefore be assumed to yield reliable age estimates of sediment formation, so that they can be employed to develop a reliable sediment chronology for the record Co1305.

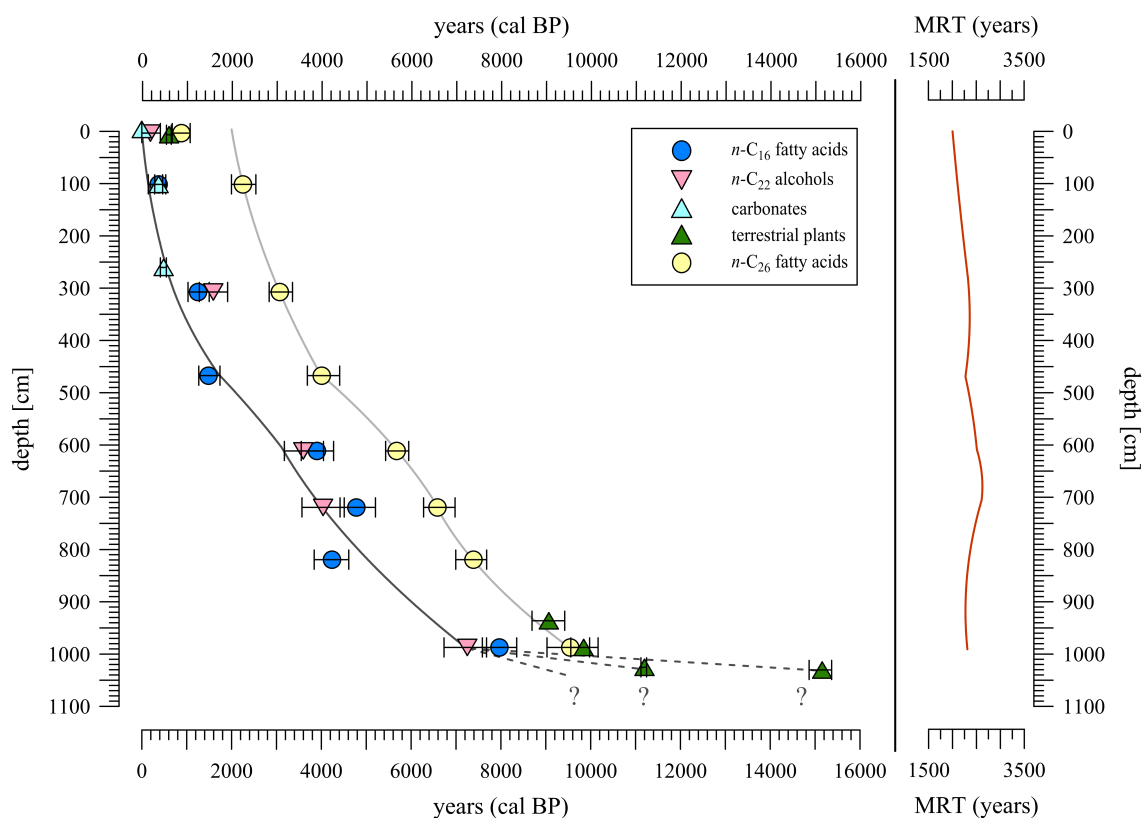


Figure 6.2: Calibrated ages (years BP) of *n*-C₁₆ fatty acids, *n*-C₂₂ alcohols and carbonates as marine components and terrestrial plant macrofossils and *n*-C₂₆ fatty acids as terrestrial components against depth. Black line: age model of Unit IV and III for the core Co1305, derived from ages of marine samples. Dashed line shows possible age models of units I-III. Grey line: age model of terrigenous samples derived from *n*-C₂₆ fatty acid ages. On the right hand side: red line indicates the mean residence time (MRT) of terrigenous organic matter against core depth. MRT is derived from the difference of the age model of terrigenous compounds and the age model of marine compounds.

Table 6.2: fMC values of biomarker compounds are corrected for blank and derivatization. Calibration of ^{14}C ages was performed with Calib 7.1. Calibration curve SHcal was used for terrestrial samples and calibration curve Marine13 was used for marine samples and TOC, with $\Delta R = +320$. Calibrated ages (in years BP) display the median age probability. + and - display the age range.

depth [cm]	sample type	compound	F ^{14}C corrected fMC	^{14}C age [years BP]	Cal age [years BP]	+	-
surface	carbonate			719 ± 42	recent		
0–2	TOC		0.862 ± 0.004	1192 ± 35	494	49	59
4–9	fatty acids	<i>n</i> -C ₂₆	0.881 ± 0.012	1022 ± 106	880	197	204
4–9	alkanes	<i>n</i> -C ₂₉₊₃₁	0.882 ± 0.012	1008 ± 106	868	198	191
4–9	alcohols	<i>n</i> -C ₂₂	0.897 ± 0.014	872 ± 129	192	220	192
4–9	alcohols	<i>n</i> -C ₂₆	0.925 ± 0.013	624 ± 113	585	154	145
10–12	terrestrial plant			662 ± 39	605	51	56
103–108	fatty acids	<i>n</i> -C ₁₆	0.876 ± 0.011	1060 ± 100	374	158	230
103–108	fatty acids	<i>n</i> -C ₂₆	0.752 ± 0.010	2295 ± 112	2254	286	256
105–107	TOC		0.779 ± 0.004	2003 ± 43	1243	82	92
105–107	marine plant			1082 ± 40	403	76	99
105–107	carbonate			1055 ± 44	377	88	90
264–266	carbonate			1179 ± 42	485	62	73
308–313	fatty acids	<i>n</i> -C ₁₆	0.778 ± 0.010	2022 ± 107	1254	246	226
308–313	fatty acids	<i>n</i> -C ₂₆	0.692 ± 0.010	2963 ± 118	3075	283	239
308–313	alkanes	<i>n</i> -C ₂₉₊₃₁	0.700 ± 0.012	2870 ± 138	2974	383	251
308–313	alcohols	<i>n</i> -C ₂₂	0.747 ± 0.014	2338 ± 146	1591	322	309
310–312	TOC		0.660 ± 0.004	3337 ± 44	2788	103	88
468–473	fatty acids	<i>n</i> -C ₁₆	0.756 ± 0.010	2251 ± 110	1488	253	220
468–473	fatty acids	<i>n</i> -C ₂₆	0.630 ± 0.011	3709 ± 134	4008	401	321
468–473	alkanes	<i>n</i> -C ₂₇₊₂₉	0.646 ± 0.012	3505 ± 150	3741	358	361
468–473	alcohols	<i>n</i> -C ₂₆	0.690 ± 0.013	2979 ± 147	3097	307	333
472–474	TOC		0.633 ± 0.003	3678 ± 37	3220	115	116
612–617	fatty acids	<i>n</i> -C ₁₆	0.590 ± 0.010	4235 ± 133	3901	371	348
612–617	fatty acids	<i>n</i> -C ₂₆	0.539 ± 0.010	4970 ± 145	5677	269	244
612–617	alkanes	<i>n</i> -C ₂₇₊₂₉	0.559 ± 0.012	4666 ± 175	5299	363	453
612–617	alcohols	<i>n</i> -C ₂₂	0.608 ± 0.013	3992 ± 170	3595	454	420
614–616	TOC		0.466 ± 0.003	6138 ± 52	6238	118	125
720–725	fatty acids	<i>n</i> -C ₁₆	0.544 ± 0.010	4896 ± 145	4780	424	364
720–725	fatty acids	<i>n</i> -C ₂₆	0.485 ± 0.010	5814 ± 160	6585	393	309
720–725	alkanes	<i>n</i> -C ₃₁₊₃₃	0.449 ± 0.012	6429 ± 219	7268	399	488
720–725	alcohols	<i>n</i> -C ₂₂	0.583 ± 0.013	4337 ± 178	4041	468	472
722–724	TOC		0.457 ± 0.004	6289 ± 65	6382	159	124
820–825	fatty acids	<i>n</i> -C ₁₆	0.572 ± 0.010	4483 ± 139	4234	377	394
820–825	fatty acids	<i>n</i> -C ₂₆	0.443 ± 0.010	6537 ± 174	7386	296	392
848–850	TOC		0.314 ± 0.002	9305 ± 51	9634	176	124
940–942	terrestrial plant		0.362 ± 0.006	8172 ± 127	9070	350	377
988–993	fatty acids	<i>n</i> -C ₁₆	0.378 ± 0.009	7822 ± 199	7967	385	380
988–993	fatty acids	<i>n</i> -C ₂₆	0.344 ± 0.009	8573 ± 219	9543	621	517
988–993	alkanes	<i>n</i> -C ₂₉₊₃₁	0.366 ± 0.010	8078 ± 227	8926	530	499
988–993	alcohols	<i>n</i> -C ₂₂	0.414 ± 0.012	7079 ± 230	7252	427	518
988–993	alcohols	<i>n</i> -C ₂₆	0.376 ± 0.012	7864 ± 250	8698	614	530
990–992	TOC		0.299 ± 0.002	9686 ± 63	10206	191	144
990–992	terrestrial plant		0.333 ± 0.004	8832 ± 101	9842	133	285
1029–1031	terrestrial plant			9798 ± 37	11197	48	77
1034–1036	terrestrial plant		0.204 ± 0.002	12768 ± 61	15160	208	294
1040–1042	TOC			14172 ± 415	16186	1289	1227

A few marine macrofossils that were recovered from the upper part of the sediment core provide supplementary robust ^{14}C data that can be used for the age model. The good match between the radiocarbon ages of a carbonate shell and of $n\text{-C}_{16}$ fatty acids at 103 cm core depth (tab. 6.2, fig. 6.2) supports the assumption that $n\text{-C}_{16}$ fatty acids reliably reflect the radiocarbon signature of marine biomass. Nevertheless, the general assignment of $n\text{-C}_{16}$ fatty acids and $n\text{-C}_{22}$ alcohols to marine sources is simplified (for the calibration of their ^{14}C ages, these biomarkers were assumed to be 100% marine). Proportions of marine and land-derived homologues of these biomarkers in the sediments were considered to mainly depend on the relation between marine productivity and terrigenous supply as well as on the extent of post-depositional alteration of their initial compositions over time. In order to minimize the impact of "pre-aged" terrigenous biomarkers, only the sample that yielded the youngest ^{14}C age at a respective depth was considered for the sediment chronology.

Age estimates of samples from two investigated core depths seem to be potentially biased because of specific environmental factors. At 371 cm, particularly intense post-depositional degradation of marine biomass is assumed to have altered radiocarbon inventories of sedimentary $n\text{-C}_{16}$ fatty acids and $n\text{-C}_{22}$ alcohols substantially. Radiocarbon ages of these samples were therefore excluded from a chronological application. At a depth of 823 cm not redox conditions in the sediments but a temporally lowered marine reservoir effect was assumed to be responsible for the relatively young ^{14}C age of the $n\text{-C}_{16}$ fatty acid sample (fig. 6.2). It is generally assumed that the variation of reservoir ages was quite small for the surface-water mass of the Southern Ocean during the mid to late Holocene (Van Beek et al., 2002; Hall et al., 2010). However, spatial variability is just poorly documented and reconstructions of past ventilation changes are very challenging. Recent modeling results suggest at least a distinct Holocene variability and local differences of marine reservoir ages for the Atlantic sector of the Southern Ocean (Balmer et al., 2016; Sarnthein et al., 2015).

In the coastal marine setting of LJL, local processes may have had a considerably higher impact on the temporal variability of reservoir ages. Rapid melting of the local glaciers may have caused a high IRD supply at 823 cm core depth but also significant fresh-water supply, which possibly lowered the marine reservoir age in LJL at that time substantially. Another factor, which may have contributed to a lower marine reservoir age is possibly an increasing wind strength that may have enhanced the CO_2 exchange between atmosphere and ocean. Anyhow, ΔR was not varied for the calibration of ^{14}C ages because reservoir age variability cannot be definitely constrained and therefore remains speculative. The $n\text{-C}_{16}$ fatty acid sample from 823 cm core depth was therefore not considered for the chronology.

Based on these considerations, a likely confident sediment chronology was compiled for Units III and IV of the LJL record (fig. 6.2). The age model was derived by polynomial fitting of the chosen calibrated biomarker and macrofossil ^{14}C ages. For the lacustrine stage of the record (Unit II), chronological control is weak, since compound-specific radiocarbon data is not available and since analyzed plant macrofossils are likely "pre-aged". However, linear

extrapolation of the agetmodel of Unit III and IV to the basis of the lacustrine stage of the record yielded an approximate age of basal lake sediment formation of roughly 10,000 yrs BP.

A potential uncertainty in the calibration of all marine-derived radiocarbon ages that were used for the establishment of the sediment chronology is the estimate of the recent local marine reservoir age. It is not clear if ^{14}C enrichment in the ocean water, as a consequence of nuclear weapons testing, may have affected the ^{14}C age of the carbonate shell, which was used for the reservoir correction ($\Delta\text{R} = + 320$).

6.3.3 Mean Residence Time of Organic Matter in Terrestrial Reservoirs

The fate of terrigenous organic matter buried in coastal marine sediments was investigated in a number of studies (Eglinton et al., 1997; Uchida et al., 2001; Smittenberg et al., 2004; Goni et al., 2005; Drenzek et al., 2007; Mollenhauer and Eglinton, 2007; Kusch et al., 2010a; Vonk et al., 2010; Galy and Eglinton, 2011; Feng et al., 2013; Tao et al., 2015). It was widely observed that this material is often depleted in ^{14}C , possibly because of long transport pathways and multiple retention possibilities, which might have caused long time lags between synthesis and subsequent deposition of the organic matter. Therefore, it is generally assumed that investigations of radiocarbon inventories of terrigenous biomarkers in marginal marine sediments are important to obtain information on environmental processes, but their application for chronological purposes is hampered by high mean residence times (MRTs).

For lacustrine environments, MRTs of terrigenous biomarkers are highly unexplored. Small lakes with small watersheds are assumed to reveal a tighter coupling between terrestrial and lacustrine environments, leading to a rapid transfer between these systems. Additionally, a constant turnover of nearby vegetation is inferred to result in a dominance of fresh material in the terrigenous input (Uchikawa et al., 2008).

Since plant macrofossils are sometimes scarce in lacustrine sediments and hard-water effects possibly preclude that aquatic plant remains can be used for radiocarbon dating, the applicability of terrigenous biomarkers for the establishment of lacustrine sediment chronologies was investigated in a few studies (Uchikawa et al., 2008; Douglas et al., 2014; Gierga et al., 2016). Close agreement between terrigenous biomarker and macrofossil ages was found by Uchikawa et al. (2008) and Gierga et al. (2016), whereas "pre-aged" biomarkers (by 20–520 years) are reported by Douglas et al. (2014).

The investigated lacustrine environment of ALA appears to be very different from the lakes in these studies. "Pre-aging" of terrigenous biomarkers and of macrofossils appears to be relatively severe (c.1900 years) and constant over time.

In order to derive a chronology of terrigenous biomarkers of the LJL record, polynomial fitting of $n\text{-C}_{26}$ fatty acids ages was performed. The difference between the agetmodels of marine samples and of terrigenous biomarkers can be interpreted as MRT of terrigenous

organic matter in intermediate reservoirs (Douglas et al., 2014). The red line in fig. 6.2 indicates the variability of MRTs throughout the record Co1305. MRTs seem to be somewhat higher ($\sim 2,000 - 2,600$ years) in the setting of LJL than of ALA. A longer transport pathway due to a larger catchment of LJL in contrast to ALA may explain the higher MRTs. However, the magnitude of "pre-aging" of terrigenous organic matter is very similar for both environments. Therefore, superordinate processes that affect both environments similarly may have had a major influence on the radiocarbon inventories of terrigenous organic matter. Similar ^{14}C ages of plant macrofossils and co-occurring terrigenous biomarkers (tab. 6.2) indicate a common fate of the material. This find supports the argumentation, that large fractions of the terrigenous biomarker pools likely derived from plant debris in the sediments. These findings are important, since plant macrofossils are often investigated exclusively, when sufficient amounts are found in lake sediments. If processes like intermediate storage are not fully understood for the investigated depositional systems, ages of terrigenous organic matter can be misleading. When respective samples are used for sediment chronologies, considerable deviations from the time of deposition can result and lead to false chronologies. It seems therefore recommendable to always investigate radiocarbon inventories of different sample types, in order to identify site-specific effects.

6.3.4 Biomarkers and Proxies - Co1308

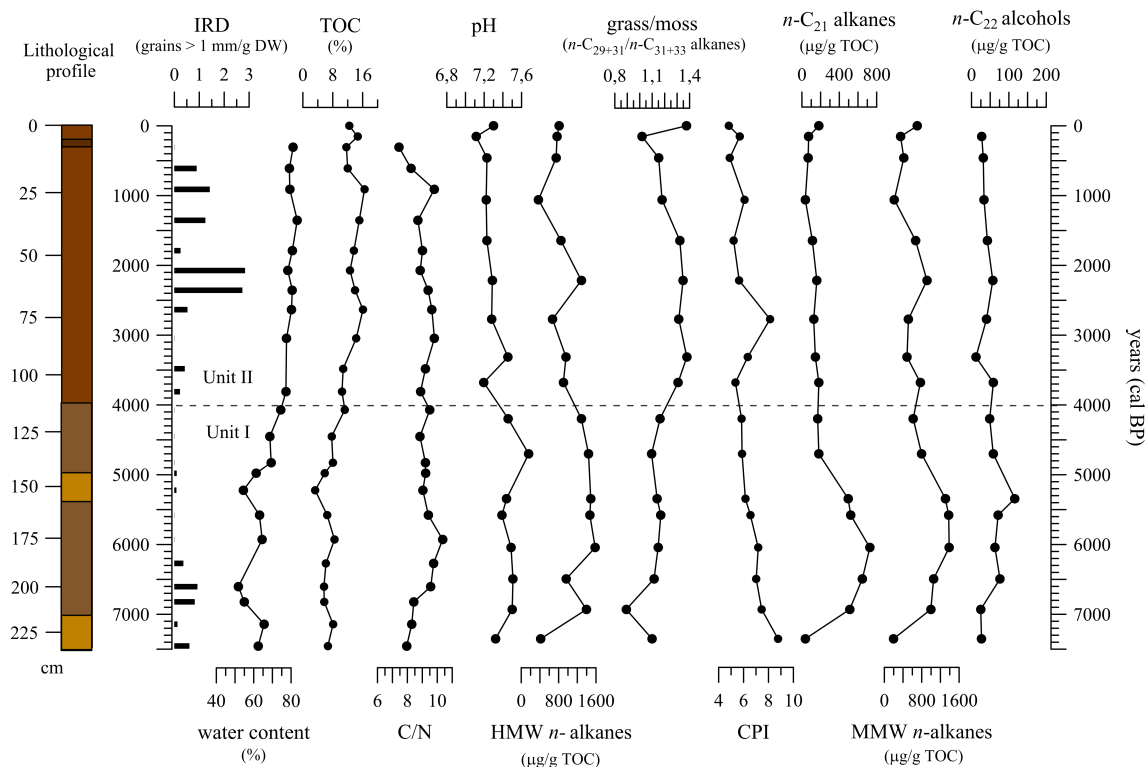


Figure 6.3: Lithological profile of the core Co1308, biomarker and proxy records against sediment age.

The 2.33 m long composite core Co1308 comprises c. 7480 years of sedimentation history in Allen Lake A (fig. 6.3). It consists of generally dark brown, organic-rich sediments which include plenty of macroscopic plant remains. The sedimentary record can be subdivided in two distinct units that are characterized by differing sediment properties. The transition between the units occurs at c. 1.1 m core depth (around c. 4,000 cal BP) and is visibly marked by a color change, from more yellowish brown sediments in the lower Unit I towards more reddish brown sediments in upper Unit II. The sediment color gives a tentative approximation of the variability of the organic matter content in the sediments. Generally lower TOC concentrations in Unit I (3.3 - 8.1 %) contrast higher concentrations in Unit II (10.5 - 16.5%). Lowest TOC contents were detected within two distinct sediment layers of lighter color that occur between 2.15 - 2.33 m and between of 1.42 - 1.64 m core depth. In contrast, a small band of darker sediments at c. 5 cm core depth exhibits a particularly high TOC concentration. Besides of the variations that are displayed within and between the two units, TOC shows a generally increasing trend from the bottom to the top of the sedimentary record. Quite the same increasing trend is also displayed for the water content of the sediments, increasing from 51.8 - 69.3% in Unit I to 74.5 - 83.3% in Unit II. A strong co-variation between TOC and water contents is given for the entire record.

Assuming a mainly aquatic origin of n -C₂₂ alcohols also in the lake, small autochthonous contributions are indicated by generally low abundances of n -C₂₂ alcohols throughout the record (fig. 6.3). Concentrations are similar in both units and exhibit values between 12 - 76 $\mu\text{g/g}$ OC. An exception is displayed around 5,300 cal BP, where a higher n -C₂₂ alcohol concentration of 116 $\mu\text{g/g}$ OC was detected. However, this peak coincides with the lowest TOC concentration in the record and therefore possibly reflects a higher proportion of aquatic organic matter in the TOC of the sediments, rather than a particularly high autochthonous productivity at that time. HMW n -alkanes, that are assumed to represent terrestrial productivity most accurately, display differing concentrations in Units I and II. Except a relatively low concentration of 417 $\mu\text{g/g}$ OC at the base of the record, sediments of Unit I are characterized by generally higher abundances of HMW n -alkanes (962 - 1487 $\mu\text{g/g}$ OC) than those of Unit II (369 - 1287 $\mu\text{g/g}$ OC) (fig. 6.3). The highest concentration of HMW n -alkanes in Unit II coincides with a high concentration of coarse sediments (grains > 1mm), possibly pointing to increased erosion between c. 2,500 and 2,000 cal BP. The generally decreasing concentrations of HMW n -alkanes between c. 7,200 and c. 1,000 cal BP can not be interpreted as indicator for a general reduction in terrestrial productivity, since TOC concentrations show an increasing trend in this period. The decreasing concentrations of HMW n -alkanes more likely indicate a transition in the plant communities. The climax vegetation of South Georgia is characterized by the dominance of tussock grass species (Leader-Williams et al., 1987). In earlier stages of plant succession, moss species have played a significant role. n -Alkane distributions of contemporary plants revealed highest abundances of n -C₂₉ and n -C₃₁ in the tussock grass sample and of n -C₃₁ and n -C₃₃ in the moss sample. The ratio of these n -alkanes ($(n\text{-C}_{29}+n\text{-C}_{31})/(n\text{-C}_{31}+n\text{-C}_{33})$), termed

grass/moss ratio, may be used to identify changes in the composition of the vegetation in the catchment of ALA throughout the sedimentation history. In Unit I, generally low grass/moss ratios of 0.9 - 1.2 point to a dominance of moss species between c. 7,450 and c. 4,000 cal BP. In Unit II, a dominance of grass species is indicated by generally higher ratios of 1.2 - 1.4. A distinct drop to a value of 1 around 200 cal BP potentially indicates that grasses were temporarily replaced by mosses at that time. The general trend of increasing proportions of grasses likely reflects plant succession in the study area. The inverse relation between decreasing concentrations of HMW *n*-alkanes and increasing proportions of grasses can therefore potentially be interpreted as a result of generally lower HMW *n*-alkane concentrations in grasses than in mosses. This is possibly the case if mosses contain more lipids than grasses, which might reveal higher proportions of sugars in their tissue. If so, the variability in the sum of HMW *n*-alkane record possibly integrates both changes in productivity and changes in plant communities.

A further indication for high abundances of mosses in Unit I is revealed by the *n*-C₂₁ alkane record which shows particularly high concentrations of 495 - 727 $\mu\text{g/g}$ OC between c. 7,000 and 5,300 cal BP (fig. 6.3). *n*-C₂₁ alkanes were found to be dominant in the *n*-alkane inventory of *Henediella heimii*, a bryophyte species that occurs in saline environments, such as coastal salt marshes (Harada et al., 1995). This halophyte moss is a dominant species in the Antarctic environment (Barrett et al., 2006) and was also found on South Georgia (Van der Putten et al., 2009). The trend of *n*-C₂₁ alkane concentrations is not consistent with the trend of the grass/moss ratio throughout the record. Concentrations of *n*-C₂₁ alkanes increase between the beginning of the record at 7,450 cal BP from 36 $\mu\text{g/g}$ OC to a peak concentration of 727 $\mu\text{g/g}$ OC around 6,400 cal BP. From that time on, concentration decreases again and exhibits quite constant values of 37-181 $\mu\text{g/g}$ OC from c. 4,700 cal BP to present. Since *Henediella heimii* apparently enhances the upward migration of salt solutions (Barrett et al., 2006), the abundance of *n*-C₂₁ alkanes in the lacustrine record may be interpreted as indicator for the influence of ocean water in the catchment of the ALA, which is located proximal to the shore of Allen Bay. The course of the *n*-C₂₁ alkane record therefore possibly documents the variability of the RSL.

Mid-molecular-weight (MMW) *n*-alkanes are characteristic for aquatic (submerged or floating) plant species (Ficken et al., 2000) as well as for Sphagnum species (Ficken et al., 1998a). The course of the MMW *n*-alkane record resembles the variability that is displayed by the *n*-C₂₁ *n*-alkane record, with generally high concentrations of 798 -1387 $\mu\text{g/g}$ OC in Unit I (except in the lowermost depth, where concentrations of just 197 $\mu\text{g/g}$ OC occur) and lower concentrations of 213-912 $\mu\text{g/g}$ OC in Unit II. The attribution to aquatic plants or to terrestrial mosses is not clear, but the similarity between the MMW *n*-alkane and the other *n*-alkane records suggests a common terrestrial source of these biomarkers. Highest concentrations of MMW *n*-alkanes coincide with relatively high C/N ratios between 6,500 and 5,500 cal BP, supporting a terrigenous origin of these biomarkers. The C/N variability within the sedimentary sequence is relatively small, with values of 7.4 - 8.4 in the uppermost and the lowermost parts of the record and with values of 8.7 to 10.4 between c. 6,500 and 700 cal BP.

Low CPI values point to high proportions of even-numbered *n*-alkanes in the sediments of Co1308. Since metabolization by microbes favors even numbered chain lengths, CPI can be used as an indicator for degraded sources of *n*-alkanes (Cranwell, 1981). However, CPI values vary for different plant species, so that CPI variability can also reflect changing sources of *n*-alkanes. The contemporary moss sample revealed a CPI value of c. 10, whereas the tussock grass sample had a value of c. 20 (Berg et al., 2019). CPI values successively decrease from 8.8 to 4.8 between the bottom to the top of the record, likely pointing to increasing proportions of degraded *n*-alkanes in the sediments. An exception for this trend is displayed by a relatively high value of 8.1 around 2,800 cal BP. Together with decreasing CPIs, grain-size of the sediments increases from clay and silt in Unit I to silt with increasing proportions of fine sand in Unit II. Consistently with the fine sand fraction, also the record of coarser grains of > 1 mm increases in Unit II and reaches particularly high counts between 2,500 and 2,000 cal BP. The vegetational change in the catchment of the lake may have favored the transition in grain size. The fine material in the lower part of the record likely consists of larger fractions of fresh moss organic matter, indicated by similar CPI values of sedimentary *n*-alkanes and contemporary moss sample. The moss-dominated vegetation in Unit I, possibly retained large parts of coarser material within the moss layer. With an increasing proportion of more unconsolidated tussock grass stands, run-off possibly canalized between the stands and transported higher fractions of coarser sediments to the site. Increasing heterogeneity of the sediments in the course of the record and higher fractions of degraded material were possibly mobilized during the grass-dominated phase. However, the consistently decreasing CPI values throughout the record can also partly reflect progressive degradation of *n*-alkanes since the time when vegetation establishment at the end of the LGM.

6.3.5 Biomarkers and Proxies - Co1305

The subdivision of the sedimentary record Co1305 into four Units was discussed in chapter 4. The beginning of lacustrine sedimentation, marking the transition between Unit I (the diamictic base of the record) and Unit II can only be anticipated to have happened around c. 10,000 years BP. A detailed interpretation of the onset of lacustrine sedimentation, will be given in later in this chapter.

The lacustrine stage of the record Co1305, comprising the time interval between c.10,000 and 7,300 cal BP, is characterized by generally low concentrations of aquatic as well as of terrigenous biomarkers (fig. 6.4). Highly variable TOC concentrations of 0.8-2.3% may indicate large fluctuations in the supply of clastic material to the site or variable preservation conditions in the lacustrine environment. The vegetation in the watershed of the lake seems to be dominated by high proportions of mosses, indicated by relatively small grass/moss

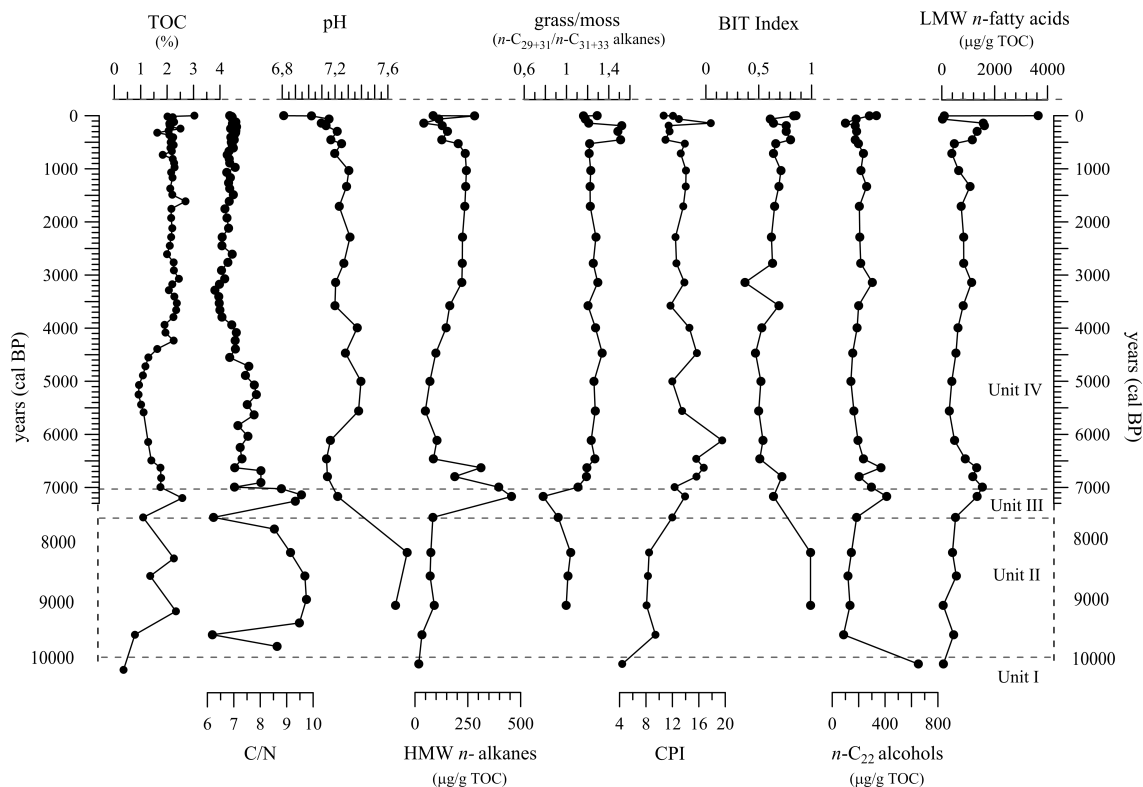


Figure 6.4: Biomarker and proxy records of Co1305 against sediment age. Dashed vertical lines indicate the inferred sediment ages of Unit II, derived from extrapolation of the agemodel of Unit IV and III.

ratios of 0.9 - 1. CPI values of 8.1-9.4, which are similar to the CPI of the recent moss sample, likely support the predominance of this vegetation type during the lacustrine stage of the record. High pH values of 7.7 are an indicator for just poorly developed, young soils in the catchment of the lake. The fresh soil signal in the sediments supports the interpretation that CPI values do not reflect degraded n -alkanes but the source of the plant biomass. Irrespective of the seemingly high concentration of HMW n -alkanes in mosses, lacustrine sediments reveal only low abundances of these biomarkers (33 to 91 $\mu\text{g/g OC}$). Therefore, it can possibly be assumed that vegetation density was low between 10,000 and 7,300 cal BP. However, despite of an apparently low productivity of the terrestrial biosphere, dominant contributions of terrigenous organic matter to the sediments are indicated for largest parts of in the lacustrine stage by C/N ratios of 8.5-9.7. An exception is revealed at c. 9,600 cal BP, where a C/N ratio of just 6.2 may points to a short period of relatively high proportions of aquatic organic matter in the sediments. In contrast to the persistently low concentrations of HMW n -alkanes, $n\text{-C}_{22}$ alcohols and $n\text{-C}_{16}$ fatty acids exhibit generally increasing concentrations between 10,000 and 7,300 cal BP, resulting in a high proportion of aquatic sedimentary biomass at the transition from Unit II to Unit III, which is reflected by a C/N ratio of 6.2 around 7,300 cal BP. The variability of $n\text{-C}_{16}$ fatty acid concentrations (27 - 330 $\mu\text{g/g OC}$) is much higher than that of $n\text{-C}_{22}$ alcohols (86 - 146 $\mu\text{g/g OC}$), possibly supporting the suggestion of variable preservation condition in the lacustrine stage of the record.

Transgression from lacustrine towards marine conditions (Berg et al., 2019) started c. 7,300 cal BP and ended c. 7,000 cal BP. The sediments of this stage reveal high TOC concentrations of 2.6 % and a large proportion of terrigenous organic matter, indicated by C/N ratios of 8.8 - 9.6. A marked peak in the record of HMW *n*-alkanes supports a particularly high supply of terrigenous biomass to the sediments (fig. 6.4). However, the large abundances of HMW *n*-alkanes (396-457 $\mu\text{g/g}$ OC) unlikely result from high terrigenous productivity alone. Intense erosion of catchment areas, which had only minor contributions to the sedimentation in previous phases, may partly have caused the high amounts of terrigenous organic matter in the sediment. Erosional products from these areas are apparently characterized by a relatively low pH of 7.2 which indicates large proportions of aged soils. If assuming that the lake level was way below the sill of LJJL when the marine transgression started, entering ocean water probably flushed the slopes of the catchment and mobilized organic matter of older soil deposits. Additionally, mosses which likely colonized the steep flanks of the watershed were possibly eroded to a high extent by the inflowing water, causing particularly low grass/moss ratios of 0.8 -1 during the transgression.

High erosion rates may have caused a large nutrient supply to the aquatic site at that time. Enhanced aquatic productivity is likely reflected by high concentrations of *n*-C₂₂ alcohols and *n*-C₁₆ fatty acids in the sediments (297-412 and 880-891, respectively). However, allochthonous supply of marine biomass, transported within the ocean water, may also have contributed to the high abundances of sedimentary *n*-C₂₂ alcohols and *n*-C₁₆ fatty acids. Erosion of land surfaces, which seems to have largely dominated the composition of sedimentary organic matter at the beginning of the transgression, likely decreased at the end of this phase. When full marine conditions established around 7,000 cal BP, a C/N ratio of 7 indicates high proportions of marine biomass in the sediment composition. Plankton species, which were possibly not as vital in the brackish waters, were likely favored from that time on.

Multiple effects apparently determined the sediment composition during the marine transgression, including high terrigenous and marine productivity as well as increased erosion of land-derived organic material. Enhanced preservation conditions due to high sedimentation rates possibly also played an important role for the distribution of biomarkers during this stage of the record.

A short time interval after the marine transgression, between c. 7,000 and 6,600 cal BP, reveals still high concentrations of marine as well as of terrigenous biomarkers (fig. 6.4). A dominant contribution of terrigenous organic matter to the sediments is indicated by C/N ratios between 9.7 and 8 and a maximum concentration of HMW *n*-alkanes of 312 $\mu\text{g/g}$ OC. TOC has a constant concentration of 1.8% between c. 7,000 and 6,600 cal BP and then decreases gradually to a minimum of 0.9 % around 5,500 cal BP. Concentrations of *n*-C₂₂ alcohols and of *n*-C₁₆ fatty acids decrease as well from values of 369 and 761 $\mu\text{g/g}$ OC at c. 6,600 cal BP to values of 141 and 158 $\mu\text{g/g}$ OC at c. 5,500 cal BP, respectively. HMW *n*-alkane concentrations show a distinct drop after c. 6,600 cal BP and display lowest

abundances of 49 $\mu\text{g/g}$ OC around 5,500 cal BP. C/N ratios of 7 - 7.7 likely reflect the decreasing proportion of terrigenous organic matter during this period.

A transition in composition of the terrestrial vegetation is indicated by increasing grass/moss ratios up to 1.3 around 6,400 cal BP. The assumption of the succession of grass species is also supported by increasing CPI values, which exhibit a maximum of 19.5, close to the CPI of a recent grass sample, around 6,000 cal BP. However, despite of the establishment of new plant communities in the catchment of LJJ, low pH values of 7.1 - 7.2 apparently point to a persistent erosion of aged soils until 6,000 cal BP, possibly caused by a further increasing RSL after the marine transgression. After 5,500 cal BP, erosion of mainly recent soils is indicated by higher pH values. However, the development and aging of these soils has resulted in a persistent decrease from a pH of 7.4 around 5,500 cal BP to a pH of 6.8 in present times.

After 5,500 cal BP, when TOC and all biomarkers displayed minima of their abundances, concentrations slowly increase again until c. 4,200 cal BP. In this phase of the record, grass/moss ratios remain stable but CPI values vary between 12 and 15.7, possibly indicating variable contributions of degraded *n*-alkanes to the site, rather than variable sources.

A small variability in the concentrations of TOC (2 -2.4%), of C/N ratios (7.1- 6.3) and of HMW *n*-alkanes (47-243 $\mu\text{g/g}$ OC) is revealed for the time interval between c. 4,200 and 500 cal BP, pointing to relatively constant environmental conditions. *n*-C₂₂ alcohol and *n*-C₁₆ fatty acid concentrations are also quite uniform during this period with values of 189-216 $\mu\text{g/g}$ OC and of 231-608 $\mu\text{g/g}$ OC, respectively. However, around 3,200 cal BP particularly high concentrations of *n*-C₂₂ alcohols (412 $\mu\text{g/g}$ OC) and a low BIT Index of just 0.4 may point to a period of exceptionally high marine productivity.

Between c. 500 cal BP and present, nearly all records display a high variability. A high marine productivity is indicated for the period between 500 and 140 cal BP by *n*-C₁₆ fatty acids concentrations of 632 -1067 $\mu\text{g/g}$ OC. These high abundances of *n*-C₁₆ fatty acids contrast low HMW *n*-alkane concentrations of 41- 154 $\mu\text{g/g}$ OC during this phase. However, low abundances of HMW *n*-alkanes unlikely reflect low terrigenous productivity but rather a differing composition of plant communities. Particularly high proportions of grasses are indicated by an exceptionally high grass/moss ratios of c. 1.5 during this period. Increased erosion of (degraded) soils in this grass-dominated environment is likely reflected by BIT indices of 0.6-0.9 as well as by relatively low CPI values of 11.0-11.6. Between 140 cal BP and present, BIT indices are particularly high (0.8-0.9). The low pH of just 6.8 of the surface sediments may suggests a higher contribution of aged soils in recent times.

6.3.6 GDGT-derived Temperature Reconstructions - Co1305

Besides of the utilization of GDGTs as lipid biomarkers, the correlation of their structural differences with environmental factors like air temperature, sea-surface temperature or soil pH, enables their application as environmental proxies. Several temperature calibrations and temperature proxies were developed based on investigations of the distributions of aquatic-

derived isoGDGTs, as well as of soil-derived brGDGTs, in sedimentary archives.

The coastal marine setting of LJJ enables the application of temperature proxies that are based on marine isoGDGT as well as on soil-derived brGDGTs.

Tex₈₆ proxy for SST reconstructions: The Tex₈₆ temperature proxy was developed based on the observation that the number of cyclopentane moieties in aquatic-derived isoGDGTs apparently increases with growth of temperature (Schouten et al., 2002). A high correlation of Tex₈₆ with the annual mean temperature of the upper mixed layer of the ocean enables the application of Tex₈₆ for reconstructing sea surface temperature (SST) (Kim et al., 2008). However, applying the Tex₈₆ temperature proxy in high latitudes is complicated, because the crenarchaeol regio-isomer (cren'), which is included in the Tex₈₆ proxy, is apparently insensitive to temperature variability in the polar oceans. A regional calibration (Tex₈₆^L), excluding cren', was therefore developed for these regions (Kim et al., 2010).

For the record of LJJ a Tex₈₆^L-based SST reconstruction was performed. In fig. 6.5a, reconstructed SSTs are displayed as temperature anomalies (the local deviation from the mean SST of the record). The revealed SST variability of the LJJ record can be subdivided in three distinct phases. Between c. 7,200 and c. 3,700 cal BP, SSTs are generally low and therefore result in mostly negative or slightly positive temperature anomalies of +1.8 to -18.7°C. In contrast, exclusively positive temperature anomalies of +3.2 to +18.1 °C characterize the period between c. 3,700 and c. 800 cal BP. For the time interval between c. 800 cal BP and present, reconstructed SSTs display a smaller amplitude than in the previous phases (-4.1 to +6.1°C) but a relatively high temporal variability. The unrealistically high absolute variability of SSTs indicates that the Tex₈₆^L apparently do not perform well in LJJ, as also observed in other high latitude regions (Ho et al., 2014). However, even if absolute SSTs are not reliable, the SST variability can be compared other temperature reconstructions derived from this record, so that similarities and differences of general trends e.g. between air and water temperatures can be identified and potential biases can be encountered.

MBT'/CBT proxy for MAAT reconstructions: The Methylation of Branched Tetraethers (MBT) and the Cyclization of Branched Tetraethers (CBT) indices (MBT'/CBT) rely on the apparent adaptation of brGDGT producing soil bacteria to growing conditions in the soils. Distributions of brGDGTs in a global soil dataset revealed that soil pH and mean annual air temperature (MAAT) are the major environmental factors for the structural variability of brGDGTs (Weijers et al., 2007). Alteration of the number of cyclopentyl moieties changes the membrane fluidity of brGDGTs, so that soil bacteria can survive in unfavorable habitats, when they reduce the permeability of their membranes. Apparently, the number of cyclopentane moieties in the brGDGTs can be related to soil pH, whereas the number of methyl groups can be related to both soil pH and MAAT (Peterse et al.,

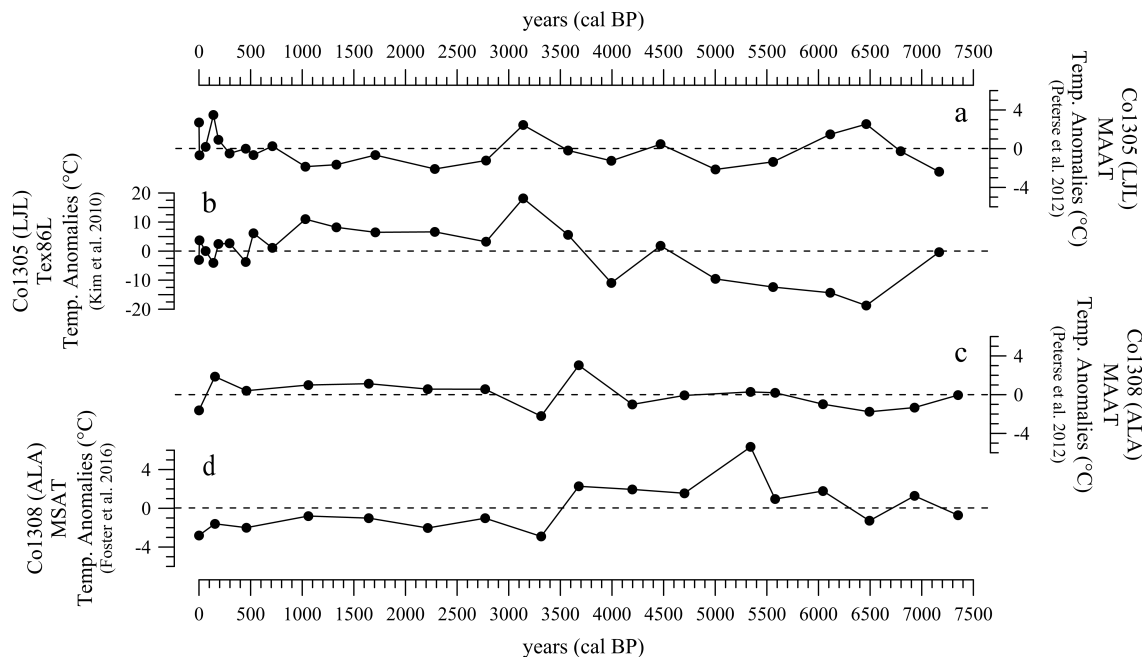


Figure 6.5: GDGT-derived Temperature Reconstructions for the records Co1308 and Co1305. Reconstructed temperatures are not displayed as absolute values but as temperature anomalies (the local deviation from the mean value of the record).

2009). Based on these relationships, and under consideration of an extended calibration soil dataset, the revised (MBT'/CBT) was developed by Peterse et al. (2009).

Several uncertainties have to be considered, because of the calibration of the MBT'/CBT proxy against MAAT and because of potential biases in the analyzed brGDGT records. Despite of the high correlation between MBT'/CBT and MAAT in the investigated global core top calibration data set, it can be assumed that MBT'/CBT would probably even better relate to soil-surface temperatures. However, soil temperatures are not documented at high spatial and temporal resolution so that they cannot be employed for a global calibration purpose. On larger regional or global scales, it is particularly true that MAAT and soil-surface temperature are virtually equal, because soil temperatures are largely governed by air temperatures. But, on a local scale the offset between the air and soil temperatures can be quite variable. The scatter resulting from this potentially variable relationship translate into a standard error of estimates of ca. 4 °C in the calibration of MBT'/CBT with MAAT (Weijers et al., 2011a).

Besides of the uncertainties that derive from the calibration of the proxy against MAAT, a seasonal bias can be introduced to the temperature signal when brGDGT-producing bacteria have a preferential growing season (Peterse et al., 2012). Generally lower correlations for high latitudes than for temperate regions were observed in the global core top dataset which may partly relate to the stronger seasonality in these regions. A temporal variability of the vegetation cover, of the precipitation amount or intensity as well as of the variable sources

Table 6.3: Results of temperature reconstructions, BIT indices and #Ringtetra indices of the record Co1305.

Little Jason Lagoon - Co1305							
depth [cm]	years cal BP	Kim et al. 2010	Peterse et al. 2012			Sinninghe-Damsté et al. 2016	
		SST (°C)	CBT	MBT'	MAAT (°C)	BIT	#Ringtetra
0	0	9.1	1.04	0.55	12.0	0.85	0.16
4	4	15.9	1.06	0.45	8.6	0.83	0.11
55	63	12.2	0.53	0.38	9.5	0.61	0.32
103	140	8.0	0.44	0.41	11.0	0.64	0.32
128	188	14.5	0.47	0.39	10.2	0.76	0.34
176	296	14.8	0.48	0.35	8.8	0.76	0.35
210	385	20.7	0.47	0.32	8.2	0.78	0.34
234	454	8.4	0.53	0.37	9.3	0.80	0.34
258	527	18.3	0.42	0.33	8.7	0.66	0.42
308	712	13.2	0.41	0.36	9.6	0.64	0.41
371	1031	23.1	0.48	0.30	7.5	0.71	0.36
418	1331	20.3	0.49	0.31	7.7	0.69	0.34
468	1708	18.6	0.47	0.34	8.7	0.65	0.39
522	2285	18.7	0.50	0.30	7.2	0.62	0.32
572	2779	15.3	0.47	0.32	8.1	0.63	0.47
612	3140	30.3	0.00	0.35	11.8	0.37	0.65
671	3576	17.7	0.48	0.36	9.1	0.69	0.33
720	3993	1.2	0.20	0.27	8.1	0.53	0.51
770	4471	13.9	0.14	0.32	9.8	0.47	0.52
820	5002	2.5	0.28	0.26	7.2	0.52	0.47
868	5561	-0.3	0.19	0.27	8.0	0.50	0.54
912	6115	-2.2	0.28	0.37	10.8	0.54	0.45
938	6462	-6.6	0.18	0.39	11.8	0.51	0.51
962	6795		0.65	0.38	9.0	0.72	0.24
988	7169	11.8	0.81	0.35	6.9	0.64	0.26
1010	8225		0.62	0.08	-0.3	0.99	0.43
1028	8772	10.7	0.46	0.12	2.0	0.99	0.30

Table 6.4: Results of temperature reconstructions and #Ringtetra indices of the record Co1308

Allen Lake A - Co1308						
depth [cm]	years cal BP	Peterse et al. 2012			Sinninghe-Damsté et al. 2016	Foster et al. 2016
		CBT	MBT'	MAAT (°C)	#Ringtetra	MSAT (°C)
0	0	1.19	0.30	3.4	0.07	7.0
4	154	1.11	0.40	6.9	0.09	8.2
12	459	1.05	0.34	5.4	0.09	7.8
28	1058	0.96	0.34	6.0	0.09	9.0
44	1644	0.92	0.34	6.2	0.12	8.7
60	2215	0.86	0.31	5.6	0.14	7.7
76	2772	0.88	0.31	5.6	0.12	8.7
92	3314	0.89	0.23	2.8	0.16	6.8
103	3679	0.68	0.36	8.0	0.18	12.0
119	4197	0.66	0.22	4.0	0.16	11.7
135	4702	0.57	0.24	4.9	0.24	11.3
156	5342	0.48	0.23	5.3	0.26	16.1
164	5580	0.64	0.26	5.2	0.19	10.7
180	6044	0.58	0.21	4.0	0.20	11.5
196	6494	0.66	0.20	3.3	0.18	8.5
212	6930	0.73	0.23	3.7	0.16	11.0
228	7351	0.87	0.29	5.0	0.16	9.0

of brGDGTs can further increase the uncertainty of the correlation between MBT'/CBT and MAAT (Sun et al., 2011).

Reconstructed MAATs of the LJJ record vary between 7.2 -12°C. For the period between c. 5,700 cal BP and present, the MAAT variability shows similar trends as the Tex_{86}^L - derived SSTs, including maximum temperatures at c. 3,200 cal BP (fig. 6.5 a,c). Between c. 5,700 and 7,200 cal BP, positive MAAT anomalies contrast negative SST anomalies.

6.3.7 GDGT-derived Temperature Reconstructions - Co1308

MBT'/CBT proxy for MAAT reconstructions: The application of the MBT'/CBT proxy is often hampered in lacustrine environments because of high amounts of brGDGTs that were produced within the lakes (Tierney and Russell, 2009; Weijers et al., 2011b). However, #Ringtetra indices which display small values for the entire record of ALA (tab. 6.4), indicate that *in situ* production is only of minor importance in the sediments of the investigated lake site. Therefore, MAATs were reconstructed for the brGDGT record of ALA, based on the MBT'/CBT proxy (fig. 6.5 c). The displayed MAAT variability is quite small for most parts of the record (3.4-6.9°C) and generally lower than for LJJ. Only between 3,680 and 3,450 cal BP, minimum and maximum values of 2.8 and 8°C were calculated.

Regional calibration for MSAT reconstructions: Because of the generally poor performance of GDGT-derived temperature reconstructions in high latitude environments, a regional calibration based on 32 lacustrine records from Antarctica and the sub-Antarctic was developed by Foster et al. (2016). Distributions of brGDGTs in these lakes showed stronger correlations with mean summer air temperature (MSAT) than with MAAT, possibly due to the seasonality of their production. Other than for MBT'/CBT, correlation of the brGDGT composition with temperature is apparently stronger than with soil pH in this dataset. Furthermore, a great importance of GDGT-IIIb in cold lacustrine environments was discovered in this study (correlation with MSAT $r^2 = 0.76$). Based on these findings, the regional MSAT calibration was developed, based on a weighted sum of IIIa, IIIb, IIa and Ib.

Reconstructed MSAT of the ALA record display a variability of 7.0-16.1°C (fig. 6.5 d). As for MBT'/CBT-derived MAAT estimates, a marked transition is also indicated by MSAT between c. 3,700 and 3,300 cal BP. Before this period, MSATs display mostly positive temperature anomalies. Between c. 3,300 cal BP and present, temperature anomalies are always negative.

6.3.8 Evaluation of Temperature Reconstructions

The spatial proximity between ALA and LJL, both located at low altitudes on the northeastern coast of South Georgia, suggests generally similar climatic conditions at these sites. However, it might be assumed that local differences, e.g. in the amplitudes of air temperatures, are possibly favored by site-specific environmental factors of the respective settings. At the site of LJL, orographic effects of the high mountain ranges, which encompass the marine inlet, potentially affect the local temperature variability. Particularly high air temperatures may occasionally be favored in this setting by föhn effects of the persisting south-westerly winds, crossing the mountain ridges (Gordon et al., 2008). On the other hand, shadowing effects of the mountains during distinct times of a day (or seasons) might promote prolonged periods of locally low air temperatures. These opposing orographic impacts might be expected to potentially cause relatively large temperature variations (on different timescales) in the setting of LJL.

Such orographic effects are probably of minor importance for the local temperature variability at the ALA site, which is located at a more exposed position on Lewin Peninsula, near the coast. It can be assumed that the setting of ALA experience a strong maritime influence, possibly resulting in a relatively small local amplitude of air temperatures.

Site-specific variability of the local amplitudes of air temperatures may partly explain differences between MAAT estimates derived from the ALA and the LJL record (fig. 6.5 a,c). However, besides of these potential local differences, it can be expected that general temperature trends are similar in both settings. The lack of coherence in reconstructed tem-

peratures, therefore might point to additional environmental differences between the sites, which strongly affect the distribution of brGDGTs in the aquatic sediments.

Most suspicious in the MAAT and MSAT reconstructions that were derived from the brGDGT record of the ALA site, is a distinct shift (or a high variability) of temperatures between c. 3,680 and 3,450 cal BP (6.5 c,d). The grass/moss ratio indicates that the proportion of grasses reached a plateau at that time, after a gradual increase. The vegetational succession in the catchment of ALA is accompanied by several sedimentological and biogeochemical changes in the lake sediments, e.g. of sediment color, grain size, TOC and biomarker concentrations (fig. 6.3), supporting a marked environmental transition in the lacustrine setting. Since succession of plant communities points to generally ameliorating climatic conditions, the opposing MSAT trend from mainly positive temperature anomalies before c. 3,680 cal BP to negative temperature anomalies after 3,450 cal BP (6.5 d), seems to reflect changing soil properties rather than climatic influences. An alteration of the habitat of soil bacteria may have led to a change in bacterial communities or to an adaptation to environmental factors by structural modification of brGDGTs. Correlations between significant changes in reconstructed MAAT (derived from MBT'/CBT) and environmental transitions were previously documented. A considerable drop of reconstructed MAAT from a peat record was found to coincide with a transition from the *Carex* dominated fen peat to *Sphagnum* dominated bog peat (Weijers et al., 2011b). Humidity was also considered to have an effect on the MBT index, since Huguët et al. (2010) found lower MBT indices at wetter fen sites and higher MBT indices at drier bog sites. It seems plausible that environmental changes might have overprinted the temperature signal in the brGDGT record of the ALA site. Therefore, brGDGT-based temperature reconstructions derived from this site are likely biased and need to be rejected from further considerations.

Such drastic environmental changes are not indicated by the sediment properties of the LJJ record. The grass/moss ratio is quite constant at this site, assuming that vegetational transitions were not as pronounced. Therefore, it can be expected that the brGDGT-based temperature reconstructions derived from the record of the LJJ site are much less biased by these environmental changes and may result in more reliable MAAT estimates for this region. Different from sedimentary sites that are supplied by large river systems, the site of LJJ receives sediments from a relatively small catchment area. Mixing of soil types that have different degradabilities, and that are therefore exported on different timescales, distorting the temperature record (De Jonge et al., 2016; Sinninghe Damsté, 2016) is not indicated in the setting of LJJ.

Despite of the unrealistic absolute temperatures derived from the Tex_{86} proxy, the relatively good match in the general trends, compared to the MBT'/CBT derived temperatures, may indicate that the SST variability can be derived by Tex_{86} in the setting of LJJ. However, a good accordance between the trends of the Tex_{86} and the MBT'/CBT proxies is revealed

for most of the record. The mismatch in the older part of the record can point to erosion of older soils from warmer periods, so that MAAT is overestimated. More likely, MAAT and SST really differed at that time. The high IRD supply may indicate that air temperature was high, resulting in high melting rates. Inflow of large amounts of ice and melt water into the inlet may simultaneously have reduced SST in this environment.

6.4 Interpretation

6.4.1 Start of Sedimentation in LJJ: $> 15,200 - < 11,200$ cal BP

At the base of the sedimentary record Co1305 from LJJ, diamictic sediments document a former glaciation at the coring site, where the prospective lake and later the marine inlet evolved. A plant remain that was recovered from the deepest lake sediments at 10.34 m, few centimeters above the diamicton, yielded an age of $15,160 \pm 250$ cal BP (tab. 6.2 and fig. 6.2). To date, the oldest direct evidence for ice-free conditions on South Georgia is documented by the onset of lacustrine sedimentation in Block Lake on Tønsberg peninsula, prior to 18,600 cal BP (Rosqvist et al., 1999). Other records from South Georgia provide basal ages of peat and sediment sequences of c. 12,000 to 9,000 cal BP (tab. 6.5), marking the start of the Holocene. The find of the plant remain in the sedimentary record of LJJ reveals that on Lewin Peninsula deglaciation took place prior to $15,160 \pm 250$ cal BP, since soil development was apparently far enough progressed to enable plant succession in ice-free areas. This supports the idea of a rapid ice retreat from the shelf to the islands shortly after the LGM maximum extend (Barlow et al., 2016; Graham et al., 2017). Fast colonization of early ice-free refugia, indicated for Tønsberg peninsula (Rosqvist et al., 1999), can therefore also be expected for Lewin Peninsula.

Interestingly, just five centimeter above this find, a second plant remain (from a sediment section not included in the composite profile) reveals an age of just $11,200 \pm 60$ years cal BP. The large temporal offset between the ages of the two plant remains matches quite well the timing of glacier advances in Cumberland Bay (c. 15,170 and 13,340 yr ago) associated to the ACR (Graham et al., 2017). Re-advance of local glaciers in the course of the ACR is also documented by "Stage 3" moraines (termed by Clapperton et al. (1989)) around LJJ (White et al., 2018), indicating that plant succession was probably restricted in the watershed of LJJ, at that time.

Based on the ages of the two plant remains, the onset of lacustrine sedimentation at site Co1305 can be drawn by different scenarios (indicated by dashed lines in fig. 6.2)):

1. Lacustrine conditions established after the deglaciation that followed the LGM (prior to c. 15,200 cal BP). The lake was then overridden by re-advancing glaciers during the ACR, interrupting sedimentation until the glaciers retreated again at the end of the ACR (prior to c. 11,200 years cal BP). However, if assuming that site Co1305 experienced a further glaciation after the establishment of lacustrine conditions, alternating lacustrine and diamictic

sediments would be expected in the lower part of the record. Since a disruption of lacustrine sedimentation cannot be identified based on sediment properties, the first scenario appears unlikely. The second scenario, implying a sedimentation rate of just 1 cm/1000 years, seems also quite unrealistic. Moreover, ice-free conditions at site Co1305 during the ACR seem implausible, since an extensive glaciation in this area is indicated by sub-aquatic moraines in the fjords of the Cumberland Bay (Graham et al., 2017), as well as by moraines around present shore of LJJ (White et al., 2018).

2. The lake formed after the post-LGM glacier retreat but remained unaffected by the re-advancing ACR glaciers that did not reach the site. The particularly severe cooling in the South Atlantic sector during the ACR (Pedro et al., 2015) restricted glacial and fluvial inflow into the lake and/or favored a persistent ice cover on the lake, resulting in a very small lacustrine sedimentation rate between c. 15,200 and 11,200 cal BP.

3. First ice-free conditions after the LGM prevailed somewhere else in the catchment of LJJ, but the site Co1305 remained glaciated, or at least the lake was not yet formed, at that time. Re-advancing ACR glaciers covered the vegetation and plants that grew in ice-free areas were stored under the ice until the end of the cold period. Formation of the lake started just by the end of the ACR and the older plant remain, that has been released by the melting ice, was deposited at the site shortly after the onset of lacustrine sedimentation.

Therefore, an onset of lacustrine sedimentation at site Co1305, only after the glacier retreat that followed the ACR, appears most likely. Melting of the ACR glaciers, possibly caused a rapid infill of the newly exposed basin of LJJ with debris-laden meltwater prior to the commence of lacustrine sedimentation at the site. A transition from coarse diamictic material at the base of the record Co1305 to finer water-rich diamictic sediments are possibly a witness of this process. However, the time of lake formation may still be overestimated by the younger plant age of 11200 ± 60 years cal BP. At other depths of the record, ages of plant remains indicate distinct "pre-aging" of the terrigenous organic material. Therefore, lacustrine sedimentation possibly started just 10,000 cal BP or later, when glaciers were already extensively retreated from the lower zones of the north-eastern coast of South Georgia (Rosqvist and Schuber, 2003).

6.4.2 Lacustrine Stage of LJJ: < 11,200 - c. 7,300 cal BP

The early Holocene that started on the Southern Hemisphere c. 11,000 years BP with the establishment of an interglacial climate (Nielsen et al., 2004) is reflected by the lacustrine sequence of the LJJ record. This sequence comprises c. 70 cm and ends with a marine transgression around 7,300 cal BP. The low sedimentation rate during the lacustrine stage as well as the fine lamination of the sediments point to a low energy discharge regime during that period. The IRD record documents continuous glacial activity in the catchment. This

Table 6.5: Basal peat and lake sediment radiocarbon dates. This overview is taken from Van Der Putten and Verbruggen (2005)

Sample Type	Author	Age cal BP
lake sediments	Rosqvist et al. (1999)	19550-18050
peat	Clapperton et al. (1987)	9690-9420
peat	Barrow et al. (1983)	12150-9650
peat	Clapperton et al. (1989)	11600-10550
peat	Smith (1981)	11050-10500
peat	Smith (1981)	11200-10250
peat	Smith (1981)	9920-9550
peat	Smith (1981)	9760-9530
peat	Van der Putten and Verbruggen (2005)	10700-9900
peat	Van der Putten and Verbruggen (2005)	9410-9030
peat	Van der Putten et al. (2004)	10560-10230
peat	Van der Putten et al. (2004)	11200-10550
lake sediments	Van der Putten and Verbruggen (2005)	9500-9140
lake sediments	Van der Putten and Verbruggen (2005)	10400-9970

supports the assumption that the local glaciers were already extensively retreated when lacustrine sedimentation started in LJJ. Advanced deglaciation at the beginning of the early Holocene is as well indicated by the onset of lake sediment and peat accumulation in many records of South Georgia between c.11,000 to 9,000 yrs BP (tab.) (Smith, 1981; Rosqvist et al., 1999; Van der Putten et al., 2004; Van Der Putten and Verbruggen, 2005; Van der Putten et al., 2009). Evidences from palynological studies reveal that nearly all plant species were already present on the north-eastern shore of South Georgia at the beginning of the Holocene (Barrow, 1983; Van Der Putten and Verbruggen, 2005). This indicates that plants survived in refugia that remained ice-free during the ACR and rapidly colonized ice-free zones after ice retreat (Rosqvist et al., 1999; Smith, 1981; Björck et al., 1991; Van der Putten et al., 2009). Rapid colonization of the uncovered land by plants is indicated by the continuous record of HMW *n*-alkanes in the lacustrine stage (6.4). CPI values of 8.1-9.4 support that *n*-alkanes, most likely, derived from fresh vegetation and not from older degraded sources in the catchment. However, generally low concentrations of HMW *n*-alkanes in the lacustrine sediments of LJJ, indicate that productivity on land was restricted at that time (fig. 6.4). Low terrestrial productivity in the study area may have been due to a cooling trend between 9000 and 7000 cal BP that is documented in the sub-Antarctic (Bianchi and Gersonde, 2004), may have caused the .

6.4.3 Mid-Holocene Hypsithermal: c. 7,500 (7,300) - 5,800 cal BP

A climatic optimum in the sub-Antarctic region, between c. 7,500 and 6,000 years BP, is indicated by e.g. particularly high SSTs of the Ross Sea (Steig, 1998; Michalchuk et al., 2009) (fig. 6.6). For South Georgia, a general warming trend after 8,400 cal BP (Rosqvist et al., 1999) and a mid-Holocene warm peak at 6,100 cal BP (Rosqvist and Schuber, 2003) were identified in lacustrine records from Tønsberg Peninsula.

Consistent with the observed warm phase in these studies, reconstructed MAATs of the LJJ

record reveal positive temperature anomalies between 7,000 and 5,800 cal BP (fig. 6.6d). Generally high concentrations of HMW *n*-alkanes and of *n*-C₂₁ alkanes (fig.6.7e,g), as well as a low grass/moss ratio point to dominant proportions of mosses in the catchment of ALA at that time (fig.6.7f) . Relatively wet climatic conditions after 6,200 cal BP are possibly indicated by the establishment of *Juncus sp.* (fig.6.7 h), a species of flushed wet habitats (Clapperton et al., 1989). In contrast to the positive temperature anomalies of the MAAT record, reconstructed SSTs display negative values during the same phase (fig. 6.5b). This situation might have resulted because high air temperatures may have caused melting of the local glaciers at that time. Increasing IRD counts after 6,500 cal BP together with decreasing TOC concentrations point to glacial supply of clastic sediments to the site. The inflow of large quantities of glacial melt water possibly caused low water temperatures in LJJ, explaining the low SST estimates. Peak MAAT temperature anomalies around 6,500 cal BP (fig. 6.5a), coincide with the drainage of an ice-dammed lake in Stormness Bay (prior 6.300 years BP (Bentley et al., 2007)), supporting a possibly strong effect of air temperatures on the loss of continental ice at that time.

Just MAATs of the time after 7,000 cal BP are considered for the interpretation, because erosion of aged soils during transgression potentially has biased the MAAT reconstruction in the period before by possibly integrating temperature signals of broader time span.

Rising RSL - Coastal Erosion: Since the last glacial termination, persistent melting of the polar ice masses caused an immense release of fresh water into the oceans and led to a dramatic eustatic sea level rise. Isostatic uplift of the island of South Georgia, caused by the vanishing continental ice load after the LGM, compensated a part of the effect, but around 7,300 cal BP relative sea level (RSL) apparently rose above the sill of LJJ. As a consequence, ocean water flooded the basin of LJJ and replaced the fresh water of the lake. Erosion of older soils from the adjacent slopes of LJJ is indicated by relatively low pH values at that time (fig. 6.4). CPI values of 8.5 - 12 and low grass/moss ratios of 0.8 -1 indicate high contributions of moss biomass to the sedimentary material during the marine transgression. Inundation of the low-lying parts of the catchment likely reduced the vegetated area of the catchment. The relatively long duration of the transgression and the weak lamination of the sediments support that inflow of ocean water into the LJJ basin probably happened gradually and not by an abrupt flooding event.

Rising of the RSL, that is documented by the marine transgression in LJJ between 7,300 and 7,000 years BP, continued beyond this event. Raised beaches in the adjacent Enten Valley (Barlow et al., 2016) indicate that a highstand was probably reached when the sea level was c. 8 m above of the sill, which connects LJJ with the Cumberland fjord in recent times. Persisting coastal erosion until 6,600 cal BP, as a consequence of the progressively rising RSL, is indicated in the setting of LJJ by relatively high C/N ratios of 8 to 9.3 and a BIT index of 0.7 (fig. 6.4). Relatively low pH values of 7.1 may even point to further erosional inputs until c. 6,000 cal BP.

The setting of ALA lies c. 17 m above the assumed sea-level highstand of +8 m. However,

due to the position of the lake proximal to the shore, an influence of ocean water in the catchment of ALA can be expected. The strikingly consistent increase of n -C₂₁ alkane concentrations between c. 7,500 and c. 6,000 cal BP, as well as the equally consistent decrease after 6,000 BP may document the effect of sea spray or the accessibility of salt water from upward migration for the habitat of salt marsh mosses. Optimum conditions for halophytic vegetation around 6,000 cal BP can be interpreted as a result of the proximity between ocean and lake, marking peak RSL at this time.

Based on pH values of LJJ and on the n -C₂₁ alkane record of ALA, a highstand of RSL around 6,000 cal BP is indicated. Compared to the study of Barlow et al. (2016), the assumed timing of peak RSL post-dates the minimum age estimate of the formation of raised beaches in Enten Valley (4,350 ± 100 years BP) but pre-dates than the most probable modeled highstand (c. 8,000 years BP).

6.4.4 "Neoglacial": c. 5,800 - c. 4,500 cal BP

A rapid cooling followed the mid-Holocene hypsithermal and led to negative temperature anomalies in the MAAT record of LJJ between c. 5,800 - c. 4,500 cal BP (fig. 6.6d). This cooling trend and the establishment of a "neoglacial" climate was observed in several regions of the world (Hodell et al., 2001). It caused e.g. glacier re-advances in Antarctica between 6,000 and 4,500 cal BP (Michalchuk et al., 2009) and in South America and New Zealand between 5,400 and 4,900 cal BP as well as sea ice expansion in the Atlantic sector of the Southern Ocean around 5,000 cal BP (Hodell et al., 2001). The block lake record from Tønsberg Peninsula documents cooler climatic conditions between 5,200 and 4,400 cal BP for South Georgia (Rosqvist and Schuber, 2003), characterized by glacier re-advances (Clapperton et al., 1989; Bentley et al., 2007; White et al., 2018).

The particularly high IRD record of LJJ (fig. 6.6c) supports the assumption of a pronounced glacial activity during that period, also in the setting of the marine inlet. Glaciers of the catchment as well as icebergs from the Neumayer Glacier, which entered the inlet, are possible sources of the IRD. Variable CPI values possibly point to varying erosion of degraded n -alkanes by glaciers (fig. 6.4). The re-advance of glaciers was probably not only caused because of cooler temperatures but also because of high precipitation during this phase. Humid climatic conditions are indicated by maximum abundances of *Juncus sp.* (fig. 6.7h) and high concentrations of mosses (fig. 6.7f) in the catchment of ALA. Large abundances of mosses were also found in peat sequences from Stromness Bay, which were deposited in the time interval c. 8,000 to 4,000 cal BP (Van der Putten et al., 2009). Low TOC concentrations in both the ALA and the LJJ record (fig.6.6a,b) likely reflect a generally reduced productivity at that time and possibly dilution of organic matter by clastic material. Relatively high pH values of 7.4 point to development of fresh soils in the setting of LJJ in this phase (fig. 6.4).

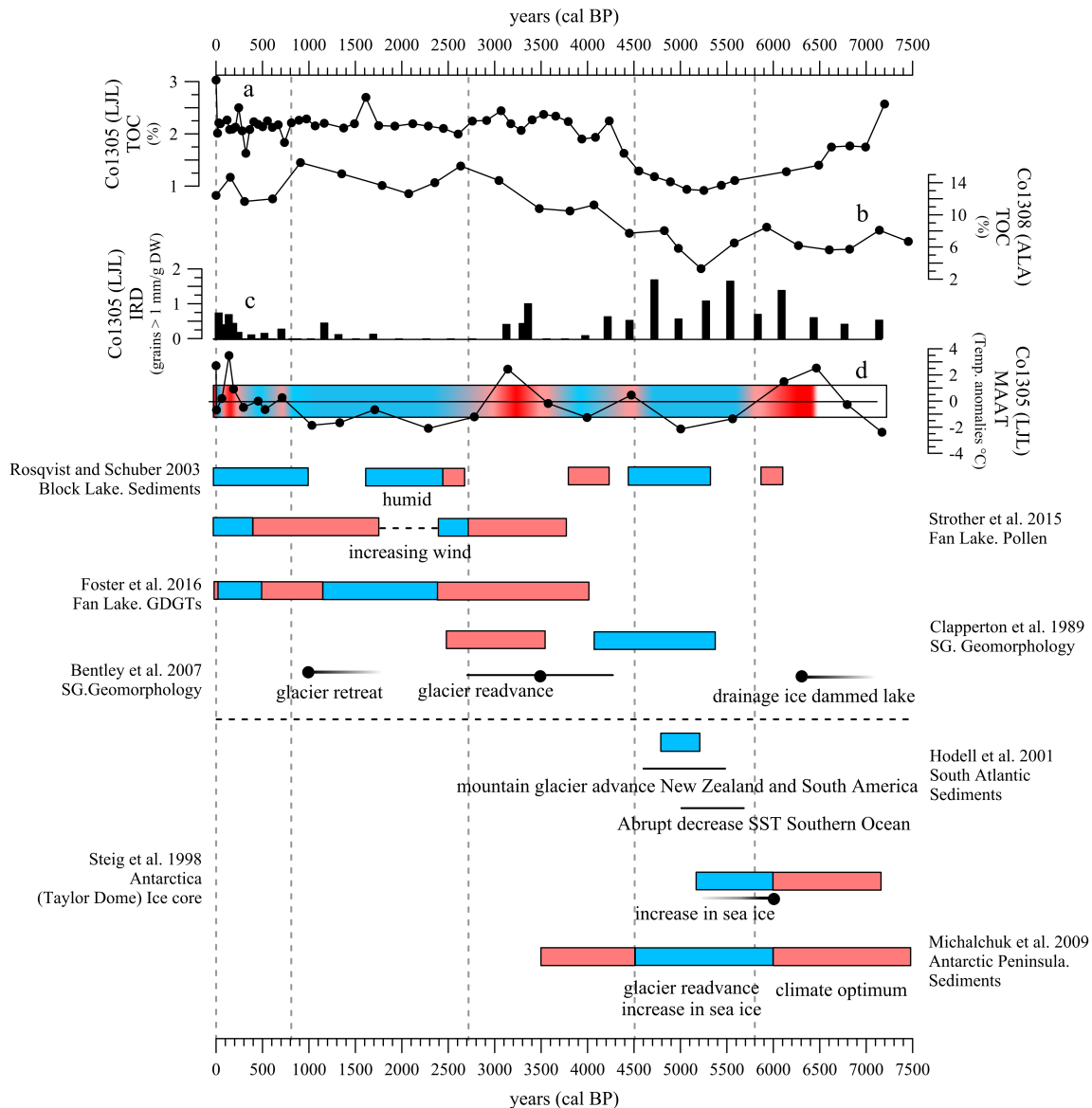


Figure 6.6: TOC records of Co1305 and Co1308, MAAT and IRD record of Co1305 against time. Regional overview of climatic reconstructions.

6.4.5 Late Holocene Hypsithermal: c. 4,500 - c. 2,700 cal BP

A period of significant warmth, the so-called hypsithermal, followed the "neoglacial" and is indicated in several records from the Antarctic and sub-Antarctic region (Bentley et al., 2007). On the South Shetland islands, a gradual warming and increasing humidity is suggested for the period between 4,000 and 2,500 yrs BP, with an optimum at 3,000 yrs BP (Björck et al., 1993). A warming trend is also evident in the Block lake record of South Georgia for the time interval 4,400 to 3,800 cal BP (Rosqvist and Schuber, 2003).

The MAAT record of LJL indicates a short period of positive temperature anomalies between 4,500 and 4,300 cal BP and significant warmth around 3,100 cal BP (fig.6.6d). Glacier retreat after 4,000 years BP in Cumberland East Bay (Bentley et al., 2007) and in Enten

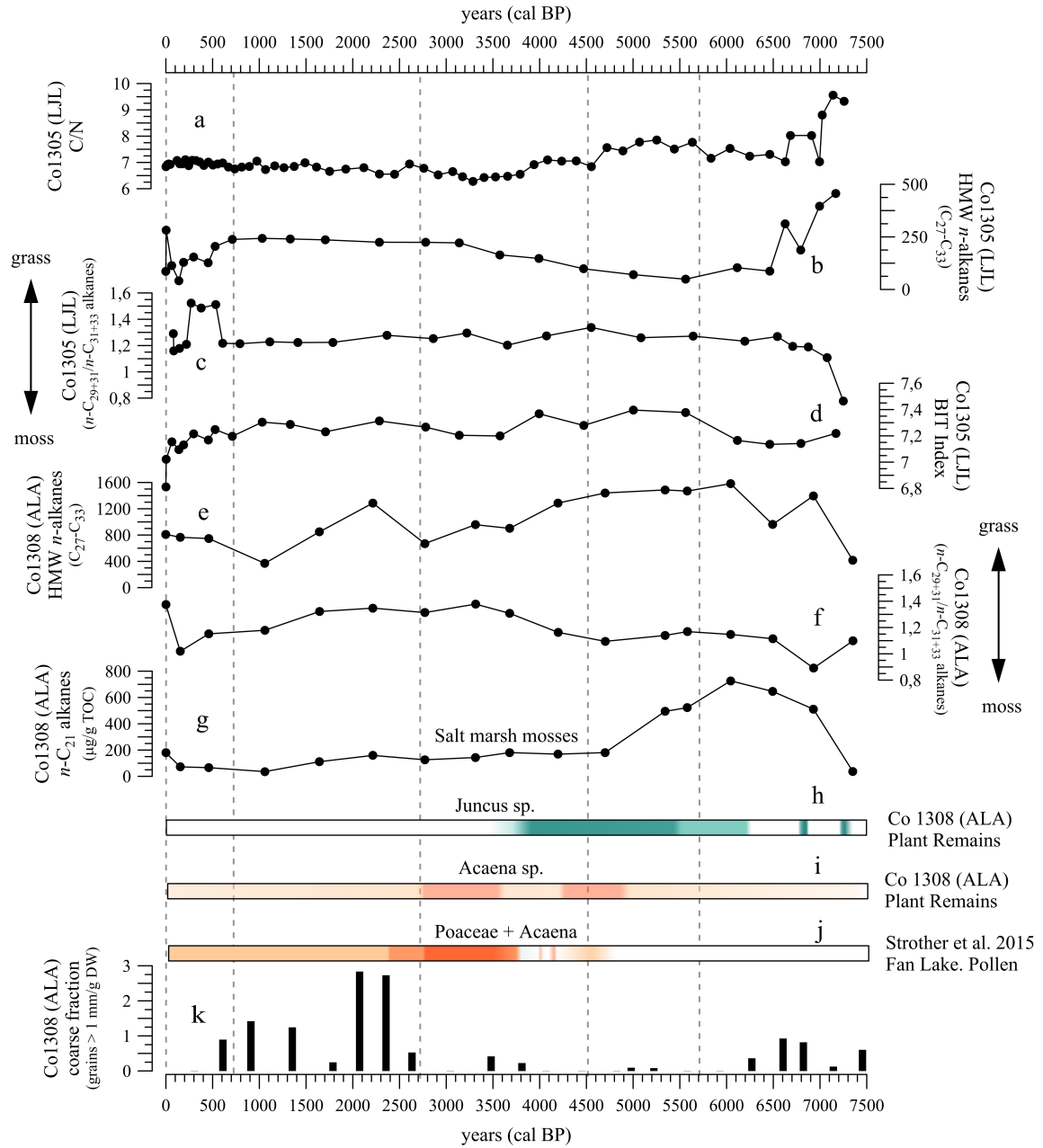


Figure 6.7: Selected biomarker and proxy records of Co1305 and Co1308 against time.

Bay (Barlow et al., 2016) apparently followed the climatic change. In LJL, a decreasing influence of glacial supply is not only visible in the low IRD record at that time (fig.6.6c), but also by a shift towards generally younger TOC ages which point to decreasing proportions of glacially supplied ancient OC (details in chapter 4). Increasing TOC concentrations between c. 4,500 - c. 2,700 cal BP in both the LJL and the ALA record (fig. 6.6a,b) indicate increasing productivity due to ameliorated climatic conditions. A marked transition in plant communities towards a landscape with higher proportions of grasses is indicated by increasing grass/moss ratios of the ALA record (fig.6.7f). Increasing aridity as a consequence of the southward shift of the westerlies at c. 4,000 cal BP is seen in a number of proxy records

of South America (Bentley et al., 2007). A transition towards dry climate conditions is may indicated in the setting of ALA by the replacement of *Juncus sp.* by *Acena sp.* around 4,000 cal BP, coinciding with maximum concentrations of *Acena sp.* and *Poacea sp.* pollen that were found in the record of Fan Lake of South Georgia (Strother et al., 2015) (fig.6.7f,i,j). Warm and dry conditions are also indicated at Kanin Point between 4,400 and 3,400 cal BP (Van der Putten et al., 2009) and on Tønsberg Peninsula between 4,100 and 2,800 cal BP (Van der Putten et al., 2004). However, negative temperature anomalies between 4,300 and 3,600 BP (fig.6.6d) indicate a short break of the warming trend in the study area. The prominent advance of South Georgia tidewater glaciers around 3,600 years BP may be associated to decreasing temperatures at that time and not as suggested by Bentley et al. (2007), to high precipitations. Around 3,300 to 3,100 cal BP, high IRD concentrations in LJL were possibly caused by high air temperatures, indicated by positive MAAT anomalies (fig. 6.6 c,d). Peak concentrations of LMW fatty acids and *n*-C₂₂ alcohol as well as a small BIT index (fig. 6.4) point to an intensification of the marine productivity at that time, possibly associated to particularly high temperatures and possibly also to an increased nutrient supply from the melting glaciers.

6.4.6 Climate Deterioration : c. 2,700 - c. 800 cal BP

Climate deterioration after the late Holocene "climate optimum" is indicated by negative temperature anomalies between c. 2,700 - c. 800 cal BP (fig. 6.6d). A transition to cool and wet conditions after 2,700 cal BP is also revealed in other lacustrine records from South Georgia (Rosqvist and Schuber, 2003; Strother et al., 2015; Foster et al., 2016). Glacier advances in Cumberland Bay are indicated for the Nordenskjöld Glacier after 2,000 cal BP (Gordon, 1987) and for tidewater glaciers of the Moraine fjord between 1,500 and 1,300 cal BP (Clapperton et al., 1989). However, low IRD records between 1,600 and 1,200 cal BP in LJL indicate that glaciers are retreated to higher altitudes in the catchment of LJL at that time (fig. 6.6c). Despite of a deterioration of climatic conditions, this phase seems to be characterized by a relatively stable productivity, reflected by only minor changes in biomarker and TOC records of both sites (fig. 6.4 and 6.3).

6.4.7 High Climatic Variability: c. 800 cal BP - Today

The phase between c. 800 cal BP and present seems to be characterized by variable climatic conditions, possibly associated to short-term climatic events. Around 700 cal BP (1,250 AD), slightly positive temperature anomalies and high terrigenous as well as marine productivity are indicated in the LJL record (fig. 6.4 and 6.6 d), possibly associated with the Medieval Warm Period (MWP). Slightly negative temperature anomalies between c. 600 cal BP (1,350 AD) and cal 300 BP (1,650 AD) may reflect the Little Ice Age (LIA) climatic event. Concentrations of HMW *n*-alkanes in the LJL record are quite low at that time as well as TOC concentrations in ALA (fig.6.7b and 6.6b). A particularly high grass/moss ratio, together with a BIT index of 0.8 and a low CPI in the setting of LJL (fig. 6.4)

may indicate a clear predominance a grass and high erosion rates of soils and degraded *n*-alkanes. A high marine productivity and/or good preservation conditions are indicated by high concentrations of *n*-C₁₆ fatty acids. The cold event seems to have ended with a sharp temperature increase, culminating around 150 BP (1,800 AD). IRD concentration increases simultaneously, but also *n*-C₁₆ fatty acids reach a maximum concentration and high CPI values point to the input of fresh terrigenous organic matter. It seems that biomarker trends and MAAT reconstructions are possibly not fully consistent in this phase. An offset between different signals is associated with variable pathways of the sedimentary material (e.g. high MRT of terrigenous components). This effect is possibly expressed because of the high resolution of the data in this part of record.

6.5 Conclusions

The investigation of individual biomarkers for a chronological purpose was beneficial in order to develop a confident sediment chronology for the coastal marine record Co1305 of Little Jason Lagoon. The combination of *n*-C₂₂ alcohol ages along with *n*-C₁₆ fatty acid ages resulted in a chronology of c. 10,000 years.

The lacustrine sediment chronology for the record Co1308 of Allen Lake A was based on calibrated radiocarbon ages of terrigenous macrofossils and HMW *n*-alkanes and yielded a basal age of 7,500 years. It was found that despite of a small catchment and a small lake size, biomarkers as well as macrofossils are severely "pre-aged" in this setting. Similar ¹⁴C ages of plant macrofossils and terrigenous biomarkers pointed to common sources and transport mechanisms of these materials. Because of the remarkably coherent age-depth relationship between both sample types in the record, a constant deviation of 1,900 years was applied for the chronology.

The good match between the timing of transitions in both records indicates that the sediment chronologies, that were derived from different sample types, are likely reliable. Moreover, similar trends in the records suggest significant environmental changes of regional extend.

After a lacustrine stage in the setting of LJJ, when the prospective marine inlet was disconnected from the ocean, marine transgression started around 7.300 cal BP. Fully marine conditions established around 7.000 cal BP but RSL seems to have further increased until c. 6.000 cal BP. Indications on RSL development were found in both records. In the LJJ record C/N ratios, BIT indices and pH values indicate a RSL highstand between 6,600 and 6,000 cal BP. The concentration of *n*-C₂₁ alkanes in the sediments of ALA was interpreted as indicator for RSL fluctuations in the lacustrine environment, based on the assumption that *n*-C₂₁ alkanes are characteristic biomarkers of salt marsh mosses. *n*-C₂₁ alkanes have not been used before to reconstruct RSL variations, but possibly they have good potential

to identify salt-rich habitats.

An important environmental transition is indicated to have happened around 4,000 cal BP, when climatic conditions ameliorated after a cold period. In the lacustrine core Co1308 of Allen Lake A several changes were traced at that time, probably associated to the dominant effect of plant succession in this setting. The changing landscape is apparently characterized by a transition from moss dominated vegetation to a grass dominated vegetation and a replacement of *Juncus sp.* by *Acena sp.*. Vegetational changes appear to be recorded in the distribution of HMW *n*-alkanes in the sediments of ALA. It seems that the vegetational succession has a dominant effect on several sedimentological and biogeochemical properties of the record and can therefore mislead environmental interpretations e.g. of productivity based on the sum of HMW *n*-alkanes or of temperature signals derived from brGDGT distributions.

Chapter 7

Summarizing Remarks and Perspectives

The studies comprising this thesis identified various depositional processes affecting distributions and radiocarbon inventories of terrigenous and marine biomarkers in aquatic sediments of South Georgia. Compound-specific ^{14}C ages of different sedimentary biomarkers were evaluated with regard to their potential for chronological applications. The investigation of two continuous sedimentary records from a lake and a marine inlet resulted in the reconstruction of Holocene environmental changes of the study area.

Retention of Organic Matter on Land: Transport of terrigenous organic matter from land into aquatic environments was found to be delayed by approximately 1,900 to 2,600 years. Similar radiocarbon ages of terrigenous biomarkers (HMW *n*-fatty acids and HMW *n*-alkanes) and of macroscopic plant remains indicates that large fractions of the sedimentary pools of terrigenous biomarkers likely derived from plant debris and not from heterogeneous soil reservoirs. Climatic conditions were assumed to have a major controlling function on the preservation and storage of the organic matter in the sub-Antarctic setting of South Georgia.

An important question arising from the find that transport of terrigenous organic matter is delayed relates to the paleoenvironmental information of this material in sedimentary archives. When "pre-aged" terrigenous organic matter in the sediments is co-occurring with more recently produced compounds, interpretations of paleoenvironmental signals may relate to different times. The parallel variations of marine and terrigenous biomarkers (*n*-C₁₆ and *n*-C₂₆ fatty acids) in most parts of the record Co1305, therefore, appear somehow doubtful. However, they can possibly be explained by the strong impact of preservation conditions in the sediments on the distributions of both respective biomarkers. Moreover, the temporal resolution in the record is possibly too low to reveal distinct offsets between the abundances of *n*-C₁₆ and *n*-C₂₆ fatty acids. Not only when comparing biomarkers of marine and terrigenous origin, temporal offsets need to be considered. This is also the case when deriving MAAT reconstructions from brGDGTs with a certain MRT in soils and re-

lating the variability in other biomarker records to these temperature estimates. Therefore, it appears necessary to better constrain the delay in the deposition of different biomarkers more specifically. Whereas many investigations focussed on the ^{14}C of biomarkers in marine sediments, there are only few ^{14}C studies on biomarkers in soils. More systematic studies are needed in order to better understand ^{14}C distributions in soils, including different soil components (e.g. biomarkers, size or density fractions). It is desirable to not only investigate ^{14}C ages in depth profiles of soils, but also on the entire transport pathway from source to sink regions. Moreover, influences of variable climatic conditions, discharge regimes, catchment sizes, topography etc. need to be considered in these studies. Since pathways of soil components can be very complex in large watersheds, these systems likely offer various interpretations due of a range of opposed effects. For the identification of most important environmental factors for the transport of soil components, small catchments like that of ALA are possibly good study sites.

Carbon Redistribution from Land to the Ocean: Transport of terrigenous (plant and soil) organic matter was assumed to mainly rely on fluvial processes, indicated by the irregular distribution of HMW *n*-fatty acids in fjord sediments. In contrast, clear distributional trends of ancient OC in the fjords of Cumberland Bay point to an exclusive role of glaciers for the mobilization of this material by mechanical erosion of the bedrock. This find is in concert with other studies, which revealed that OC from petrogenic sources in fjords derived mainly from physical erosion of sedimentary rocks.

Burial of OC in marine sediments is an important mechanism of long-term carbon sequestration. Continental margins are known as highly productive areas, which play a major role in the global carbon cycle. Fjords are characterized by particularly high rates of OC burial, so that these environments may have considerable importance for climate regulation on glacial–interglacial timescales. Distinguishing between different carbon sources is very important, because timescales of carbon transitions between reservoirs vary. Quantification of OC sources in aquatic sediments, however, is a topical problem. To derive the proportional contributions of three endmembers, and therefore to distinguish between different allochthonous OC fractions, dual isotope mass balances based on $\Delta^{14}\text{C}$ and $\delta^{13}\text{C}$ were applied in several studies. A challenge in this approach is the attribution of $\delta^{13}\text{C}$ to the different land-derived endmembers. $\Delta^{14}\text{C}$ mass balance calculations with ratios of biomarkers (e.g. *n*-fatty acids) seem promising to overcome the difficulties of potentially non-conclusive $\delta^{13}\text{C}$ values. CSRA of biomarkers additionally helps to constrain endmember $\Delta^{14}\text{C}$ values.

Marine Sediment Chronologies based on Radiocarbon Ages of Biomarkers: Calibrated ^{14}C ages of marine biomarkers (*n*- C_{16} fatty acids and *n*- C_{22} alcohols) were applied to develop a sediment chronology for the coastal marine record Co1305 of Little Jason Lagoon. It seems that ^{14}C ages of these biomarkers can yield a confident approximation of the time of sediment formation in the study area.

Compound-specific radiocarbon ages of n -C₁₆ fatty acids were previously employed to establish marine sediment chronologies in coastal Antarctic regions. However, the coastal marine setting of Little Jason Lagoon differs from these Antarctic environments by the fact that supply of terrigenous material also introduces n -C₁₆ fatty acids to the site. Here, combination of ¹⁴C ages of labile n -C₁₆ fatty acids together with ages of more refractory n -C₂₂ alcohols seems to improve the accuracy of the chronology. In the upper part of the record, n -C₁₆ fatty acids yield more precise age estimates, whereas in the lower part, younger ages of n -C₂₂ alcohols indicate smaller fractions of "pre-aged" terrigenous compounds.

Despite the elaborate laboratory preparation procedure, radiocarbon analysis of biomarkers seems to be particularly eligible to establish or enhance sediment chronologies. The investigation of different biomarkers is very useful to trace diagenetical differences and to select the most promising material for chronological purposes.

Lacustrine Sediment Chronologies based on Radiocarbon Ages of Plant Macrofossils: The sediment chronology for the lake record Co1308 was developed based on calibrated radiocarbon ages of terrigenous macrofossils and HMW n -alkanes. Because of the remarkably coherent age-depth relationship between both sample types in the record, a constant deviation from the time of production of 1,900 years was applied for the chronology.

Allen Lake A is very small and has also a small watershed. The considerable "pre-aging" of terrigenous organic matter in this environment challenges the general assumption that macrofossils are transported with small delay in such environments. Cool and moist climatic condition together with the slowly decomposing character of the investigated plant types possibly accounted for the good preservation of the material on land. This find is important, since plant macrofossils are often investigated exclusively, when they are found in sufficient amounts in lake sediments. When processes like intermediate storage are not fully understood for the investigated depositional systems, ages of terrigenous organic matter can be misleading. When respective samples are used for sediment chronologies, considerable deviations from the time of deposition can result and lead to weak chronologies. It seems therefore recommendable to investigate different sample types to identify site-specific effects.

Effect of Plant Succession on Sedimentological and Biogeochemical Proxies: Plant succession from a moss-dominated vegetation to a grass-dominated vegetation was identified to have caused several sedimentological and biogeochemical changes in the sediments of the lake record Co1308. Mosses were assumed to contain higher concentrations of lipids than grasses, so that distributions of HMW n -alkanes in the sediments were interpreted to reflect the inputs of a respective plant community, rather than terrigenous productivity as a whole. It was assumed the replacement of a relatively dense moss cover by single grass stands resulted in the erosion of sediments of larger grain sizes, which were

previously retained by the mosses. Suspicious and implausible changes of reconstructed air temperatures from brGDGTs, coinciding with the proposed vegetational transition, pointed to changing soil properties and adaptation of brGDGT producing soil bacteria to these changes.

All the sedimentological and geochemical changes in the record Co1308 impressively demonstrate how vegetational succession can change soil characteristics as well as transport mechanisms. The effect of these changes on the distribution and composition of biomarkers can distort the interpretation of corresponding proxies. Particularly when long records are analyzed, the effect of environmental changes on the used proxies has to be considered. The effect of vegetational changes can be expected to be particularly strong in the setting of Allen Lake A, because of its small catchment size. Reasons why such a clear succession did not happen in the setting of LJJ are probably a more diverse vegetation and more diverse soils as well as other environmental factors (like glaciers) that influence the terrestrial biosphere. Analysis of plants from the catchment (more species than in this study) seems recommendable to identify endmembers of sedimentary biomarkers, so that changes in biomarker distributions associated to vegetational changes can be identified.

More Unusual Biomarkers for Environmental Reconstructions: An important finding of this study is that sources of HMW *n*-alcohols (C₂₂ to C₂₈) cannot simply be derived from the chain lengths of these biomarkers, as commonly assumed when HMW biomarkers are ascribed to terrigenous origins. This indicates that it can be crucial to investigate biomarker sources for each site specifically to prevent possibly inappropriate allocation of biomarkers to generalized sources.

n-Alkanes with intermediate chain lengths, like *n*-C₂₅, were found to be characteristic for Sphagnum species. The potential of *n*-C₂₁ alkanes as specific biomarkers of halophyte moss species was not yet investigated. Further studies would be desirable to assess the validity of *n*-C₂₁ alkanes records for the characterization of the influence of sea water in coastal marine environments and to reconstruct changes of the RSL.

Investigation of Lacustrine together with Marine Records: A high-resolution reconstructions of Holocene environmental and climatic conditions have been obtained based on two sedimentary records, Co1305 from Little Jason Lagoon and Co1308 from Allen Lake A. The investigation of independent records from the same region seems advantageous to distinguish between regional implications of climatic changes and more local processes. The identification of significant environmental transitions, recorded in both settings, further helps to better constrain the timing of these events and to evaluate the accuracy of the respective sediment chronologies. It seems therefore desirable, particularly in regions where age control is limited, to combine the data of independent aquatic environments to derive a refined picture of environmental changes in the study region.

Bibliography

- Ackman, R. G. (1989). Fatty acids. *Marine biogenic lipids, fats and oils*, 1:103–137.
- Albers, C. S., Kattner, G., and Hagen, W. (1996). The compositions of wax esters, triacylglycerols and phospholipids in Arctic and Antarctic copepods: Evidence of energetic adaptations. *Marine Chemistry*, 55(3-4):347–358.
- Andrews, J. T., Domack, E. W., Cunningham, W. L., Leventer, A., Licht, K. J., Jull, A., DeMaster, D. J., and Jennings, A. E. (1999). Problems and Possible Solutions Concerning Radiocarbon Dating of Surface Marine Sediments, Ross Sea, Antarctica. *Quaternary Research*, 52(2):206–216.
- Atkinson, A., Whitehouse, M. J., Priddle, J., Cripps, G. C., Ward, P., and Brandon, M. A. (2001). South Georgia, Antarctica: a Productive, Cold Water, Pelagic Ecosystem. *Marine Ecology Progress Series*, 216:279–308.
- Balmer, S., Sarnthein, M., Mudelsee, M., and Grootes, P. M. (2016). Refined modeling and ^{14}C plateau tuning reveal consistent patterns of glacial and deglacial ^{14}C reservoir ages of surface waters in low-latitude Atlantic. *Paleoceanography*, 31(8):1030–1040.
- Bard, E. (1988). Correction of Accelerator Mass Spectrometry ^{14}C Ages measured in planktonic foraminifera: Paleoceanographic implications. *Paleoceanography*, 3(6):635–645.
- Bard, E., Arnold, M., Hamelin, B., Tisnerat-Labore, N., and Cabioch, G. (1998). Radiocarbon calibration by means of mass spectrometric $^{230}\text{Th}/^{234}\text{U}$ and ^{14}C ages of corals: an updated database including samples from Barbados, Mururoa and Tahiti. *Radiocarbon*, 40(3):1085–1092.
- Bard, E., Hamelin, B., Fairbanks, R. G., and Zindler, A. (1990). Calibration of the ^{14}C timescale over the past 30,000 years using mass spectrometric U-Th ages from Barbados corals. *Nature*, 345(6274):405–410.
- Bard, E., Rostek, F., and Sonzogni, C. (1997). Interhemispheric synchrony of the last deglaciation inferred from alkenone palaeothermometry. *Nature*, 385(6618):707.
- Barlow, N., Bentley, M., Spada, G., Evans, D., Hansom, J., Brader, M., White, D., Zander, A., and Berg, S. (2016). Testing models of ice cap extent, South Georgia, sub-Antarctic. *Quaternary Science Reviews*, 154:157–168.

- Barrett, J. E., Virginia, R. A., Hopkins, D. W., Aislabie, J., Bargagli, R., Bockheim, J. G., Campbell, I. B., Lyons, W. B., Moorhead, D. L., Nkem, J. N., Sletten, R. S., Steltzer, H., Wall, D. H., and Wallenstein, M. D. (2006). Terrestrial ecosystem processes of Victoria Land, Antarctica. *Soil Biology and Biochemistry*, 38(10):3019–3034.
- Barrow, C. (1978). Postglacial pollen diagrams from South Georgia (sub-Antarctic) and West Falkland island (South Atlantic). *Journal of Biogeography*, 5(3):251–274.
- Barrow, C. J. (1983). Palynological studies in South Georgia: III. Three profiles from near King Edward Cove, Cumberland East Bay. *British Antarctic Survey Bulletin*, 58:43–60.
- Bentley, M. J., Evans, D. J. A., Fogwill, C. J., Hansom, J. D., Sugden, D. E., and Kubik, P. W. (2007). Glacial geomorphology and chronology of deglaciation, South Georgia, sub-Antarctic. *Quaternary Science Reviews*, 26(5-6):644–677.
- Bentley, M. J., Hodgson, D. A., Smith, J. A., Cofaigh, C. Ó., Domack, E. W., Larter, R. D., Roberts, S. J., Brachfeld, S., Leventer, A., Hjort, C., Hillenbrand, C. D., and Evans, J. (2009). Mechanisms of Holocene palaeoenvironmental change in the Antarctic Peninsula region. *The Holocene*, 19(1):51–69.
- Berg, S., White, D. A., Jivcov, S., Melles, M., Leng, M. J., Rethemeyer, J., Allen, C., Perren, B., Bennike, O., and Viehberg, F. (2019). Holocene glacier fluctuations and environmental changes in subantarctic south georgia inferred from a sediment record from a coastal inlet. *Quaternary Research*, 91(1):132–148.
- Berkman, P. A. and Forman, S. L. (1996). Pre-bomb radioacarbon and the reservoir correction for calcareous marine species in the Southern Ocean. *Geophysical Research Letters*, 23(4):363–366.
- Bhatia, M. P., Das, S. B., Xu, L., Charette, M. A., Wadham, J. L., and Kujawinski, E. B. (2013). Organic carbon export from the Greenland ice sheet. *Geochimica et Cosmochimica Acta*, 109:329–344.
- Bianchi, C. and Gersonde, R. (2004). Climate evolution at the last deglaciation: The role of the Southern Ocean. *Earth and Planetary Science Letters*, 228(3-4):407–424.
- Bianchi, T. S., Mitra, S., and McKee, B. A. (2002). Sources of terrestrially-derived organic carbon in lower Mississippi River and Louisiana shelf sediments: Implications for differential sedimentation and transport at the coastal margin. *Marine Chemistry*, 77(2-3):211–223.
- Björck, S., Håkansson, H., Olsson, S., Barnekow, L., and Janssens, J. (1993). Palaeoclimatic studies in South Shetland Islands, Antarctica, based on numerous stratigraphic variables in lake sediments. *Journal of Paleolimnology*, 8(3):233–272.

- Björck, S., Håkansson, H., Zale, R., Karlen, W., and Jonsson, B. (1991). A late Holocene lake sediment sequence from Livingston Island, South Shetland Islands, with palaeoclimatic implications. *Antarctic Science*, 3(1):61–72.
- Blair, N. and Aller, R. (2012). The fate of terrestrial organic carbon in the marine environment. *Annual Review of Marine Science*, 4(1):401–423.
- Blair, N. E., Leithold, E. L., Ford, S. T., Peeler, K. A., Holmes, J. C., and Perkey, D. W. (2003). The persistence of memory: The fate of ancient sedimentary organic carbon in a modern sedimentary system. *Geochimica et Cosmochimica Acta*, 67(1):63–73.
- Blunier, T., Chappellaz, J., Schwander, J., Dällenbach, A., Stauffer, B., Stocker, T. F., Raynaud, D., Jouzel, J., Clausen, H. B., Hammer, C. U., and Johnsen, S. J. (1998). Asynchrony of Antarctic and Greenland climate change during the last glacial period. *Nature*, pages 739–743.
- Bohrmann, G. (2013). The expedition of the research vessel "polarstern" to the antarctic in 2013 (ant-xxix/4). *Berichte zur Polar-und Meeresforschung = Reports on polar and marine research*, 668.
- Bol, R., Huang, Y., Meridith, J. a., Eglinton, G., Harkness, D. D., and Ineson, P. (1996). The ^{14}C age and residence time of organic matter and its lipid constituents in a stagnohumic gley soil. *European Journal of Soil Science*, 47(2):215–222.
- Bolin, B. (1970). The Carbon Cycle. *Scientific American*, 223(3):124–135.
- Borrione, I. and Schlitzer, R. (2013). Distribution and recurrence of phytoplankton blooms around South Georgia, Southern Ocean. *Biogeosciences*, 10(1):217–231.
- Bowman, S. (1990). *Radiocarbon dating. Interpreting the past*. British Museum Press.
- Bray, E. E. and Evans, E. D. (1961). Distribution of *n*-paraffins as a clue to recognition of source beds. *Geochimica et Cosmochimica Acta*, 22(1):2–15.
- Broecker, W. S. (1998). Paleocan circulation during the 1st deglaciation: A bipolar seasaw? *Paleoceanography*, 13(2):119–121.
- Burke, a. and Robinson, L. F. (2012). The Southern Ocean's Role in Carbon Exchange During the Last Deglaciation. *Science*, 335(6068):557–561.
- Cacho, I., Grimalt, J. O., Sierro, F. J., Shackleton, N., and Canals, M. (2000). Evidence for enhanced Mediterranean thermohaline circulation during rapid climatic coolings. *Earth and Planetary Science Letters*, 183(3-4):417–429.
- Canuel, E. A. and Martens, C. S. (1996). Reactivity of recently deposited organic matter: Degradation of lipid compounds near the sediment-water interface. *Geochimica et Cosmochimica Acta*, 60(10):1793–1806.

- Clapperton, C. M., Sugden, D. E., Birnie, J., and Wilson, M. J. (1989). Late-glacial and Holocene glacier fluctuations and environmental change on South Georgia, Southern Ocean. *Quaternary Research*, 31(2):210–228.
- Cranwell, P. A. (1981). Diagenesis of free and bound lipids in terrestrial detritus deposited in a lacustrine sediment. *Organic Geochemistry*, 3:79–89.
- Cripps, G. C., Watkins, J. L., Hill, H. J., and Atkinson, A. (1999). Fatty acid content of Antarctic krill *Euphausia superba* at South Georgia related to regional populations and variations in diet. *Marine Ecology Progress Series*, 181:177–188.
- Cui, X., Bianchi, T. S., Jaeger, J. M., and Smith, R. W. (2016). Biospheric and petrogenic organic carbon flux along southeast Alaska. *Earth and Planetary Science Letters*, 452:238–246.
- Cui, X., Bianchi, T. S., and Savage, C. (2017). Erosion of modern terrestrial organic matter as a major component of sediments in fjords. *Geophysical Research Letters*, 44:1457–1465.
- Damsté, J. S. S., Schouten, S., Hopmans, E. C., van Duin, A. C. T., and Geenevasen, J. A. J. (2002). Crenarchaeol: the characteristic core glycerol dibiphytanyl glycerol tetraether membrane lipid of cosmopolitan pelagic crenarchaeota. *Journal of Lipid Research*, 43(10):1641–1651.
- De Jonge, C., Stadnitskaia, A., Cherkashov, G., and Sinninghe Damsté, J. S. (2016). Branched glycerol dialkyl glycerol tetraethers and crenarchaeol record post-glacial sea level rise and shift in source of terrigenous brGDGTs in the Kara Sea (Arctic Ocean). *Organic Geochemistry*, 92:42–54.
- De Jonge, C., Stadnitskaia, A., Fedotov, A., and Sinninghe Damsté, J. S. (2015). Impact of riverine suspended particulate matter on the branched glycerol dialkyl glycerol tetraether composition of lakes: The outflow of the Selenga River in Lake Baikal (Russia). *Organic Geochemistry*, 83-84:241–252.
- Denton, G. H., Anderson, R. F., Toggweiler, J. R., Edwards, R. L., Schaefer, J. M., and Putnam, A. E. (2010). The Last Glacial Termination. *Science*, 328(June):1652–1656.
- Dewald, A., Heinze, S., Jolie, J., Zilges, A., Dunai, T., Rethemeyer, J., Melles, M., Staubwasser, M., Kuczewski, B., Richter, J., Radtke, U., Von Blanckenburg, F., and Klein, M. (2013). CologneAMS, a dedicated center for accelerator mass spectrometry in Germany. *Nuclear Instruments and Methods in Physics Research, Section B: Beam Interactions with Materials and Atoms*, 294:18–23.
- Diefendorf, A. F. and Freimuth, E. J. (2016). Extracting the most from terrestrial plant-derived *n*-alkyl lipids and their carbon isotopes from the sedimentary record: A review. *Organic Geochemistry*, 103:1–21.

- Domack, E., Leventer, A., Dunbar, R., Taylor, F., Brachfeld, S., and Sjunneskog, C. (2001). Chronology of the Palmer Deep site, Antarctic Peninsula: A Holocene palaeoenvironmental reference for the circum-Antarctic. *Holocene*, 11(1):1–9.
- Domack, E. W., Jull, a. J. T., Anderson, J. B., and Williams, C. R. (1989). of Tandem Accelerator Mass-Spectrometer Dating to Application Sediments of the East Antarctic Late Pleistocene-Holocene Continental Shelf. *Quaternary Research*, 31:277–287.
- Douglas, P. M. J., Pagani, M., Eglinton, T. I., Brenner, M., Hodell, D. A., Curtis, J. H., Ma, K. F., and Breckenridge, A. (2014). Pre-aged plant waxes in tropical lake sediments and their influence on the chronology of molecular paleoclimate proxy records. *Geochimica et Cosmochimica Acta*, 141:346–364.
- Drenzek, N. J., Montluçon, D. B., Yunker, M. B., Macdonald, R. W., and Eglinton, T. I. (2007). Constraints on the origin of sedimentary organic carbon in the Beaufort Sea from coupled molecular ^{13}C and ^{14}C measurements. *Marine Chemistry*, 103(1-2):146–162.
- Eglinton, G. and Calvin, M. (1967). Chemical Fossils. *Scientific American*, 216(1):32–43.
- Eglinton, G. and Hamilton, R. J. (1967). Leaf Epicuticular Waxes. *Science*, 156(3780):1322–1335.
- Eglinton, T. I., Aluwihare, L. I., Bauer, J. E., Druffel, E. R., and McNichol, A. P. (1996). Gas chromatographic isolation of individual compounds from complex matrices for radiocarbon dating. *Analytical Chemistry*, 68(5):904–912.
- Eglinton, T. I., Benitez-Nelson, B. C., Pearson, A., McNichol, A. P., Bauer, J. E., and Druffel, E. R. M. (1997). Variability in Radiocarbon Ages of Individual Organic Compounds from Marine Sediments. *Science*, 277(5327):796–799.
- Feng, X., Benitez-Nelson, B. C., Montluçon, D. B., Prahl, F. G., McNichol, A. P., Xu, L., Repeta, D. J., and Eglinton, T. I. (2013). ^{14}C and ^{13}C characteristics of higher plant biomarkers in Washington margin surface sediments. *Geochimica et Cosmochimica Acta*, 105:14–30.
- Ficken, K. J., Barber, K. E., and Eglinton, G. (1998a). Lipid biomarker, $\delta^{13}\text{C}$ and plant macrofossil stratigraphy of a Scottish montane peat bog over the last two millennia. *Organic Geochemistry*, 28(3-4):217–237.
- Ficken, K. J., Li, B., Swain, D. L., and Eglinton, G. (2000). An *n*-alkane proxy for the sedimentary input of submerged/floating freshwater aquatic macrophytes. *Organic Geochemistry*, 31(7-8):745–749.
- Ficken, K. J., Street-Perrott, F. A., Perrott, R. A., Swain, D. L., Olago, D. O., and Eglinton, G. (1998b). Glacial/interglacial variations in carbon cycling revealed by molecular and isotope stratigraphy of Lake Nkunga, Mt. Kenya, East Africa. *Organic Geochemistry*, 29(5-7):1701–1719.

- Ficken, K. J., Wooller, M. J., Swain, D. L., Street-Perrott, F. A., and Eglinton, G. (2002). Reconstruction of a subalpine grass-dominated ecosystem, Lake Rutundu, Mount Kenya: A novel multi-proxy approach. *Palaeogeography, Palaeoclimatology, Palaeoecology*, 177(1-2):137–149.
- Filley, T. R., Freeman, K. H., Bianchi, T. S., Baskaran, M., Colarusso, L. A., and Hatcher, P. G. (2001). An isotopic biogeochemical assessment of shifts in organic matter input to Holocene sediments from Mud Lake, Florida. *Organic Geochemistry*, 32(9):1153–1167.
- Foster, L. C., Pearson, E. J., Juggins, S., Hodgson, D. A., Saunders, K. M., Verleyen, E., and Roberts, S. J. (2016). Development of a regional glycerol dialkyl glycerol tetraether (GDGT)-temperature calibration for Antarctic and sub-Antarctic lakes. *Earth and Planetary Science Letters*, 433:370–379.
- Fraser, C. I., Nikula, R., Spencer, H. G., and Waters, J. M. (2009). Kelp genes reveal effects of subantarctic sea ice during the Last Glacial Maximum. *Proceedings of the National Academy of Sciences of the United States of America*, 106(9):3249–3253.
- Fretwell, P. T., Tate, A. J., Deen, T. J., and Belchier, M. (2009). Compilation of a new bathymetric dataset of South Georgia. *Antarctic Science*, 21(2):171–174.
- Fricke, H., Gercken, G., Schreiber, W., and Oehlenschläger, J. (1984). Lipid, Sterol and Fatty Acid Composition of Antarctic Krill. *Lipids*, 19(11):821–827.
- Galy, V. and Eglinton, T. (2011). Protracted storage of biospheric carbon in the Ganges-Brahmaputra basin. *Nature Geoscience*, 4(12):843–847.
- Galy, V., France-Lanord, C., and Lartiges, B. (2008). Loading and fate of particulate organic carbon from the Himalaya to the Ganga-Brahmaputra delta. *Geochimica et Cosmochimica Acta*, 72(7):1767–1787.
- Galy, V., Peucker-Ehrenbrink, B., and Eglinton, T. (2015). Global carbon export from the terrestrial biosphere controlled by erosion. *Nature*, 521:204–208.
- Geprägs, P., Torres, M. E., Mau, S., Kasten, S., Römer, M., and Bohrmann, G. (2016). Carbon cycling fed by methane seepage at the shallow Cumberland Bay, South Georgia, sub-Antarctic. *Geochemistry, Geophysics, Geosystems*, 17(4):1401–1418.
- Gierga, M., Hajdas, I., van Raden, U. J., Gilli, A., Wacker, L., Sturm, M., Bernasconi, S. M., and Smittenberg, R. H. (2016). Long-stored soil carbon released by prehistoric land use: Evidence from compound-specific radiocarbon analysis on Soppensee lake sediments. *Quaternary Science Reviews*, 144:123–131.
- Goñi, M. A., Ruttenger, K. C., and Eglinton, T. I. (1998). A re-assessment of the sources and importance of land-derived organic matter in surface sediments from the Gulf of Mexico. *Geochimica et Cosmochimica Acta*, 62(18):3055–3075.

- Goni, M. A., Yunker, M. B., Macdonald, R. W., and Eglinton, T. I. (2005). The supply and preservation of ancient and modern components of organic carbon in the Canadian Beaufort Shelf of the Arctic Ocean. *Marine Chemistry*, 93:53–73.
- Gordon, J. E. (1987). Radiocarbon dates from Nordenskjold Glacier, South Georgia, and their implications for late Holocene glacier chronology. *British Antarctic Survey Bulletin*, 76:1–5.
- Gordon, J. E. and Harkness, D. D. (1992). Magnitude and geographic variation of the radiocarbon content in Antarctic marine life: Implications for reservoir corrections in radiocarbon dating. *Quaternary Science Reviews*, 11(7-8):697–708.
- Gordon, J. E., Haynes, V. M., and Hubbard, A. (2008). Recent glacier changes and climate trends on South Georgia. *Global and Planetary Change*, 60(1-2):72–84.
- Graham, A. G., Fretwell, P. T., Larter, R. D., Hodgson, D. A., Wilson, C. K., Tate, A. J., and Morris, P. (2008). A new bathymetric compilation highlighting extensive paleo-ice sheet drainage on the continental shelf, south georgia, sub-antarctica. *Geochemistry, Geophysics, Geosystems*, 9(7):1–21.
- Graham, A. G. C., Kuhn, G., Meisel, O., Hillenbrand, C.-D., Hodgson, D. A., Ehrmann, W., Wacker, L., Wintersteller, P., Dos Santos Ferreira, C., Römer, M., White, D., and Bohrmann, G. (2017). Major advance of South Georgia glaciers during the Antarctic Cold Reversal following extensive sub-Antarctic glaciation. *Nature communications*, 8:14798.
- Gregory, J. (1915). The physiography of South Georgia as shown by Mr Ferguson's photographs. *Geological Observations in South Georgia - Transaction of the Royal Society of Edinburgh*, 50:814–816.
- Grobe, H. (1987). A Simple Method for the Determination of Ice-Rafted Debris in Sediment Cores. *Polarforschung*, 57(3):123–126.
- Häggi, C., Sawakuchi, A. O., Chiessi, C. M., Mulitza, S., Mollenhauer, G., Sawakuchi, H. O., Baker, P. A., Zabel, M., and Schefuß, E. (2016). Origin, transport and deposition of leaf-wax biomarkers in the Amazon Basin and the adjacent Atlantic. *Geochimica et Cosmochimica Acta*, 192:149–165.
- Hall, B. L., Henderson, G. M., Baroni, C., and Kellogg, T. B. (2010). Constant Holocene Southern-Ocean ^{14}C reservoir ages and ice-shelf flow rates. *Earth and Planetary Science Letters*, 296(1-2):115–123.
- Harada, N., Handa, N., Fukuchi, M., and Ishiwatari, R. (1995). Source of hydrocarbons in marine sediments in Lützow-Holm Bay, Antarctica. *Organic Geochemistry*, 23(3):229–237.
- Hedges, J. I. (1992). Global biogeochemical cycles: progress and problems. *Marine Chemistry*, 39:67–93.

- Hedges, J. I., Hu, F. S., Devol, A. H., Hartnett, H. E., Tsamakis, E., and Keil, R. G. (1999). Sedimentary organic matter preservation: A test for selective degradation under oxic conditions. *American Journal of Science*, 299(7-9):529–555.
- Hedges, J. I., Keil, R. G., and Benner, R. (1997). What happens to terrestrial organic matter in the ocean? *Organic Geochemistry*, 27(5):195–212.
- Ho, S. L., Mollenhauer, G., Fietz, S., Martínez-García, A., Lamy, F., Rueda, G., Schipper, K., Méheust, M., Rosell-Melé, A., Stein, R., and Tiedemann, R. (2014). Appraisal of TEX₈₆ and TEX_{86L} thermometries in subpolar and polar regions. *Geochimica et Cosmochimica Acta*, 131:213–226.
- Hobbie, S. E., Schimel, J. P., Trumbore, S. E., and Randerson, J. R. (2000). Controls over carbon storage and turnover in high-latitude soils. *Global Change Biology*, 6(Suppl. 1):196–210.
- Hodell, D. A., Kanfoush, S. L., Shemesh, A., Crosta, X., Charles, C. D., and Guilderson, T. P. (2001). Abrupt Cooling of Antarctic Surface Waters and Sea Ice Expansion in the South Atlantic Sector of the Southern Ocean at 5000 cal yr B.P. *Quaternary Research*, 56(2):191–198.
- Hodgson, D. A., Graham, A. G., Roberts, S. J., Bentley, M. J., Cofaigh, C. Ó., Verleyen, E., Vyverman, W., Jomelli, V., Favier, V., Brunstein, D., et al. (2014). Terrestrial and submarine evidence for the extent and timing of the last glacial maximum and the onset of deglaciation on the maritime-antarctic and sub-antarctic islands. *Quaternary Science Reviews*, 100:137–158.
- Hogg, A., Southon, J., Turney, C., Palmer, J., Ramsey, C. B., Fenwick, P., Boswijk, G., Buntgen, U., Friedich, M., Helle, G., Hughen, K., Jones, R., Bernd Kromer, Noronha, A., Reining, F., Reynard, L., Straff, R., and Wacker, L. (2016). Decadally resolved laeglacial radiocarbon evidence from New Zealand Kauri. *Radiocarbon*, pages 1–25.
- Hood, E., Fellman, J., Spencer, R. G. M., Hernes, P. J., Edwards, R., Amore, D. D., Scott, D., D'Amore, D., and Scott, D. (2009). Glaciers as a source of ancient and labile organic matter to the marine environment. *Nature*, 462(7276):1044–7.
- Hopmans, E. C., Weijers, J. W. H., Schefuß, E., Herfort, L., Sinninghe Damsté, J. S., and Schouten, S. (2004). A novel proxy for terrestrial organic matter in sediments based on branched and isoprenoid tetraether lipids. *Earth and Planetary Science Letters*, 224(1-2):107–116.
- Hughen, K., Lehman, S., Southon, J., Overpeck, J., Marchal, O., Herring, C., and Turnbull, J. (2004). C Activity and Global Carbon. *Science*, 303(January):202–207.

- Huguet, A., Fosse, C., Laggoun-Défarge, F., Toussaint, M. L., and Derenne, S. (2010). Occurrence and distribution of glycerol dialkyl glycerol tetraethers in a French peat bog. *Organic Geochemistry*, 41(6):559–572.
- Huguet, C., Hopmans, E. C., Febo-Ayala, W., Thompson, D. H., Sinninghe Damsté, J. S., and Schouten, S. (2006). An improved method to determine the absolute abundance of glycerol dibiphytanyl glycerol tetraether lipids. *Organic Geochemistry*, 37(9):1036–1041.
- Huguet, C., Smittenberg, R. H., Boer, W., Schouten, S., and Sinninghe Damsté, J. S. (2007). Twentieth century proxy records of temperature and soil organic matter input in the Drammensfjord, southern Norway. *Organic Geochemistry*, 38:1838–1849.
- Ingalls, A. E., Aller, R. C., Lee, C., and Wakeham, S. G. (2004). Organic matter diagenesis in shallow water carbonate sediments. *Geochimica et Cosmochimica Acta*, 68(21):4363–4379.
- Ingalls, A. E. and Pearson, A. (2005). Ten years of compound-specific radiocarbon analysis. *Oceanography*, 18(3):18–31.
- Ishiwatari, R., Uzaki, M., and Yamada, K. (1994). Carbon isotope composition of individual *n*-alkanes in recent sediments. *Organic Geochemistry*, 21(6-7):801–808.
- Jaffé, R., Mead, R., Hernandez, M. E., Peralba, M. C., and Diguida, O. A. (2001). Origin and transport of sedimentary organic matter in two subtropical estuaries: a comparative, biomarker-based study. *Organic Geochemistry*, 32:507–526.
- Johns, R. B., Gillan, F. T., and Volkman, J. K. (1980). Early diagenesis of phytol esters in a contemporary temperate intertidal sediment. *Geochimica et Cosmochimica Acta*, 44(2):183–188.
- Ju, S. J. and Harvey, H. R. (2004). Lipids as markers of nutritional condition and diet in the Antarctic krill *Euphausia superba* and *Euphausia crystallorophias* during austral winter. *Deep-Sea Research Part II: Topical Studies in Oceanography*, 51(17-19):2199–2214.
- Juul-Pedersen, T., Arendt, K. E., Mortensen, J., Blicher, M. E., Søgaard, D. H., and Rysgaard, S. (2015). Seasonal and interannual phytoplankton production in a sub-Arctic tidewater outlet glacier fjord, SW Greenland. *Marine Ecology Progress Series*, 524:27–38.
- Kattner, G., Albers, C., Graeve, M., and Schnack-Schiel, S. B. (2003). Fatty acid and alcohol composition of the small polar copepods, *Oithona* and *Oncaea*: Indication on feeding modes. *Polar Biology*, 26(10):666–671.
- Kim, J. H., Schouten, S., Hopmans, E. C., Donner, B., and Sinninghe Damsté, J. S. (2008). Global sediment core-top calibration of the TEX₈₆-paleothermometer in the ocean. *Geochimica et Cosmochimica Acta*, 72(4):1154–1173.

- Kim, J. H., van der Meer, J., Schouten, S., Helmke, P., Willmott, V., Sangiorgi, F., Koç, N., Hopmans, E. C., and Damsté, J. S. (2010). New indices and calibrations derived from the distribution of crenarchaeal isoprenoid tetraether lipids: Implications for past sea surface temperature reconstructions. *Geochimica et Cosmochimica Acta*, 74(16):4639–4654.
- Kuli, K., Monika, K., Lege, J., Gluchowska, M., and Zaborska, A. (2014). Particulate organic matter sinks and sources in high Arctic fjord. *Journal of Marine Systems*, 139:27–37.
- Kusch, S., Eglinton, T. I., Mix, A. C., and Mollenhauer, G. (2010a). Timescales of lateral sediment transport in the Panama Basin as revealed by radiocarbon ages of alkenones, total organic carbon and foraminifera. *Earth and Planetary Science Letters*, 290(3-4):340–350.
- Kusch, S., Rethemeyer, J., Hopmans, E. C., Wacker, L., and Mollenhauer, G. (2016). Factors influencing ^{14}C concentrations of algal and archaeal lipids and their associated sea surface temperature proxies in the Black Sea. *Geochimica et Cosmochimica Acta*, 188:35–57.
- Kusch, S., Rethemeyer, J., Schefuß, E., and Mollenhauer, G. (2010b). Controls on the age of vascular plant biomarkers in Black Sea sediments. *Geochimica et Cosmochimica Acta*, 74(24):7031–7047.
- Landais, A., Masson-Delmotte, V., Stenni, B., Selmo, E., Roche, D. M., Jouzel, J., Lambert, F., Guillevic, M., Bazin, L., Arzel, O., Vinther, B., Gkinis, V., and Popp, T. (2015). A review of the bipolar see-saw from synchronized and high resolution ice core water stable isotope records from Greenland and East Antarctica. *Quaternary Science Reviews*, 114:18e32.
- Leader-Williams, N., Smith, R. I. L., and Rothery, P. (1987). Influence of Introduced Reindeer on the Vegetation of South Georgia: Results From a Long-Term Exclusion Experiment. *Journal of Applied Ecology*, 24(3):801–822.
- Libby, W. F., Anderson, E. C., and Arnold, J. R. (1949). Age Determination by Radiocarbon Content: World-Wide Assay of Natural Radiocarbon. *Science*, 109(2827):227–228.
- Licht, K. J., Cunningham, W. L., Andrews, J. T., Domack, E. W., and Jennings, A. E. (1998). Establishing chronologies from acid-insoluble organic ^{14}C dates on antarctic (Ross Sea) and arctic (North Atlantic) marine sediments. *Polar Research*, 17(2):203–216.
- Licht, K. J., Jennings, A. E., Andrews, J. T., and Williams, K. M. (1996). Chronology of late Wisconsin ice retreat from the western Ross Sea, Antarctica. *Geology*, 24(3):223–226.
- Lichtfouse, E., Derenne, S., Mariotti, A., and Largeau, C. (1994). Possible algal origin of long chain odd n -alkanes in immature sediments as revealed by distributions and carbon isotope ratios. *Organic Geochemistry*, 22(6):1023–1027.

- Loomis, S. E., Russell, J. M., and Sinninghe Damsté, J. S. (2011). Distributions of branched GDGTs in soils and lake sediments from western Uganda: Implications for a lacustrine paleothermometer. *Organic Geochemistry*, 42(7):739–751.
- Marson, J. M., Wainer, I., Mata, M. M., and Liu, Z. (2014). The impacts of deglacial meltwater forcing on the South Atlantic Ocean deep circulation since the Last Glacial Maximum. *Climate of the Past*, 10(5):1723–1734.
- Marwick, T. R., Tamooch, F., Teodoru, C. R., Borges, A. V., Darchambeau, F., and Boillon, S. (2015). The age of river-transported carbon: A global perspective. *Global Biogeochemical Cycles*, 29:122–137.
- Mayewski, P. A., Rohling, E. E., Stager, J. C., Karlén, W., Maasch, K. A., Meeker, L. D., Meyerson, E. A., Gasse, F., van Krevelend, S., Holmgren, K., Lee-Thorp, J., Rosqvist, G., Rack, F., Staubwasser, M., Schneider, R. R., and Steig, E. J. (2004). Holocene climate variability. *Quaternary Research*, 62(3):243–255.
- McCormac, F. G., Hogg, A. G., Blackwell, P. G., Buck, C. E., Higham, T. F. G., and Reimer, P. J. (2004). SHcal04 Southern Hemisphere Calibration, 0–11.0 cal kyr BP. *Radiocarbon*, 46(3):1078–1092.
- Méjanelle, L., Sanchez-Gargallo, A., Bentaleb, I., and Grimalt, J. O. (2003). Long chain *n*-alkyl diols, hydroxy ketones and sterols in a marine eustigmatophyte, *Nannochloropsis gaditana*, and in *Brachionus plicatilis* feeding on the algae. *Organic Geochemistry*, 34(4):527–538.
- Melles, M., Viehberg, F., Ritter, B., Bennike, O., and White, D. (2013). 6. holocene and pleistocene environmental history of south georgia. *Expedition Programme No. 91 RV Polarstern*, page 18.
- Meyers, P. A. (1994). Preservation of elemental and isotopic source identification of sedimentary organic matter. *Chemical Geology*, 114(3-4):289–302.
- Meyers, P. A. (1997). Organic geochemical proxies of paleoceanographic, plaeolimnologic, and plaeoclimatic processes. *Organic Geochemistry*, 27(5):213–250.
- Meyers, P. A. (2003). Application of organic geochemistry to paleolimnological reconstruction: a summary of examples from the Laurentian Great Lakes. *Organic Geochemistry*, 34:261–289.
- Meyers, P. A. and Ishiwatari, R. (1993). Lacustrine organic geochemistry - an overview of indicators of organic matter sources and diagenesis in lake sediments. *Organic Geochemistry*, 20(7):867–900.
- Michalchuk, B. R., Anderson, J. B., Wellner, J. S., Manley, P. L., Majewski, W., and Bohaty, S. (2009). Holocene climate and glacial history of the northeastern Antarctic Peninsula:

- the marine sedimentary record from a long SHALDRIL core. *Quaternary Science Reviews*, 28(27-28):3049–3065.
- Mollenhauer, G. and Eglinton, T. I. (2007). Diagenetic and sedimentological controls on the composition of organic matter preserved in California Borderland Basin sediments. *Limnology and Oceanography*, 52(2):558–576.
- Mollenhauer, G., Kienast, M., Lamy, F., Meggers, H., Schneider, R. R., Hayes, J. M., and Eglinton, T. I. (2005). An evaluation of ^{14}C age relationships between co-occurring foraminifera, alkenones, and total organic carbon in continental margin sediments. *Paleoceanography*, 20(1):1–12.
- Mollenhauer, G. and Rethemeyer, J. (2009). Compound-specific radiocarbon analysis - Analytical challenges and applications. *IOP Conference Series: Earth and Environmental Science*, 5:012006.
- Müller, P. J. and Suess, E. (1979). Productivity, sedimentation rate, and sedimentary organic matter in the oceans-I. Organic carbon preservation. *Deep Sea Research Part A, Oceanographic Research Papers*, 26(12):1347–1362.
- Muller, R. A. (1977). Radioisotope Dating with a Cyclotron. *Science*, 196(4289):489–494.
- Naeher, S., Peterse, F., Smittenberg, R. H., Niemann, H., Ziegler, P. K., and Schubert, C. J. (2014). Sources of glycerol dialkyl glycerol tetraethers (GDGTs) in catchment soils, water column and sediments of Lake Rotsee (Switzerland) - Implications for the application of GDGT-based proxies for lakes. *Organic Geochemistry*, 66:164–173.
- Nielsen, S. H. H., Koç, N., and Crosta, X. (2004). Holocene climate in the Atlantic sector of the Southern Ocean: Controlled by insolation or oceanic circulation? *Geology*, 32(4):317–320.
- Ohkouchi, N. (2003). Radiocarbon Dating of Individual Fatty Acids As a Tool for Refining Antarctic Sediment Chronologies. *Radiocarbon*, 45(1):17–24.
- Ohkouchi, N. and Eglinton, T. I. (2008). Compound-specific radiocarbon dating of Ross Sea sediments: A prospect for constructing chronologies in high-latitude oceanic sediments. *Quaternary Geochronology*, 3(3):235–243.
- Pancost, R. D. and Boot, C. S. (2004). The palaeoclimatic utility of terrestrial biomarkers in marine sediments. *Marine Chemistry*, 92(1-4 SPEC. ISS.):239–261.
- Pearson, a. and Eglinton, T. I. (2000). An organic tracer for surface ocean radiocarbon. *October*, 15(5):541–550.
- Pearson, A., McNichol, A. P., Benitez-Nelson, B. C., Hayes, J. M., and Eglinton, T. I. (2001). Origins of lipid biomarkers in Santa Monica Basin surface sediment: A case study using compound-specific $\Delta^{14}\text{C}$ analysis. *Geochimica et Cosmochimica Acta*, 65(18):3123–3137.

- Pedro, J. B., Bostock, H. C., Bitz, C. M., He, F., Vandergoes, M. J., Steig, E. J., Chase, B. M., Krause, C. E., Rasmussen, S. O., Markle, B. R., and Cortese, G. (2015). The spatial extent and dynamics of the Antarctic Cold Reversal. *Nature Geoscience*, 9(1):51–55.
- Peterse, F., Kim, J. H., Schouten, S., Kristensen, D. K., Koç, N., and Sinninghe Damsté, J. S. (2009). Constraints on the application of the MBT/CBT palaeothermometer at high latitude environments (Svalbard, Norway). *Organic Geochemistry*, 40(6):692–699.
- Peterse, F., van der Meer, J., Schouten, S., Weijers, J. W. H., Fierer, N., Jackson, R. B., Kim, J. H., and Sinninghe Damsté, J. S. (2012). Revised calibration of the MBT-CBT paleotemperature proxy based on branched tetraether membrane lipids in surface soils. *Geochimica et Cosmochimica Acta*, 96:215–229.
- Phleger, C. F., Nelson, M. M., Mooney, B. D., and Nichols, P. D. (2002). Interannual and between species comparison of the lipids, fatty acids and sterols of Antarctic krill from the US AMLR Elephant Island survey area. *Comparative Biochemistry and Physiology - B Biochemistry and Molecular Biology*, 131(4):733–747.
- Rampen, S. W., Willmott, V., Kim, J. H., Rodrigo-Gámiz, M., Uliana, E., Mollenhauer, G., Schefuß, E., Sinninghe Damsté, J. S., and Schouten, S. (2014). Evaluation of long chain 1,14-alkyl diols in marine sediments as indicators for upwelling and temperature. *Organic Geochemistry*, 76:39–47.
- Raymond, P. A. and Bauer, J. E. (2001). Use of ^{14}C and ^{13}C natural abundances for evaluating riverine, estuarine, and coastal DOC and POC sources and cycling: A review and synthesis. *Organic Geochemistry*, 32(4):469–485.
- Reimer, P. J., Baillie, M. G. L., Bard, E., Bayliss, A., Beck, J. W., Bertrand, C. J. H., Blackwell, P. G., Buck, C. E., Burr, G. S., Cutler, K. B., Damon, P. E., Edwards, R. L., Fairbanks, R. G., Friedrich, M., Guilderson, T. P., Hogg, A. G., Hughen, K. A., and Kromer, B. (2004). Marine04 Marine radiocarbon age calibration 0-26 cal kyr BP. *Radiocarbon*, 46(3):0–26.
- Reimer, P. J., Bard, E., Bayliss, A., Beck, J. W., Blackwell, P. G., Ramsey, C. B., Buck, C. E., Cheng, H., Edwards, R. L., Friedrich, M., Grootes, P. M., Guilderson, T. P., Hafidason, H., Hajdas, I., Hatté, C., Heaton, T. J., Hoffmann, D. L., Hogg, A. G., Hughen, K. A., Kaiser, K. F., Kromer, B., Manning, S. W., Niu, M., Reimer, R. W., Richards, D. A., Scott, E. M., Southon, J. R., Staff, R. A., Turney, C. S. M., and van der Plicht, J. (2013). IntCal13 and Marine13 Radiocarbon Age Calibration Curves 0-50,000 Years cal BP. *Radiocarbon*, 55(04):1869–1887.
- Rethemeyer, J., Fülöp, R. H., Höffle, S., Wacker, L., Heinze, S., Hajdas, I., Patt, U., König, S., Stapper, B., and Dewald, A. (2013). Status report on sample preparation facilities for ^{14}C analysis at the new CologneAMS center. *Nuclear Instruments and Methods in Physics Research, Section B: Beam Interactions with Materials and Atoms*, 294:168–172.

- Rethemeyer, J., Kramer, C., Gleixner, G., and Schwark, L. (2004). Complexity of soil organic matter. *Radiocarbon*, 46(1):1111–1150.
- Rosenheim, B., Santoro, J., Gunter, M., and Domack, E. (2013). Improving Antarctic Sediment ^{14}C Dating Using Ramped Pyrolysis: An Example from the Hugo Island Trough. *Radiocarbon*, 55(1):115–126.
- Rosenheim, B. E., Day, M. B., Domack, E., Schrum, H., Benthien, A., and Hayes, J. M. (2008). Antarctic sediment chronology by programmed-temperature pyrolysis: Methodology and data treatment. *Geochemistry, Geophysics, Geosystems*, 9(4).
- Rosqvist, G. C., Rietti-Shati, M., and Shemesh, A. (1999). Late glacial to middle Holocene climatic record of lacustrine biogenic silica oxygen isotopes from a Southern Ocean island. *Geology*, 27(11):967–970.
- Rosqvist, G. C. and Schuber, P. (2003). Millennial-scale climate changes on South Georgia, Southern Ocean. *Quaternary Research*, 59(3):470–475.
- Sarnthein, M., Balmer, S., Grootes, P. M., and Mudelsee, M. (2015). Planktic and benthic ^{14}C reservoir ages for three ocean basins, calibrated by a suite of ^{14}C plateaus in the glacial-to-deglacial suigetsu atmospheric ^{14}C record. *Radiocarbon*, 57(1):129–151.
- Schlesinger, W. H. et al. (1995). An overview of the carbon cycle. In *Soils and global change*, volume 25, pages 9–25. CRC Press: Boca Raton, FL, USA.
- Schouten, S., Hopmans, E. C., Pancost, R. D., and Sinninghe Damsté, J. S. (2000). Widespread occurrence of structurally diverse tetraether membrane lipids: evidence for the ubiquitous presence of low-temperature relatives of hyperthermophiles. *Proceedings of the National Academy of Sciences of the United States of America*, 97(26):14421–14426.
- Schouten, S., Hopmans, E. C., Schefuß, E., and Sinninghe Damsté, J. S. (2002). Distributional variations in marine crenarchaeotal membrane lipids: A new tool for reconstructing ancient sea water temperatures? *Earth and Planetary Science Letters*, 204(1-2):265–274.
- Schouten, S., Hopmans, E. C., and Sinninghe Damsté, J. S. (2013). The organic geochemistry of glycerol dialkyl glycerol tetraether lipids: A review. *Organic Geochemistry*, 54:19–61.
- Schouten, S., Huguet, C., Hopmans, E. C., Kienhuis, M. V., and Sinninghe Damsté, J. S. (2007). Analytical methodology for tex_{86} paleothermometry by high-performance liquid chromatography/atmospheric pressure chemical ionization-mass spectrometry. *Analytical Chemistry*, 79(7):2940–2944.
- Simoneit, B. R. (2004). Biomarkers (molecular fossils) as geochemical indicators of life. *Advances in Space Research*, 33(8):1255–1261.

- Singer, G. a., Fasching, C., Wilhelm, L., Niggemann, J., Steier, P., Dittmar, T., and Battin, T. J. (2012). Biogeochemically diverse organic matter in Alpine glaciers and its downstream fate. *Nature Geoscience*, 5(10):710–714.
- Sinninghe Damsté, J. S. (2016). Spatial heterogeneity of sources of branched tetraethers in shelf systems: The geochemistry of tetraethers in the Berau River delta (Kalimantan, Indonesia). *Geochimica et Cosmochimica Acta*, 186:13–31.
- Sinninghe Damsté, J. S., Rijpstra, W. I. C., and Reichart, G. J. (2002). The influence of oxic degradation on the sedimentary biomarker record II. Evidence from Arabian Sea sediments. *Geochimica et Cosmochimica Acta*, 66(15):2737–2754.
- Skidmore, M. (1972). The Geology of South Georgia. *British Antarctic Survey Scientific Reports*, 73.
- Smith, R. I. L. (1981). Types of peat forming veg from South Georgia. *British Antarctic Survey Bulletin*, 53:119–139.
- Smith, R. W., Bianchi, T. S., Allison, M., Savage, C., and Galy, V. (2015). High rates of organic carbon burial in fjord sediments globally. *Nature Geoscience*, 8(May):450–453.
- Smittenberg, R. H., Hopmans, E. C., Schouten, S., Hayes, J. M., Eglinton, T. I., and Sinninghe Damsté, J. S. (2004). Compound-specific radiocarbon dating of the varved Holocene sedimentary record of Saanich Inlet, Canada. *Paleoceanography*, 19(2):1–16.
- Southon, J. R., Nelson, D. E., Vogell, J. S., and Fraser, S. (1990). A record of past ocean-atmosphere radiocarbon differences from the Northeast Pacific. *Paleoceanography*, 5(2):197–206.
- Spencer, R. G. M., Vermilyea, A., Fellman, J., Raymond, P., Stubbins, A., Scott, D., and Hood, E. (2014). Seasonal variability of organic matter composition in an Alaskan glacier outflow: insights into glacier carbon sources. *Environmental Research Letters*, 9:055005.
- Steig, E. J. (1998). Synchronous Climate Changes in Antarctica and the North Atlantic. *Science*, 282(5386):92–95.
- Strother, S. L., Salzmann, U., Roberts, S. J., Hodgson, D. A., Woodward, J., Van Nieuwenhuyze, W., Verleyen, E., Vyverman, W., and Moreton, S. G. (2015). Changes in Holocene climate and the intensity of Southern Hemisphere Westerly Winds based on a high-resolution palynological record from sub-Antarctic South Georgia. *The Holocene*, 25:263–279.
- Stuiver, M. and Pearson, G. W. (1993). High precision bidecadal calibration of the radiocarbon time scale, AD 1950-500 BC and 2500-6000 BC. *Radiocarbon*, 35(1):1–23.
- Stuiver, M., Pearson, G. W., and Braziunas, T. (1986). Radiocarbon age calibration of marine samples back to 9,000 cal yr BP. *Radiocarbon*, 28(2B):980–1021.

- Stuiver, M. and Polach, H. a. (1977). Reporting of ^{14}C Data. *Radiocarbon*, 19(3):355–363.
- Subt, C., Fangman, K. A., Wellner, J. S., and Rosenheim, B. E. (2016). Sediment chronology in antarctic deglacial sediments: Reconciling organic carbon ^{14}C ages to carbonate ^{14}C ages using ramped pyrox. *The Holocene*, 26(2):265–273.
- Suess, H. (1955). Radiocarbon concentration in modern wood. *Science*, 122(3166):415–417.
- Suess, H. E. (1986). Secular Variations of Cosmogenic ^{14}C on Earth: Their Discovery and Interpretation. *Radiocarbon*, 28(2A):259–265.
- Sugden, D. E. and Clapperton, C. M. (1977). The maximum ice extent on island groups in the Scotia sea, Antarctica. *Quaternary Research*, 7(2):268–282.
- Sun, M.-Y. and Wakeham, S. G. (1994). Molecular evidence for degradation and preservation of organic matter. *Geochimica et Cosmochimica Acta*, 58(16):3395–3406.
- Sun, Q., Chu, G., Liu, M., Xie, M., Li, S., Ling, Y., Wang, X., Shi, L., Jia, G., and Lü, H. (2011). Distributions and temperature dependence of branched glycerol dialkyl glycerol tetraethers in recent lacustrine sediments from China and Nepal. *Journal of Geophysical Research: Biogeosciences*, 116(1):1–12.
- Tao, S., Eglinton, T. I., Montluçon, D. B., McIntyre, C., and Zhao, M. (2015). Pre-aged soil organic carbon as a major component of the Yellow River suspended load: Regional significance and global relevance. *Earth and Planetary Science Letters*, 414:77–86.
- Taylor, H. W., Gordon, A., and Molinelli, E. (1978). Climatic characteristics of the Antarctic Polar Front zone. *Journal of Geophysical Research: Oceans*, 83(C9):4572–4578.
- Tesi, T., Semiletov, I., Dudarev, O., Andersson, A., and Gustafsson, Ö. (2016). Matrix association effects on hydrodynamic sorting and degradation of terrestrial organic matter during cross-shelf transport in the Laptev and East Siberian shelf seas. *Journal of Geophysical Research G: Biogeosciences*, 121(3):731–752.
- Tierney, J. E. and Russell, J. M. (2009). Distributions of branched GDGTs in a tropical lake system: Implications for lacustrine application of the MBT/CBT paleoproxy. *Organic Geochemistry*, 40(9):1032–1036.
- Trumbore, S. (2009). Radiocarbon and Soil Carbon Dynamics. *Annual Review of Earth and Planetary Sciences*, 37(1):47–66.
- Trumbore, S. E. (1993). Comparison of carbon dynamics in tropical and temperate soils using radiocarbon measurements. *Global Biogeochemical Cycles*, 7(2):275–290.
- Trumbore, S. E. (1997). Accumulation and turnover of carbon in organic and mineral soils of the BOREAS northern study area. *Journal of Geophysical Research*, 102(D24):28817–28830.

- Turnbull, J. C., Fletcher, S. E., Ansell, I., Brailsford, G. W., Moss, R. C., Norris, M. W., and Steinkamp, K. (2017). Sixty years of radiocarbon dioxide measurements at Wellington, New Zealand: 1954-2014. *Atmospheric Chemistry and Physics*, 17(23):14771–14784.
- Uchida, M., Shibata, Y., Ohkushi, K., Yoneda, M., Kawamura, K., and Morita, M. (2005). Age discrepancy between molecular biomarkers and calcareous foraminifera isolated from the same horizons of Northwest Pacific sediments. *Chemical Geology*, 218:73–89.
- Uchida, M., Yasuyuki Shibata, B., Kimitaka Kawamura, B., Yuichiro Kumamoto, B., Minoru Yoneda, B., Ken, B., Ohkushi, I., Naomi Harada, B., Masashi Hirota, B., Hitoshi Mukai, B., Atsushi Tanaka, B., Masashi Kusakabe, B., and Masatoshi Morita, B. (2001). Compound-specific radiocarbon ages of fatty acids in marine sediments from the western North Pacific. *Radiocarbon*, 43(2):949–956.
- Uchikawa, J., Popp, B. N., Schoonmaker, J. E., and Xu, L. (2008). Direct application of compound-specific radiocarbon analysis of leaf waxes to establish lacustrine sediment chronology. *Journal of Paleolimnology*, 39(1):43–60.
- Van Beek, P., Reyss, J. L., Paterne, M., Gersonde, R., van der Loeff, M. R., and Kuhn, G. (2002). ²²⁶Ra in barite: Absolute dating of Holocene Southern Ocean sediments and reconstruction of sea-surface reservoir ages. *Geology*, 30(8):731–734.
- Van der Putten, N., Stieperaere, H., Verbruggen, C., and Ochyra, R. (2004). Holocene palaeoecology and climate history of South Georgia (sub-Antarctica) based on a macrofossil record of bryophytes and seeds. *The Holocene*, 14(3):382–392.
- Van Der Putten, N. and Verbruggen, C. (2005). The onset of deglaciation of Cumberland Bay and Stromness Bay, South Georgia. *Antarctic Science*, 17(1):29–32.
- Van der Putten, N., Verbruggen, C., Ochyra, R., Spassov, S., de Beaulieu, J. L., De Dapper, M., Hus, J., and Thouveny, N. (2009). Peat bank growth, Holocene palaeoecology and climate history of South Georgia (sub-Antarctica), based on a botanical macrofossil record. *Quaternary Science Reviews*, 28(1-2):65–79.
- Volkman, J. K., Barrett, S. M., Blackburn, S. I., Mansour, M. P., Sikes, E. L., and Gelin, F. (1998). Microalgal biomarkers: A review of recent research developments. *Organic Geochemistry*, 29(5-7):1163–1179.
- Volkman, J. K., Barrett, S. M., Dunstan, G. A., and Jeffrey, S. W. (1992). C₃₀C-₃₂ alkyl diols and unsaturated alcohols in microalgae of the class Eustigmatophyceae. *Organic Geochemistry*, 18(1):131–138.
- Volkman, J. K., Johns, R. B., Gillan, F. T., and Perry, G. J. (1980). Microbial lipids of an intertidal sediment - Fatty acids and hydrocarbons. *Geochimica et Cosmochimica Acta*, 44:1133–1143.

- Vonk, J. E., Sánchez-García, L., Semiletov, I., Dudarev, O., Eglinton, T., Andersson, A., and Gustafsson, O. (2010). Molecular and radiocarbon constraints on sources and degradation of terrestrial organic carbon along the Kolyma paleoriver transect, East Siberian Sea. *Biogeosciences*, 7(10):3153–3166.
- Wacker, L., Nemeč, M., and Bourquin, J. (2010). A revolutionary graphitisation system: Fully automated, compact and simple. *Nuclear Instruments and Methods in Physics Research, Section B: Beam Interactions with Materials and Atoms*, 268(7-8):931–934.
- Wakeham, S. G. and Canuel, E. A. (2016). The nature of organic carbon in density-fractionated sediments in the Sacramento-San Joaquin River Delta (California). *Biogeosciences*, 13(2):567–582.
- Wakeham, S. G., Lee, C., Hedges, J. I., Hernes, P. J., and Peterson, M. J. (1997). Molecular indicators of diagenetic status in marine organic matter. *Geochimica et Cosmochimica Acta*, 61(24):5363–5369.
- Ward, P., Atkinson, A., Murray, A. W. A., Wood, A. G., Williams, R., and Poulet, S. A. (1995). The summer zooplankton community at South Georgia: biomass, vertical migration and grazing. *Polar Biology*, 15(3):195–208.
- Ward, P., Meredith, M. P., Whitehouse, M. J., and Rothery, P. (2008). The summertime plankton community at South Georgia (Southern Ocean): Comparing the historical (1926/1927) and modern (post 1995) records. *Progress in Oceanography*, 78(3):241–256.
- Ward, P., Shreeve, R., Whitehouse, M., Korb, B., Atkinson, A., Meredith, M., Pond, D., Watkins, J., Goss, C., and Cunningham, N. (2005). Phyto- and zooplankton community structure and production around South Georgia (Southern Ocean) during Summer 2001/02. *Deep-Sea Research Part I: Oceanographic Research Papers*, 52(3):421–441.
- Weber, Y., De Jonge, C., Rijpstra, W. I. C., Hopmans, E. C., Stadnitskaia, A., Schubert, C. J., Lehmann, M. F., Sinninghe Damsté, J. S., and Niemann, H. (2015). Identification and carbon isotope composition of a novel branched GDGT isomer in lake sediments: Evidence for lacustrine branched GDGT production. *Geochimica et Cosmochimica Acta*, 154:118–129.
- Weijers, J. W. H., Bernhardt, B., Peterse, F., Werne, J. P., Dungait, J. A. J., Schouten, S., and Sinninghe Damsté, J. S. (2011a). Absence of seasonal patterns in MBT-CBT indices in mid-latitude soils. *Geochimica et Cosmochimica Acta*, 75(11):3179–3190.
- Weijers, J. W. H., Schouten, S., Spaargaren, O. C., and Sinninghe Damsté, J. S. (2006). Occurrence and distribution of tetraether membrane lipids in soils: Implications for the use of the TEX₈₆ proxy and the BIT index. *Organic Geochemistry*, 37(12):1680–1693.

- Weijers, J. W. H., Schouten, S., van den Donker, J. C., Hopmans, E. C., and Sinninghe Damsté, J. S. (2007). Environmental controls on bacterial tetraether membrane lipid distribution in soils. *Geochimica et Cosmochimica Acta*, 71(3):703–713.
- Weijers, J. W. H., Schouten, S., Van Der Linden, M., Van Geel, B., and Sinninghe Damsté, J. S. (2004). Water table related variations in the abundance of intact archaeal membrane lipids in a Swedish peat bog. *FEMS Microbiology Letters*, 239(1):51–56.
- Weijers, J. W. H., Steinmann, P., Hopmans, E. C., Schouten, S., and Sinninghe Damsté, J. S. (2011b). Organic Geochemistry Bacterial tetraether membrane lipids in peat and coal: Testing the MBT/CBT temperature proxy for climate reconstruction. *Organic Geochemistry*, 42(5):477–486.
- White, D. A., Bennike, O., Melles, M., Berg, S., and Binnie, S. A. (2018). Was south georgia covered by an ice cap during the last glacial maximum? *Geological Society, London, Special Publications*, 461(1):49–59.
- Wild, E., Golser, R., Hille, P., Kutschera, W., Priller, A., Puchegger, S., Rom, W., Steier, P., and Vycudilik, W. (1998). First ^{14}C results from archaeological and forensic studies at the Vienna Environmental Research Accelerator. *Radiocarbon*, 40(1):273–281.
- Winkelmann, D. and Knies, J. (2005). Recent distribution and accumulation of organic carbon on the continental margin west off Spitsbergen. *Geochemistry, Geophysics, Geosystems*, 6(9):1–22.
- Wood, R. (2015). From revolution to convention: The past, present and future of radiocarbon dating. *Journal of Archaeological Science*, 56:61–72.
- Wündsche, M., Haberzettl, T., Meadows, M. E., Kirsten, K. L., Kasper, T., Baade, J., Daut, G., Stoner, J. S., and Mäusbacher, R. (2016). The impact of changing reservoir effects on the ^{14}C chronology of a Holocene sediment record from South Africa. *Quaternary Geochronology*, 36:148–160.
- Xiao, W., Esper, O., and Gersonde, R. (2016). Last Glacial - Holocene climate variability in the Atlantic sector of the Southern Ocean. *Quaternary Science Reviews*, 135:115–137.
- Yamane, M., Yokoyama, Y., Miyairi, Y., Suga, H., Matsuzaki, H., Dunbar, R. B., and Ohkouchi, N. (2014). Compound-specific ^{14}C dating of IODP expedition 318 core U1357A obtained off the Wilkes Land Coast, Antarctica. *Radiocarbon*, 56(3):1009–1017.
- Young, E. F., Thorpe, S. E., Banglawala, N., and Murphy, E. J. (2014). Variability in transport pathways on and around the South Georgia shelf, Southern Ocean: Implications for recruitment and retention. *Journal of Geophysical Research: Oceans*, 119(1):241–252.
- Zell, C., Kim, J. H., Dorhout, D., Baas, M., and Sinninghe Damsté, J. S. (2015). Sources and distributions of branched tetraether lipids and crenarchaeol along the Portuguese

continental margin: Implications for the BIT index. *Continental Shelf Research*, 96:34–44.

Zencak, Z., Reddy, C. M., Teuten, E. L., Xu, L., McNichol, A. P., and Gustafsson, Ö. (2007). Evaluation of gas chromatographic isotope fractionation and process contamination by carbon in compound-specific radiocarbon analysis. *Analytical Chemistry*, 79(5):2042–2049.

Ziolkowski, L. A. and Druffel, E. R. M. (2009). Quantification of extraneous carbon during compound specific radiocarbon analysis of black carbon. *Analytical Chemistry*, 81(24):10156–10161.

Zonneveld, K. A. F., Versteegh, G. J. M., Kasten, S., Eglinton, T. I., Emeis, K.-C., Huguet, C., Koch, B. P., de Lange, G. J., de Leeuw, J. W., Middelburg, J. J., Mollenhauer, G., Prahl, F. G., Rethemeyer, J., and Wakeham, S. G. (2010). Selective preservation of organic matter in marine environments; processes and impact on the sedimentary record. *Biogeosciences*, 7(2):483–511.

Ich versichere, dass ich die von mir vorgelegte Dissertation selbstständig angefertigt, die benutzten Quellen und Hilfsmittel vollständig angegeben und die Stellen der Arbeit- einschließlich Tabellen, Karten und Abbildungen-, die anderen Werken in Wortlaut oder dem Sinn nach entnommen sind, in jedem Einzelfall als Entlehnung kenntlich gemacht habe; dass diese Dissertation noch keiner anderen Fakultät oder Universität zur Prüfung vorgelegen hat; dass sie - abgesehen von unten angegebenen Teilpublikationen- noch nicht veröffentlicht worden ist sowie, dass ich eine solche Veröffentlichung vor Abschluss des Promotionsverfahrens nicht vornehmen werde. Die Bestimmungen der Promotionsordnung sind mir bekannt. Die von mir vorgelegte Dissertation ist von Dr. Sonja Berg betreut worden.

Köln, den 28. März 2019

Sandra Jivcov

Sandra Jivcov